

Novel Pervaporation for Separating Acetic Acid and Water Mixtures Using Hollow Fiber Membranes

A Thesis
Presented to
The Academic Faculty

By

Fangbin Zhou

In Partial Fulfillment
Of the Requirements for the Degree of
Doctor of Philosophy in Chemical Engineering

School of Chemical and Biomolecular Engineering
Georgia Institute of Technology
August 2005

Copyright © 2005 by Fangbin Zhou

Novel Pervaporation for Separating Acetic Acid and Water Mixtures Using Hollow Fiber Membranes

Approved by:

Dr. William J. Koros, Advisor
School of Chemical and Biomolecular
Engineering
Georgia Institute of Technology

Dr. Charles A. Eckert
School of Chemical and Biomolecular
Engineering
Georgia Institute of Technology

Dr. Aryn S. Teja
School of Chemical and Biomolecular
Engineering
Georgia Institute of Technology

Dr. F. Joseph Schork
School of Chemical and Biomolecular
Engineering
Georgia Institute of Technology

Dr. Wallace W. Carr
School of Polymer, Textile and Fiber
Engineering
Georgia Institute of Technology

Dr. Stephen J. Pietsch
PTA Process Research
BP Chemicals

Date Approved: June 16, 2005

To my loving husband, Ken

Acknowledgements

First and foremost, I owe a deep debt of gratitude to my advisor, Prof. William Koros, for his continuous guidance, support, and encouragement through this study. Not only did Prof. Koros introduce me to this fascinating research field and provide me with invaluable advice in the research, but he has also guided my personal development and maturation as an independent, confident, and strong researcher, something I never could have learned from a book. His enthusiasm for work, his dedication to research, and his vast knowledge have created an excellent model for me to learn from. He is the greatest professor I have ever met in my life, and I will always keep this precious experience in my heart.

I would like to extend my deepest gratitude to Dr. Steve Pietsch and to BP-Amoco for their financial support. I appreciate Dr. Steve's advice for overcoming culture difference and achieving a successful career. His trust made me feel like a superstar and helped me to beat all the challenges in both research and life.

I would like to thank constructive suggestions and valuable comments from other committee members: Dr. Eckert, Dr. Teja, Dr. Schork, and Dr. Carr. My special thanks also go to Prof. Mostafa A. El-Sayed, Dr. Wei Qian, Dr. Lulu Song, and Dr. Xianyong Wang for their help on fluorescence measurement and interpretation.

I am fortunate to work in a wonderful group and I appreciate all of the kind help from the past and present members of Dr. Koros' group. My special thanks go to Dr. David Wallace and Shabbir Husain for teaching me to spin a hollow fiber, Dr. Ted Moore for revising my English writing, Preeti for proof reading my dissertation draft, Madden

and Alexis for helping me to understand American culture and politics, and JR for correcting my English pronunciation.

I am also deeply indebted to my parents, Juan Zhou and Xianxian Jia, for their endless support, understanding, encouragement, and love, which inspired me to pursue my dream and finish my Ph.D study in the United States.

Last, but definitely not least, I would like to thank my husband, Ken, who has stood by me throughout this long journey. His love and friendship have helped me to overcome many obstacles. Without his spiritual support, this dissertation would not have been possible.

Table of Contents

Acknowledgements.....	iv
List of Tables	xi
List of Figures	xiii
Summary	xx
Chapter 1: Introduction	1
1.1 Industrial Motivations.....	1
1.2 Membrane Based-Pervaporation Separation.....	5
1.3 Research Objectives and Strategies	7
1.4 Organization of Dissertation	10
1.5 References.....	12
Chapter 2: Background and Theory	14
2.1 Membrane Material Selection.....	14
2.2 Gas Transport in Amorphous Glassy Polymers.....	16
2.3 Asymmetric Defect-Free Hollow Fiber Membranes	23
2.3.1 Formation of Defect-Free Outer Skin Layer.....	25
2.3.2 Large Bore Size Hollow Fibers.....	27
2.4 Gas Transport in Asymmetric Defect-Free Hollow Fibers.....	28
2.5 Mechanism of Pervaporation Transport.....	34
2.6 Plasticization and Stabilization of Hollow Fibers.....	37
2.7 Summary	39
2.8 References.....	39
Chapter 3: Hollow Fiber Spinning from Matimid [®]	45
3.1 Introduction.....	45
3.2 Mechanism of Phase Separation	48
3.3 Dope Preparation	50
3.4 Fiber Spinning.....	55
3.4.1 Formation of Integrally-Skinned Defect-Free Outer Layer	57
3.4.2 Formation of Open Porous Substructure.....	59
3.4.3 Macroscopic Morphology	60

3.4.4 Key Spinning Variables to Control Fiber Size	62
3.5 Solvent Exchange and Drying	66
3.6 Fiber Characterizations and Iterations	68
3.6.1 Pure Gas Permeation Tests	68
3.6.2 Microscopy Tests	72
3.7 Summary	73
3.8 References	74
Chapter 4: Pervaporation to Separate HAc/H ₂ O Mixtures Using Matrimid [®] Hollow Fibers.....	79
4.1 Introduction.....	79
4.2 Pervaporation Module Fabrication	80
4.3 Pervaporation Set-up	81
4.4 Pervaporation Experiments.....	83
4.4.1 Procedures.....	83
4.4.2 Sample Analysis.....	84
4.5 Experimental Results and Discussion.....	86
4.5.1 "Proof of Concept" Work.....	88
4.5.2 Effects of Bore Size on Fiber Performance	95
4.5.3 Water Effects on Fiber Performance.....	97
4.5.4 Effects of HAc Concentration in Feeds on Fiber Performance ..99	
4.5.5 Long Term Pervaporation Results	102
4.5.6 Effects of Operation History on Fiber Performance	104
4.6 Summary	109
4.7 References.....	110
Chapter 5: Mathematical Model to Demonstrate Bore Pressure Change Effects on Fiber Performance.....	113
5.1 Introduction.....	113
5.2 Model Development.....	114
5.3 Results and Discussion	121
5.3.1 Model Results with Pure Gas Permeation Tests	121
5.3.2 Model Results for Pervaporation Tests with Pure DI Water Feeds	124
5.3.3 Model Results for Pervaporation Tests with 20% HAc/H ₂ O Feeds	

.....	128
5.4 Summary	132
5.5 References	133
Chapter 6: Pervaporation of HAc/H ₂ O Mixtures Using Thermally Annealed Hollow Fibers	135
6.1 Introduction	135
6.2 Spectroscopy Technology	137
6.2.1 FTIR	138
6.2.2 ¹ H NMR	138
6.2.3 Fluorescence Spectroscopy	139
6.3 One Application of Fluorescence Technology in Benzophenone-Type Polyimides	141
6.4 Thermal Annealing Procedures	142
6.5 Separation Results with and without Thermal Annealing for 20% wt HAc Concentration Feeds	143
6.5.1 Heating Temperature	143
6.5.2 Spectroscopy Results for Annealed Hollow Fibers	145
6.5.3 Heating Time	149
6.5.4 Heating Environment	153
6.5.5 Long Term Separation Performance with Annealed Fibers	154
6.6 Separation Results with and without Thermal Annealing for 50% wt HAc Concentration Feeds	155
6.6.1 Heating Time	156
6.6.2 Heating Environment	157
6.7 Modeling Work to Estimate Overall Selectivity of Annealed Fibers in a Cross-Flow Separator	158
6.7.1 Permeabilities of Water and Acetic Acid	159
6.7.2 Model Development	161
6.7.3 Simulation Results	165
6.8 Summary	168
6.9 References	170
Chapter 7: Sorption-Induced Swelling Tests	173
7.1 Introduction	173

7.2	Sorption-Induced Swelling Experiments	174
7.3	Swelling Effects on Hollow Fibers with and without Heat Treatment	176
7.4	Summary	178
7.5	References	179
Chapter 8: Conclusions and Recommendations for Future Work		182
8.1	Summary of Conclusions	182
8.1.1	Spinning a Large Bore Size Defect-Free Fiber	183
8.1.2	Pervaporation of HAc/H ₂ O Mixtures Using Hollow Fibers	185
8.1.3	Model to Simulate Pressure Change in Bore Side of Hollow Fibers	186
8.1.4	Investigation of Thermally Annealed Fibers in Separating HAc/H ₂ O Mixtures	187
8.1.5	Sorption-Induced Swelling Tests	190
8.2	Recommendations for Future Work	191
8.2.1	Performance Evaluation for Contaminated Feeds	192
8.2.2	Platicization by HAc and Potential Contaminates	193
8.3	References	194
Appendix A: Manufacture of Lab-Scale Hollow Fiber Modules for Gas Permeation [1]		196
A.1	Parts	196
A.2	Procedure	197
A.3	References	198
Appendix B: Pure Gas Permeation Tests for Hollow Fiber Modules		199
B.1	Setup	199
B.2	Purge Modules	200
B.3	Testing	200
B.4	Analysis	202
Appendix C: Fabrication of Hollow Fiber-Based Pervaporation Modules		203
C.1	Parts	203
C.2	Procedures	204
C.3	Notes	205

C.4	References.....	205
Appendix D:	Pervaporation Tests for Hollow Fiber-Based Pervaporation Modules	206
D.1	Bore vs. Shell Feed	207
D.2	Operation Procedures.....	207
D.3	Analysis.....	209
D.4	Emergency Stop.....	211
D.5	Notes	211
Appendix E:	Exploration of Reverse Osmosis Technology	212
E.1	Introduction.....	212
E.2	RO Model.....	213
E.3	References.....	219
Bibliography	221

List of Tables

Table 1.1:	Boiling points and vaporization enthalpies for H ₂ O and HAc	2
Table 2.1:	Collision diameters of selected substances * calculated by the equation of $\sigma = 8.33V_c^{\frac{1}{3}}$ [36], $V_c = 0.171\text{m}^3/\text{kgmol}$ [37].....	22
Table 3.1:	Boiling temperature and solubility level with water for solvents and non-solvents commonly used for asymmetric membrane formation *: Solubility with water or EtOH on a relative scale: 1-insoluble; 2-slightly soluble; 3-soluble; 4-very soluble; 5-miscible.....	52
Table 3.2:	Dope and bore fluid formulas used to spin regular diameter (~ 250 μm) and large diameter (~ 500 μm) fibers in this project	55
Table 3.3:	Key variables used to spin regular and large diameter fibers	66
Table 3.4:	Potential non-solvent candidates for the solvent exchange process [22]	67
Table 3.5:	Permeability and selectivity of Matrimid [®] films tested @ 35°C, upstream pressure of 50-65 psi (A), (B), and (C) represent different Matrimid [®] sources	68
Table 3.6:	Gas permeation data for a dense film and five different state fibers @ 35°C, upstream pressure of 100 psi. $\pm 2\%$ Error.....	70
Table 4.1:	Pure gas permeation results for defect-free hollow fibers that are used to separate HAc/H ₂ O mixtures in pervaporation * Calculated based upon pure gas permeation tests using equation 3.3	87
Table 4.2:	Pervaporation results with a model 20% wt HAc/H ₂ O mixture feed for FB5.6_5 and FB5.6_10 modules. * FB5.6_5 has been tested with pure DI water for 14 days before taking a model 20% wt HAc solution feed on day #15 ** FB5.6_10 was directly tested with a model 20% wt HAc solution feed.....	98
Table 5.1:	Parameters used as model inputs for FB1.4 fiber in pure gas permeation tests	122
Table 5.2:	Comparison between uncorrected and corrected bore pressure changes for FB1.4 fiber	122
Table 5.3:	Inner diameter and skin thickness of hollow fibers used in the model	

	*: Calculated based upon pure gas permeation tests (N ₂ and O ₂) using Equation 3.3	125
Table 6.1:	Comparison of separation results between a virgin hollow fiber and an annealed hollow fiber.....	145
Table 6.2:	Pure gas permeation results for hollow fibers with different annealing times	152
Table 6.3:	Optimal heating variables	154
Table A.1:	Parts for assembling double-ended lab scale hollow fiber modules	196
Table C.1:	Parts for assembling a hollow fiber-based pervaporation module.....	204
Table C.2:	Technique parameters for Stycast [®] 2651 and Loctite [®] Depend [®] 330 [™] epoxies	205
Table E.1:	T _c and P _c for water and HAc [7-8].....	217

List of Figures

Figure 1.1:	Flow chart for manufacturing terephthalic acid (TA).....	2
Figure 1.2:	Vapor-liquid equilibrium graph for HAc/H ₂ O system [2].....	3
Figure 1.3:	Hypothetical hybrid process for separating HAc/H ₂ O mixtures in the dehydration tower	4
Figure 1.4:	Schematic diagram of membrane-based pervaporation separation processes (a) vacuum operation (b) permeate-side sweep stream operation	7
Figure 1.5:	Schematic flowchart of our research procedures	10
Figure 2.1:	Repeat unit for Matrimid [®] polymer	16
Figure 2.2:	Schematic of specific volume vs. temperature for an amorphous polymer [27]	17
Figure 2.3:	Schematic chart showing gas separation through amorphous dense polymeric films	18
Figure 2.4:	Typical sorption isotherm for amorphous glassy polymeric materials.	20
Figure 2.5:	Solubility vs. pressure for amorphous glassy polymeric materials...	21
Figure 2.6:	Cartoon pictures showing an idealized diffusion step and the difference in diffusion between large and small molecules in a glassy polymer... ..	22
Figure 2.7:	Surface area per unit volume with geometric configurations [28] ...	25
Figure 2.8:	Cartoon picture showing coating technique for the defective outer skin layer of a hollow fiber.....	26
Figure 2.9:	Pressure change in the bore side along the axial direction of hollow fibers with shell feed (A) A small diameter fiber with a large pressure change (B) A large diameter fiber with a small pressure change	27
Figure 2.10:	Structure of a typical asymmetric hollow fiber and its outer separation skin layer.....	28

Figure 2.11: Cartoon picture showing the total resistance from both skin and substrate of hollow fibers	31
Figure 2.12: The relationship between the membrane selectivity of $\alpha_{\text{He}/\text{N}_2}$ and the ratio of $\phi / (\frac{\ell_{\text{skin}}}{P_{\text{He}}})$	33
Figure 2.13: Cartoon picture showing an ideal pervaporation process	35
Figure 2.14: Schematic diagram of HAc permeability vs. HAc concentration in feeds showing the HAc-induced swelling effects	38
Figure 3.1: Steps involved in the formation of a large bore size hollow fiber with defect-free outer skin layer	46
Figure 3.2: Schematic flowchart for the fiber spinning set-up	47
Figure 3.3: Ternary-phase diagram of polymer-solvent-nonsolvent system	49
Figure 3.4: Ternary-phase diagram of the Matrimid [®] /(THF+NMP)/EtOH system, showing the starting point of a dope composition [2]	53
Figure 3.5: Ternary-phase diagram of the Matrimid [®] /NMP/H ₂ O system showing the concentration point of a bore fluid [2]	54
Figure 3.6: Structure of “the first generation” spinneret used in this work [27] (a) whole picture, (b) parts, (c) bottom view	56
Figure 3.7: Mass transfer in the “dry jet, wet quench” spinning process	57
Figure 3.8: Phase separation in the air gap	58
Figure 3.9: Phase separation in the quench bath	59
Figure 3.10: SEM picture showing a non-concentric hollow fiber	60
Figure 3.11: Cartoon picture showing the non-concentric hollow fiber due to design weakness of the spinneret	61
Figure 3.12: The take-up rate effects on the O.D. of hollow fibers	63
Figure 3.13: The effects of the bore fluid extrusion rate on the I.D. with the same dope extrusion rate	64
Figure 3.14: Cartoon picture showing the crinkling problem in the spinning process	65

Figure 3.15: Experimental set-up for pure gas permeation tests	69
Figure 3.16: SEM picture showing the cross section of a hollow fiber with the defect-free skin layer and the outer diameter of 450 μm	73
Figure 3.17: SEM picture of FB5.4 fiber showing a skin layer, transition layer and open porous substructure	73
Figure 4.1: Laboratory single-fiber pervaporation module (A) Cartoon picture showing a double-ended module (B) Optical microscopy picture showing a pot-face with an open bore	81
Figure 4.2: A hollow fiber-based pervaporation system	82
Figure 4.3: Calibration curves to measure the HAc concentration in aqueous mixtures $\pm 2\%$ Error (a) Low HAc concentration window (permeate side) (b) High HAc concentration window (feed side).....	84
Figure 4.4: Schematic testing procedures for DW24.3_3 and FB4.7_2 modules. The numbers of “(1), (2), (3), and (4)” represent the testing step.....	89
Figure 4.5: Water flux and separation factor, $\beta_{\text{H}_2\text{O}/\text{HAc}}$, for DW24.3_3 and FB4.7_2 modules	89
Figure 4.6: Cartoon pictures showing the competition effect caused by the presence of HAc in a membrane system. The symbol of \odot represents the free volume accessible to A/water in the glassy polymer in the absence of B/HAc that is a strongly competitive agent. During exposure to a HAc/H ₂ O mixture, the water permeation pathway is hindered by HAc molecules, thereby reducing the water permeability in contrast to a pure DI water feed.....	92
Figure 4.7: Schematic testing procedures for DW24.2_1 and FB2.6_1 modules. The numbers of “(1), (2), (3), and (4)” represent the testing step.....	93
Figure 4.8: Water flux and separation factor for DW24.2_1 and FB2.6_1 modules	94
Figure 4.9: Water and HAc fluxes and separation factor vs. bore size for 20% wt HAc concentration feeds	95
Figure 4.10: The variation of the water flux with the bore size for pure DI water feeds	97


Figure 4.11: Water permeance for pure DI water feeds (FB5.6_5), and replaced by a model 20% HAc concentration feed on day #15.	98
Figure 4.12: Schematic testing procedures for FB4.7_2 module. The numbers of “(1), (2), ..., and (8)” represent the testing step.	100
Figure 4.13: Water flux and acetic acid flux with different HAc concentration feeds	100
Figure 4.14: Permeance and separation factor/membrane selectivity with different HAc concentration feeds.....	101
Figure 4.15: Water permeance with different HAc concentration and pure DI water feeds for FB4.7_1 module.....	102
Figure 4.16: Membrane selectivity with different HAc concentration feeds for FB4.7_1 module.....	103
Figure 4.17: The variations of water and HAc permeances with time for 20% wt and 55% wt HAc concentration feeds	105
Figure 4.18: The variation of membrane selectivity with time for 20% wt and 55% wt HAc concentration feeds.....	105
Figure 4.19: Cartoon pictures showing plasticization effects caused by the presence of HAc in a membrane system. The symbol of  represents the free volume accessible to A/water or B/HAc in the glassy polymer. The purple arrows represent transport pathway of water, while the black arrows represent transport pathway of HAc. Additional arrows shown in “during swelling” case illustrates the increased flux of water and HAc during the B/HAc-induced plasticization. Clearly, More HAc molecules go through the polymer, thereby reducing the membrane selectivity... ..	106
Figure 4.20: Cartoon picture showing the separating process in a cross-flow separator	107
Figure 4.21: Schematic testing procedures for FB4.7_3 module	108
Figure 4.22: Permeance and selectivity for FB4.7_3 module on day #11, 12, 13, and 14.....	108
Figure 5.1: Schematic diagram of the finite element method for a one-ended module	115
Figure 5.2: Schematic diagram of the j^{th} element in a hollow fiber	116

Figure 5.3:	Schematic diagram of sealed end and pot face of a fiber	118
Figure 5.4:	Modeled pressure distribution of N ₂ , O ₂ , and He inside the bore of FB1.4 fiber	123
Figure 5.5:	Variation of water permeability vs. bore size with and without bore pressure change correction.....	126
Figure 5.6:	Modeled pressure distribution inside the bore for different bore size fibers	127
Figure 5.7:	Comparison of water flux between model and experimental results for different bore size fibers with pure DI water feeds.....	128
Figure 5.8:	Comparison of water flux between model and experimental results for different bore size fibers with 20% wt HAc/H ₂ O feeds.....	129
Figure 5.9:	Comparison of HAc flux between model and experimental results for different bore size fibers with 20% wt HAc/H ₂ O feeds.....	129
Figure 5.10:	HAc permeability and HAc partial pressure inside the bore for different bore size fibers with bore pressure change correction	130
Figure 5.11:	Water permeabilities with bore pressure change correction for different bore size fibers	131
Figure 6.1:	Chemical structure of Matrimid [®] showing electron acceptive and donative groups [9-11]	137
Figure 6.2:	Jablonski diagram illustrating the processes involved in the creation of an excited electronic singlet state by optical absorption and subsequent emission of fluorescence [16]	139
Figure 6.3:	Fluorescence spectrum of a benzophenone-type aromatic polyimide PI (BTDA/DPM) film.....	141
Figure 6.4:	Intra- and inter-molecular charge transfer complexes for PI(BTDA/DPM) polymer [9].....	142
Figure 6.5:	Effects of heating temperature on water and acetic acid permeances	144
Figure 6.6:	Effects of heating temperature on the membrane selectivity α_{mem}	144

Figure 6.7: Chemical structure of Matrimid® and FTIR absorption spectra for virgin and annealed fibers at room temperature	146
Figure 6.8: Chemical structure of Matrimid® and ¹ H NMR absorption spectra for virgin and annealed fibers at room temperature	147
Figure 6.9: Variations of micro-fluorescence emission spectra for the fibers cured at different temperatures	148
Figure 6.10: Variations of micro-fluorescence emission spectra for the fibers cured at different times	150
Figure 6.11: Effects of annealing times on water permeance and membrane selectivity	151
Figure 6.12: Effects of heating environments on water permeance and membrane selectivity	153
Figure 6.13: Permeance and separation factor of module FB5.6_511 for long term separation experiments.....	155
Figure 6.14: Effects of heating time on water permeance and membrane selectivity with a model 50% wt HAc/H ₂ O mixture feed	156
Figure 6.15: Effects of heating environments on water permeance and membrane selectivity with a model 50% wt HAc/H ₂ O mixture feed.....	158
Figure 6.16: Schematic diagrams of dead-end flow and cross-flow separators	159
Figure 6.17: Water and HAc permeances and membrane selectivity vs. HAc concentration (% wt) in feeds	160
Figure 6.18: Asymmetric hollow fiber-based separation in a cross-flow separator..	162
Figure 6.19: HAc concentration distribution in the shell and bore sides for a hollow fiber-based cross-flow separator	166
Figure 6.20: Normalized HAc and H ₂ O flowrate distributions in the shell and bore sides for a hollow fiber-based cross-flow separator	166
Figure 6.21: (A) HAc loss and removed water (% wt) vs. normalized feed flowrate (B) Overall membrane selectivity vs. normalized feed flowrate	168
Figure 7.1: Experimental set-up for a hollow fiber-based swelling test.....	175

Figure 7.2: Length extension measurement of hollow fibers with and without heat treatment in different HAc concentration solutions.....	176
Figure 7.3: Equilibrium data of length extension for virgin and annealed fibers	177
Figure 8.1: Flow diagram showing our achievements.....	183
Figure 8.2: Chemical structure of Torlon®	194
Figure A.1: Parts for assembling double-ended lab scale hollow fiber modules	197
Figure A.2: Parts for a blank module	197
Figure A.3: Brass male adapter with Tygon tubing piece	198
Figure C.1: Pervaporation module used for separating acetic acid-water mixtures	203
Figure D.1: A hollow fiber-based pervaporation system	206
Figure E.1: Typical RO membrane desalination system with energy recovery [2].	212
Figure E.2: Flowchart of a hollow fiber-based RO separator	213
Figure E.3: Osmotic pressure vs. HAc concentration on the upstream and downstream sides of the membrane	215
Figure F.4: Hypothetical RO cross-flow separator	217
Figure F.5: Variations of osmotic pressure and HAc concentration on the upstream side vs. distance down the length of hollow fibers	218
Figure F.6: Overall membrane selectivity and energy cost vs. applied pressure	218

Summary

Commercial pure terephthalic acid (PTA) manufacturing generates process streams mainly containing acetic acid (HAc) and water. A large financial incentive exists to replace the costly and energy intensive distillation column used to recycle HAc-water mixtures. This work focuses on the development of pervaporation technology to separate HAc-water mixtures using a hollow fiber-based membrane unit.

Membrane processes can separate azeotropic or close-boiling temperature components if a proper membrane material is selected. Hollow fiber membranes are “self-supporting” and enable high productivity as a result of high surface area per unit volume. Currently a 250 μm outer diameter Matrimid[®] hollow fiber is used in industry for gas separations. Due to the difference between gas and liquid separations, the fiber performance associated with high flux in pervaporation is limited by a pressure change inside the bore along the axial direction of the fiber. A mathematical model was developed to describe the bore pressure change in pervaporation in this work, which demonstrated that spinning a large bore size fiber was a good solution to minimize the bore pressure change.

Spinning technology has been adapted to obtain a *large bore size defect-free* Matrimid[®] hollow fiber. In addition to a large bore size, the asymmetric fiber exhibits an intrinsically defect-free selective layer supported on an open porous substrate. This eliminates the post-treatment with a “caulking layer” that is a costly and time-consuming process in industry, and has a special advantage for aggressive liquid separations.

A proof of concept was provided by testing both small and large bore size defect-free fibers with a model 20% wt HAc feed in a pervaporation system at 101.5°C. The membrane selectivity (~ 25) and water flux ($\sim 4.5 \text{ kg/m}^2\text{hr}$) were increased by about 150% with a diameter (O.D. $\sim 500 \mu\text{m}$) twice as large as the regular fiber. Further, a decrease in the HAc flux was observed with the increased bore size due to the reduction

in HAc-induced plasticization. This “*win-win*” situation leads to a significant increase of membrane selectivity in pervaporation of acetic-acid and water mixtures.

Sub- T_g thermal annealing was used to stabilize the fiber by suppressing HAc-induced plasticization. Micro-fluorescence spectra provide concrete proof that thermal annealing can intensify charge transfer complexes and reduce the free volume. This improves the polymer discrimination of shape and size for penetrants although no chemical reaction occurs with thermal annealing. The resulting membrane selectivity was increased from 10 to about 95 using a *large bore size defect-free annealed* fiber with acceptable flux ($\sim 1.5 \text{ kg/m}^2\text{hr}$) for 20% wt HAc concentration feed streams.

These improvements make Matrimid[®] hollow fiber membranes very attractive for future scale-up and commercial development.

Chapter 1: Introduction

1.1 Industrial Motivation

Purified terephthalic acid (PTA), an intermediate product in the polyester industry, has been commercially available since 1965 [1]. The key technology in producing PTA involves a separate step to attain the high product purity required for polyester manufacture. Several processes have been developed to produce purified terephthalic acid and they all use acetic acid (HAc) as a solvent to remove the main byproduct -- water.

To produce PTA in industry, acetic acid, air, p-xylene, and catalyst are fed continuously into an oxidation reactor that is maintained at 175-225°C and 1500-3000 kPa, as shown in Figure 1.1. Once the oxidation reaction described below is completed, two moles of water are formed per mole of p-xylene reacted.

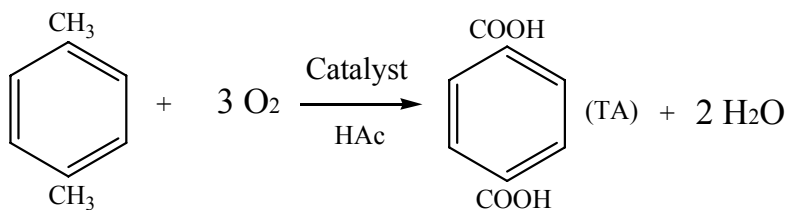


Figure 1.1 shows a typical flow chart of this oxidation process. The oxidation is generally exothermic to the extent of 2×10^8 J/kg of p-xylene reacted, and the produced heat allows the solvent and water mixture to boil in the reactor. The vapor composed mostly of HAc and water goes to the top of the reactor. One portion is condensed and refluxed to the reactor, and the other portion is delivered to a dehydration tower to further remove water and to concentrate the HAc in the solution.

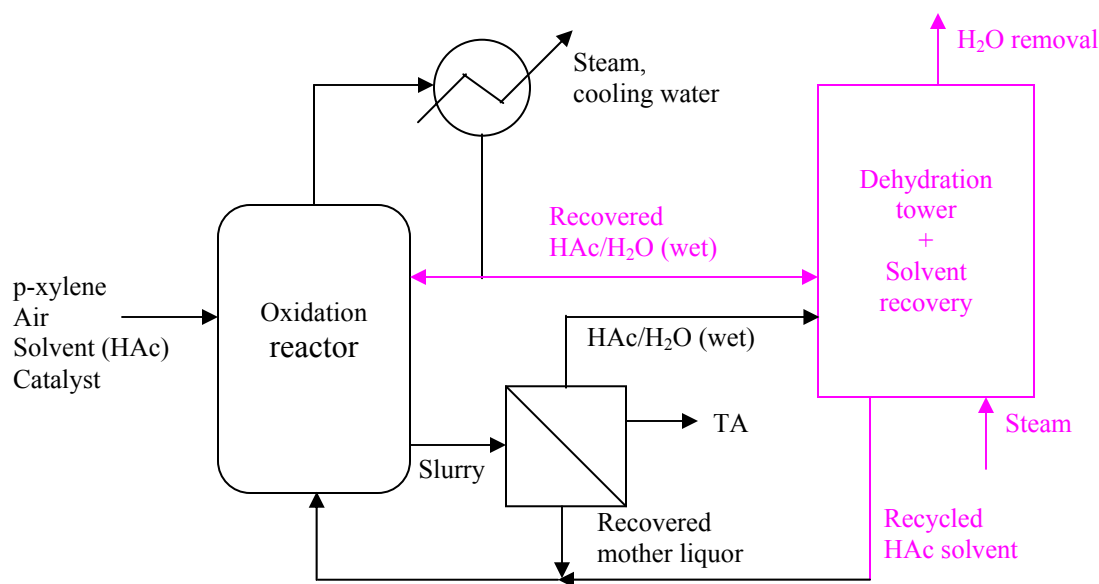


Figure 1.1: Flow chart for manufacturing terephthalic acid (TA)

A conventional dehydration process for solvent (HAc) recovery is completed by a distillation column with 45-60 theoretical stages. This separation is energy intensive because the relative volatility between water and HAc is close to unity. The normal boiling temperatures, T_b , and the molar enthalpies of vaporization, $\Delta_{\text{vap}}H$, at T_b are given in Table 1.1.

Table 1.1 Boiling points and vaporization enthalpies for H_2O and HAc

Compounds	T_b ($^{\circ}\text{C}$)	$\Delta_{\text{vap}}H$ (T_b) (kJ/mol)
H_2O	100	40.65
HAc	117.9	23.70

Figure 1.2 shows the vapor-liquid equilibrium graph for the HAc/H₂O system. In the region of the low HAc (high water) concentration, it becomes even more difficult for distillation as the compositions of HAc in liquid and vapor phase approach each other.

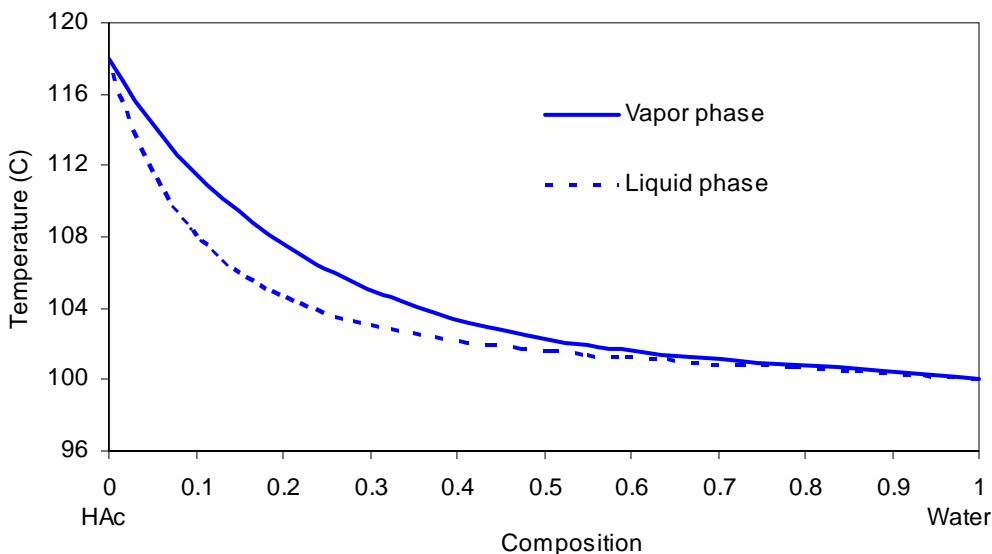


Figure 1.2: Vapor-liquid equilibrium graph for HAc/H₂O system [2]

Membrane-based pervaporation or vapor permeation is a promising alternative to distillation since it is an energy-saving one-step separation process. If the proper membrane material is selected, pervaporation can separate azeotropic mixtures and close-boiling mixtures that traditional distillation has difficulties in processing [3].

A so-called “hybrid system” is preferable for the dehydration of acetic acid-water mixtures, depending upon the contribution of distillation and pervaporation to the HAc/H₂O concentration range within which each is most efficient. The hybrid system combines pervaporation with distillation, adsorption, or any other complementary technique to obtain the most benefits from each process [2]. Figure 1.3 schematically illustrates such a hybrid system in the dehydration tower of PTA plants.

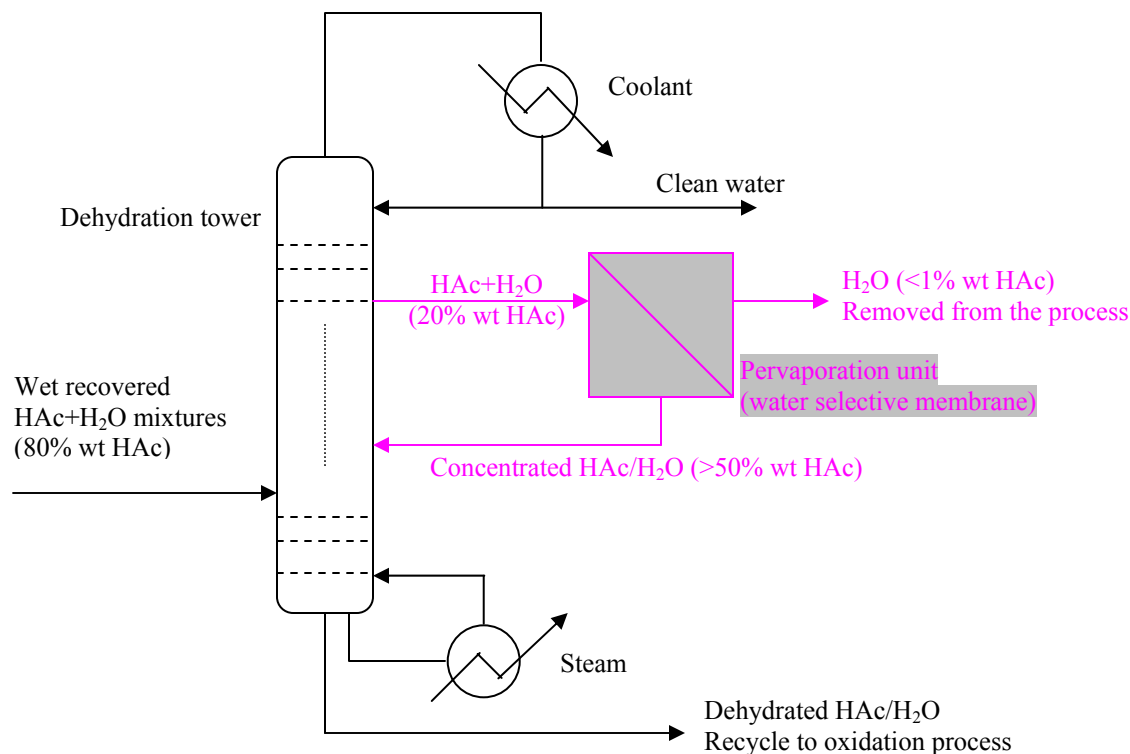


Figure 1.3: Hypothetical hybrid process for separating HAc/H₂O mixtures in the dehydration tower

Since it is difficult to achieve high efficiency at the low HAc concentration stream in distillation, as discussed above, a highly water-selective membrane unit can be used on a vapor-side draw taken from the water-rich portion of the tower. The water can be permeated with minimal acetic acid loss because of the membrane's high selectivity, and then the water can be removed from the system. This removal of water significantly reduces the energy consumption in the reboiler required to operate the tower. The high selectivity of the membrane also allows the volume of the retentate stream to be minimized.

For a typical large-scale PTA plant of 500KMT (Kilo Metric Tons) per annum capacity, acetic acid-water mixtures of around 1000 KMT are produced and must be dehydrated. As compared to capital cost of US\$2 million for membrane units, a minimum operating cost of US\$0.5 million can be saved per year if a highly selective membrane unit is successfully incorporated into the current distillation column [2]. This offers a significant payback.

1.2 Membrane-Based Pervaporation Separation

The origins of pervaporation date back to the 19th century, but the process was first studied in a systematic fashion at the laboratory level by Binning, Lee and co-workers [4] at American Oil in the early 1950s. Because of the limitations of membrane fabrication at that time, the pervaporation process was not commercialized until 1980. With the advanced development of membrane technology in the last 20 years, some applications have been successfully industrialized using pervaporation separation. One is the separation of water from concentrated alcohol solutions. GFT in Germany is the leader in this field and installed their first major plant in 1982 [5]. The other application of pervaporation is the separation of small amounts of organic solvents from contaminated water, for which the technology has been developed by MTR in USA [6]. In addition, a pervaporation unit can be integrated into a bioreactor to improve bioconversion rate and reduce downstream processing costs, if membranes can selectively remove volatile inhibitory substances from fermentation broths [7]. Compared to the relatively easy separation of non-aggressive chemicals from water in industry, very few commercial systems have been developed to separate aggressive organics-water systems such as the HAc-water system [8-11].

The most significant opportunity to use pervaporation is in splitting an azeotrope or a close boiling-temperature mixture, where distillation is less efficient due to the huge amount of energy consumption. Although a binary mixture with acetic acid and water does not have an azeotrope, removing pure water by distillation is still difficult due to their close-boiling temperatures. Thus, pervaporation may be a useful method to separate such a mixture.

Theoretically, if a liquid feed contacts a nonporous membrane with vacuum downstream, the vaporization rate of each component in the liquid is limited by the membrane permeability. In other words, the concentration distribution of each component in the liquid and vapor is not only controlled by the thermodynamic equilibrium [12], but also is governed by the membrane permeability. In this case, the membrane is sometimes referred to as a “mass separating agent”. Nevertheless, the membrane-mediated evaporation is generally regarded as pervaporation. In order to maximize the driving force, i.e. an activity difference between a feed liquid and permeate vapor, heating the feed liquid at the boiling temperature on one side of the membrane and pulling a vacuum or cooling the permeate vapor to condense on the other side are generally applied in the pervaporation process [3]. These approaches are more complex than the purely gas and vapor feed cases without evaporation and condensation. Two types of widely used pervaporation separation schemes are shown in Figure 1.4.

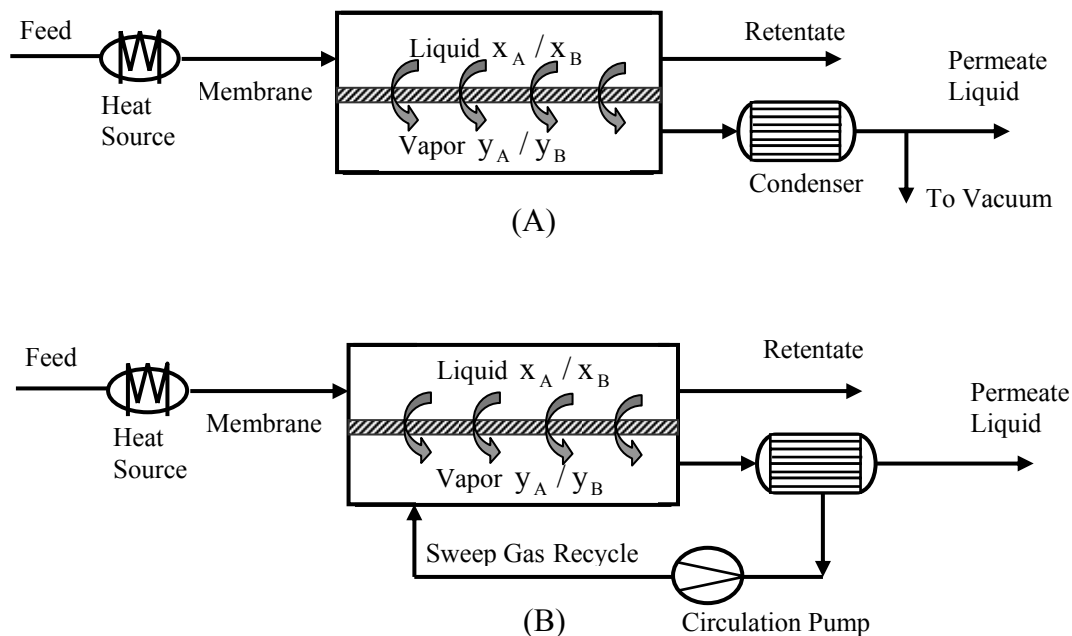


Figure 1.4: Schematic diagram of membrane-based pervaporation separation processes
(a) vacuum operation (b) permeate-side sweep stream operation

1.3 Research Objectives and Strategies

The overarching goal of this research is to produce a high performance hollow fiber membrane for separating aggressive organic/organic and organic/water mixtures by pervaporation. Using HAc/H₂O mixtures as a model system, the practical goal is to investigate the feasibility of adapting gas separation hollow fiber membranes to a pervaporation process and to identify the different requirements of gas and liquid separations.

The following strategies have been pursued to develop a high performance Matrimid[®] hollow fiber membrane to separate acetic acid and water mixtures.

The first step of this research is to spin a large bore size defect-free hollow fiber membrane. Theoretically, the pressure change in the bore side of a hollow fiber plays an important role in determining fluxes of penetrant molecules with shell feed. Water

permeation is influenced by pressure change much more than acetic acid due to its high flux through the membrane in the HAc/H₂O system. In principle, the pressure buildup on the downstream side of the membrane created by water-enriched product can reduce the driving force for water and decrease the water flux disproportionately to that for HAc. This will undoubtedly underestimate the membrane selectivity and deteriorate the fiber performance. Spinning a large bore size defect-free hollow fiber is a good solution to minimize the bore pressure change. Matrimid[®] fibers, created with the “dry jet, wet quench” spinning method, have been used by others to produce a typical diameter (O.D. ~ 250μm) defect-free hollow fiber membrane; these fibers exhibit good gas separation properties [13-14]. In this work, this spinning technology has been successfully improved to obtain a large bore size defect-free hollow fiber membrane using Matrimid[®].

The second step in process development is to separate a model 20% wt HAc concentration solution by pervaporation using both a small and large bore size hollow fiber with a defect-free outer skin layer supported on an open porous substrate. This second step enables us to test models of pervaporation performance. The relationship between membrane morphology and pervaporation performance is studied in depth. Specifically, a mathematical model is developed to consider the bore pressure change of a hollow fiber to evaluate inherent membrane selectivity.

Clearly, a HAc/H₂O feed is more aggressive than typical gas separation feeds, and the swelling tendency of the HAc/H₂O feed needs to be dealt with. It is known that thermal annealing causes stabilization of Matrimid[®] for gas separation [15-16]. The third step, therefore, is to stabilize a hollow fiber using thermal annealing. The interaction between penetrants and Matrimid[®] polymer is studied by sorption tests. As expected, it

has been observed that HAc has strong swelling effects on the fiber, while the water swelling effects are negligible. In order to maximize the membrane selectivity of HAc/H₂O mixtures, heat treatment has proven very helpful to suppress the plasticization effects of HAc and enhance the membrane selectivity significantly. Figure 1.5 shows the schematic procedures followed in this work.

In summary, this thesis focuses on the separation of a model acetic acid and water mixture by pervaporation using a Matrimid[®] large bore size defect-free hollow fiber membrane. Theory and fundamentals are applied to guide and explain the experimental results, although more emphasis is placed on the practicality of implementation. The ultimate process development used in this work can, in principle, be applied broadly to other organic/water, or even to organic/organic separators.

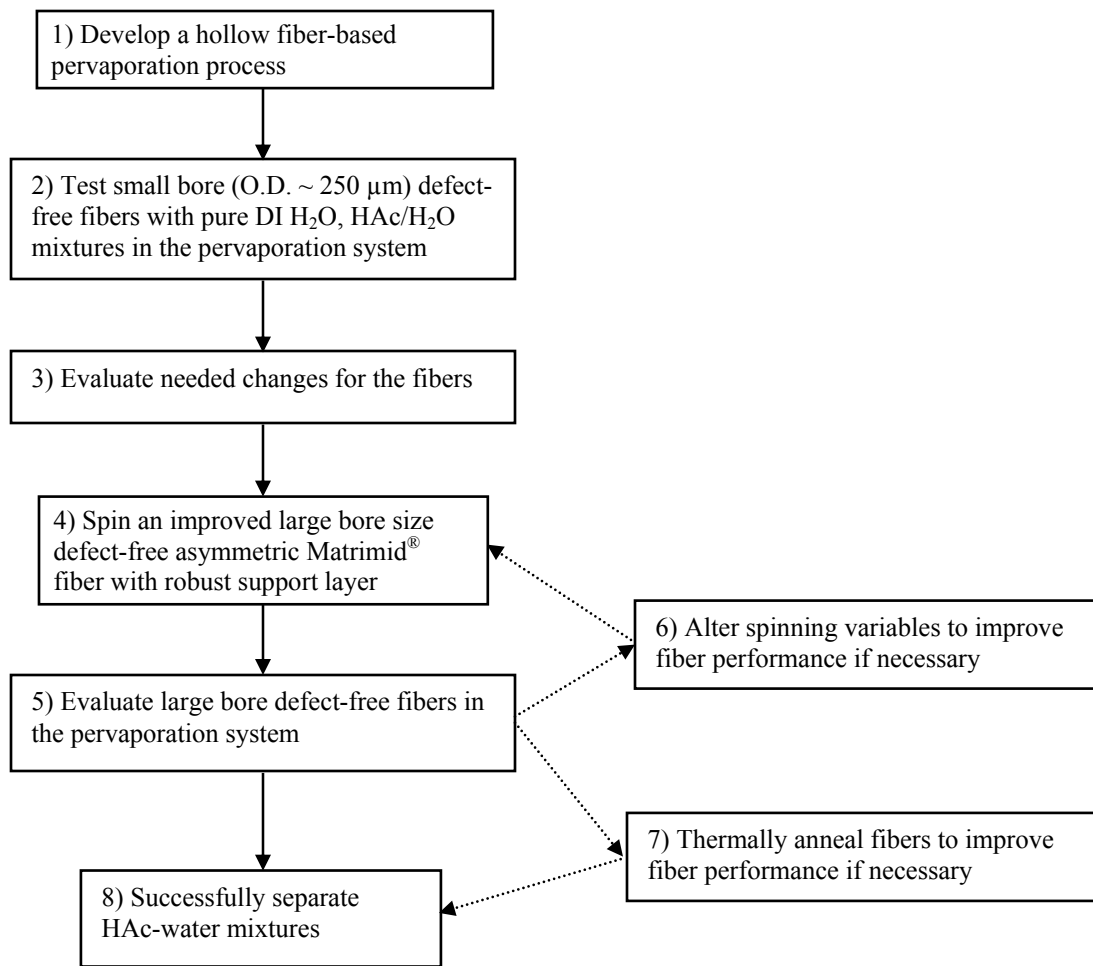


Figure 1.5: Schematic flowchart of our research procedures

1.4 Organization of Dissertation

This thesis comprises eight chapters and five appendices.

Chapter 1 provides introductory information, including industry motivation to modify the current distillation column for separating acetic acid and water mixtures, principles of membrane-based pervaporation separation, economic motivation for the hybrid process of distillation and pervaporation, research objectives and strategies, as well as overall organization of this dissertation.

Chapter 2 presents background and theory for this work. This includes membrane material selection, gas transport fundamentals in glassy polymers, specific properties of asymmetric hollow fibers, transport mechanism of pervaporation processes, and stabilization of hollow fibers.

Chapter 3 focuses on a step-by-step approach to spin a large bore size defect-free hollow fiber membrane using Matrimid[®]. In each step of the “dry jet, wet quench” spinning process, the theoretical analysis and explanation are provided. Challenges to control the bore size and defect-free outer skin layer are addressed. Current spinning technology is improved by refining and optimizing the key operation variables. In addition, the characterization of a defect-free outer skin layer of a hollow fiber is included.

Chapter 4 discusses the separation results of HAc/H₂O mixtures by a pervaporation process with model HAc concentration feeds. The pervaporation experimental setup is illustrated. The water flux and membrane selectivity for both small and large bore size fibers are compared.

Chapter 5 proposes a hypothetical model to describe the pressure change in the bore side of a hollow fiber. The proposed model is developed based on the modified Hagen-Poiseuille equation and mass balance in each divided finite element of a hollow fiber. The bore pressure change is taken into consideration to obtain the inherent membrane selectivity.

Chapter 6 evaluates thermally annealed fiber performance by pervaporation of HAc/H₂O mixtures. The heating variables are investigated and optimized. Micro-fluorescence spectroscopy is used to identify the formation of charge transfer complexes

and characterize the packing density of polymer chains. In addition to a model 20% wt HAc concentration feed, higher HAc concentration feeds are explored and discussed using annealed fibers. In the last section, a mathematical model is developed to evaluate the overall membrane selectivity of annealed fibers in an industrial cross-flow separator.

Chapter 7 provides sorption data of hollow fibers with and without heat treatment. With different HAc concentration solutions, length extension measurements are applied to estimate the solvent-induced swelling conditions of hollow fibers.

Chapter 8 presents the conclusions and ties together the various aspects of this work. Several suggestions and recommendations are discussed for future study.

The appendices contain some additional information, including the fabrication of gas permeation and pervaporation modules, standard operation procedures of pure gas permeation and pervaporation experiments. Further, reverse osmotic technology is explored to determine whether it may be substituted for pervaporation or vapor separation.

1.5 References

- [1] Kirk, R.E. and Othmer, D.F. *Encyclopedia of chemical technology*. John Wiley & Sons, Inc. 4th Ed. New York. 2000, 18, 1006-1012.
- [2] Personal Communication with Dr. Steve Pietsch from BP, 2004-2005.
- [3] Huang, R.Y.M. *Pervaporation membrane separation processes*. Elsevier Science Publishing Company, Inc. New York. 1991, 1-46.
- [4] Binning R.C., R.J. Lee, Jennings J.F. and Martin E.C. *Separation of Liquid Mixtures by Permeation*. Ind. Eng. Chem. 1961, 53, 45-50.
- [5] Ballweg A.H., Brtischke H.E.A., Schneider W.H. and Tiisel G.F. *Pervaporation Membranes*. Proceedings of the Fifth International Alcohol Fuels Symposium. John McIndoe, Dunedin, New Zealand. 1982.

- [6] Blume I., Wijmans J.G. and Baker R.W. *The separation of dissolved organics from water by pervaporation*. J. Membr. Sci. 1990, 49(3), 253-286.
- [7] Gudernatsch, W., Kimmerle, K., Stroh, N., and Chmiel, H. *Recovery and concentration of high vapor pressure bioproducts by means of controlled membrane separation*. J. Membr. Sci. 1998, 36, 331-342.
- [8] Deng, S., Sourirajan, S., Matsuura, T. *Study of polydimethylsiloxane/aromatic polyamide laminated membranes for separation of acetic acid/water mixtures by pervaporation process*. Sep. Sci. Technol. 1994, 29, 1209-1216.
- [9] Sano, T., Ejiri, S., Yamada, K., Kawakami, Y., and Yanagishita, H. *Separation of acetic acid-water mixtures by pervaporation through silicalite membrane*. J. Membr. Sci. 1997, 123, 225-233.
- [10] Huang, S.C., Ball, I.J., and Kaner, R.B. *Polyaniline membranes for pervaporation of carboxylic acids and water*. Macromolecules. 1998, 31, 5456-5464.
- [11] Yoshikawa, M., Kuno, S.T., and Kitao, T. *Specialty polymeric membranes 3. Pervaporation separation of acetic acid/water mixtures through polymeric membranes having a pyridine moiety as a side group*. J. Appl. Polym. Sci. 1994, 51, 1021-1027.
- [12] Lee, E.K. and Koros, W.J. *Membrane, Synthetic, Applications*. Encyclopedia of Physical Science and Technology. 3rd Ed. Academic Press. 2001, 279-344.
- [13] Clausi, D. T. *Formation and characterization of asymmetric polyimide hollow fiber membranes for gas separations* Ph.D. Dissertation, The University of Texas at Austin, 1998.
- [14] McKelvey, S.A. *Formation and characterization of hollow fiber membranes for gas separation*. Ph.D. Dissertation, The University of Texas at Austin, 1997.
- [15] Kawakami, H., Mikawa, M., and Nagaoka, S. *Gas transport properties in thermally cured aromatic polyimide membranes*. J. Membr. Sci. 1996, 118, 223-230.
- [16] Krol, J.J., Boerrigter, M., and Koops, G.H. *Polyimide hollow fiber gas separation membranes: preparation and the suppression of plasticization in propane/propylene environments*. J. Membr. Sci. 2001, 184, 275-286.

Chapter 2: Background and Theory

2.1 Membrane Material Selection

Membranes are molecular level selective barriers. By allowing the passage of one component preferentially over another, a wide variety of materials such as polymers, carbon molecular sieves, and zeolites can be used to form membranes [1]. Quite a few organic/inorganic membranes have been formed and reported for purpose of separating acid and water mixtures. Some of these membranes have been highly water-selective and thus effective at dehydrating acid and water mixtures [2-5]. Examples of these membranes include cross-linked polybutadiene membranes, polydimethylsiloxane/aromatic polyamide laminated membranes, acrylonitrile grafted poly(vinyl alcohol) membranes, and thin mordenite and ZSM-5 zeolite membranes. Several other publications are focused on the acid- preferential membrane materials [6-8]. For example, Qin et al. developed a liquid membrane consisting of reactive extractants, to separate dilute aqueous HAc solution. Wang et al. prepared a composite membrane of polyacrylic acid (PAA) dip-coated on an asymmetric poly(4-methyl-1-pentene) (TPX) membrane. Recently a “mixed matrix” membrane has been considered [9] since this membrane incorporates zeolite or carbon molecular sieve into a polymer. This mixed matrix membrane takes advantage of the processing ability of polymers and also the high selectivity of molecular sieves [10]. However, mixed matrix membranes are still in the early stages of development and have not yet been applied to HAc/H₂O separation. Only polymeric membranes are considered in this work because they are currently the dominant membranes that offer a wide spectrum of properties with considerable cost

advantages in industry.

Since gas separation systems are the most studied cases, the fundamentals of material structure-property relations are understood best for this class of applications. Nevertheless, pervaporation, vapor permeation, gas separation, and even reverse osmosis all rely upon similar molecular principles; thus, the insights from gas separation can apply to these other systems. To achieve high gas selectivity and permeability for a potential polymer candidate, two key factors must be considered. First, the polymer has to have a stiff molecular backbone, and second, the chain packing has to be sufficiently open but well defined enough to produce a narrow free volume distribution. This enables local “transient gaps” between chain segments that allow size selective diffusion selectivity. Aromatic polyimides have been discovered having excellent mass transfer characteristics and unique physicochemical properties such as high thermal and chemical stability and superior mechanical properties. These advantages make polyimides extraordinary materials for separation and purification technologies [11]. Today polyimides membranes are widely used in the gas separation industry including hydrogen recovery [12-16], helium purification [17], natural gas sweetening [13, 16], and so on. As opposed to the applications of polyimide membranes in gas separation, very few reports concentrate on pervaporation for separating acid and water mixtures using polyimide membranes. Huang et al. [18-19] investigated the sorption and transport behavior of pure water vapor in dense and asymmetric polyimide membranes (PMDA-50DDS/50ODA and BPDA-50DDS/50ODA).

Matrimid[®], a commercially available polyimide with excellent thermal and mechanical properties, has been studied for gas separation and exhibits good permeability and selectivity in a hollow fiber form [20-21]. However, to our knowledge this material has not been studied for pervaporation of the HAc/H₂O system. Matrimid[®] is selected as a model material in pervaporation of acetic acid and water mixtures in this research. The chemical structure of Matrimid[®] is shown in Figure 2.1 [22].

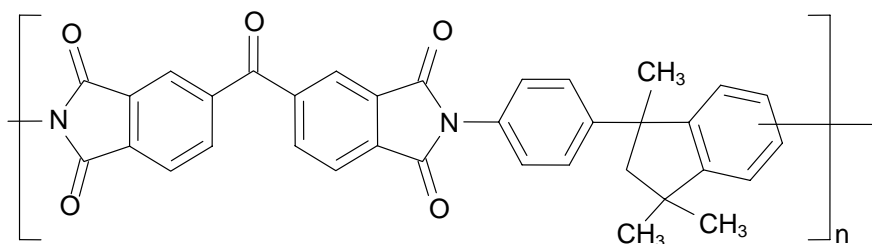


Figure 2.1: Repeat unit for Matrimid[®] polymer

2.2 Gas Transport in Amorphous Glassy Polymers

Since a membrane is defined basically as a barrier that separates two phases and restricts transport of various components in a selective manner, the driving force for permeation is a chemical potential difference related to the concentration or pressure difference imposed between the feed and permeate sides of the membrane [23-25]. Matrimid[®] used in this work has a high glass transition temperature (305°C ~ 315°C) [26] and is a typical amorphous glassy polymer over a broad temperature range.

An amorphous polymer exists in either rubbery or glassy state; the state changes based upon the operating temperature. As shown in Figure 2.2 [27], a discontinuity is observed in the slope of the specific volume versus temperature curve at the so-called “glass transition temperature”, T_g . As a rubbery polymer changes to a glassy state, the

sudden decrease in segmental mobility with the decreased temperature “traps” the polymer chains into non-equilibrium configurations, resulting in excess un-relaxed free volume [28]. In the glassy region, the non-equilibrium configuration can be relaxed towards its equilibrium state with time. This limiting case can be reached by extrapolating the V vs. T in the rubbery region below T_g and is shown as a dashed line in Figure 2.2. The excess free volume of $V_g - V_l$ at any temperature promotes excess sorption above that in the rubbery state, and thus is an important factor to determine the gas permeation in the glassy polymer. Meanwhile, the diffusion of penetrants can also be influenced by the rigidity of the polymer chains. Creating adequately large local transient gaps to enable diffusion of penetrant molecules requires energy, thereby greatly favoring diffusion of the smaller penetrant vs the larger one.

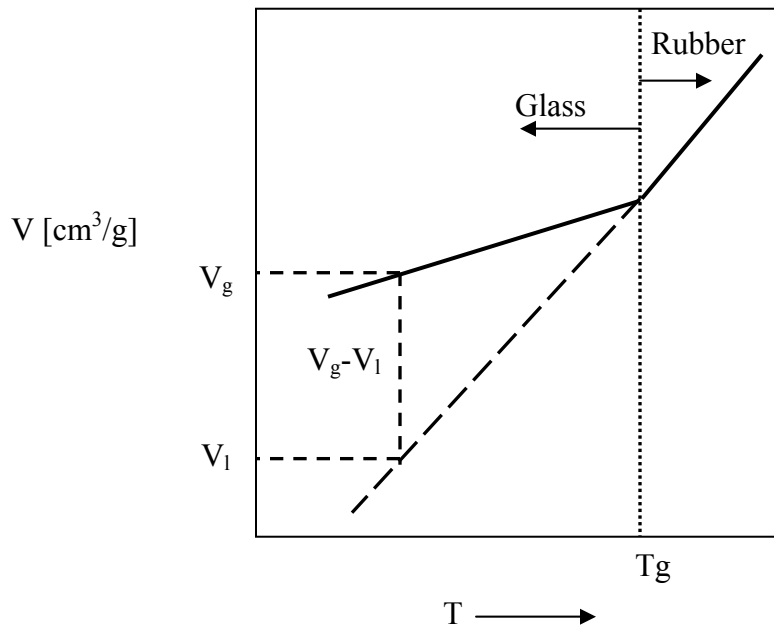


Figure 2.2: Schematic of specific volume vs. temperature relationship for an amorphous polymer [27]

For a homogeneous nonporous dense film membrane used in *gas* or *vapor* separation, the “solution-diffusion” model [13, 29] is commonly used to explain the gas transport mechanism. Gas molecules sorb on the upstream side of the membrane, diffuse through the membrane, and finally desorb on the downstream side, as illustrated in Figure 2.3. The permeability, \mathcal{P}_i , for a given component i can be written as:

$$\mathcal{P}_i = D_i \cdot S_i \quad (2.1)$$

where D_i and S_i represent diffusion and solubility coefficients of component i , respectively. The effects of solubility and diffusivity (mobility) on permeability results are discussed below.

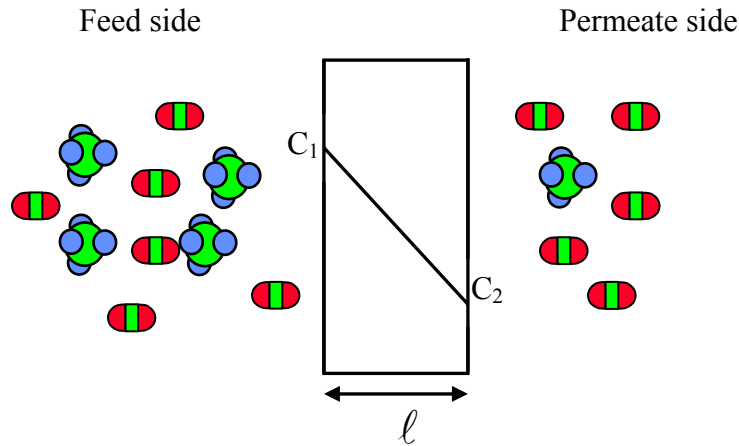


Figure 2.3: Schematic chart showing gas separation through amorphous dense polymeric films

- **Solubility Coefficient**

The solubility coefficient characterizes the interaction between a penetrant and polymer, determining the amount of the penetrant that can be accommodated in the polymer at a given activity or partial pressure at equilibrium. The dual mode model is the simplest and most widely used model to describe the solubility of gases in glassy

polymers, which have complex “dual environments” due to their non-equilibrium natures (see Figure 2.2) [30]. The dual mode model postulates the presence of two types of sorption environments reflective of the “well-packed equilibrium nature” and local “packing disruptions” that cause an out-of-equilibrium aspect in the glass. In the first mode, gas molecules follow the Henry’s law and dissolve in the densified regions of the polymer. The second mode, termed as “Langmuir sorption”, is associated with the excess un-relaxed free volume that formed from the inter-segmental defects due to the non-equilibrium properties in the glassy polymer. Generally speaking, the gas molecules sorbed in the Langmuir sites are less diffusively mobile than those in the Henry’s law sorption sites due to their lower sorption enthalpies [30-32]. The equilibrium part of this theory can be expressed for the isotherm by the following equation:

$$C = C_D + C_H = k_D p + \frac{C'_H b p}{1 + b p} \quad (2.2)$$

where C is the penetrant concentration in the polymer (solubility), C_D is the penetrant concentration in the Henry’s law sites, C_H is the penetrant concentration in the Langmuir sites, k_D is the Henry’s law constant, C'_H is the Langmuir capacity, b is the Langmuir affinity constant, and p is the applied pressure (or partial pressure for a mixture) in equilibrium with the membrane. At low pressure, the Langmuir sites are occupied preferentially with the penetrant molecules because sorption in these sites has the most negative sorption enthalpy, which is characteristic of “hole filling” uptakes in materials like zeolites [13]. As pressure increases, the Henry’s law sorption dominates, due to the saturation of the Langmuir sites.

Figure 2.4 shows a typical sorption isotherm for glassy polymers. The effective sorption coefficient S_i for component i , can be experimentally determined by the ratio of C_i/p_i . As shown in Figure 2.5, in the low and intermediate pressure region, the solubility coefficient decreases until the excess free volumes (Langmuir sites) are saturated. Thereafter, the solubility coefficient remains constant with increased pressure unless strong penetrant-induced swelling occurs. In other words, although the Langmuir sites have been fully occupied in very high pressure, the penetrants can keep dissolving in the densified polymer region because of the swelling effects. This eventually causes the further increment of solubility coefficient in the high partial pressure region [1]. As a consequence, the swelled and dilated polymer chains lose their former shape and size discrimination of penetrants and thus decrease the membrane selectivity.

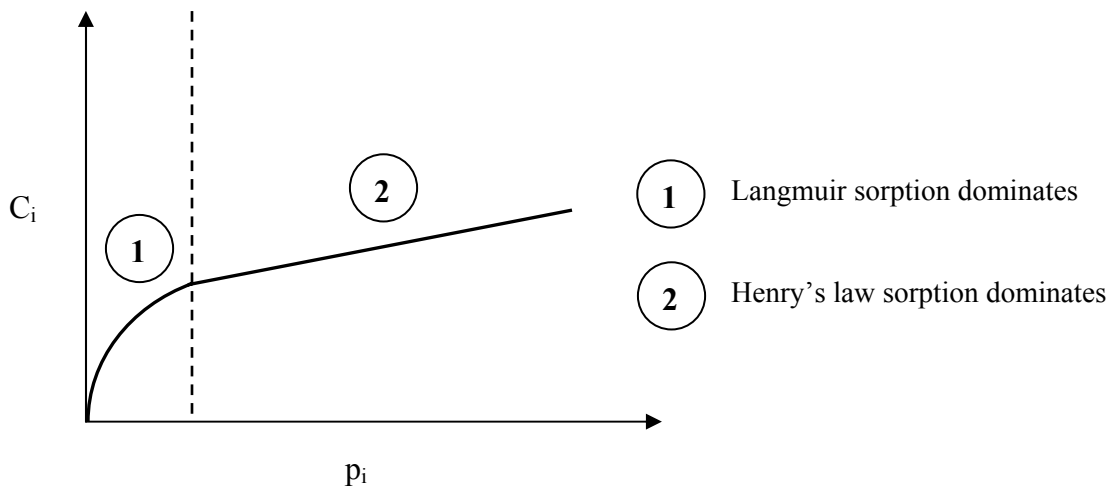


Figure 2.4: Typical sorption isotherm for amorphous glassy polymeric materials

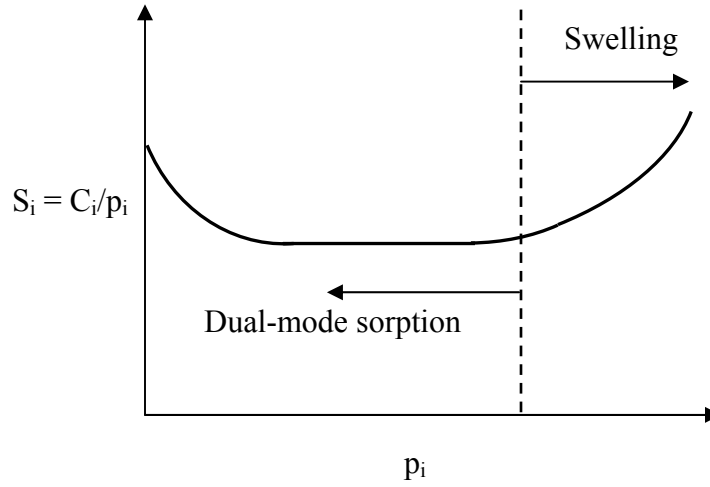


Figure 2.5: Solubility vs. pressure for amorphous glassy polymeric materials

- **Diffusion**

Diffusion of gas molecules in the glassy polymer is achieved by activated jumps through the molecular-scale “gaps” created by random polymer chain segmental motion. In terms of transition state theory [33-34], the penetrant jump rate constant, k_{jump} , and jump length, λ , can be obtained by stochastic simulations. The diffusion coefficient D can then be calculated by the following equation [35]:

$$D = \frac{1}{6} k_{\text{jump}} \lambda^2 \quad (2.3)$$

The diffusion coefficient obeys the Arrhenius rule as follows:

$$D = D_0 \exp(-E_d/RT) \quad (2.4)$$

where D_0 is a temperature independent pre-exponential constant, E_d is the activation energy, R is the universal gas constant, and T is temperature. The larger gas molecule needs higher activation energy to open a transient gap between the polymer chains to enable jumps and thus exhibits much lower diffusion coefficient. The cartoon pictures

shown in Figure 2.6 illustrate the difference of diffusivity between large and small penetrants in the glassy polymer.

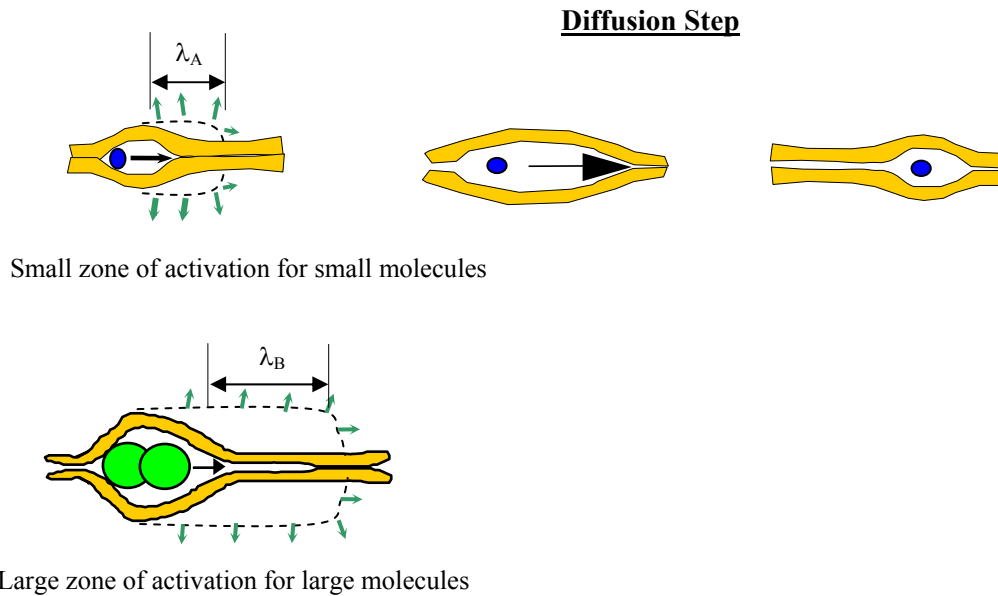


Figure 2.6: Cartoon pictures showing an idealized diffusion step and the difference in diffusion between large and small molecules in a glassy polymer

Collision diameters, as a useful measure for the physical size of a gas molecule, are given for a number of pure substances in Table 2.1 [36].

Table 2.1: Collision diameters of selected substances

* calculated by the equation of $\sigma = 8.33V_c^{\frac{1}{3}}$ [36], $V_c = 0.171\text{m}^3/\text{kgmol}$ [37]

Molecule	Collision diameter ($\sigma \times 10^{10} \text{ m}$)
N ₂	3.80
O ₂	3.47
He	2.55
H ₂	2.83
H ₂ O	2.64
HAc	4.62*

The intrinsic permeability of a homogeneous dense film for a given component i , \mathcal{P}_i , physically can be defined as a pressure and thickness normalized flux, viz.,

$$\mathcal{P}_i = \frac{Q_i}{\Delta p_i / \ell} \quad (2.5)$$

where ℓ is the thickness of a dense film, Q_i is the flux of component i , and Δp_i is the partial pressure difference of component i between the upstream and downstream membrane face. The units for permeability are Barrers where

$$1 \text{ Barrer } [=] 10^{-10} \frac{\text{cc(STP)} \cdot \text{cm}}{\text{cm}^2 \cdot \text{sec} \cdot \text{cmHg}} \quad (2.6)$$

The intrinsic selectivity for components A and B, $\alpha_{A/B}$, defined in terms of the ratio of downstream to upstream component mole or mass fraction, can be expressed as the ratio of the corresponding permeabilities when downstream pressure is negligible, viz.,

$$\alpha_{A/B} = \frac{y_A / y_B}{x_A / x_B} \approx \frac{\mathcal{P}_A}{\mathcal{P}_B} \quad (2.7)$$

where y_A and y_B represent the mole or mass fractions on the permeate side of the membrane for components A and B, and x_A and x_B represent the mole or mass fractions on the feed side of the membrane for components A and B.

2.3 Asymmetric Defect-Free Hollow Fiber Membranes

In asymmetric membranes, the porosity changes from one surface of the membrane to the other, with the highest density part being the functional separation layer. This layer has a density essentially equal to that of a normally dense glassy polymer. A defect-free hollow fiber membrane is a specific type of asymmetric membrane. Its

structure is composed of three distinct regions, a thin skin (selective) layer, a transition layer, and a porous substructure. Ideally, the skin layer carries out the separation function, while the transition and porous substructure provide mechanical support with negligible transport resistance.

Asymmetric hollow fibers offer several important advantages over dense films for industrial application. First, a hollow fiber has a self-supporting structure with the highest available separation area per unit volume of all membrane types, and thus is well suited for practical applications. Figure 2.7 shows a comparison of surface area per unit volume between hollow fibers and other geometric configurations. Even for a large diameter fiber (O.D. $\sim 750\ \mu\text{m}$) with a packing factor of 50%, fibers have a separation area per unit volume that is much higher than spiral-wound and plate-in-frame forms. Second, the outer defect-free skin layer is very thin (100-700 nm), while maintaining similar selectivity to a standard polymer film, thereby providing much higher productivity. Third, the open porous substrate, comprising the majority of the fiber wall, provides mechanical support for pressure drop across the membrane with negligible transport resistance. Finally, a hollow fiber is more forgiving in length and diameter when it experiences swelling effects from aggressive feeds as opposed to typical flat-plate modules. Thus, a hollow fiber membrane is selected to separate HAc/H₂O mixtures in this research.

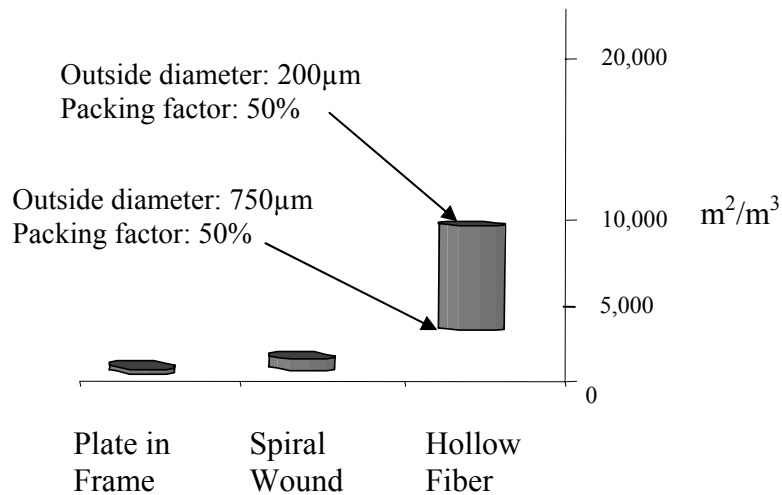


Figure 2.7: Surface area per unit volume with geometric configurations [28]

2.3.1 Formation of Defect-Free Outer Skin Layer

The most critical issue in spinning a hollow fiber is the formation of the outer defect-free skin layer. Due to the complicated spinning process, hollow fibers with integrally skinned structure are difficult to obtain. Some defects might appear in the outer separation layer, resulting in a concomitant sacrifice of selectivity. One type of these defects is “pores” in the outer selective layer, which can permit the passage of most penetrant gases across the membrane without the need to pass through the polymer [38]. The polymer nodules aggregated in the outer skin, instead of a uniformly dense layer, can be another type of defects because even a small channel between the nodules can cause a large loss in selectivity.

Due to inherent defects in the outer skin layer of hollow fibers, they are seldom used commercially unless these defects are repaired by “caulking” or “coating” techniques [39-40]. The purpose of “caulking” or “coating” is to plug defects (pores or channels) and force the gas molecule through the skin layer. This caulking is generally

termed as “post-treatment”. Henis and Tripodi [38, 40] used polydimethylsiloxane (PDMS) as a coating material, since PDMS is highly permeable to most gases with little additional resistance. Polyamides can be used as another caulking material [41-44]. By theoretically “cutting” a hollow fiber in the radial direction, it can be flattened and viewed as a flat sheet. Figure 2.8 demonstrates the coating concepts for repairing the defective outer skin layer of a hollow fiber based on a “flat sheet”.

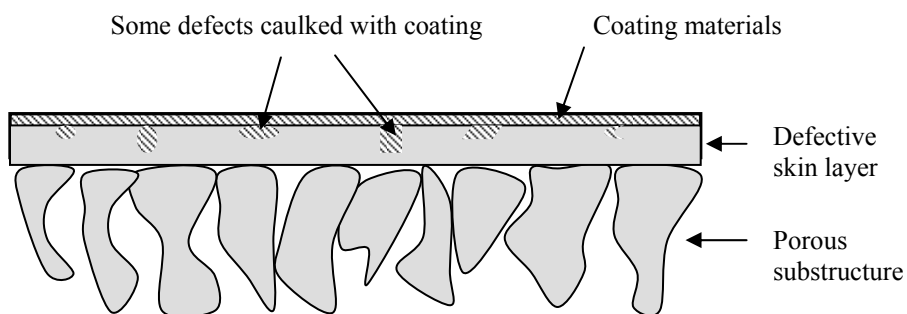


Figure 2.8: Cartoon picture showing coating technique for the defective outer skin layer of a hollow fiber

Commercial membrane products are usually composed of very thin and defective skins initially and are thereafter caulked with some fillings, as the post-treatment methods have been well developed. While adequate for gas separation, this method fails for pervaporation separation and especially for aggressive streams such as HAc/H₂O mixtures. The main problem appears to be that the aggressive streams can be detrimental to the affinity between the polymer and caulking material, and can dislodge the caulking material under an extreme condition. Therefore, formation and characterization of an integral defect-free outer skin layer are key factors in spinning a hollow fiber in this work and will be discussed in detail in Chapter 3.

2.3.2 Large Bore Size Hollow Fibers

To obtain the maximum separation area per unit volume of a fiber, a relatively small diameter hollow fiber is apparently attractive in industry. However, a very small diameter or long fiber may lead to complicated permeation behavior with shell feed. That is, whenever gas or vapor permeates through a hollow fiber, a pressure change associated with gas flux will be generated in the bore side along the axial direction of the fibers, as shown in Figure 2.9. This phenomenon is much more pronounced for highly permeable gases.

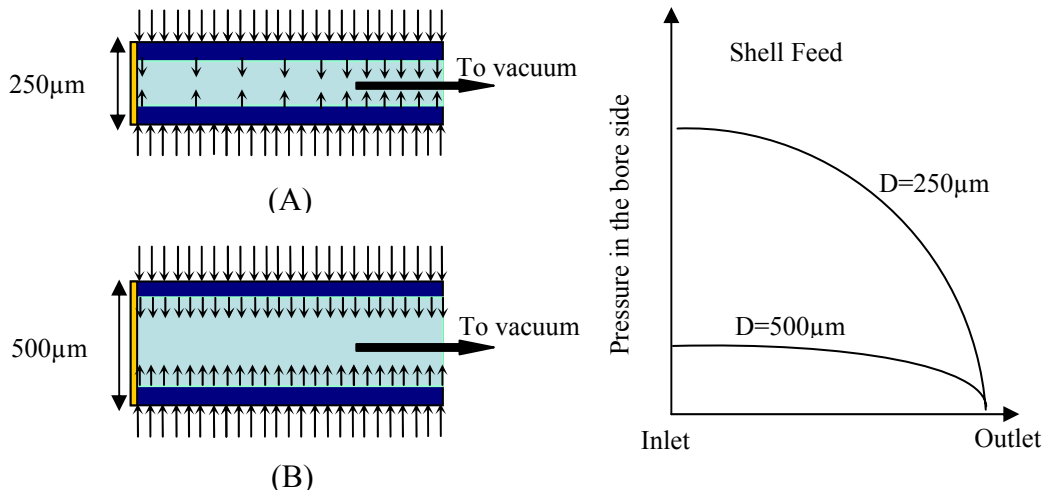


Figure 2.9: Pressure change in the bore side along the axial direction of hollow fibers with shell feed
(A) A small diameter fiber with a large pressure change
(B) A large diameter fiber with a small pressure change

The pressure change in the bore side of a hollow fiber plays an important role in transport behaviors of penetrants and can be modeled in terms of the Hagen-Poiseuille equation [45-48]. Since the bore pressure change affects the highly permeable gas much more than the less permeable one, the membrane selectivity for the high permeable/low

permeable gas pair is underestimated if the pressure buildup inside the bore is not accounted for properly. It is not surprising that both permeance and selectivity will be lower than the intrinsic polymer values without correcting for the bore pressure change effects. Spinning a large bore size fiber is considered to be a feasible solution to decrease the effects of the bore pressure change, as this can avoid the pressure buildup of total permeable gases in the bore side. Current spinning technology for a regular gas separation hollow fiber (O.D. $\sim 250\ \mu\text{m}$) has been successfully improved to spin a large diameter fiber of about $500\ \mu\text{m}$ in this work. The detailed spinning process is described in Chapter 3. Chapter 5 provides a mathematical model developed by the Hagen-Poiseuille and mass balance equations to account for the bore pressure change to obtain the inherent polymer selectivity.

2.4 Gas Transport in Asymmetric Defect-Free Hollow Fibers

Figure 2.10 shows the structure of an asymmetric hollow fiber with three distinct regions, i.e. a thin skin (selective) layer, a transition layer, and a porous substructure.

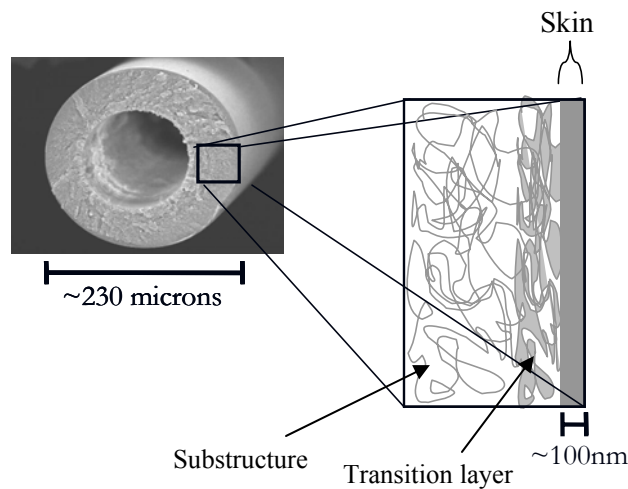


Figure 2.10: Structure of a typical asymmetric hollow fiber and its outer separation skin layer

Ideally, only the outer skin layer is capable of separating penetrants, while the transition layer and open porous substructure provide mechanical support without any selective function. As the skin thickness is difficult to measure for a hollow fiber membrane due to its complex morphology [28], permeance $(\frac{P}{\ell})_i$, is used to characterize the permeability of component i for the hollow fiber membrane. This can eliminate the need to know the actual thickness, ℓ , of the selective layer. Gas Permeation Units (GPUs) are a generally reported unit for permeance.

$$(\frac{P}{\ell})_i = \frac{Q_i}{\Delta p_i} \quad (2.8)$$

$$1 \text{ GPU} [=] 10^{-6} \frac{\text{cc(STP)}}{\text{cm}^2 \cdot \text{cmHg} \cdot \text{sec}} \quad (2.9)$$

where ℓ is the thickness of the dense skin, Q_i is the flux of component i, and Δp_i is the partial pressure difference of component i between the upstream and downstream membrane faces. Thus, the corresponding selectivity for components A and B, $\alpha_{A/B}$, can be written as the ratio of the permeance at negligible downstream pressure, viz.,

$$\alpha_{A/B} \approx \frac{(\frac{P}{\ell})_A}{(\frac{P}{\ell})_B} \quad (2.10)$$

If a hollow fiber membrane exhibits intrinsic or near-intrinsic selectivity, the thickness of the outer selective skin layer ℓ , can be estimated by taking the ratio of the intrinsic permeability of a dense film and the permeance of an asymmetric hollow fiber for component i, viz.,

$$\ell = \frac{\mathcal{P}_i}{\left(\frac{\mathcal{P}}{\ell}\right)_i} \quad (2.11)$$

The scanning electron photomicrograph (SEM) test can also be used to obtain an approximate estimate of the thickness for the outer skin layer visually.

- **Substrate Resistance**

As discussed above, ideally the defect-free skin layer of a hollow fiber provides high productivity and selectivity. However, if resistance exists in the transition layer or open porous substructure, which is generally called substrate resistance, the fluxes of the penetrants will unavoidably decrease. In addition, the “fast” permeate gas is inhibited more than the “slow” gas, resulting in a decrease in the membrane selectivity between the high and low permeable gas pair [49]. The most common measure of substrate resistance is the selectivity comparison between a dense film and hollow fiber for the oxygen/nitrogen (O_2/N_2) and helium/nitrogen (He/N_2) pairs. The gas permeation rate follows “ $\text{He} \gg \text{O}_2 > \text{N}_2$ ”. If the substrate resistance is not negligible, the selectivity of the He/N_2 pair drops down much more than that of the O_2/N_2 pair for a given hollow fiber. In other words, the higher permeability of He “overloads” the support layer’s carrying capability compared to the lower permeability of O_2 and N_2 . Figure 2.11 illustrates the essence of the substrate resistance [22].

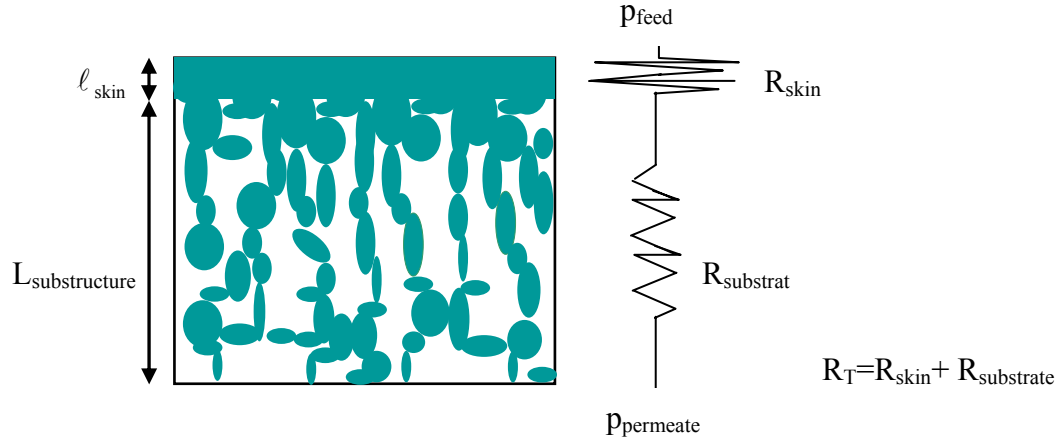


Figure 2.11: Cartoon picture showing the total resistance from both skin and substrate of hollow fibers

The selectivity of hollow fiber membranes can be expressed with negligible downstream pressure as follows:

$$\alpha_{A/B} = \frac{y_A / y_B}{x_A / x_B} = \frac{\text{Flux}_A / \text{Flux}_B}{x_A / x_B} \quad (2.12)$$

$$\underset{\text{Vacuum downstream}}{=} \frac{\left(\frac{x_A \cdot p_T - 0}{R_{T,A}} \right) / \left(\frac{x_B \cdot p_T - 0}{R_{T,B}} \right)}{x_A / x_B} = \frac{R_{T,B}}{R_{T,A}}$$

where y_A and y_B represent the mole or mass fractions on the permeate side of the membrane for components A and B, and x_A and x_B represent the mole or mass fractions on the feed side of the membrane for components A and B. The symbols of $R_{T,A}$ and $R_{T,B}$ represent the total resistance for components A and B. The symbol of p_T represents the total pressure on the upstream membrane face.

It can be seen that the membrane selectivity is inversely proportional to the ratio of the total resistance for components A and B. If the substrate resistance is negligible, the total resistance is equal to the skin resistance, i.e.,

$$\text{Flux} = \frac{\text{Driving force}}{\text{Resistance}} = \frac{\Delta p_i}{\left(\frac{\ell_{\text{skin}}}{\mathcal{P}_i}\right)} \longrightarrow R_{\text{skin},i} = \left(\frac{\ell_{\text{skin}}}{\mathcal{P}_i}\right) \quad (2.13)$$

where $R_{\text{skin},i}$ is the resistance in the outer skin layer for component i , ℓ_{skin} is the thickness of the outer skin layer for an asymmetric hollow fiber membrane, Δp_i is the partial pressure difference across the membrane for component i , and \mathcal{P}_i is the permeability of the skin layer for component i . Thus, the membrane selectivity is simplified to be the skin selectivity and equation 2.12 goes back to equation 2.10, i.e.,

$$\alpha_{A/B} = \frac{R_{T,B}}{R_{T,A}} = \frac{R_{\text{skin},B}}{R_{\text{skin},A}} = \frac{\left(\frac{\mathcal{P}_A}{\ell_{\text{skin}}}\right)}{\left(\frac{\mathcal{P}_B}{\ell_{\text{skin}}}\right)} \quad (2.10)$$

If the substrate resistance cannot be neglected, the Knudsen diffusion mechanism will dominate for penetrant diffusion in the substrate. The resistance of Knudsen diffusion for component i , $R_{\text{substrate_layer},i}$, is defined as [36],

$$R_{\text{substrate_layer},i} = \phi(\text{polymer structure}) \cdot \sqrt{\frac{\text{MW}_i}{T}} \quad (2.14)$$

where ϕ is the function of the polymer structure such as tortuosity and porosity, T is temperature, and MW_i represents the molecular weight of component i . The total resistance for component i through a hollow fiber membrane wall should be expressed as below:

$$R_{T,i} = R_{\text{skin},i} + R_{\text{substrate_layer},i} = \frac{\ell_{\text{skin}}}{\mathcal{P}_i} + \phi(\text{polymer structure}) \cdot \sqrt{\frac{\text{MW}_i}{T}} \quad (2.15)$$

For example, a gas pair of He and N₂ is used to characterize the substrate resistance quantitatively. The following conditions are given at $T=35^\circ\text{C}$,

$$\left\{ \begin{array}{l} MW_{\text{He}} = 4, \quad MW_{\text{N}_2} = 28 \\ \alpha_{\text{skin,He/N}_2} = \frac{\left(\frac{\mathcal{P}}{\ell_{\text{skin}}} \right)_{\text{He}}}{\left(\frac{\mathcal{P}}{\ell_{\text{skin}}} \right)_{\text{N}_2}} = 90 \quad \text{Solution - Diffusion} \\ \alpha_{\text{substrate_layer,He/N}_2} = \sqrt{\frac{MW_{\text{N}_2}}{MW_{\text{He}}}} = 2.7 \quad \text{Knudsen Diffusion} \end{array} \right. \quad (2.16)$$

The corresponding selectivity $\alpha_{\text{He/N}_2}$ can then be calculated, viz.,

$$\alpha_{\text{He/N}_2} = \frac{R_{\text{T,N}_2}}{R_{\text{T,He}}} = \frac{\frac{\ell_{\text{skin}}}{\mathcal{P}_{\text{N}_2}} + \frac{\phi}{\sqrt{T}} \sqrt{MW_{\text{N}_2}}}{\frac{\ell_{\text{skin}}}{\mathcal{P}_{\text{He}}} + \frac{\phi}{\sqrt{T}} \sqrt{MW_{\text{He}}}} = \frac{90 \cdot \frac{\ell_{\text{skin}}}{\mathcal{P}_{\text{He}}} + \frac{\phi}{\sqrt{T}} \sqrt{28}}{\frac{\ell_{\text{skin}}}{\mathcal{P}_{\text{He}}} + \frac{\phi}{\sqrt{T}} \sqrt{4}} \quad (2.17)$$

In terms of the balance between the skin and substrate resistance, the membrane

selectivity of $\alpha_{\text{He/N}_2}$ vs. the ratio of $\phi / \left(\frac{\ell_{\text{skin}}}{\mathcal{P}_{\text{He}}} \right)$ at $T=35^\circ\text{C}$ is shown in Figure 2.12.

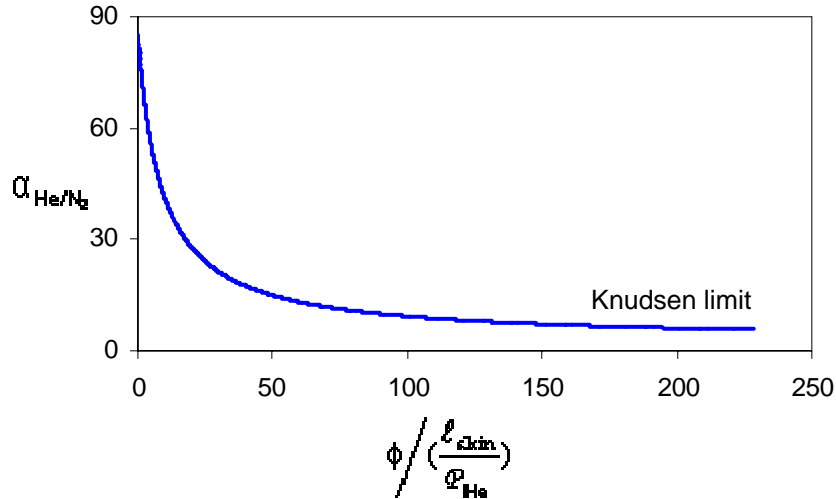


Figure 2.12: The relationship between the membrane selectivity of $\alpha_{\text{He/N}_2}$ and the ratio

of $\phi / \left(\frac{\ell_{\text{skin}}}{\mathcal{P}_{\text{He}}} \right)$

When the substrate resistance starts to be dominant, the highly permeable gas of He will be dramatically reduced, while the less permeable gas of N₂ is relatively unchanged in terms of the order of magnitude, i.e., $R_{T,He}=R_{skin,He}+R_{substrate_layer,He}$ and $R_{T,N_2}=R_{skin,N_2}$. Thus, it is not surprising that the membrane selectivity decreases quickly with the increase in $\phi / (\frac{\ell_{skin}}{P_{He}})$ due to high substrate resistance. The lower selectivity of a high/low permeable gas pair is usually an initial indicator of the substrate resistance of a hollow fiber. Further, the membrane selectivity can fall all of the way to the Knudsen limit in the worst case, as shown in Figure 2.12.

2.5 Mechanism of Pervaporation Transport

In a pervaporation process, a liquid feed is in contact with a membrane, and a permeate is evolved in the vapor state from the opposite side of the membrane, which is kept under low pressure (vacuum pervaporation), or swept by a stream of gas (sweeping-gas pervaporation). Eventually, the permeate is collected in a liquid state by condensation in a cooled container [50]. Unlike gas separation described in equations 2.8-10, although pervaporation follows the solution-diffusion model, the transport mechanism of pervaporation through a pore-free selective film can be conveniently visualized to involve three steps. The first step is the partitioning of the upstream components between a feed liquid and its equilibrium vapor that is in contact with one side of the membrane. The second step is the partitioning and diffusion of penetrants in the selective membrane. The last step is the desorption of permeates, which takes place at the other side of the membrane. Figure 2.13 demonstrates these idealized three steps in a pervaporation process.

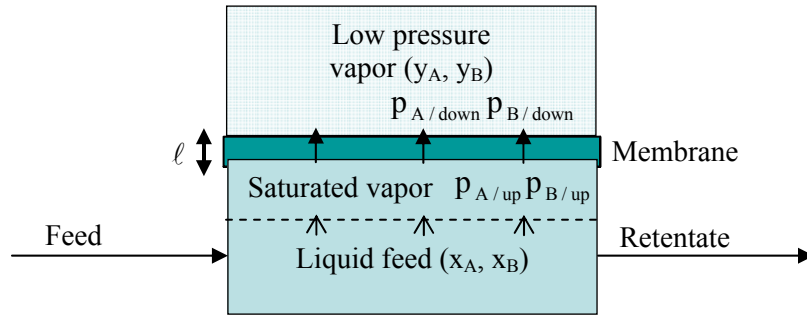


Figure 2.13: Cartoon picture showing an ideal pervaporation process

The pervaporation separation factor, $\beta_{A/B}$, can be defined as the ratio of composition of components in the permeate vapor over the ratio of composition of components in the feed liquid, as follows:

$$\beta_{A/B} = \frac{\text{ratio of components in the permeate vapor}}{\text{ratio of components in the feed liquid}} = \frac{y_A/y_B}{x_A/x_B} \quad (2.18)$$

where x_A and x_B are the mole or mass fractions of A and B in the feed liquid side, and y_A and y_B are the mole or mass fractions of A and B in the vapor permeate side of the membrane.

The ratio of the mole or mass fraction for components A and B on the permeate side is equal to the ratio of the corresponding flux across the membrane wall. Based upon the definition of permeance in equation 2.8, the pervaporation separation factor $\beta_{A/B}$ can be further derived as follows:

$$\begin{aligned} \beta_{A/B} &= \frac{y_A/y_B}{x_A/x_B} = \frac{\text{Flux}_A/\text{Flux}_B}{x_A/x_B} \\ &= \frac{\left(\frac{\mathcal{P}}{\ell}\right)_A \Delta p_A}{\left(\frac{\mathcal{P}}{\ell}\right)_B \Delta p_B (x_A/x_B)} = \frac{\left(\frac{\mathcal{P}}{\ell}\right)_A (p_{A/up} - p_{A/down})}{\left(\frac{\mathcal{P}}{\ell}\right)_B (p_{B/up} - p_{B/down}) (x_A/x_B)} \end{aligned} \quad (2.19)$$

where $p_{A/up}$ and $p_{B/up}$ represent the partial pressures (or fugacities) on the feed side for components A and B. The corresponding partial pressures (or fugacities) on the permeate side are represented by $p_{A/down}$ and $p_{B/down}$. The symbols of $(\frac{\mathcal{P}}{\ell})_A$ and $(\frac{\mathcal{P}}{\ell})_B$ represent the permeances for components A and B, respectively. Ideally $p_{A/down}$ and $p_{B/down}$ are negligible under the vacuum permeate condition. Since the partial pressure on the upstream side for component i can be expressed as $p_{i/up} = \gamma_i x_i p_i^*$, equation 2.19 is simplified to a convenient form, viz.,

$$\beta_{A/B} = \frac{(\frac{\mathcal{P}}{\ell})_A p_{A/up}}{(\frac{\mathcal{P}}{\ell})_B p_{B/up} (x_A / x_B)} = \frac{(\frac{\mathcal{P}}{\ell})_A (\gamma_A x_A p_A^*)}{(\frac{\mathcal{P}}{\ell})_B (\gamma_B x_B p_B^*) (x_A / x_B)} = \underbrace{\left[\frac{(\frac{\mathcal{P}}{\ell})_A}{(\frac{\mathcal{P}}{\ell})_B} \right]}_{\alpha_{mem}} \underbrace{\left[\frac{\gamma_A p_A^*}{\gamma_B p_B^*} \right]}_{\alpha_{EVAP}} \quad (2.20)$$

where γ_A and p_A^* represent the activity coefficient and saturated vapor pressure at the operating temperature for component A, and γ_B and p_B^* represent the activity coefficient and saturated vapor pressure at the operating temperature for component B. The symbols of α_{mem} and α_{EVAP} represent the membrane selectivity and “evaporation factor”, respectively. As a result, the membrane selectivity of α_{mem} in pervaporation is the same as that in gas separation, but the overall separation factor is more complex.

With zero downstream pressure, the pervaporation separation factor can be simply expressed as follows:

$$\beta_{A/B} = \alpha_{mem} \cdot \alpha_{EVAP} \quad (2.21)$$

2.6 Plasticization and Stabilization of Hollow Fibers

A glassy polymer is a non-equilibrium material because it contains excess unrelaxed free volume. The interaction between polymers and penetrants must be considered for glassy polymer materials as it plays an important part in membrane permeability and selectivity. In a few cases, the interaction is negligible due to “non-swelling” properties of penetrants such as oxygen, nitrogen, and helium. However, most penetrants and especially aggressive molecules such as CO₂ and organics can interact with the polymer matrix to increase the segmental mobility of the polymer chains, resulting in a change in the free volume and its distribution. This phenomenon, defined as swelling or plasticization, can deteriorate the membrane performance and lower the membrane selectivity dramatically [51]. For example, CO₂-induced swelling in polyimide membranes can cause a severe problem in natural gas purification. The swelling agent of CO₂ (fast penetrant) generates more free volume among the polymer chains. This enables relatively more CH₄ molecules (slow penetrant) to pass through the membrane and leads to a lower membrane selectivity of $\alpha_{\text{CO}_2/\text{CH}_4}$ [52-54]. The swelling effects generally favor slow gas molecules much more than fast ones [55].

Although Matrimid[®] has excellent thermal and chemical stability; these penetrant-induced swelling stresses can still lead to polymer plasticization especially in aggressive environments such as HAc/H₂O mixtures. In this case, it has been observed that water has trivial effects on the polymer, while acetic acid can swell the fiber significantly. Acetic acid is not only a swelling agent, but also a “slow” molecule in this work. Therefore, the plasticization from acetic acid helps the acid itself to permeate through the membrane much more than it helps water. The relatively larger increase in the HAc flux than water

flux results in the decreased membrane selectivity of $\alpha_{\text{H}_2\text{O}/\text{HAc}}$. The experimental results shown in Figure 2.14 illustrate the variation of HAc permeability with different HAc concentration (HAc partial pressure) in feeds at about 101.5°C for a hollow fiber membrane in this research. Clearly, the HAc permeability increases with the increment of the HAc concentration in feeds.

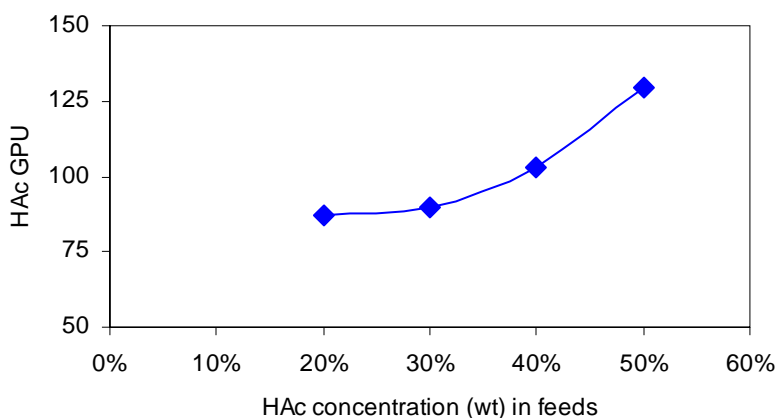


Figure 2.14: Schematic diagram of HAc permeability vs. HAc concentration in feeds showing the HAc-induced swelling effects

Swelling phenomena are complicated since they depend on a number of factors, such as how aggressive the penetrants are. The HAc-induced plasticization starts immediately from the 20% wt HAc concentration feed.

Two methods have been widely used to suppress plasticization. Switching to a different polymer for a particular separation problem is a solution in principle; however, it is an extreme approach. The other option is to modify the polymer of interest in such a way that it can diminish the swelling effects, which is generally called “stabilization”. Several attempts have been made to stabilize polyimide membranes for gas separation such as chemical cross-linking and blending [54, 56]. Heat treatment (below T_g) has proven very helpful in suppressing the organics-induced plasticization for polyimide

membranes because it reduces the free volume and prompts the formation of charge transfer complexes [57-58]. Both effects can limit the mobility of segmental polymer chains, and thus inhibit the swelling from aggressive penetrants. Heat treatment is used to control plasticization caused by acetic acid in this work, which is discussed in Chapter 6.

2.7 Summary

This chapter provided fundamental knowledge needed to understand gas transport in glassy polymers as well as specific properties of asymmetric large bore size defect-free hollow fibers, the mechanism of pervaporation transport, challenges faced in an aggressive environment, and approaches to address the plasticization.

In order to separate HAc/H₂O mixtures effectively with a hollow fiber membrane unit, spinning a large bore size defect-free hollow fiber is certainly the first step of this project. The following chapter will discuss the spinning process in detail based upon theoretical and practical standpoints.

2.8 References

- [1] Wallace, D.W. *Crosslinked hollow fiber membranes for natural gas purification and their manufacture from novel polymers*. Ph.D. Dissertation, The University of Texas at Austin, 2004.
- [2] Deng, S., Sourirajan, S., Matsuura, T. *Study of polydimethylsiloxane/aromatic polyamide laminated membranes for separation of acetic acid/water mixtures by pervaporation process*. Sep. Sci. Technol. 1994, 29, 1209-1216.
- [3] Sano, T., Ejiri, S., Yamada, K., Kawakami, Y., and Yanagishita, H. *Separation of acetic acid-water mixtures by pervaporation through silicalite membrane*. J. Membr. Sci. 1997, 123, 225-233.
- [4] Huang, S.C., Ball, I.J., and Kaner, R.B. *Polyaniline membranes for pervaporation of carboxylic acids and water*. Macromolecules. 1998, 31, 5456-5464.

- [5] Yoshikawa, M., Kuno, S.T., and Kitao, T. *Specialty polymeric membranes 3. Pervaporation separation of acetic acid/water mixtures through polymeric membranes having a pyridine moiety as a side group*. J. Appl. Polym. Sci. 1994, 51, 1021-1027.
- [6] Hofmann, T., Hapke, R.L., Sengupta, A., and Roberts, D.L. *Acetic acid and butyric acid recovery from aqueous solutions by pervaporation*. Presented at the Conference of the North American Membrane Society, San Diego, CA, 1991.
- [7] Bai, J., Fouda, A.E., Matsuura, T., and Hazlett, J.D. *Study on the preparation and performance of polydimethylsiloxane-coated polyetherimide membranes in pervaporation*. J. Appl. Polym. Sci. 1993, 48, 999-1008.
- [8] Yoshikawa, M., Kuno, S.L., Wano, T., and Kitano, T. *Specialty polymeric membranes. 4. Pervaporation separation of acetic acid/water mixtures through modified polybutadiene membranes*. Poly. Bull. 1993, 31, 607-613.
- [9] Mahajan, R., *Formation, characterization and modeling of mixed matrix membrane materials*. Ph.D. Dissertation, The University of Texas at Austin at Austin, 2000.
- [10] Zimmerman, C.Z. Singh, A. and Koros, W.J., *Tailoring mixed matrix composite membranes for gas separations*. J. Membr. Sci. 1997, 137, 145-154.
- [11] Ohya, H., Kudryavtsev, V.V., and Semenova, S.I. *Polyimide membranes: applications, fabrications, and properties*. Gordon and Breach Inc. 1996.
- [12] Porter, M.C., *Handbook of industrial membrane technology*. Noyes Publications, Park Ridge, NJ 1990.
- [13] Kesting, R.E. and Fritzsche, A.K. *Polymeric gas separation membranes*. John Wiley and Sons, Inc., New York 1993.
- [14] Paul, D.R. and Yampol'skii, Y.P. *Polymeric gas separation membranes*. CRC Press, Boca Raton, FL 1994.
- [15] Ho, W.S.W. and Sirkar, K.K. *Membrane handbook*. Van Nostrand Reinhold, New York 1992.
- [16] Spillman, R.W. *Economics of gas separation membranes*. Chem. Eng. Proc. January 1989, 41-62.
- [17] Kim, T. H., Koros, W. J., Husk, G. R., and O'Brien, K. C. *Relationship between gas separation properties and chemical structure in a series of aromatic polyimides*. J. Membr. Sci. 1988, 37, 45-62.

- [18] Huang, J.G., Cranford, R.J., Matsuura, T., and Roy, C. *Sorption and transport behavior of water vapor in dense and asymmetric polyimide membranes*. J. Membr. Sci. 2004, 241, 187-196.
- [19] Huang, J.G., Cranford, R.J., Matsuura, T., and Roy, C. *Water vapor permeation properties of aromatic polyimides*. J. Membr. Sci. 2003, 215, 129-140.
- [20] Clausi, D.T., Koros, W.J. *Formation of defect-free polyimide hollow fiber membranes for gas separations*. J. Membr. Sci. 2000, 167, 79-89.
- [21] Tin, P.S., Chung, T.S., Liu, Y., Wang, R., Liu, S.L., and Pramode, K.P. *Effects of cross-linking modification on gas separation performance of Matrimid[®] membranes*. J. Membr. Sci. 2003, 225, 77-90.
- [22] McKelvey, S.A. *Formation and characterization of hollow fiber membranes for gas separation*. Ph.D. Dissertation, The University of Texas at Austin, 1997.
- [23] Lee, E.K. and Koros, W.J. *Membrane, synthetic, applications*. Encyclopedia of Physical Science and Technology, 2001, 279-344.
- [24] Paul, D.R. and Y.P. Yampol'skii, *Polymeric gas separation membranes*. Boca Raton: CRC Press 1994.
- [25] Mulder, M., *Basic principles of membrane technology*. Kluwer Academic Publishers: Dordrecht 1996.
- [26] Vu, D.Q., *Formation and characterization of asymmetric carbon molecular sieve and mixed matrix membranes for natural gas purification*. Ph.D. Dissertation, The University of Texas at Austin, 2001.
- [27] Koros, W.J. and Paul, D.R., *CO₂ sorption in poly(ethylene terephthalate) above and below the glass transition*. J. Poly. Sci.: Phys. Ed. 1978, 16, 1947-1964.
- [28] Clausi, D. T. *Formation and characterization of asymmetric polyimide hollow fiber membranes for gas separations* Ph.D. Dissertation, The University of Texas at Austin, 1998.
- [29] Ohya, H., Kudryavtsev, V.V., and Semenova, S.I. *Polyimide membranes: applications, fabrications, and properties*. Gordon and Breach Inc. 1996.
- [30] Koros, W.J. and Paul, D.R. et al. *Carbon dioxide sorption and transport in polycarbonate*. J. Polym. Sci., Polym. Phys. 1976 Ed. 14, 687-702.
- [31] Chan, A.H., Koros, W.J. and Paul, D.R. *Analysis of hydrocarbon gas sorption and transport in ethyl cellulose using the dual sorption/partial immobilization models*. J. Membr. Sci. 1978, 3, 117-130.

- [32] Paul, D.R. and Koros, W.J. *Effect of partially immobilizing sorption on permeability and the diffusion lag time*. J. Poly. Sci., Poly. Phys. 1976, 14, 675-685.
- [33] Gray-Weale, A.A. and Henchman, R.H. *Transition-state theory model for the diffusion coefficients of small penetrants in glassy polymers*. Macromolecules. 1997, 30(23), 7296-7306.
- [34] Greenfield, M.L. and Theodorou, D.N. *Molecular modeling of methane diffusion in glassy atactic polypropylene via multidimensional transition state theory*. Macromolecules. 1998, 31(20), 7068-7090.
- [35] Bueche, F. *Physical properties of polymers*. New York: Interscience, Inc. 1962.
- [36] Hines, A.L. and Maddox, R.N. *Mass transfer fundamentals and applications*. Prentice Hall Inc. 1985.
- [37] Lide, D.R. *Handbook of chemistry and physics*. CRC Press 1995-1996, 76th, 6-57.
- [38] Henis, J.M.S. and Tripodi, M.K. *Composite hollow fiber membranes for gas separation: the resistance model approach*. J. Membr. Sci. 1981, 8, 233-246.
- [39] Ekiner, O.M., Hayes, R.A., and Manos, P. *Reactive post treatment for gas separation membranes*. United States Patent 5,091,216, E.I. du Pont de Nemours 1992.
- [40] Henis, J.M.S. and Tripodi, M.K. *Multicomponent membranes for gas separations*. United States Patent 4,230,463, Monsanto Co. 1980.
- [41] Makino, H., Kusuki, Y., Yoshida, H., and Nadamura, A. United States Patent 4,378,324, 1983.
- [42] Makino, H., Kusuki, Y., Harada, T., and Shimazaki, H. United States Patent 4,373,400, 1983.
- [43] Makino, H., Kusuki, Y., Harada, T., and Shimazaki, H. United States Patent 4,440,643, 1984.
- [44] Makino, H., Kusuki, Y., Harada, T., Shimazaki, H., and Isida, T. United States Patent 4,528,004, 1985.
- [45] Pan C. Y. and Habgood H. W. *Gas separation by permeation: Part I. Calculation methods and parametric analysis*. Canadian J. Chem. Eng. 1978, 56, 197-209.

- [46] Pan C. Y. and Habgood H. W. *Gas separation by permeation: Part II. Effect of permeate pressure drop and choice of permeate pressure*. Canadian J. Chem. Eng. 1978, 56, 210-217.
- [47] Thundiyil M. J. and Koros W. J. *Mathematical modeling of gas separation permeators - for radial crossflow, countercurrent, and cocurrent hollow fiber membrane modules*. J. Membr. Sci. 1997, 125, 275-291.
- [48] Bird R. B., Stewart W. E. and Lightfoot E. N. *Transport Phenomena* John Wiley & Sons, Inc., New York, 1960.
- [49] Clausi, D.T., S.A. McKelvey, and W.J. Koros, *Characterization of substructure resistance in asymmetric gas separation membranes*. J. Membr. Sci. 1999, 160, 51-64.
- [50] Huang, R.Y.M. *Pervaporation membrane separation processes*. Elsevier Science Publishing Company, Inc. New York. 1991, 1-46.
- [51] Koros, W.J. and Hellums, M.W. *Transport properties, in encyclopedia of polymer science and engineering*, 2nd ed., John Wiley and Sons: New York, 1989; Supplement. Vol., 724-803.
- [52] Bos, A., Punt, I.G.M., Wessling, M., and Strathmann, H. *Plasticization-resistant glassy polyimide membranes for CO₂/CH₄ separations*. Sep. Purif. Technol. 1998, 14, 27-39.
- [53] Wind, J.D., Sirard, S.M., Paul, D.R., Green, P.F., Johnston, K.P., and Koros, W.J. *Relaxation dynamics of CO₂ diffusion, sorption, and polymer swelling for plasticized polyimide membranes*. Macromolecules. 2003, 36, 6442-6448.
- [54] Wind, J.D., Claudia, S.B., Paul, D.R., and Koros, W.J. *Solid-state covalent cross-linking of polyimide membranes for carbon dioxide plasticization reduction*. Macromolecules. 2003, 36, 1882-1888.
- [55] Bos, A. *CO₂/CH₄ separation with glassy polymer membranes: Aspects of CO₂-induced plastization*. University of Twente 1996.
- [56] Bos, A., Punt, I.G.M., Strathmann, H., and Wessling, M. *Suppression of gas separation membrane plasticization by homogeneous polymer blending*. AIChE J. 2001, 47, 1088-1093.
- [57] Kawakami, H., Mikawa, M., and Nagaoka, S. *Gas transport properties in thermally cured aromatic polyimide membranes*. J. Membr. Sci. 1996, 118, 223-230.

- [58] Krol, J.J., Boerrigter, M., and Koops, G.H. *Polyimide hollow fiber gas separation membranes: preparation and the suppression of plasticization in propane/propylene environments*. J. Membr. Sci. 2001, 184, 275-286.

Chapter 3: Hollow Fiber Spinning from Matrimid[®]

3.1 Introduction

The technology to spin a hollow fiber membrane was developed soon after the pioneering work of Loeb and Sourirajan to form flat sheet asymmetric membranes [1]. As discussed in Chapter 2.3, currently hollow fiber membranes with an ultra-thin separation layer have been produced to satisfy high productivity in industry, but some defects in the thin separation layer have to be caulked to get an intrinsic selectivity. The post-treatment technology functions successfully in gas separation; however, it may fail in pervaporation because aggressive organic feeds can dislodge those fillings and deteriorate the membrane performance.

The Koros group has developed the “dry jet, wet quench” spinning method [2-4] that can form a defect-free thin skin layer with around 250 μm outer diameter fiber. This technology is important for the application of hollow fibers in pervaporation [5-7]. Matrimid[®], a commercially available polymer, exhibits good permeation properties and processability in contrast to other readily available polymers in gas separation. Combined with other good properties such as high glass transition temperature ($T_g > 300^\circ\text{C}$), good mechanical strength, and chemical- and thermo- resistance, Matrimid[®] appears to be an attractive candidate polymer for pervaporation of HAc/H₂O mixtures.

The pressure change in the bore side can influence the permeation of all the penetrants with shell feed due to high flux through the membrane in a pervaporation process, while the “fast” gases are affected more significantly than the “slow” ones. The membrane selectivity can be underestimated to be lower than the inherent value.

Spinning a large bore size fiber is ideally a simple solution to diminish the effects of the bore pressure change in terms of theoretical analysis; however, modifying the current spinning process and facilities to obtain a large bore size defect-free fiber is not trivial.

Figure 3.1 shows a procedure flowchart that is used to spin a defect-free large bore size hollow fiber membrane by the “dry-jet, wet-quench” method.

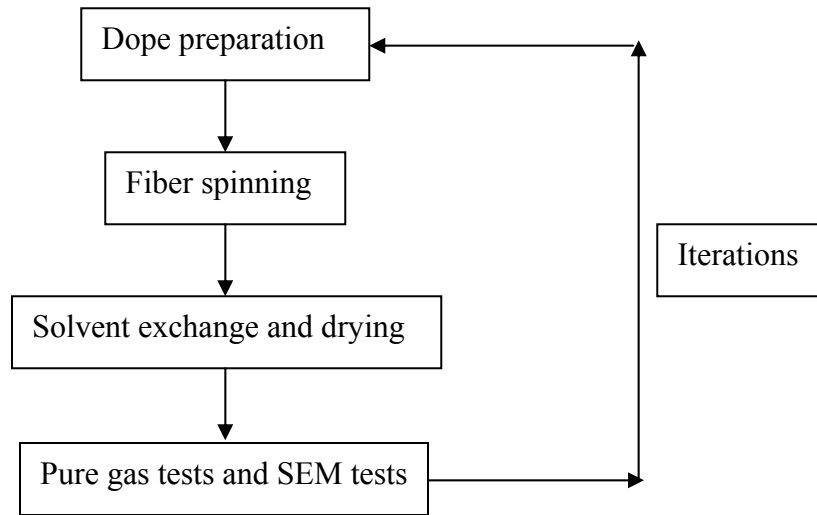


Figure 3.1: Steps involved in the formation of a large bore size hollow fiber with defect-free outer skin layer

An asymmetric hollow fiber is formed by the phase separation of a polymer solution. As shown in Figure 3.2, an appropriate homogeneous polymer solution called “dope”, with a bore fluid composed of non-volatile solvent and water, are extruded through an annular spinneret into air at the initial stage. Once a nascent fiber is driven into the air gap, the volatile solvent will evaporate immediately at the outer periphery of the fiber. This process increases the polymer concentration quickly at the outermost layer of the fiber and ideally vitrifies this layer to form a defect-free selective skin layer [8]. When the nascent fiber hits a quench (water) bath, phase separation occurs in the

underlying-skin layer region instantaneously to produce an open porous non-selective substructure [9]. A subsequent solvent exchange process plays an important role in the resulting membrane morphology and permeation performance. The collapse of the porous substructure of the fiber can be avoided as high surface tension water is replaced by low surface tension solvents [10-11]. The last step involves pure gas permeation and SEM tests. Iterations might be necessary if the fiber properties have to be modified.

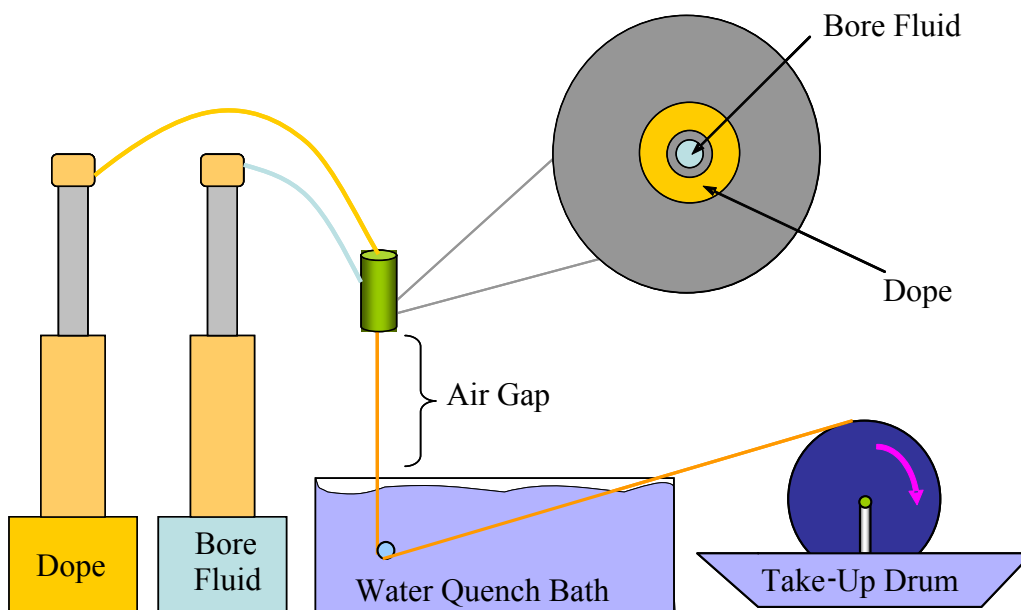


Figure 3.2: Schematic flowchart for the fiber spinning set-up

This chapter focuses on the improvement of current spinning technology [2-4] to produce a large bore size defect-free hollow fiber membrane from Matrimid[®] by adjusting the dope composition and spinning parameters. The mechanisms of phase separation, the formation of a defect-free non-nodular skin layer, key factors to control outer and inner diameters of hollow fibers, and fiber characterization by pure gas permeation tests are summarized below.

3.2 Mechanism of Phase Separation

Non-solvent induced phase separation is used to produce an asymmetric hollow fiber in this work. This approach involves a complicated relationship between thermodynamic and kinetic factors of a ternary system (polymer, solvent, and non-solvent). From a thermodynamic point of view, a ternary phase diagram shown in Figure 3.3 can be used to study the interactions among polymer, solvents and non-solvents.

In a ternary-phase diagram, the corners of the triangle represent pure components (polymer, solvent, and non-solvent). The axes of the triangle represent the binary combination of two components. Any point within the triangle represents a ternary mixture of three components [12]. Three regions exist in this ternary-phase diagram including homogeneous/1-phase region, metastable region, and unstable/2-phase region. The boundary between the homogeneous and metastable region is called the “binodal curve”, while the boundary between the metastable and stable region is referred to as the “spinodal curve”. The critical point lies at their intersection. The colored region at the top represents the glassy region or vitrified region, in which polymer chains have very low mobility and inhibited ability to rearrange themselves due to high polymer concentration. A thin skin layer at the outermost surface of a hollow fiber is formed from this vitrification mechanism and functions as a selective layer.

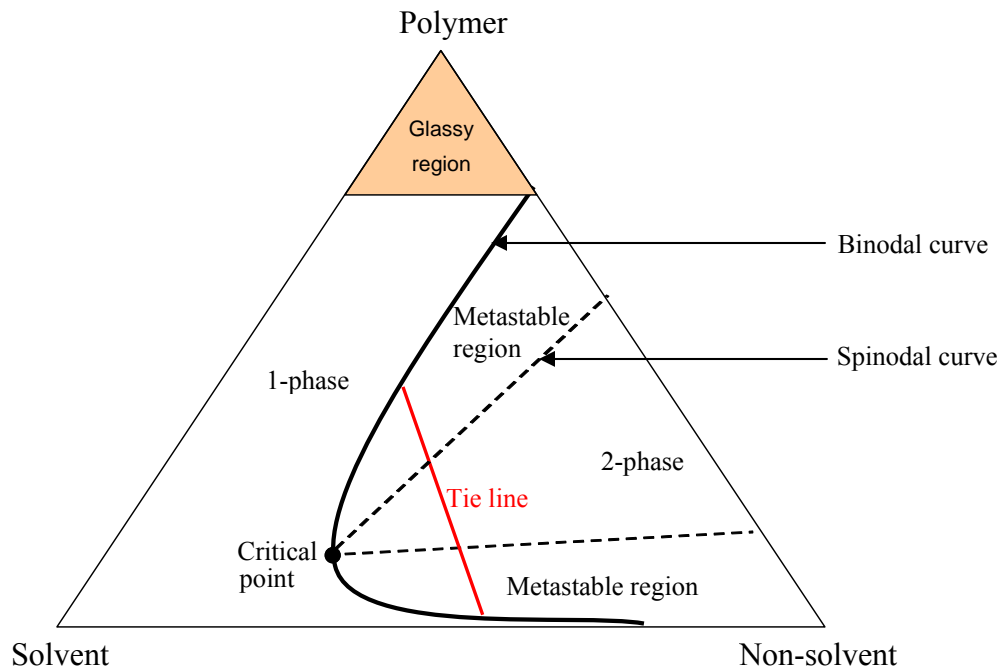


Figure 3.3: Ternary-phase diagram of polymer-solvent-nonsolvent system

In the stable region, the dope/polymer solution is in a homogeneous status. When a solvent evaporates from or non-solvent dissolves in a polymer solution, a homogeneous dope will cross the binodal curve into the metastable region and demixing will occur. A “nucleation and growth” mechanism [4, 13] is considered to describe the phase separation in the metastable region. For a given composition located within the metastable region, the equilibrium composition of the polymer-lean phase and that of the polymer-rich phase are decided by the intercept of the tie-line with the binodal curve. The volumetric ratio of polymer-rich to polymer-lean phase is given by the lever rule [14]. When demixing starts somewhere below the critical point, the polymer-rich phase nucleates and grows, resulting in low-integrity powdery agglomerates. Generally this

case must not happen, as such a polymer morphology is not practical for membrane formation.

On the other hand, the nucleation and growth of the polymer-lean phase occur when demixing starts somewhere above the critical point due to the highly concentrated polymer solution. Under this condition, the free energy associated with phase separation decreases and a nucleus of polymer-lean phase larger than the critical size grows. A nucleus less than the critical size will simply “re-dissolve” into the homogeneous polymer solution. This results in the formation of a sponge-like cell structure and the cell walls of this structure must rupture to yield a desirable open cell foam support [13, 15-16].

Spinodal decomposition occurs in the unstable region. A bi-continuous network of the polymer-lean and polymer-rich phases is directly produced without any nucleation and growth due to instantaneous demixing [17]. A truly bi-continuous network formed via either mechanism promotes an open porous membrane support without selective function ideally.

3.3 Dope Preparation

A typical dope for spinning an asymmetric hollow fiber is a homogeneous multi component solution, including polymer, solvents (a more volatile solvent and a less volatile solvent), and non-solvent [18-19]. The selection of solvents and non-solvent, and the composition of each component have significant influences on phase separation, which determines the final morphology of a hollow fiber membrane and its separation performance.

Water miscibility is the first consideration to select solvents and non-solvent due to an aqueous quenched membrane formation process in this work. That is, solvents have to be exchanged with water to drive the dope composition into the unstable region of the ternary-phase diagram to cause instantaneous demixing. Good miscibility of volatile and non-volatile solvents with the polymer is also necessary because the regular polymer concentration of the dope is very high (25-30% wt). In addition to being miscible with water, the volatile solvent has to be sufficiently volatile for the instantaneous vitrification to form a thin skin layer in the air gap. Carruthers [20] found that the amount of volatile components in a spinning dope plays an important role in forming a thin skin layer in the air gap. In this work, tetrahydrofuran (THF) is chosen as a highly volatile solvent because it is a strong solvent of Matrimid[®] and also very miscible with water. Considering a relatively benign environment, 1-methyl-2-pyrrolidinone (NMP) is used as a less volatile solvent that can also strongly dissolve Matrimid[®] and is miscible with water.

The choice of non-solvent is more challenging since limited guidelines can be followed. Although economical water can be used as a coagulant in the quench bath, its non-solvent strength is too high to be of practical use [21]. In other words, only a little bit of water can induce phase separation immediately in a polymer, solvent, and non-solvent system, which makes the window of available dope composition in a ternary-phase diagram very narrow. Aliphatic alcohols are miscible with water and lower molecular weight alcohols are more volatile than water. Thus, ethanol (EtOH) is chosen as a non-solvent due to its strong interaction with water, relatively lower non-solvent strength, and benign nature. Table 3.1 shows the boiling temperature and the solubility level with water for commonly used solvents and non-solvents in the fiber formation process [22].

Table 3.1: Boiling temperature and solubility level with water for solvents and non-solvents commonly used for asymmetric membrane formation
*: Solubility with water or EtOH on a relative scale: 1-insoluble; 2-slightly soluble; 3-soluble; 4-very soluble; 5-miscible

Solvent	Boiling temp.(°C)	Solubility level with H ₂ O*	Solubility level with EtOH*
Tetrahydrofuran (THF)	65-67	3	4
1-Methyl-2-Pyrrolidinone (NMP)	202	4	4
Dimethylformamide (DMF)	153	5	5
Non-solvent	Boiling temp. (°C)	Solubility level with H ₂ O*	
Methanol (MeOH)	64.6	5	
Ethanol (EtOH)	78.2	5	
1-Propanol	97.2	5	
2-Propanol	82.3	5	

Once components of a spinning dope are chosen, the composition of each component can be represented by a ternary phase diagram. Basically the starting point of a dope should be as close as possible to a binodal curve, while still being stable to allow reasonable handling. This proximity to the binodal curve can assist the instantaneous demixing (i.e. evaporation of volatile solvents or absorption of water vapor from air) after the dope is extruded from a spinneret. Further, the polymer concentration has to be controlled to a certain degree to reach the best spinning condition. A low polymer concentration dope is difficult to extrude and draw smoothly due to its low viscosity. On the other hand, with a high polymer concentration, it is hard to produce highly porous

substructure due to the kinetic factors of phase separation [3], resulting in additional substrate resistance. Thus, the lowest polymer concentration, while maintaining the sufficient viscosity, is the best option for spinning a hollow fiber. In this work, the dope is formulated with 27% wt Matrimid[®] (polymer), 15-20% wt THF (volatile solvent), 41-46% wt NMP (less volatile solvent), and 12% wt EtOH (non-solvent). The binodal curve for this system can be decided by the cloud point method [23]. The red solid circle shows the dope composition in Figure 3.4. Although more advanced spinning techniques have been developed to use two dope solutions to form a more economical and high performance fiber [24-25], only one polymer layer with a bore fluid using a monolithic spinneret is presented in this work. The spinning concepts can easily be extended to multi-layer composite fibers.

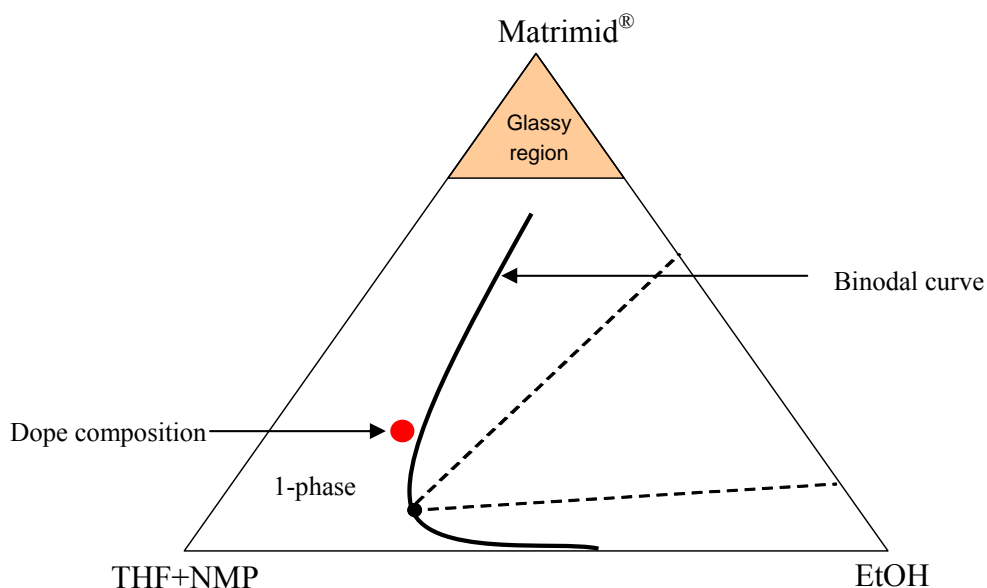


Figure 3.4: Ternary-phase diagram of the Matrimid[®]/(THF+NMP)/EtOH system, showing the starting point of a dope composition [2]

The dope has to be co-extruded with a bore fluid through an annular spinneret. Many chemicals can be used to make a bore fluid provided that they are comprised of non-volatile solvents and non-solvents. The purpose of a bore fluid is to prevent a nascent

hollow fiber from collapsing in the air gap and make a hollow morphology available. If a bore fluid contains too much solvent, it will dissolve the inner layer polymer of a hollow fiber and slow the phase separation process in the quench bath. In addition, some amount of debris will appear inside the hollow space that is supposed to be empty. Too much non-solvent/water in a bore fluid can drive the inner layer polymer of a hollow fiber into the vitrification region in the air gap, resulting in both inner and outer skin layers (double layers). Thus, a bore fluid should act neither as a strong solvent nor as a strong non-solvent, and the interaction between the bore fluid and the polymer must be minimized. A bore fluid composed of NMP (less volatile solvent to Matrimid[®]) and water is used in this work and the concentration of each component can be determined by a ternary phase diagram. As shown in Figure 3.5, the concentration point of a bore fluid can be extrapolated from a line tangent to the binodal curve to the NMP/water axis.

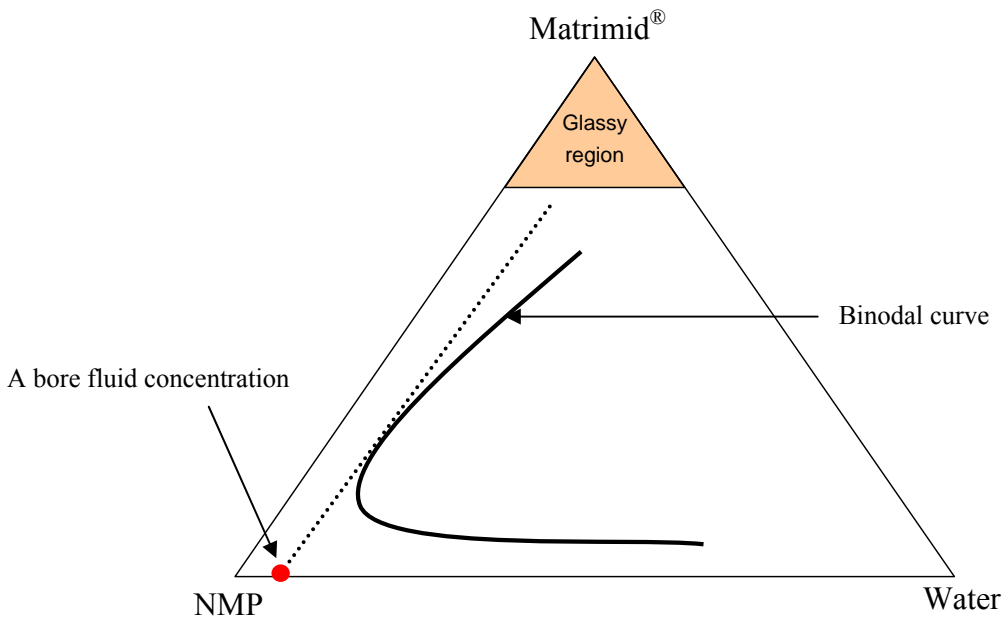


Figure 3.5: Ternary-phase diagram of the Matrimid[®]/NMP/H₂O system showing the concentration point of a bore fluid [2]

Table 3.2 summaries the dope and bore fluid composition used to spin regular diameter ($\sim 250 \mu\text{m}$) [2] and large diameter ($\sim 500 \mu\text{m}$) fibers in this project. As it can be

seen, the feasible concentration window of each component in the dope is refined and narrowed for the large diameter fiber spinning relative to the case for small diameter fibers. Although the concentration of total solvents is maintained constant, the NMP and THF concentrations are pushed to their lower-bound and upper-bound regions, respectively. This is very helpful to form a densified defect-free outer skin layer, because adding more volatile solvent (reducing less volatile solvent) in a dope can drive the polymer solution to the vitrification region much more easily in the air gap.

Table 3.2: Dope and bore fluid formulas used to spin regular diameter (~ 250 μm) and large diameter (~ 500 μm) fibers in this project

Chemicals	Weight percentage (%)			
	Small Diameter (~250 μm)		Large Diameter (~500 μm)	
	Dope	Bore Fluid	Dope	Bore Fluid
Matrimid [®]	27		27	
NMP (less volatile solvent)	40-55	4-6	41-46	4-6
THF (more volatile solvent)	0-20		15-20	
EtOH (weak non-solvent)	10-15		12	
H ₂ O (strong non- solvent)		94-96		94-96

3.4 Fiber Spinning

The well mixed dope is first poured into a pump for overnight to degas. The bore fluid is delivered into a separate pump the next day. The spinneret designed by Pesek [26]

is used in this work, which is also called “the first generation spinneret” in our group. The spinneret structure is shown in Figure 3.6. The bore inside diameter, outside diameter, and annular outside diameter are 0.2, 0.45, and 0.9 mm, respectively. Before being pumped into the spinneret, the bore fluid and dope have to be filtered with a 2 μm and 60 μm sintered metal filter, respectively.

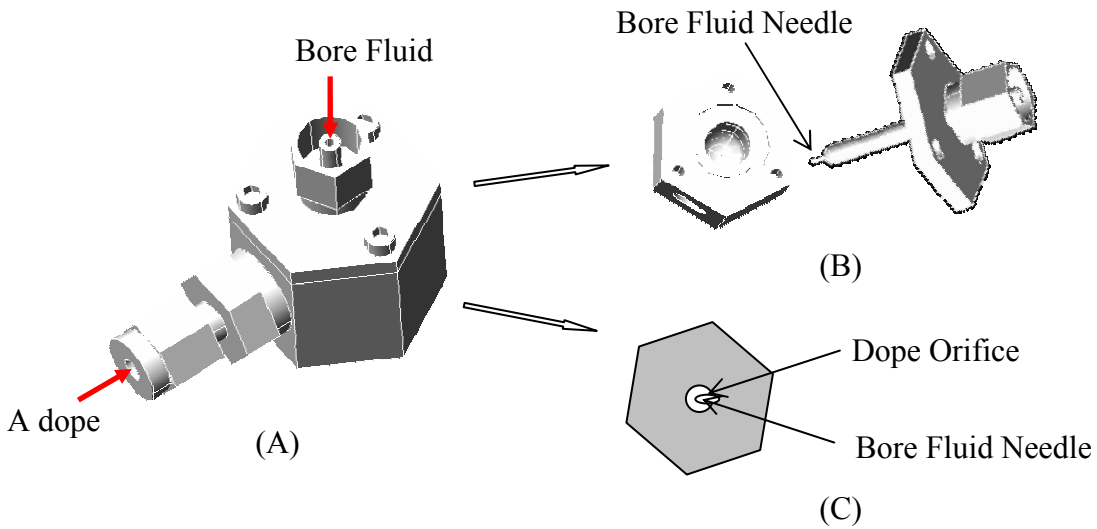


Figure 3.6: Structure of “the first generation” spinneret used in this work [27]
(a) whole picture, (b) parts, (c) bottom view

The polymeric dope is extruded through an annular orifice of the spinneret, while a bore fluid is extruded through the center of annulus to form a bore. After a nascent fiber comes out from the spinneret, it is initially exposed to air and drawn, then quenched in a water bath, and finally collected on a take-up drum. Figure 3.7 illustrates mass transfer in each step of the “dry-jet, wet-quench” spinning procedures.

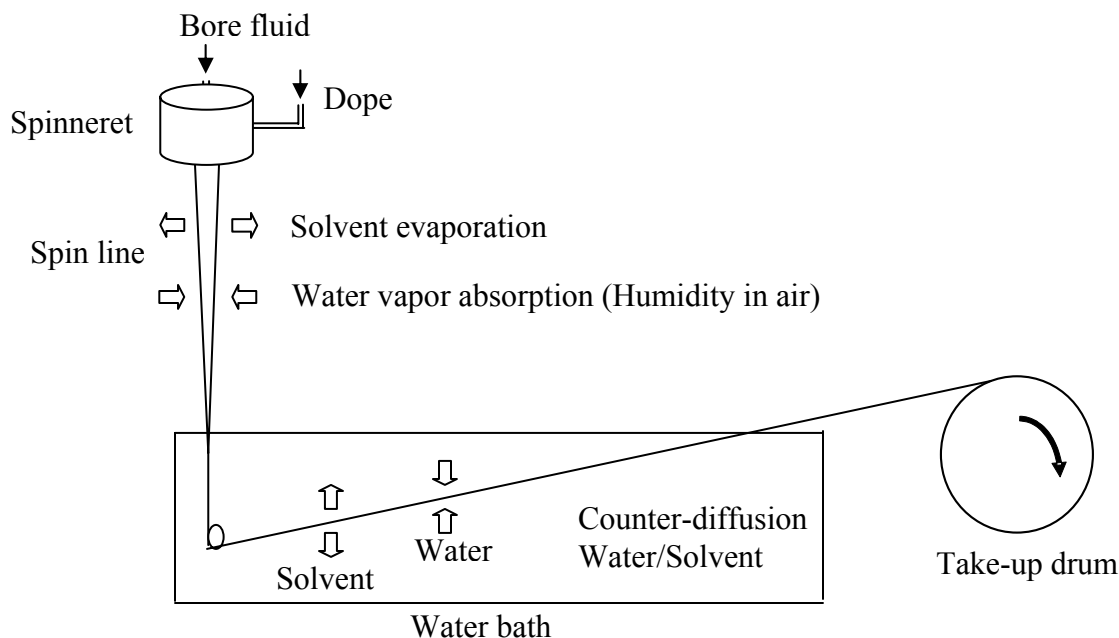


Figure 3.7: Mass transfer in the “dry jet, wet quench” spinning process

3.4.1 Formation of Integrally-Skinned Defect-Free Outer Layer

Phase separation in the air gap negatively affects the formation of a defect-free outer skin layer [28-29]. That is, the volatile solvent evaporation should ideally drive the dope composition from the starting point (shown in Figure 3.8) to the vitrification region, resulting in a non-nodular defect-free outer skin layer that will *not phase separate* in the aqueous quench bath. Typically the operation variables such as the height of air gap, the polymer concentration in the dope, the temperature of the spinneret, and the convection rate in air have to be increased to favor the solvent evaporation in the air gap. However, some limitations exist for these variables. For example, the spinneret temperature can not be too high as it can lower the dope viscosity and cause the spin line to become unstable [3]. The increase of the air gap is restricted by the spin line stability and tension, although it can extend the evaporation time.

Carruthers [20] recently proposed a framework that shows how the skin formation depends on the polymer solution in the outer periphery of a fiber at the point of demixing. If the polymer concentration is sufficiently high, the mobility of the polymer chains is so limited that most polymer chains are entangled upon phase separation. In this research, more volatile solvents are added into the dope to promote their evaporation in the air gap, while the weight percentage of the polymer remains constant. This can make the outer skin layer more likely defect-free due to its high polymer concentration in the air gap, while the open porous substructure can still be achieved in the water bath. If necessary, forced-convective evaporation can be used in the air gap [29-30]. A forced convective stream consisting of an inert gas is helpful to remove the volatile solvent from the outermost region of the hollow fiber and can reduce the external mass transfer resistance; however, this is not found to be necessary in the present work.

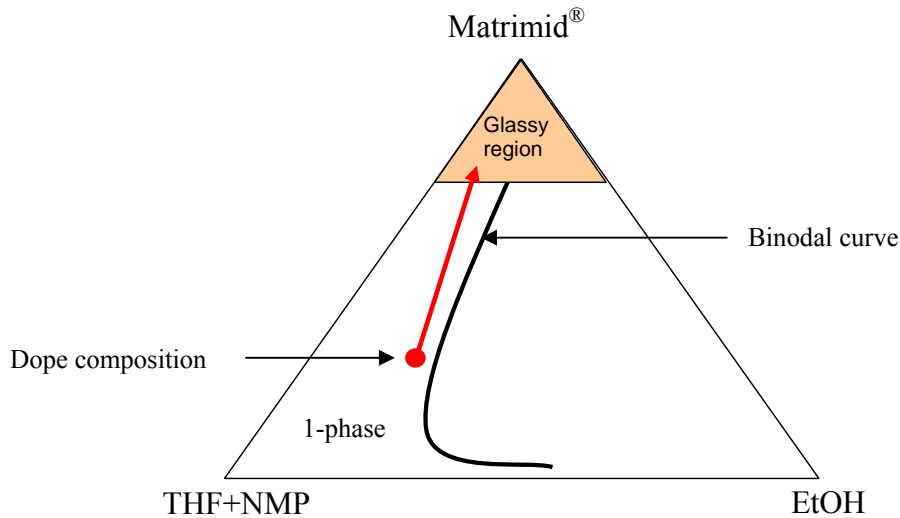


Figure 3.8: Phase separation in the air gap

3.4.2 Formation of Open Porous Substructure

The underlying region beneath the nascent skin layer remains in a fluid state until it is immersed into an aqueous quench bath. Based upon the counter-diffusion of solvents and water, the starting point of the dope composition in the ternary phase diagram is driven to the metastable or unstable region, as shown in Figure 3.9. An open porous support layer without diffusive separation function can be formed in the bulk of the fiber regardless of nucleation and growth, or spinodal decomposition mechanism.

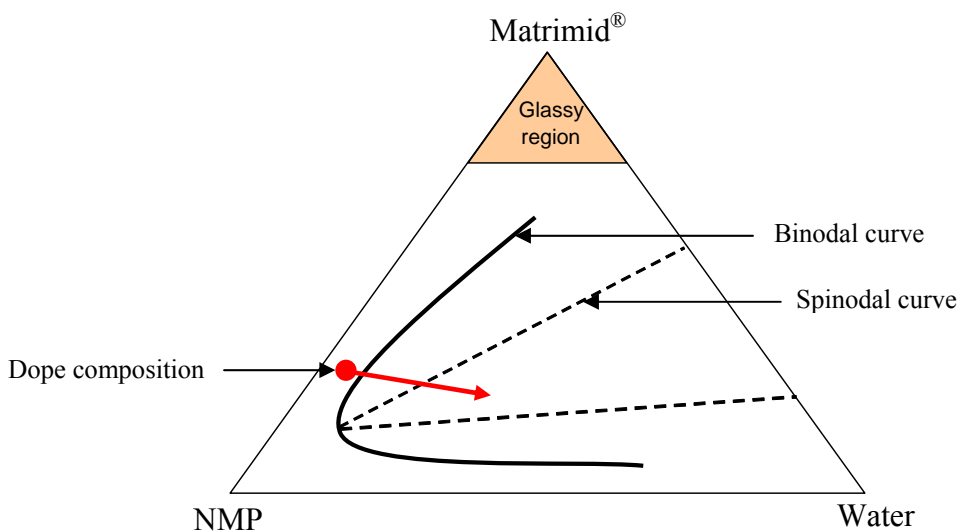


Figure 3.9: Phase separation in the quench bath

Instantaneous demixing by spinodal decomposition is preferred in the quench bath in order to produce the ideal bi-continuous and inter-connected open porous substructure. Non-solvent strength is the first criterion when selecting a coagulant as it induces rapid phase separation. Water is a strong non-solvent and adequately miscible with many chemicals such as NMP and THF. In addition, water is economical, safe, and easy-to-handle. Thus, water is usually used as a coagulant in the quench bath.

The aqueous quench bath is operated at 25°C in this work. Depending on the desired separation characteristics of a hollow fiber, sometimes the quench bath temperature can be increased [3]. A high temperature quench can accelerate the counter diffusion of solvents and water; however, it weakens the non-solvent strength of water and also adds to the operation costs.

3.4.3 Macroscopic Morphology

Macroscopic morphology refers to the appearance of hollow fibers in this work, primarily including inner and outer diameters and concentric circles of hollow fibers. A fiber that is not concentric may not withstand a high pressure drop across the membrane and may collapse easily in the thin wall region. Figure 3.10 shows a SEM picture of a non-concentric hollow fiber.

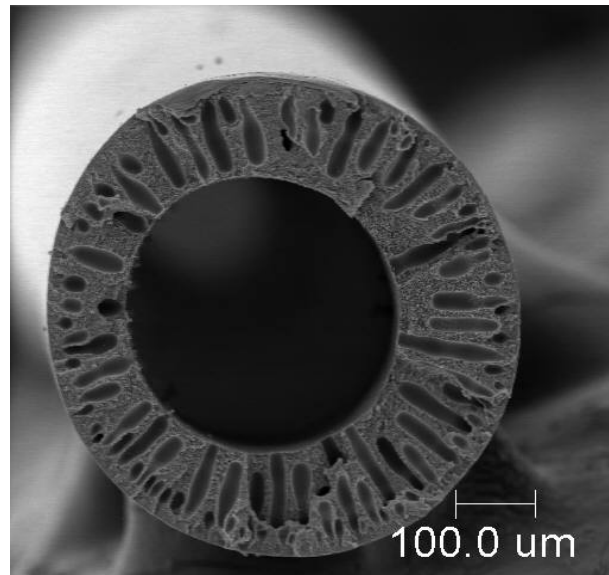


Figure 3.10: SEM picture showing a non-concentric hollow fiber

Design weakness of the first generation spinneret makes it difficult to achieve perfect alignment and is responsible for the formation of the non-concentric hollow

fibers. As shown in Figure 3.6 (B) and (C), the bore fluid needle has to be manually centered at the bottom of the spinneret, which is a difficult and time consuming process. If the tiny needle is even slightly displaced, it is hard to form a concentric hollow fiber.

The dope extrusion rate of 180 ml/hr and the bore fluid extrusion rate of 60~100 ml/hr are used in this work, respectively. A non-concentric hollow fiber is more likely to be observed when the dope extrusion rate is lower than 180 ml/hr. The cartoon picture in Figure 3.11 simplistically illustrates this phenomenon. A dope line is connected with one side of the spinneret through a NPT joint. With the lower extrusion rate, the dope inside the spinneret will not be well mixed before a nascent fiber is extruded. In other words, the dope inside the spinneret is not uniformly distributed along the “X” direction, resulting in the varied pressure drop in the “Y” direction. More dope is extruded in the position close to the dope line, while less dope is extruded in the position far from the dope line. This forces the bore to deviate from the center and makes the wall thickness unevenly distributed. Although important, improving the spinneret design is not a goal of this work.

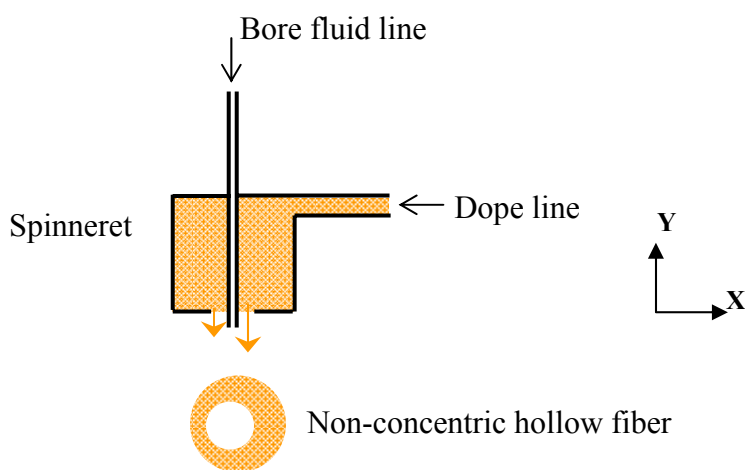


Figure 3.11: Cartoon picture showing the non-concentric hollow fiber due to design weakness of the spinneret

It is also noticed that many “macrovoids” are produced in the hollow fiber in Figure 3.10. Theoretically macrovoids jeopardize mechanical integrity, which can deteriorate the fiber performance in high pressure gas separation [3-4]. The formation of macrovoids has attracted more and more attention recently [31-34], but the clear picture has not been thoroughly addressed. Many types of instabilities exist and it is difficult to decouple each of them. McKelvey [4] proposed a hypothetical model to describe macrovoids generation and a practical framework to avoid macrovoids. In his explanation, macrovoids were generated during non-solvent induced phase separation in the quench bath through a very complicated mechanism. Paulsen et al. [34] noticed that minimizing the thickness of the fiber wall tended to dampen the macrovoid formation. However, these macrovoids do not cause any collapse or compaction of fibers in pervaporation of HAc/H₂O mixtures due to the low operating pressure (< 20 psi). Moreover, these macrovoids might actually further reduce the substructure resistance and assist penetrants through the membrane in pervaporation. As long as macrovoids exist in the support layer instead of the outer separation skin layer, the fiber performance will not be undermined in this project. It is important to promote the outer skin layer of a nascent fiber to vitrify in the air gap. Otherwise, further phase separation in the quench bath might generate macrovoids in the outer skin layer. SEM tests can be used to check the distribution of macrovoids in the fiber.

3.4.4 Key Spinning Variables to Control Fiber Size

As discussed in Chapter 2.3, spinning a large bore size hollow fiber is a solution to decrease the bore pressure change in separating HAc/H₂O mixtures. The current

spinning facility was designed to spin around 250 μm outer diameter and 150 μm inner diameter hollow fibers [26]. Modifying spinning variables, while still using the same spinning equipment (*spinneret*) to obtain a large bore size fiber, is discussed in this section.

For a given spinneret, the outer and inner diameters (O.D. and I.D.) of a hollow fiber are mainly controlled by the take-up rate and extrusion rate. The I.D. is usually $1/2 \sim 2/3$ of the O.D for practical applications [35]. Figure 3.12 shows the effects of the take-up rate on the O.D. when other spinning parameters are same. The O.D. increases with a decrease in the take-up rate. During the same time period, the length of the collected hollow fiber is reduced due to the low take-up rate, and thus the O.D. of this fiber is larger and the corresponding wall is thicker. An optical microscope is used to measure the outer and inner diameter of a hollow fiber.

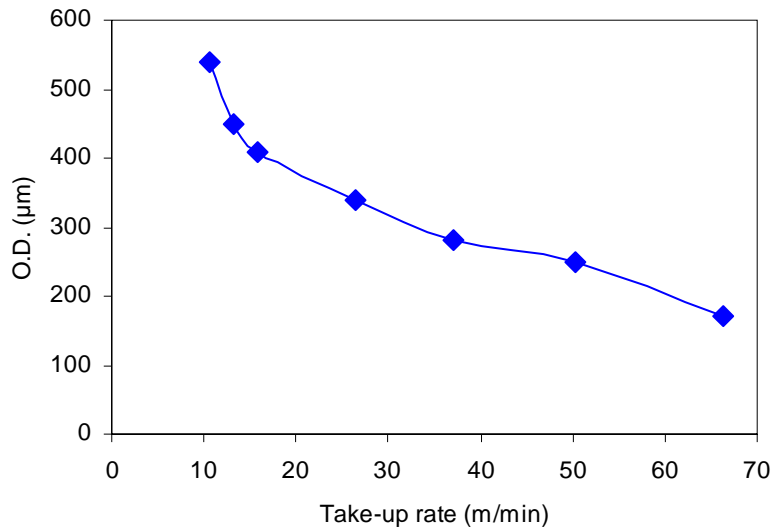


Figure 3.12: The take-up rate effects on the O.D. of hollow fibers

With the same take-up rate, the bore fluid extrusion rate mainly controls the I.D., while the O.D. is controlled by the dope extrusion rate. Typically high dope extrusion

rate is preferable as it enables high productivity for fiber fabrication. However, an excessive dope extrusion rate will cause less residence time in the water bath, which is difficult for the polymer to phase separate completely and smoothly. This might deform the cylindrical morphology of the hollow fiber if it is not sufficiently solid on the take-up drum. The dope extrusion rate is maintained around 180 ml/hr in this work [2]. Figure 3.13 shows the bore fluid extrusion rate effects on the I.D. It is reasonable that the I.D. increases with the enhancement of the bore fluid extrusion rate when the dope extrusion rate remains constant. In the mean time, the higher bore fluid extrusion rate drives the fiber wall thinner.

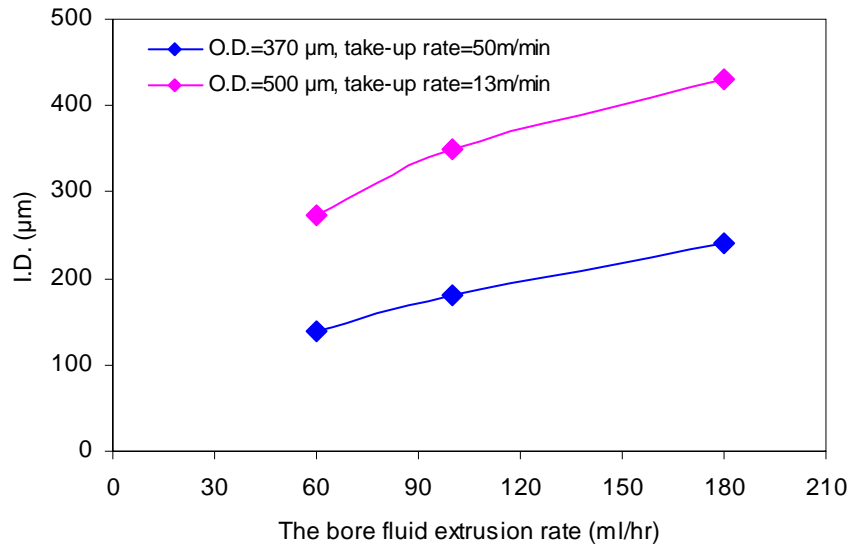


Figure 3.13: The effects of the bore fluid extrusion rate on the I.D. with the same dope extrusion rate

Ideally, slowing down the take-up rate and increasing the extrusion rate as much as possible can be used to maximize the O.D. and I.D. However, these two variables have to be properly balanced because excessively low take-up rate or excessively high extrusion rate will cause the fiber to “crinkle” in the quench bath. The cartoon picture

shown in Figure 3.14 describes this extreme condition. A nascent fiber reaches its relatively highest velocity when hitting the water bath. If the pulling velocity of the take-up drum can not overcome water viscous resistance and surface tension, the nascent fiber is difficult to go through and tends to crinkle in the water bath due to periodic instabilities. This crinkling issue can deform the fiber morphology and undermine its separation performance. The maximal outer diameter of a hollow fiber spun by the first generation spinneret is about 580 μm in this work. Thus, changing to a new spinneret is a final solution if larger diameter fibers are needed by other researchers.

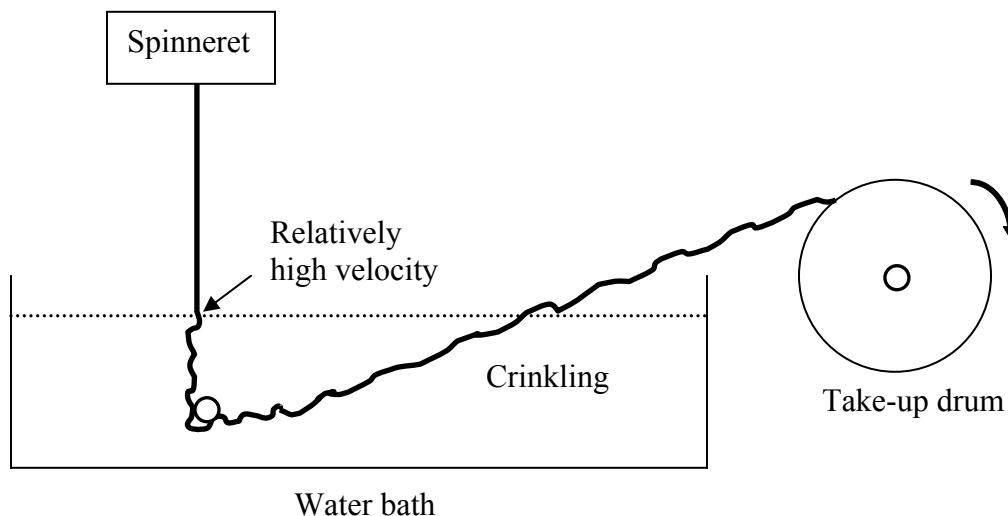


Figure 3.14: Cartoon picture showing the crinkling problem in the spinning process

Many combinations of spinning variables exist depending on the specific requirements of hollow fibers. It has been found that the take-up rate is the easiest variable to control the fiber size. In order to spin as large as possible fibers using the first generation spinneret, 12 m/min is the minimal take-up rate that can be achieved. Once the take-up rate is fixed, the variation of other major variables is strictly limited. Table 3.3

lists the key operation variables used to spin regular ($\sim 250\ \mu\text{m}$) and large diameter ($\sim 500\ \mu\text{m}$) hollow fibers in this thesis.

Table 3.3: Key variables used to spin regular and large diameter fibers

Spinning Variables	Fiber size	O.D. $\sim 250\ \mu\text{m}$ I.D. $\sim 150\ \mu\text{m}$	O.D. $\sim 500\ \mu\text{m}$ I.D. $\sim 320\ \mu\text{m}$
Take-up rate (m/min)		~ 50	~ 12
Dope extrusion rate (ml/hr)		~ 180	~ 180
Bore fluid extrusion rate (ml/hr)		~ 60	~ 100
Height of air gap (cm)		$5 \sim 20$	$7 \sim 12$
Temperature of a spinneret ($^{\circ}\text{C}$)		~ 50	~ 50
Temperature of a water bath ($^{\circ}\text{C}$)		~ 25	~ 25

3.5 Solvent Exchange and Drying

When hollow fibers are cut from the take-up drum, they have to be soaked in deionized (DI) water for a couple of days to achieve complete solvent removal. It is inevitable that the open porous substructure of the hollow fiber is filled with water. Direct drying of the fibers is not allowed, as this causes the collapse of the porous substructure, resulting in very low productivity fibers. Several methods have been proposed to safely dehydrate fibers [36-37]. Water has high surface tension and can cause enormous capillary force during drying. A solvent exchange process, in which water is replaced by volatile solvents with a lower surface tension, is usually undertaken before fibers are dried to prevent their collapse.

The first criterion to choose a liquid substitute for water is its low surface tension. The low surface tension liquid will minimize the capillary force and preserve the original morphology of the wet fibers. The second is the miscibility of this new liquid with water,

as water has to be completely expelled from the fibers. Finally, the liquid must be a non-solvent to the polymeric membranes and the interaction between this liquid and the polymer must be minimized.

A typical solvent exchange usually involves two steps. That is, a water soluble alcohol with low surface tension is used to replace water and a more volatile organic chemical with the lower surface tension is then used to substitute the alcohol. Table 3.4 lists the potential non-solvent candidates in the solvent exchange process. In this work, the fibers are solvent-exchanged with three separate 20 minutes methanol baths, followed with three 20 minutes hexane baths, exposed in air for 30 minutes, and finally dried under vacuum at 110°C for 1 hr to remove the residual non-solvents. The parameters in this phase may not be ideal, but they are workable, and time constraints do not permit optimization.

Table 3.4: Potential non-solvent candidates for the solvent exchange process [22]

Non-solvent	Normal boiling temperature (°C)	Surface tension (dynes/cm)	Molar enthalpy of vaporization at 25°C (kJ/mol)
Water	100	72.8	43.98
1-Propanol	97.4	23.8	29.62
2-Propanol	82.4	21.7	29.62
Methanol	65	22.6	37.43
Ethanol	78.5	22.8	42.32
n-Octane	125.7	21.8	41.49
n-Hexane	69	18.4	30.61
Acetone	56.2	23.7	30.99

3.6 Fiber Characterizations and Iterations

Although the fibers are used for pervaporation of HAc/H₂O mixtures, pure gas permeation must be tested first because this method can characterize the outer selective skin layer of a hollow fiber in the absence of swelling complications. The pure gas permeation results of a hollow fiber can be benchmarked with that of an intrinsic dense film to determine whether this fiber is defect-free or defective. The permeability and selectivity data for Matrimid[®] dense films are shown in Table 3.5.

Table 3.5: Permeability and selectivity of Matrimid[®] films tested @ 35°C, upstream pressure of 50-65 psi
(A), (B), and (C) represent different Matrimid[®] sources

Matrimid [®] films	Permeability (Barrers)		Selectivity	
	O ₂	He	O ₂ /N ₂	He/N ₂
(A) [38]	2.12		6.6	
(B) [39]	1.35	20.7	7.1	90
(C)	2.19	26.3	6.6	80

3.6.1 Pure Gas Permeation Tests

The technology to pot dry fibers into a double-ended module is described in Appendix A. A bubble flow method, which has been well established in our lab, is used to measure pure gas permeation of the double-ended module at a feed pressure of 100 psi and temperature of 35°C. Pure nitrogen, oxygen, and helium are most commonly used gases due to their lack of interaction with polymers (“neutral” property). The pressure on the permeate side is one atmosphere and the gas flow rates are measured with a bubble flowmeter and stopwatch. The bore pressure change has to be corrected with shell feed

for highly permeable gases, as discussed in Chapter 2.3.2. Figure 3.15 shows the pure gas permeation set-up.

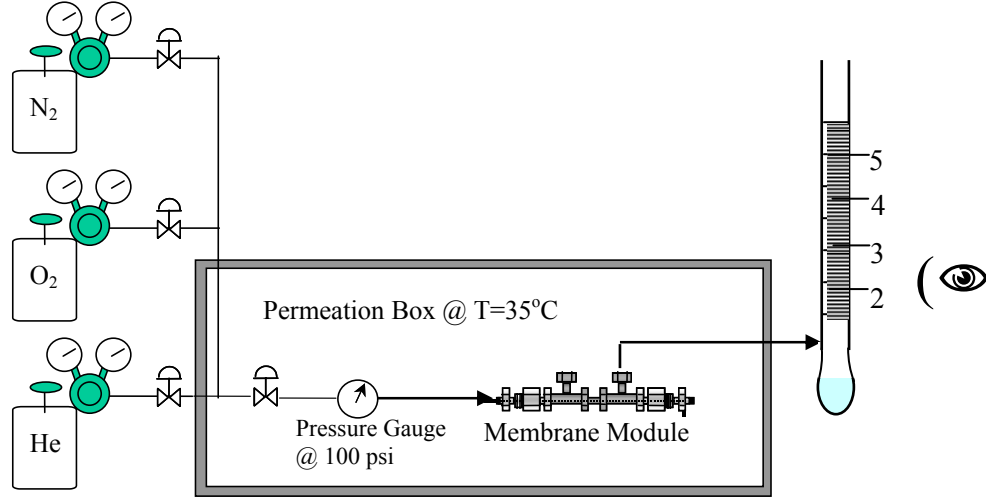


Figure 3.15: Experimental set-up for pure gas permeation tests

An example to measure N_2 permeance is discussed briefly (Appendix B provides detailed procedures for pure gas permeation tests). This can be easily applied to other pure gas permeation tests. The whole permeation system has to be purged by N_2 in the first step until a permeation flowrate and inner permeation box temperature reach the steady state. Next the permeate flowrate is measured with a bubble flowmeter for a couple of times until the tolerable errors are obtained. N_2 permeance with the unit of GPU can be calculated using equation 3.1.

$$\left(\frac{\mathcal{P}}{\ell}\right)_{N_2} [\text{GPU}] = 10^6 \cdot \frac{F \cdot 273.15}{T \cdot A \cdot \Delta p \cdot 5.17} \quad (3.1)$$

where \mathcal{P} is the permeability of N_2 , ℓ is the thickness of the outer skin layer, $\left(\frac{\mathcal{P}}{\ell}\right)_{N_2}$ is the permeance of N_2 with the unit of GPU, T is the inner box temperature with the unit of

Kelvin, A is the permeation area in cm^2 , Δp is the pressure drop between upstream and downstream sides of a membrane in psi, and F is the permeate flowrate with the unit of ml/sec. The ideal selectivity can be obtained as follows:

$$\alpha_{A/B} = \frac{\left(\frac{P}{\ell}\right)_A}{\left(\frac{P}{\ell}\right)_B} \quad (3.2)$$

In terms of the permeability of N_2 , O_2 , and He as noted earlier (equation 2.11), the theoretical or ideal thickness of the outer separation skin layer ℓ can be calculated by

$$\ell[\mu\text{m}] = \frac{P[\text{Barrer}]}{\left(\frac{P}{\ell}\right)[\text{GPU}]} \quad (3.3)$$

The fiber selectivity must be close to the intrinsic one for equation 3.3 to be meaningful.

The permeation data for five different state fibers are summarized in the following table.

Table 3.6: Gas permeation data for a dense film and five different state fibers
@ 35°C , upstream pressure of 100 psi. $\pm 2\%$ Error

Hollow fiber State ID	O.D. (μm)	Permeance (GPU)		Selectivity		Ideal skin thickness ℓ (μm)
		O_2	He	O_2/N_2	He/ N_2	
Dense film				6.6	85	
FB5.13	250	4.86	64	6.8	90	0.44
FB4.5	375	2.47	32	6.7	86	0.86
FB5.4	450	5.16	66	6.8	87	0.41
FB5.15	580	4.68	62	6.9	92	0.46
FB5.3	500	9.0	82	2.3	21	

With the outer diameter ranging from 250 μm to 580 μm , the FB5.13, FB4.5, FB5.4, and FB5.15 state fibers exhibit close or better membrane selectivity for O_2/N_2 and He/N_2 pairs than the intrinsic results within experimental uncertainty ($\pm 2\%$). This is clearly indicative of the defect-free outer skin layer. Further, physical aging is considered to be responsible for the higher selectivity in hollow fibers. Due to the non-equilibrium nature of glassy polymers, a continual evolution occurs towards its equilibrium state over time. This process is known as physical aging [40-42] that is related to the free volume relaxation, i.e. segmental mobility of the polymer chains. Although more free volume is frozen in the outer skin layer of an asymmetric hollow fiber due to its rapid phase separation, physical aging in the thin layer of a hollow fiber is believed to occur *much faster than that in a dense film* [43-46]. This allows the polymer chains of a fiber to be more tightly packed than those of a dense film and thus increases the membrane selectivity. Slightly different pure gas permeance is observed in each of these four defect-free hollow fibers due to different thickness of the outer selective layer. The higher resistance exists in the thicker outer selective layer of the hollow fiber, resulting in the decreased gas permeance.

As noted earlier, substrate resistance of a hollow fiber can be another important factor to influence permeation properties and needs to be characterized properly [47-48]. Helium is the fastest and most permeable gas and can be affected much more than others by the substrate resistance. The membrane selectivities of He/N_2 ($\alpha_{\text{He}/\text{N}_2}$) and O_2/N_2 ($\alpha_{\text{O}_2/\text{N}_2}$) pairs are usually used as an indication of the substrate resistance, as stated in Chapter 2.4. If the relative depression of $\alpha_{\text{He}/\text{N}_2}$ is much larger than $\alpha_{\text{O}_2/\text{N}_2}$ compared to a dense film (i.e. $\alpha_{\text{O}_2/\text{N}_2}$ is still close to intrinsic, but $\alpha_{\text{He}/\text{N}_2}$ is less than intrinsic), the

substrate resistance can not be neglected any more. It is clear that no substrate resistance exists for the first four state fibers. FB5.3 fiber is defective due to its very low selectivity and high permeance. If defects are small enough, the post-treatment with a silicone rubber can caulk the skin layer and recover the selectivity back to intrinsic in pure gas permeation tests [7]. However, FB5.3 fiber can not be used for pervaporation of HAc/H₂O mixtures since the caulking method often fails for aggressive liquid feeds. Iterations are necessary to solve the defective skin problem by optimizing spinning variables.

3.6.2 Microscopy Tests

Although pure gas permeation is a reliable method to characterize the outer selective layer of a hollow fiber, microscopy tests can also be used to investigate the morphology of a hollow fiber *roughly*.

The cross-section morphology of a hollow fiber can be examined using the optical microscope (Leitz Laborlux 12 ME S). 10x magnification is used to measure the outer and inner diameters of a hollow fiber in this work.

Scanning electron microscopy (Hitachi S-800 FE-SEM) is used to investigate the fiber morphology more accurately. A SEM picture for the cross-section of a large bore size defect-free hollow fiber is shown in Figure 3.16.

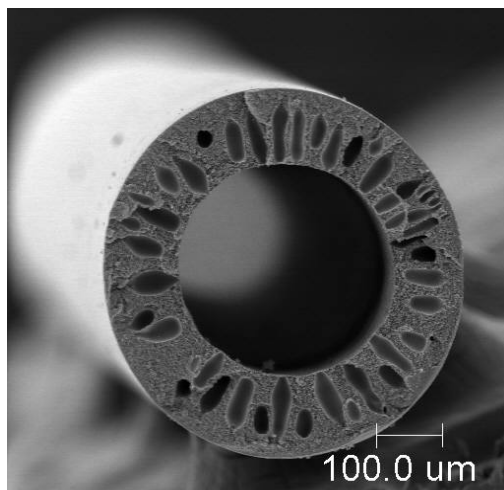


Figure 3.16: SEM picture showing the cross section of a hollow fiber with the defect-free skin layer and the outer diameter of 450 μm

With magnification higher than 3000x, a skin layer, transition layer, and open porous substructure of a hollow fiber can be distinguished using SEM. As shown in Figure 3.17, the outer skin layer of FB5.4 fiber is around 0.45 μm visually, which is very close to the pure gas permeation result.

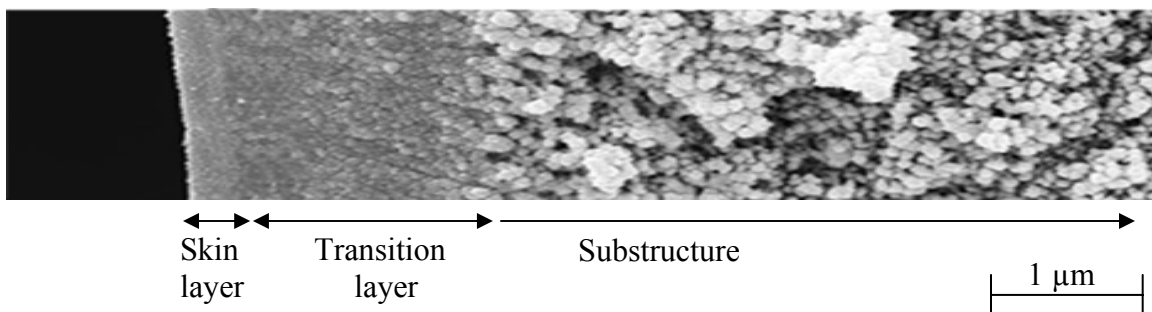


Figure 3.17: SEM picture of FB5.4 fiber showing a skin layer, transition layer and open porous substructure

3.7 Summary

Current spinning technology has been successfully improved to obtain a large bore size defect-free outer skin layer hollow fiber from Matrimid[®] in this work. From

dope preparation, fiber spinning, solvent exchange and drying, to pure gas permeation tests, this chapter elaborates systematic approaches and theoretical mechanisms (mass transfer) in depth.

The take-up rate is the most sensitive and easy to adjust variable to control the fiber size in contrast to other spinning variables. Once this variable is fixed, the variations of other variables are very limited. The dope composition plays an important role in the formation of a defect-free outer skin layer. Adding more volatile solvent and maintaining the same amount of Matrimid[®] in a dope are helpful to form a defect-free skin layer in the air gap, while still preserving an open porous substructure in the quench bath. These large bore size defect-free fibers exhibit good gas separation performance and will be used to separate HAc/H₂O mixtures in the following chapter.

3.8 References

- [1] Loeb, S. and Sourirajan, S. *Sea water demineralization by means of an osmotic membrane*. Adv. Chem. Ser. 1962, 38, 117-132.
- [2] Clausi, D.T. *Formation and characterization of asymmetric polyimide hollow fiber membranes for gas separations*. Ph.D. Dissertation, The University of Texas at Austin, 1998.
- [3] Wallace, D.W. *Crosslinked hollow fiber membranes for natural gas purification and their manufacture from novel polymers*. Ph.D. Dissertation, The University of Texas at Austin, 2004.
- [4] McKelvey, S.A. *Formation and characterization of hollow fiber membranes for gas separation*. Ph.D. Dissertation, The University of Texas at Austin, 1997.
- [5] Ekiner, O.M., Hayes, R.A., and Manos, P. *Reactive post treatment for gas separation membranes*. United States Patent 5,091,216, E.I. du Pont de Nemours, 1992.
- [6] Henis, J.M.S. and Tripodi, M.K. *Composite hollow fiber membranes for gas separation: The resistance model approach*. J. Membr. Sci. 1981, 8, 233-246.

- [7] Henis, J.M.S. and Tripodi, M.K. *Multicomponent membranes for gas separations*. United States Patent 4,230,463, Monsanto Co. 1980.
- [8] Reuvers, A.J., Van den Berg, J.W.A., and Smolders, C.A. *Formation of membranes by means of immersion precipitation. Part I. A model to describe mass transfer during immersion precipitation*. J. Membr. Sci. 1987, 34, 45-65.
- [9] Barrer, R.M. *Diffusion and permeation in heterogeneous media, in Diffusion in polymers*. J. Crank and G.S. Park, Editors. 1968, Academic Press: New York. 165-217.
- [10] Hayes R. A. *Polyimide Gas Separation membranes* United States Patent 4,705,540, E.I. Du Pont de Nemours, 1987.
- [11] Davis T.E. and Overman D. C. *Process for Drying Water-Wet Membranes* United States Patent 4,430,807, Dow Chemical 1984.
- [12] Van de Witte, P., Dijkstra, P.J., Van den Berg, J.W.A., and Feijen, *Phase separation processes in polymer solutions in relation to membrane formation*. J. Membr. Sci. 1996, 117, 1-31.
- [13] Pinnau, I. and Freeman, B.D. *Membrane formation and modification*. ACS Symposium Series 744, 1999.
- [14] Castellan, G.W. *Physical chemistry*. The Benjamin/Cummings Publishing Company, Inc. 3rd Ed. 1983.
- [15] Machado, P.S.T., Habert, A.C. and Borges, C.P. *Membrane formation mechanism based on precipitation kinetics and membrane morphology: flat and hollow fiber polysulfone membranes*. J. Membr. Sci. 1999, 155, 171-183.
- [16] Koros, W.J. and Fleming, G.K. *Membrane-based gas separation*. J. Membr. Sci. 1993, 83, 1-80.
- [17] Koros, W.J., Pinnau, I. *In polymeric gas separation membranes*; Pual, D.R. and Yampol'skii, Y.P., Eds.; CRC Press: Boca Raton, LA, 1994; Chapter 5.
- [18] Ismail, A.F. and Yean, L.P. *Review on the development of defect-free and ultrathin-skinned asymmetric membranes for gas separation through manipulation of phase inversion and rheological factors*. J. Appl. Poly. Sci. 2003, 88, 442-451.
- [19] Mckelevy, S.A., Clausi, D.T., and Koros, W.J. *A guide to establishing hollow fiber macroscopic properties for membrane applications*. J. Membr. Sci. 1997, 124, 223-232.

- [20] Carruthers, S.B., Ramos, G.L., and Koros, W.J. *Morphology of integral-skin layers in hollow-fiber gas-separation membranes*. J. Appl. Poly. Sci. 2003, 90, 399-411.
- [21] Wang, D., Li, K., and Teo, T.K. *Highly permeable polyethersulfone hollow fiber gas separation membranes prepared using water as non-solvent additive*. J. Membr. Sci. 2000, 176, 147-158.
- [22] Lide, D.R. *Handbook of chemistry and physics*. CRC press. 1995-1996, 76th, 3.3-3.330.
- [23] Boom, R.M., Boomgaard, T.v.d., Berg, J.W.A.v.d., and Smolders, C.A. *Linearized cloudpoint curve correlation for ternary systems consisting of one polymer, one solvent and one non-solvent*. Polymer. 1993, 34, 2348-2356.
- [24] Chung, T.S., E.R. Kafchinski, and R. Vora, *Development of a Defect-Free 6FDA-Durene Asymmetric Hollow Fibers and its Composite Hollow Fibers*. J. Membr. Sci. 1994, 88, 21-36.
- [25] Tao, W., J.R. Collier, and B.J. Collier, *Evaluation of Interfacial Adhesion in Sheath/Core Composite Fibers*. J. Appl. Poly. Sci. 1993, 47, 1115-1122.
- [26] Pesek, S.C. *Aqueous quenched asymmetric polysulfone flat sheet and hollow fiber membranes prepared by dry/wet phase separation*. Ph.D. Dissertation, The University of Texas at Austin, 1993.
- [27] Rhodes, E. *Spinnerets for hollow fiber membranes: design & modeling*. 2004 (Internal report in Dr. William Koros' group).
- [28] Pesek, S. C. and Koros, W.J. Aqueous quenched asymmetric polysulfone membranes prepared by dry/wet phase separation. J. Membr. Sci. 1993, 81, 71-82.
- [29] Pinnau, I. and Koros, W.J. A Qualitative skin formation mechanism for membranes made by dry/wet phase inversion. J. Poly. Sci., Poly. Phys. Ed. 1993, 31, 419-427.
- [30] Carruthers, S.B. *Integral skin formation in hollow fiber membranes for gas separations, in chemical engineering*. Ph.D. Dissertation, The University of Texas at Austin, 1997.
- [31] McHugh, A.J. and Tsay, C.S. *Dynamics of the phase inversion process*. J. Appl. Poly. Sci. 1992, 46, 2011-2021.
- [32] Tsay, C.S. and McHugh, A.J. *A rationale for structure and formation during phase inversion*. J. Poly. Sci. Part. B 1992, 30, 309-313.

- [33] Smolders, C.A., Reuvers, A.J., Boom, R.M., and Wienk, I.M. *Microstructure in phase-inversion membranes. Part I. Formation of macrovoids*. J. Membr. Sci. 1992, 73, 259-275.
- [34] Paulsen, F.G., Shojaie, S.S., and Krantz, W.B. *Effect of evaporation step on macrovoid formation in wet-cast polymeric membranes*. J. Membr. Sci. 1994, 91, 265-282.
- [35] Ekiner, O.M. and Vassilatos, G. *Polyaramide hollow fiber for hydrogen/methane separation-spinning and properties*. J. Membr. Sci. 1990, 53, 259-273.
- [36] Manos, P. *Solvent exchange drying of membranes for gas separation*. United States Patent 4,120,098.
- [37] Park, H.C., Moon, Y.S., Rhee, H.W., Won, J., Kang, Y.S., and Kim, U.Y. *Effect of solvent exchange on the morphology of asymmetric membranes, in membrane formation of modification*, Pinnau, I. and Freeman, B., Ed. 2000, ACS: Washington, D.C. 110-124.
- [38] Vu, D.Q. *Formation and characterization of asymmetric carbon molecular sieve and mixed matrix membranes for natural gas purification*. Ph.D. Dissertation, The University of Texas at Austin, 2001.
- [39] Ekiner, O.M. and Hayes, R.A. *Phenylindane-containing polyimide gas separation membranes*. United States Patent 5,015,270, E.I. du Pont de Nemours, 1991.
- [40] Kovacs, A. J. *La Contraction Isotherme du Volume des Polyme ´res Amorphes*. J. Polym. Sci. 1958, 30, 131-147.
- [41] Struik, L. C. E. *Physical Aging in Amorphous Polymers and Other Materials*. Elsevier Science Publishing Company, Inc. New York, 1978.
- [42] Aref-Azar, A. and Hay, J. N. *Physical Aging in Glassy Polymers, an I. R. Spectroscopic Investigation of Poly(ethylene terephthalate)*. Polymer. 1982, 23, 1129-1132.
- [43] McCaig, M.S. and Paul, D.R. *Effect of film thickness on the changes in gas permeability of a glassy polyarylate due to physical aging Part I. Experimental observations*. Polymer. 2000, 41, 629-637.
- [44] McCaig, M.S., Paul, D.R., and Barlow, J.W. *Effect of film thickness on the changes in gas permeability of a glassy polyarylate due to physical aging Part II. Mathematical model*. Polymer. 2000, 41, 639-648.

- [45] Dorkendo, K.D. and Pfromm, P.H. *Experimental evidence and theoretical analysis of physical aging in thin and thick amorphous glassy polymer films.* J. of Polym. Sci. Part B: Polym. Phy. 1999, 37, 2239-2251.
- [46] Rezac, M.E., Pfromm, P.H., Costello, L.M., and Koros, W.J. *Aging of thin polyimide-ceramic and polycarbonate-ceramic composite membranes.* Ind. Eng. Chem. Res. 1993, 32, 1921-1926.
- [47] Clausi, D.T., McKelvey, S.A. and W.J. Koros, *Characterization of substructure resistance in asymmetric gas separation membranes.* J. Membr. Sci. 1999, 160, 51-64.
- [48] Henis, J.M.S. and Tripodi, M.K. *Composite hollow fiber membranes for gas separation: the resistance model approach.* J. Membr. Sci. 1981, 8, 233-246.

Chapter 4: Pervaporation to Separate HAc/H₂O Mixtures Using Matrimid[®] Hollow Fibers

4.1 Introduction

As discussed in Chapter 1.1, acetic acid is an important organic chemical in the synthesis of terephthalic acid, vinyl acetate, acetic anhydride, and cellulose esters in industry. Acetic acid and water are the main components in the recycling stream. Because of the small difference in the volatility of acetic acid (b.p. 117°C) and water (b.p. 100°C), a large number of trays and high reflux ratio are used to obtain glacial acetic acid with conventional distillation [1-4]. This separation is undeniably an energy-intensive process.

Membrane-based pervaporation is attractive to separate aqueous organic mixtures due to its energy-conservative properties [5]. While evaporation separation is governed by the thermodynamic equilibrium, the separation performance of pervaporation more relies on the identities of membrane materials [6-7]. That is, a membrane is seen as separating a hypothetical vapor feed that is in equilibrium with the actual liquid feed, and the size (diffusion) and solubility (sorption) differences between penetrants are crucial factors for separation instead of thermo issues. If a proper membrane material is selected, pervaporation is superior to distillation to separate close-boiling point mixtures such as HAc/H₂O mixtures. Pervaporation combines two separation mechanisms, which are illustrated in equation 4.1 (with a negligible downstream pressure).

$$\beta_{\text{Perva}} = \alpha_{\text{mem}} \cdot \alpha_{\text{EVAP}} \quad (4.1)$$

where β_{Perva} represents the overall separation factor that characterizes the efficiency of a pervaporation system. α_{mem} represents the membrane selectivity that is related to

material identity, while α_{EVAP} is the evaporation factor that accounts for thermodynamic contributions.

This chapter will use regular and large bore size defect-free hollow fibers to separate HAc/H₂O mixtures. The experimental set-up and test procedures are presented in the first section. After that, the preliminary work is presented to investigate the possibility of utilizing a Matrimid[®] hollow fiber in pervaporation. Permeance $\frac{P}{\ell}$, separation factor β_{Perva} , and membrane selectivity α_{mem} are examined based on the bore size of fibers, HAc concentration in feeds, and operation history.

4.2 Pervaporation Module Fabrication

A hollow fiber must be mounted or potted into a vessel for pervaporation tests. The basic concept of pervaporation module fabrication remains the same with gas separation modules shown in Appendix A. The fibers have to be sealed in such a manner as to allow liquid or vapor to contact one side of the fibers, while a low pressure or vacuum is maintained on the other side, so that mass transfer can occur across the membrane. This requires an airtight seal that is referred to as a tubesheet. The tubesheet is usually formed with epoxy or similar materials.

The technique of fabricating a pervaporation module is non-trivial and represents a significant challenge for separator commercialization [8-10]. For example, the selection of potting materials involves numerous factors, including their thermal and chemical resistance, mechanical strength, interaction with polymers and penetrants. Although important, this is not our focus in this work.

A “double-ended single-fiber” pervaporation module, in which only one hollow fiber is potted at both ends, is used in this pervaporation system. Two tubesheets isolate the outer fiber surface from the fiber bore. Moreover, a clean pot face must be produced, which is referred to as the surface of a potting material permitting the gas or vapor passage through the bore. The cartoon picture of a pervaporation module is shown in Figure 4.1 (A) and Figure 4.1 (B) shows the optical microscopy picture of a pot face. Manufacture of lab-scale pervaporation modules is described in Appendix C.

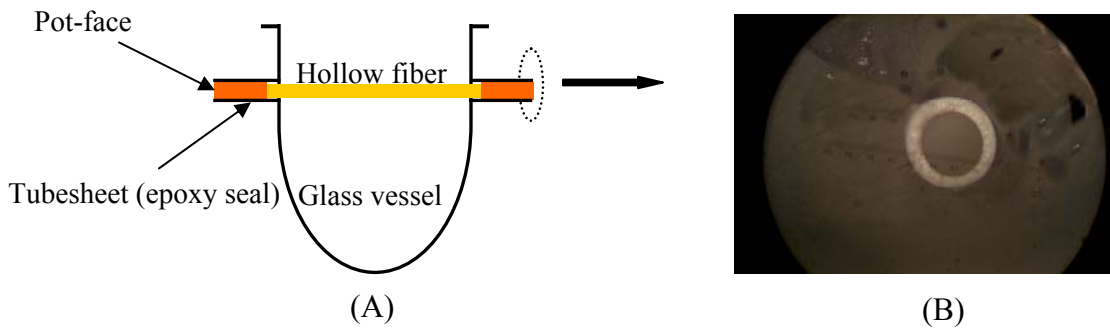


Figure 4.1: Laboratory single-fiber pervaporation module
 (A) Cartoon picture showing a double-ended module
 (B) Optical microscopy picture showing a pot-face with an open bore

4.3 Pervaporation Set-up

Once a pervaporation module is ready, it should be connected with a pervaporation system. Figure 4.2 is a schematic flowchart of a typical pervaporation process. A single-fiber module with two sealed ends is soaked in a liquid feed at about 101°C. The permeate vapor passes through the bore side of a hollow fiber and is collected at the downstream by condensing it using liquid nitrogen cold traps. It is apparent that significant opportunities exist for shell feed in this work whereas bore feed has a weakness [11]. For example, it is difficult to circulate a feed solution inside the bore with

an inner diameter of 150 - 350 μm . This can cause strong concentration-polarization inside the bore of a fiber. Although a bore pressure change associated with high flux pervaporation is significant for shell feed, it can be minimized by applying a large bore size hollow fiber in pervaporation. Moreover, excellent circulation is available for shell feed so that both concentration-polarization and external mass transfer resistance can be effectively avoided.

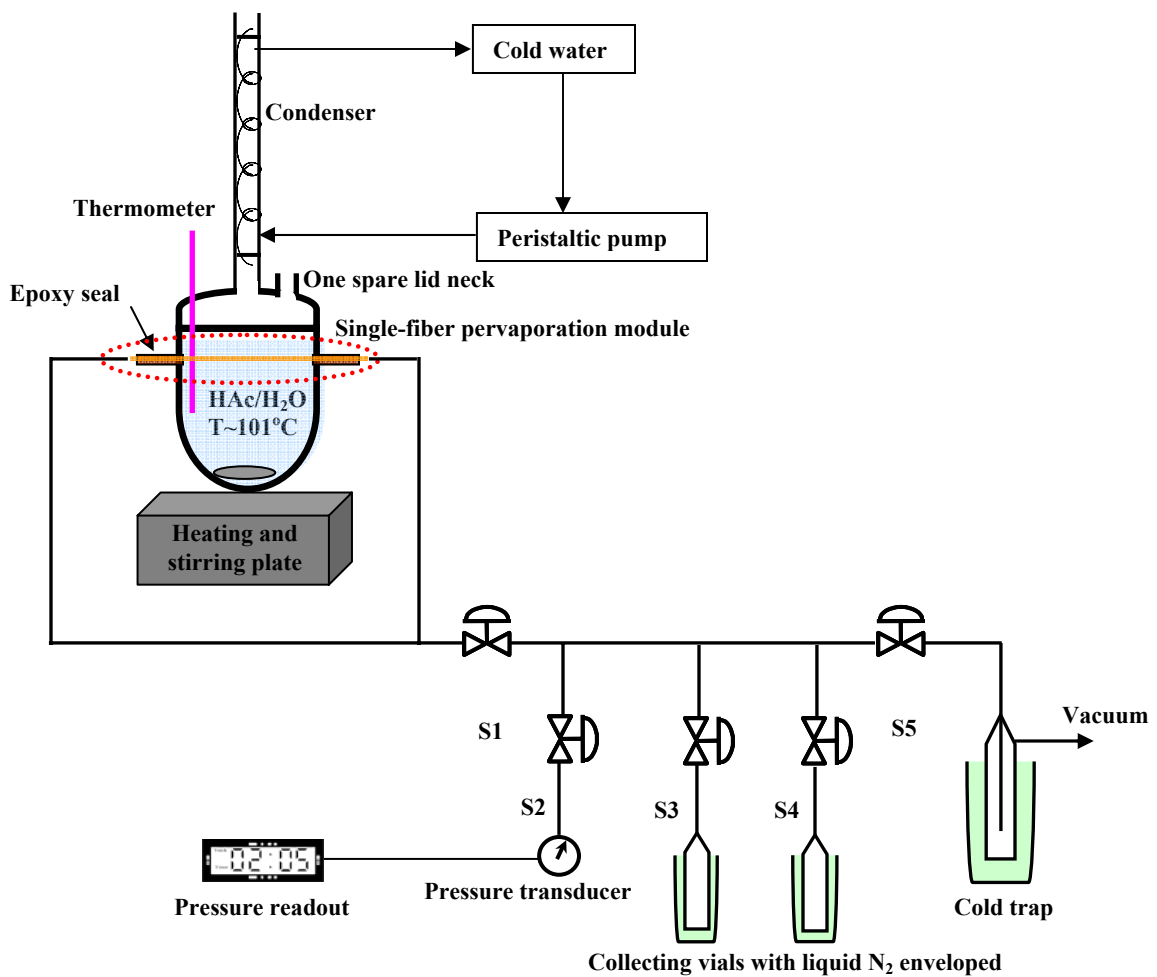


Figure 4.2: A hollow fiber-based pervaporation system

It should be pointed out that a hot vapor feed, rather than a pervaporation process, is more likely in industry. That is, the pervaporation module is fed with a saturated mixed vapor instead of a liquid mixture. From a thermodynamic standpoint, the activities of penetrants are the same at the vapor-liquid equilibrium state. The equilibrium sorption uptakes are equivalent in both cases, but the need to transfer heat of vaporization into the module is eliminated with a hot vapor feed. Thus, their separation results should not be noticeably different at the same temperature with either a liquid or its saturated vapor feed. Only a liquid feed is investigated in this research for simplicity, but it can be easily extended to a vapor case.

4.4 Pervaporation Experiments

4.4.1 Procedures

A well-prepared pervaporation module has to be connected first with a pervaporation system and then with a condenser. A peristaltic pump is used to circulate cold water in the condenser to avoid the loss of hot vapor. A continuously stirred HAc/H₂O mixture is heated until its temperature reaches the required value. In the mean time, all the valves (S1 through S5) remain open and vacuum is drawn in the whole system until the downstream pressure is less than 0.5 torr. It usually takes 2 - 3 hours to allow the system to reach the steady state. Thereafter, S5 valve is closed to shut off vacuum and permeate samples are condensed by liquid nitrogen and collected in two small vials. The samples are collected for 2 to 5 hours, depending on the required amount. The detailed operating procedure is provided in Appendix D. All the modules

are stored in a pure DI water bath before and after a pervaporation test unless it is otherwise specifically mentioned.

4.4.2 Sample Analysis

The concentration of each component in a feed solution and permeate sample can be measured accurately by the refractometer (Leica ARIAS 500) because of large differences in the refractive indices (RI) for acetic acid (RI=1.37100) and water (RI=1.33150) at 21.5~22.5°C. Two calibration curves are provided in Figure 4.3. One of them is used to test the HAc concentration in permeates in a low HAc concentration window, and the other one is applied for a high HAc concentration window.

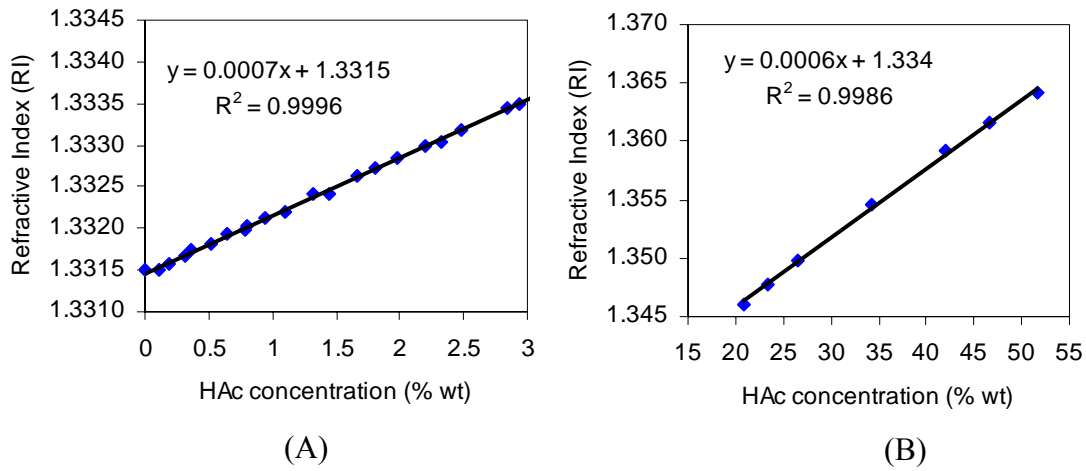


Figure 4.3: Calibration curves to measure the HAc concentration in aqueous mixtures $\pm 2\%$ Error
 (a) Low HAc concentration window (permeate side)
 (b) High HAc concentration window (feed side)

The concentration of each component can be calculated from the RI. The separation factor, $\beta_{\text{H}_2\text{O}/\text{HAc}}$, defined as the ratio of components in a permeate vapor over the ratio of components in a feed liquid, can be obtained as below,

$$\beta_{\text{H}_2\text{O}/\text{HAc}} = \frac{y_{\text{H}_2\text{O}}/y_{\text{HAc}}}{x_{\text{H}_2\text{O}}/x_{\text{HAc}}} = \frac{(1 - y_{\text{HAc}})/y_{\text{HAc}}}{(1 - x_{\text{HAc}})/x_{\text{HAc}}} \quad (4.2)$$

where $x_{\text{H}_2\text{O}}$ and x_{HAc} are the mass fractions of H_2O and HAc on the feed liquid side, and $y_{\text{H}_2\text{O}}$ and y_{HAc} are the mass fractions of H_2O and HAc on the vapor permeate side of the membrane.

The vials used to collect permeates have to be cleaned and weighed (w_1) before each pervaporation test. After the experiment is completed, these vials are taken out of liquid nitrogen dewars, covered with parafilms, warmed to room temperature, and weighed together with the permeate samples (w_2). The weight of the collected sample is equal to the weight difference before and after pervaporation, i.e. $w = w_2 - w_1$. Thus, the flux of H_2O and HAc can be calculated by

$$\begin{cases} Q_{\text{H}_2\text{O}} = \frac{w \cdot y_{\text{H}_2\text{O}}}{\Delta t \cdot (\pi D \cdot L)} \\ Q_{\text{HAc}} = \frac{w \cdot y_{\text{HAc}}}{\Delta t \cdot (\pi D \cdot L)} \end{cases} \quad (4.3)$$

where D is the outer diameter of a hollow fiber (m), L is the available module length for separation (m), Δt is the collecting time (hr), w is the weight of the total permeates (kg), and Q is the penetrant flux ($\text{kg}/\text{m}^2\text{hr}$).

If the bore size of a hollow fiber is large enough and the pressure buildup inside the bore is negligible, the permeance and membrane selectivity can be simplified as equations 4.4 and 4.5, respectively. Otherwise, both the permeance and membrane selectivity have to be corrected due to the bore pressure change. Chapter 5 provides a method to account for the bore pressure change to obtain the inherent membrane selectivity.

$$\begin{cases} \left(\frac{\mathcal{P}}{\ell}\right)_{\text{H}_2\text{O}} = \frac{Q_{\text{H}_2\text{O}}}{\gamma_{\text{H}_2\text{O}} x_{\text{H}_2\text{O}} p_{\text{H}_2\text{O}}^*} = \frac{Q_{\text{H}_2\text{O}}}{\gamma_{\text{H}_2\text{O}} \cdot (1 - x_{\text{HAc}}) \cdot p_{\text{H}_2\text{O}}^*} \\ \left(\frac{\mathcal{P}}{\ell}\right)_{\text{HAc}} = \frac{Q_{\text{HAc}}}{\gamma_{\text{HAc}} x_{\text{HAc}} p_{\text{HAc}}^*} \end{cases} \quad (4.4)$$

where $\gamma_{\text{H}_2\text{O}}$ and $p_{\text{H}_2\text{O}}^*$ represent the activity coefficient and saturated vapor pressure for H_2O , γ_{HAc} and p_{HAc}^* represent the activity coefficient and saturated vapor pressure for HAc , $\left(\frac{\mathcal{P}}{\ell}\right)_{\text{H}_2\text{O}}$ and $\left(\frac{\mathcal{P}}{\ell}\right)_{\text{HAc}}$ represent the permeances of HAc and H_2O . The corresponding membrane selectivity $\alpha_{\text{H}_2\text{O}/\text{HAc}}$, instead of the separation factor $\beta_{\text{H}_2\text{O}/\text{HAc}}$, can be expressed by

$$\alpha_{\text{H}_2\text{O}/\text{HAc}} = \frac{\left(\frac{\mathcal{P}}{\ell}\right)_{\text{H}_2\text{O}}}{\left(\frac{\mathcal{P}}{\ell}\right)_{\text{HAc}}} \quad (4.5)$$

It should be clarified that the separation factor, $\beta_{\text{H}_2\text{O}/\text{HAc}}$, and the membrane selectivity, $\alpha_{\text{H}_2\text{O}/\text{HAc}}$, are two different concepts. $\alpha_{\text{H}_2\text{O}/\text{HAc}}$ decouples the effects of operating conditions on the membrane performance and stresses the identities of membrane materials [12-13], while $\beta_{\text{H}_2\text{O}/\text{HAc}}$ characterizes the separation capability of the whole pervaporation system. Both results will be provided in the later work to get a better understanding of each aspect.

4.5 Experimental Results and Discussion

Although our goal focuses on liquid separation in this research, it is necessary to perform gas permeation first to probe the structure and properties of a fiber. In other words, pure gas permeation tests are applied to characterize the nature of a fiber -- “a

defect-free fiber vs. a defective fiber”. The intrinsic selectivity of a Matrimid[®] dense film for the O₂/ N₂ pair, α_{O_2/N_2} , is about 6.6 at 35°C [14]. A hollow fiber with selectivity greater than 90% of intrinsic (i.e. 6.0) is defined as a “defect-free” fiber. Table 4.1 shows the gas permeation results of the hollow fibers that will be used to separate HAc/H₂O mixtures for pervaporation in the following sections. As it can be seen, all the fibers are defect-free although the thickness of the outer separation skin layer varies. A pervaporation module is numbered following the fiber identification, for example, a module made with the FB1.4 state fiber is named as “FB1.4_1.”

Table 4.1: Pure gas permeation results for defect-free hollow fibers that are used to separate HAc/H₂O mixtures in pervaporation

* Calculated based upon pure gas permeation tests using Equation 3.3

Fiber Identification	O.D. (μm)	I.D. (μm)	O₂ (GPU)	Selectivity α_{O_2/N_2}	Ideal skin thickness* (μm)
DW24.2	283	168	1.70	6.9	1.25
DW24.3	272	158	2.12	6.0	1.01
FB1.4	230	136	3.80	6.9	0.56
FB2.6	487	289	2.66	6.3	0.79
FB4.5	375	229	2.47	6.7	0.86
FB4.7	520	331	3.25	6.8	0.65
FB4.12	567	431	3.47	6.6	0.61
FB5.6	520	325	3.27	6.7	0.65
FB5.13	230	140	5.01	6.8	0.43
FB5.15	580	376	4.68	6.9	0.46

For a given fiber, a typical pervaporation test begins at 100-104°C for three hours, which is more than sufficient time to reach the steady state for a thin selective layer. Thereafter, the permeate is collected for two or three hours at the same temperature. Longer term tests are also done and will be reported later.

It should be pointed out that membrane-to-membrane differences in properties are still a challenge today. Two fibers from the same spinning state might not demonstrate the exact same separation results. A small change in the key parameters, such as the packing density of polymer chains and thickness of the outer separation layer, can cause observable but acceptable discrepancies. Experimental uncertainty in this work is about $\pm 5\%$.

4.5.1 “Proof of Concept” Work

Acetic acid and water mixtures were prepared based upon the required composition for a feed solution before pervaporation tests. The concentration of each component in a feed solution was also evaluated using the refractometer.

The schematic testing procedures for DW24.3_3 module with an outer diameter of 272 μm and FB4.7_2 module with 520 μm are shown in Figure 4.4. A model 20% wt HAc/H₂O mixture was used as a feed at 101.5°C first. Next pure DI water was used to replace the mixture and perform a pervaporation test at 100°C. When this procedure was completed, the same module was tested for a model 20% wt HAc/H₂O mixture and pure DI water sequentially under the same condition. The water flux, $Q_{\text{H}_2\text{O}}$, and the separation factor, $\beta_{\text{H}_2\text{O}/\text{HAc}}$, are shown in Figure 4.5. Water is believed to have very trivial effects on Matrimid[®] since fibers are usually soaked in water to remove the residual solvents during

the spinning process [15-16]. Thus, these alternative feeds were used in pervaporation to avoid other perturbing factors.

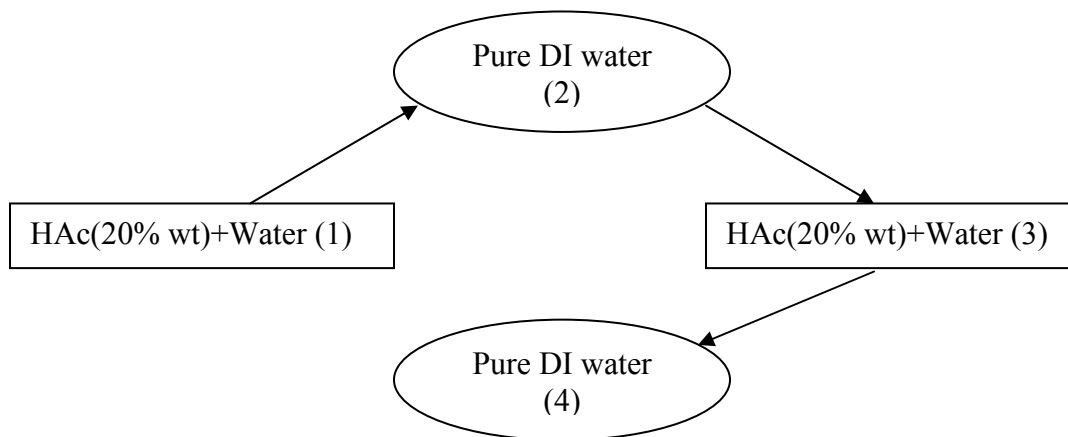


Figure 4.4: Schematic testing procedures for DW24.3_3 and FB4.7_2 modules. The numbers of “(1), (2), (3), and (4)” represent the testing step

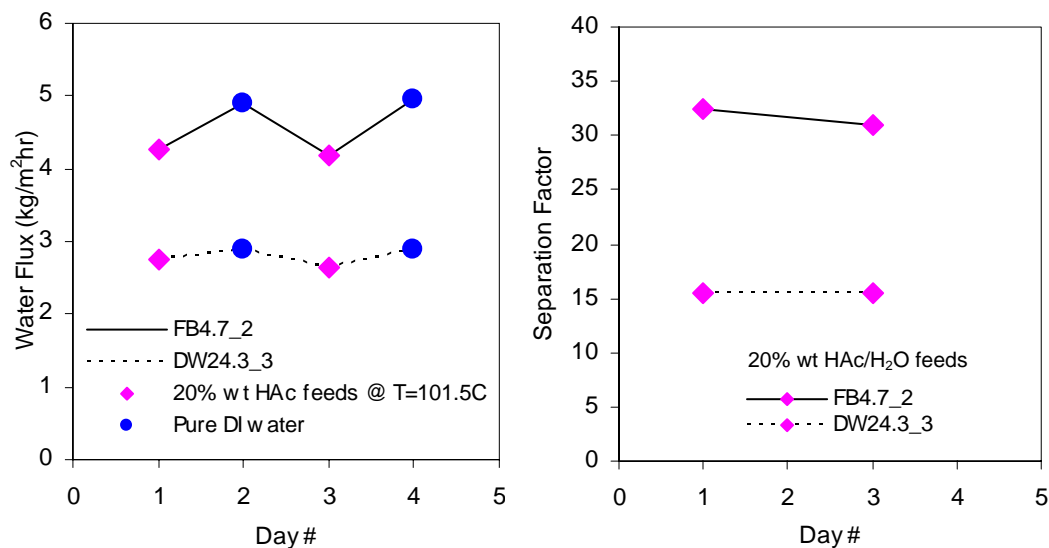


Figure 4.5: Water flux and separation factor, $\beta_{\text{H}_2\text{O}/\text{HAc}}$, for DW24.3_3 and FB4.7_2 modules

FB4.7_2 fiber with a large bore shows higher water flux and separation factor in contrast to DW24.3_3 fiber with a small bore. This clearly supports our expectation that

the bore pressure influences the “faster” gas molecule, water, much more than acetic acid. The water permeance and corresponding membrane selectivity are not given here because complicated calculations are involved in the correction of the bore pressure change. A model used to correct the bore pressure change is illustrated in Chapter 5 and its results show that the bore pressure change is negligible with the outer diameter large than 500 μm fibers. Therefore, the bore pressure change of FB4.7_2 fiber can be neglected due to its 520 μm outer diameter, i.e. the assumption of zero pressure in the bore side (downstream) is reasonable. The separation performance of FB4.7_2 can be considered as the inherent membrane property without underestimation.

FB4.7_2 fiber shows a significant increase of the water flux when a HAc/H₂O mixture feed is replaced by a pure DI water feed. The water flux can be defined using a “driving force and resistance” manner in equation 4.6,

$$Q_{\text{H}_2\text{O}} = \frac{\text{Driving force}}{\text{Resistance}} = \frac{\Delta p_{\text{H}_2\text{O}}}{\left(\frac{\ell_{\text{skin}}}{\mathcal{P}_{\text{H}_2\text{O}}}\right)} \quad (4.6)$$

where ℓ_{skin} is the thickness of the outer skin layer of an asymmetric membrane, $\Delta p_{\text{H}_2\text{O}}$ is the partial pressure difference across the membrane for water, and $\mathcal{P}_{\text{H}_2\text{O}}$ is the water permeability through the skin layer. The ratio of the water flux between a pure DI water and HAc/H₂O mixture feed can be derived with negligible downstream pressure as follows,

$$\begin{aligned}
\frac{(Q_{H_2O})_{\text{pure } H_2O}}{(Q_{H_2O})_{HAc/H_2O}} &= \frac{\left\{ \frac{\Delta p_{H_2O}}{\left(\frac{\ell_{\text{skin}}}{P_{H_2O}} \right)} \right\}_{\text{pure } H_2O}}{\left\{ \frac{\Delta p_{H_2O}}{\left(\frac{\ell_{\text{skin}}}{P_{H_2O}} \right)} \right\}_{HAc/H_2O}} \\
&= \frac{\{\Delta p_{H_2O}\}_{\text{pure } H_2O}}{\{\Delta p_{H_2O}\}_{HAc/H_2O}} \cdot \frac{\{P_{H_2O}\}_{\text{pure } H_2O}}{\{P_{H_2O}\}_{HAc/H_2O}} \\
&= \frac{(p^* - 0)}{(x_{H_2O} \gamma_{H_2O} p^* - 0)} \cdot \frac{\{P_{H_2O}\}_{\text{pure } H_2O}}{\{P_{H_2O}\}_{HAc/H_2O}} \\
&= \frac{1}{x_{H_2O} \gamma_{H_2O}} \cdot \frac{\{P_{H_2O}\}_{\text{pure } H_2O}}{\{P_{H_2O}\}_{HAc/H_2O}}
\end{aligned} \tag{4.7}$$

where the subscript of pure H₂O represents a pure DI water feed and the subscript of HAc/H₂O represents a HAc/H₂O mixture feed, x_{H_2O} is the mole fraction of water in a mixture feed, γ_{H_2O} is the water activity coefficient, and p^* is the saturated water pressure at the operating temperature. Since the following variables are known for a 20% wt HAc concentration and pure DI water feed for FB4.7_2 module, i.e., $x_{H_2O} = 0.93$, $\gamma_{H_2O} = 1.02$ [2], $(Q_{H_2O})_{HAc/H_2O} = 4.20 \text{ kg/m}^2 \text{ hr}$, and $(Q_{H_2O})_{\text{pure } H_2O} = 4.93 \text{ kg/m}^2 \text{ hr}$, the ratio of the water permeability between a pure DI water and mixture feed can be obtained below,

$$\frac{\{P\}_{\text{pure } H_2O}}{\{P\}_{HAc/H_2O}} = \frac{(Q_{H_2O})_{\text{pure } H_2O}}{(Q_{H_2O})_{HAc/H_2O}} \cdot x_{H_2O} \gamma_{H_2O} = \frac{4.93}{4.20} \times 0.93 \times 1.02 = 1.11 \tag{4.8}$$

The larger water pressure difference (driving force) across a membrane for a pure DI water feed is responsible for its higher flux in contrast to a mixture feed. However, a noticeable discrepancy of the water permeability exists between a pure DI water and mixture feed even if the driving force difference is taken into account. This might be ascribed to the competition between acetic acid and water molecules in the available separation sites among the polymer chains. The presence of a strongly competitive agent,

acetic acid, inhibits the transport of water molecules, as Matrimid® is a hydrophobic material. The competition effect is most apparent for highly absorbable or condensable penetrants such as HAc based upon the dual mode sorption theory [17]. As a result, the water diffusivity and permeability are depressed in a HAc/H₂O feed, but they can return to the original value upon the replacement of a pure DI water feed. In other words, removal of the preferentially sorbing penetrant (HAc) can push the permeability of another penetrant (H₂O) back to its virgin value. The cartoon pictures shown in Figure 4.6 illustrate this competition effect between water and HAc.

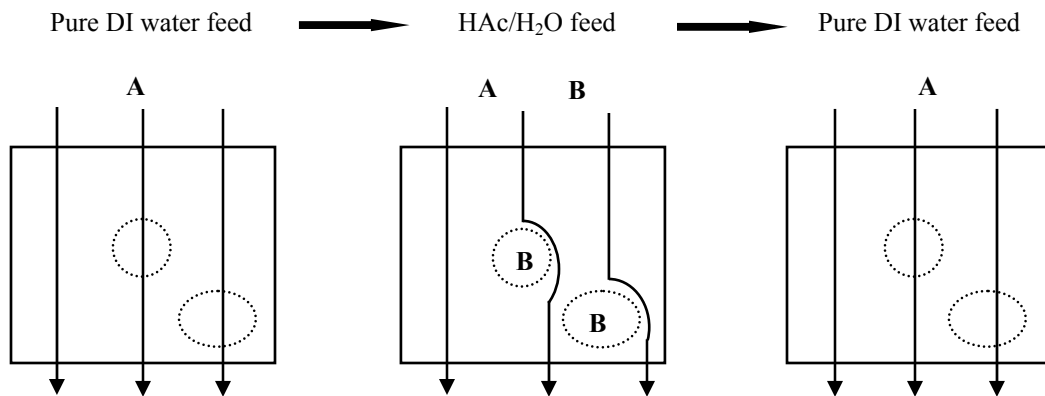


Figure 4.6: Cartoon pictures showing the competition effect caused by the presence of HAc in a membrane system. The symbol of \odot represents the free volume accessible to A/water in the glassy polymer in the absence of B/HAc that is a strongly competitive agent. During exposure to a HAc/H₂O mixture, the water permeation pathway is hindered by HAc molecules, thereby reducing the water permeability in contrast to a pure DI water feed.

It has also been observed that water demonstrates very trivial effects on the fiber in pervaporation since the experimental results are well reproduced with a mixture feed on day #3. For water, no considerable flux difference exists between a pure DI water and mixture feed with a small bore size fiber because the bore pressure change is dominant

and decreases the water flux dramatically in both feeds. Therefore, once the pressure change is corrected, a similar permeability should be obtained regardless of the fiber size for “neutral” penetrants.

Two separate pervaporation modules with small and large bore size fibers, DW24.2_1 (O.D. $\sim 283\ \mu\text{m}$) and FB2.6_1 (O.D. $\sim 487\ \mu\text{m}$), were tested using the procedures shown in Figure 4.7. Figure 4.8 illustrates the water flux and separation factor for these two modules. Model 20% wt and 30% wt HAc concentration solutions were used for pervaporation tests on day # 2 and day # 4, respectively.

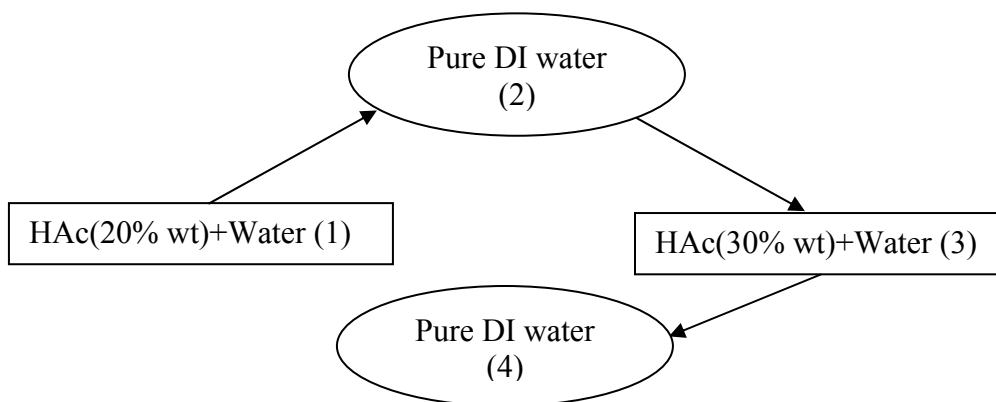


Figure 4.7: Schematic testing procedures for DW24.2_1 and FB2.6_1 modules. The numbers of “(1), (2), (3), and (4)” represent the testing step

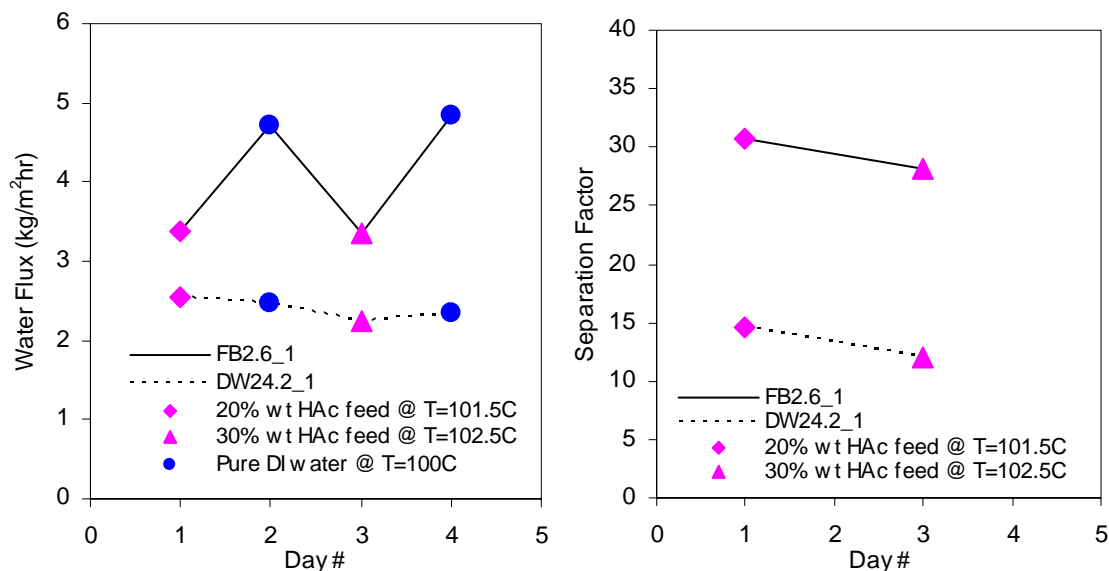


Figure 4.8: Water flux and separation factor for DW24.2_1 and FB2.6_1 modules

As observed in the previous experiment, the higher water flux is associated with the larger bore size fiber. The separation factor decreases with the increased HAc concentration feeds for both fibers. Apparently the HAc flux increases with the increased HAc concentration feed as the water flux remains almost constant. This behavior is attributed to the concentration-dependent HAc permeability (swelling). In addition, the water flux in the 30% wt HAc/H₂O feed does not show any depression in contrast to that in the 20% wt HAc/H₂O feed. This is not contrary to the expectation from competition effects. In fact, the constant water fluxes in both mixture feeds are an indirect indication of the existence of the HAc-induced plasticization. That is, the HAc-induced swelling, if present, can assist water transport through the polymer to some degree and might offset the water flux loss from competition effects. Thus, the higher HAc concentration feeds will be tested in Chapter 4.5.4 and the HAc and water permeabilities instead of their fluxes will be provided.

Nevertheless, a large bore size fiber (O.D. $\sim 500\ \mu\text{m}$) exhibits the larger water flux (productivity) and separation factor (efficiency). This clearly shows that the adaptation of large bore size defect-free Matrimid[®] hollow fibers into pervaporation of HAc/H₂O mixtures is feasible.

4.5.2 Effects of Bore Size on Fiber Performance

As shown in the preliminary work, the bore size of a hollow fiber plays an important role in determining separation results. It is useful to investigate the fiber performance in separating HAc/H₂O mixtures with different bore size fibers. Figure 4.9 shows the variation of water and HAc fluxes and separation factor with the bore size. All the feeds were 20% wt HAc concentration solutions and the operating temperature was 101.5°C.

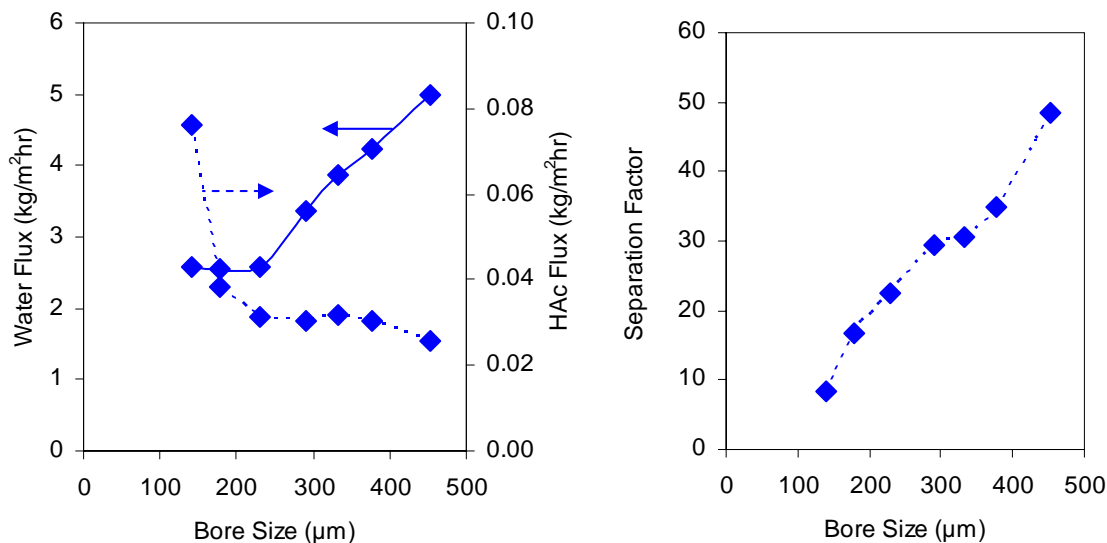


Figure 4.9: Water and HAc fluxes and separation factor vs. bore size for 20% wt HAc concentration feeds

The water flux increases with an increase of the fiber bore size. This is in good agreement with our theoretical analysis. Water diffusivity instead of solubility dominates

and causes its high flux through the membrane due to its “neutral” properties in the hydrophobic Matrimid[®] polymer. A large bore size fiber can reduce the water (highly permeable molecules) partial pressure change in the bore side and thus maximize the driving force across the membrane. However, the HAc flux does *not exhibit any increment* even with the low HAc pressure change inside the large bore. This implies that two contradictory factors might influence the HAc flux, namely 1) the enhanced HAc flux resulted from the low pressure change inside the large bore, 2) plus suppressed flux due to the reduction of HAc-induced plasticization inside the large bore. With the increment of the bore size, the second factor is predominantly in charge due to the relatively low HAc pressure change. The lower HAc concentration (lower pressure change) inside the larger bore presumably decreases the HAc-induced plasticization, resulting in the lower HAc flux through the membrane. Thus, the separation factor increases considerably due to the higher water flux and lower HAc permeation in a large bore size fiber. This “win-win” situation makes a large bore size fiber very attractive as an alternative to distillation columns.

In order to investigate how significantly the bore size can influence the water flux, only pure DI water feeds are used to decouple the HAc-induced swelling effects. Figure 4.10 shows the variation of the water flux with the bore size. The water flux with the 480 μm bore size fiber is increased by almost 300% compared to the 180 μm bore size fiber. This indicates that the bore pressure change is a key factor for the water flux in this work. A large bore size fiber is selected to investigate the *inherent* properties of the membrane in the future pervaporation tests because it can avoid the pressure buildup inside the bore.

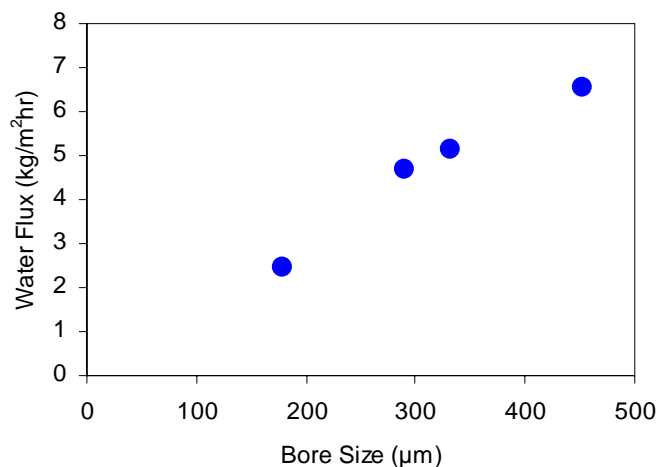


Figure 4.10: The variation of the water flux with the bore size for pure DI water feeds

4.5.3 Water Effects on Fiber Performance

The preliminary work has indirectly shown that no observable swelling interaction exists between water and the polymer, but additional evidence is necessary to prove this hypothesis. A pervaporation process with a pure DI water feed is studied to decouple HAc influences on the fibers. FB5.6_5 module (O.D. $\sim 520 \mu\text{m}$) was used to perform pervaporation tests with pure DI water feeds for 14 days. Thereafter, pure DI water was substituted by a model 20% wt HAc/H₂O mixture to continue the pervaporation test on day #15. The water permeance is shown in Figure 4.11. In the mean time, a new module of FB5.6_10 was prepared to conduct a pervaporation test with a model 20% wt HAc mixture directly without any pure water feed involved. Table 4.2 shows the comparison of water permeance and membrane selectivity between FB5.6_5 and FB5.6_10 modules.

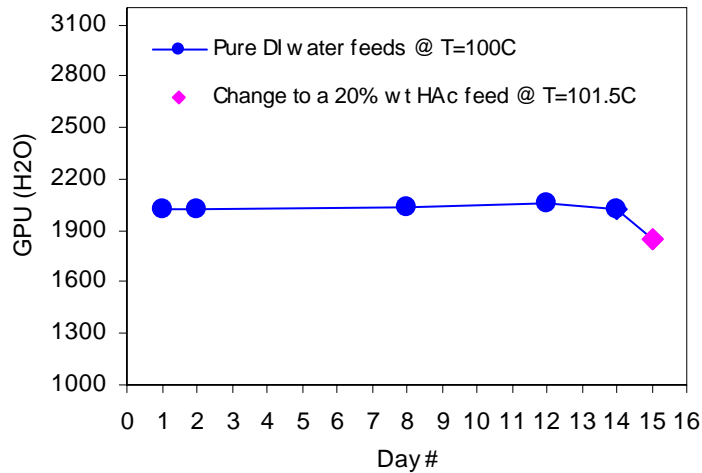


Figure 4.11: Water permeance for pure DI water feeds (FB5.6_5), and replaced by a model 20% HAc concentration feed on day #15

Table 4.2: Pervaporation results with a model 20% wt HAc/H₂O mixture feed for FB5.6_5 and FB5.6_10 modules.
 * FB5.6_5 has been tested with pure DI water for 14 days before taking a model 20% wt HAc solution feed on day #15
 ** FB5.6_10 was directly tested with a model 20% wt HAc solution feed

Fiber Identification	O.D. (μm)	I.D. (μm)	Permeance H ₂ O(GPU)	Membrane selectivity $\alpha_{H_2O/HAc}$
FB5.6_5*	520	325	1850	27
FB5.6_10**			1900	26

As it can be seen, the water permeance remains constant for almost two weeks for FB5.6_5 module. When compared to FB5.6_10 module that is not involved in any pure DI water feeds, FB5.6_5 module demonstrates very close membrane selectivity and permeance for a model 20% wt HAc concentration feed. The similar separation performance of HAc/H₂O mixtures for these two modules confirms that water does not have noticeable influence on the membrane. This conclusion is very important for the

exploration of the HAc effects on the membrane in the next section. In other words, any changes of the fiber performance in separating HAc/H₂O mixtures can be reasonably attributed to acetic acid.

4.5.4 Effects of HAc Concentration in Feeds on Fiber Performance

It has been shown that different HAc concentration solutions can influence the fiber performance. Thus, higher HAc concentration feeds are used in pervaporation to better understand the HAc effects on the membrane material. The schematic testing procedures for FB4.7_2 module (O.D. ~ 520 μ m) are shown in Figure 4.12. Figure 4.13 illustrates the water flux and acetic acid flux with the different HAc concentration feeds for FB4.7_2 module. The HAc flux increases dramatically with the higher HAc concentration feeds, while the water flux does not change very much.

In order to explore whether this behavior is ascribed to the characteristic of the polymer membrane or solely associated with the upstream partial pressure arising from the different HAc concentration feeds, the water and acetic acid permeance have to be calculated instead of their flux. The bore pressure change is reasonably assumed as zero for large bore size fibers. The permeance (including the water permeance with pure DI water feeds) and membrane selectivity are shown in Figure 4.14.

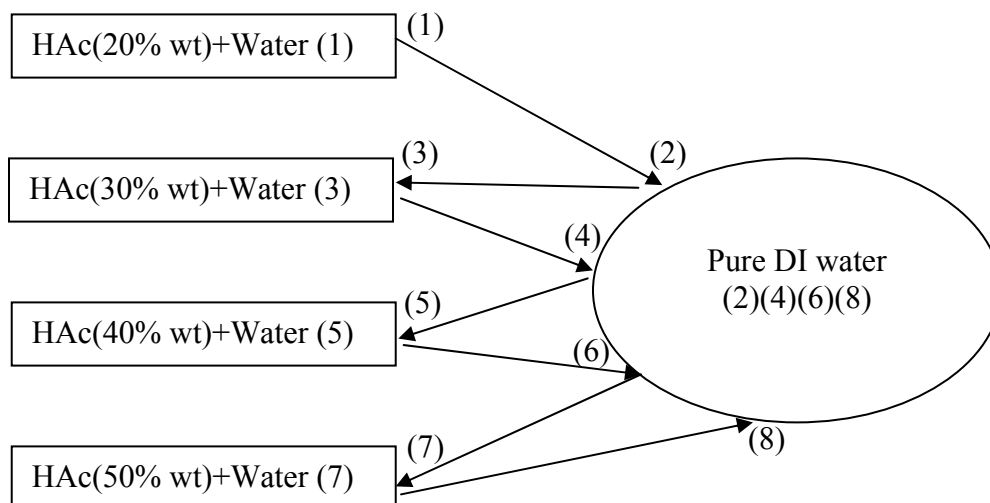


Figure 4.12: Schematic testing procedures for FB4.7_2 module. The numbers of “(1), (2), ..., and (8)” represent the testing step

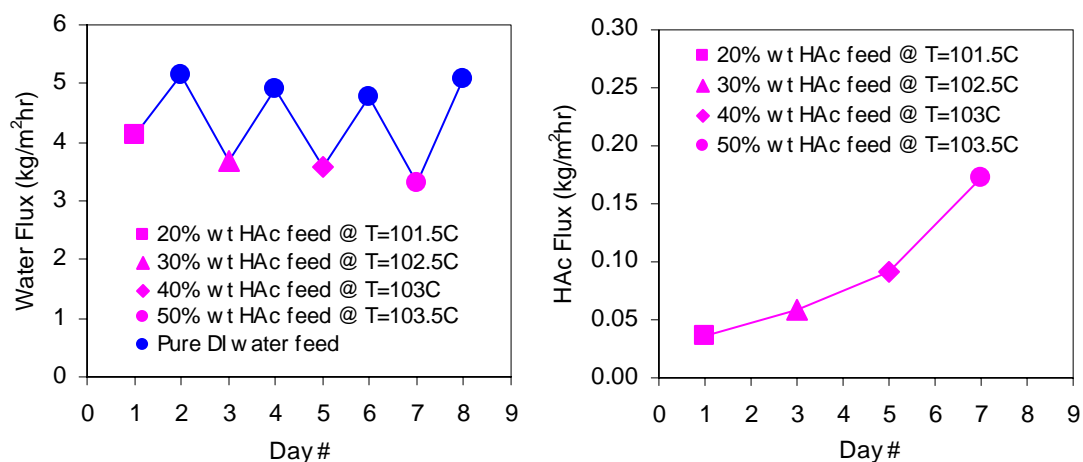


Figure 4.13: Water flux and acetic acid flux with different HAc concentration feeds

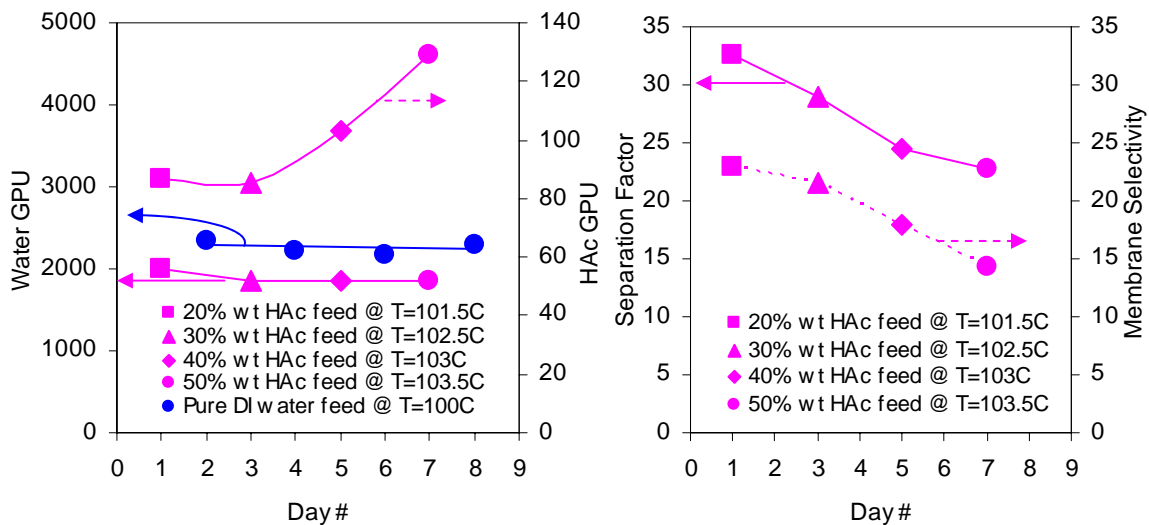


Figure 4.14: Permeance and separation factor/membrane selectivity with different HAc concentration feeds

The HAc permeance has a large increment with the high HAc concentration feeds. This is attributed to the HAc-induced plasticization on the polymer. Acetic acid can cause the microscopic changes of the polymer, including changes in the chain rigidity and chain packing density. As a consequence, the swelling effects can increase the free volume or change the free volume distribution [18-19], which mainly favors the passage of the “slow” penetrants such as acetic acid in this case. In other words, HAc molecules are much more capable of competing for the added free volume from the HAc-induced swelling and plasticization [20]. The relatively constant water permeance is attributed to the counteracting effects from competition and plasticization.

Infrared Spectroscopy (IR) was used to compare the chemical structure of membranes and no noticeable differences were observed before and after pervaporation tests. This is an indication of no chemical reaction between HAc and Matrimid®. The physical change of the polymer chains arising from acetic acid is responsible for the separation results.

4.5.5 Long Term Pervaporation Results

In addition to the basic requirements such as selectivity (separation efficiency) and permeation rate (productivity) for membranes, the life time or durability is also an important issue. Although the relative importance of each of these requirements varies with the application, ultimately all of them have to be balanced against economic costs. FB4.7_1 module was used to perform pervaporation tests for 16 days. The schematic testing procedures of FB4.7_1 module followed those of FB4.7_2 module (in Figure 4.12) twice. Pervaporation tests were completed on a daily basis. Between the testing periods, the fibers were soaked in pure DI water at room temperature. That is, the fibers were in direct contact with HAc/H₂O mixtures only during pervaporation tests. Figure 4.15 and 4.16 show the water permeance and membrane selectivity for FB4.7_1 module, respectively.

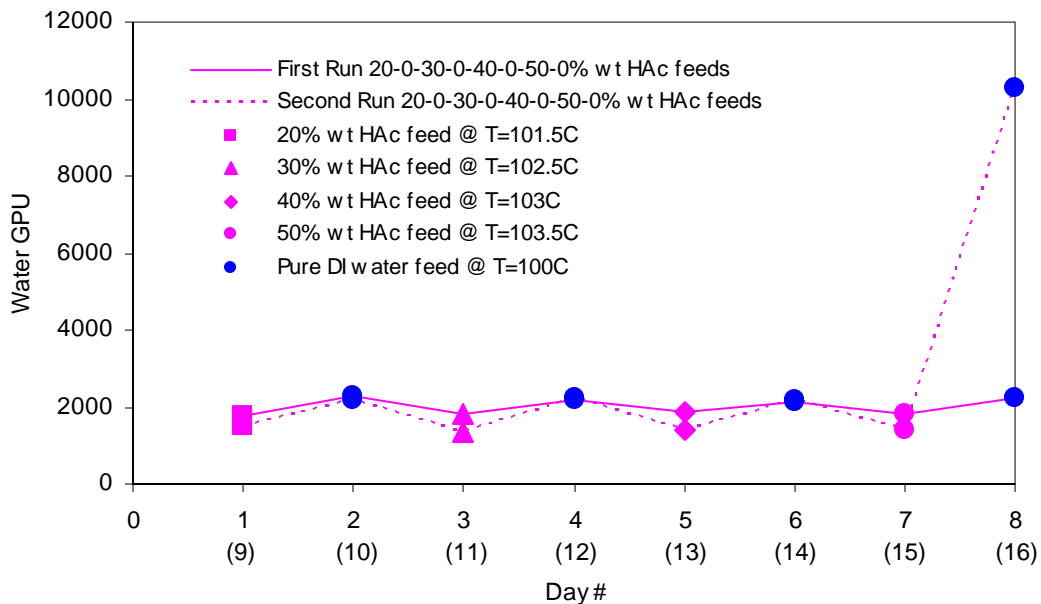


Figure 4.15: Water permeance with different HAc concentration and pure DI water feeds for FB4.7_1 module

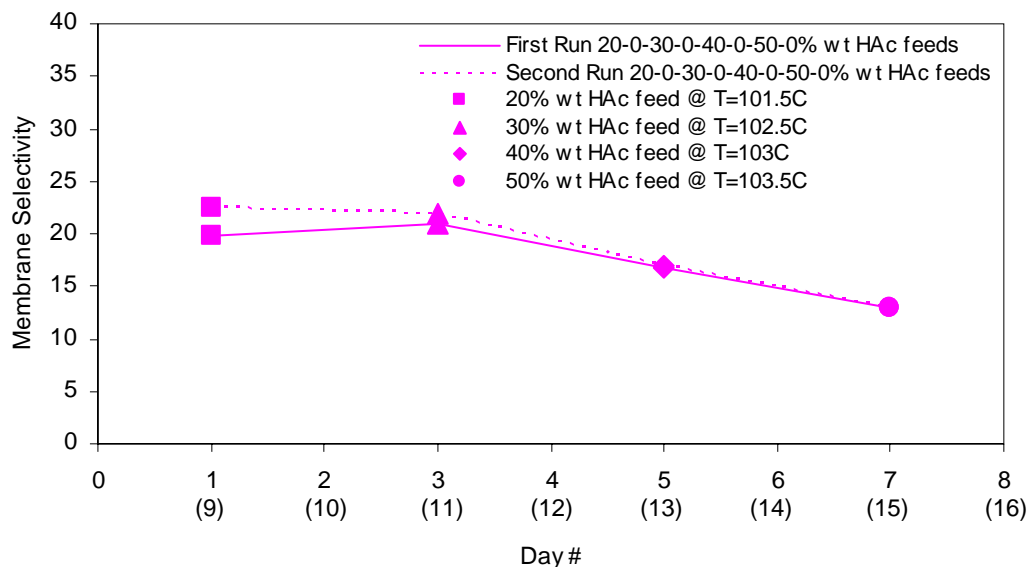


Figure 4.16: Membrane selectivity with different HAC concentration feeds for FB4.7_1 module

Both the water permeance and membrane selectivity are very close between the first and second run with 20-30-40-50% wt HAC mixture feeds. In the mean time, it was observed that the fiber extended to some degree after a HAC mixture test and shrank back upon the next step with pure DI water pervaporation. Apparently, the morphology of fibers changes during the HAC/H₂O mixture separation. The polymer chains tend to relax and dilate due to the conditioning effects of acetic acid; however, pure DI water helps them recover back to the original status. After continually dilating and recoiling, the interstitial space among the polymer chains can be narrowed down, resulting in the closer localized configuration of aromatic polyimide benzene rings. This leads to a small increase in the selectivity and the depression in water permeance in the second run. The history effect from the 50% wt HAC/H₂O feed in the first run is responsible for the apparent decrease of the membrane selectivity with the 20% wt HAC/H₂O feed in the

second run. As for the last test (day #16), an abrupt increment of the water permeance is believed to be due to epoxy leakage.

Although the high HAc concentration feed swells the polymer and causes the reduction of the membrane selectivity, pure DI water functions well in the recovery of the polymer morphology. Therefore, the permeance and membrane selectivity are consistent during the two runs and the fiber performance is very robust.

4.5.6 Effects of Operation History on Fiber Performance

As discussed earlier, pure DI water does not show observable interaction with the polymer. In addition, replacing HAc/H₂O mixtures with pure DI water can help the polymer chains to recover back and minimize the HAc conditioning effects. However, it is not practical to clean and wash membranes by pure DI water frequently in industry. Thus, it is pertinent to explore the HAc/H₂O mixture pervaporation without pure DI water involved either as a feed or storage bath. In other words, the pervaporation modules are always soaked in the corresponding HAc/H₂O solutions during pervaporation tests at about 101°C or waiting status at room temperature. Figure 4.17 - 4.18 show the water permeance, HAc permeance and membrane selectivity for FB4.7_3 and FB4.7_5 modules with 20% and 55% wt HAc concentration feeds, respectively.

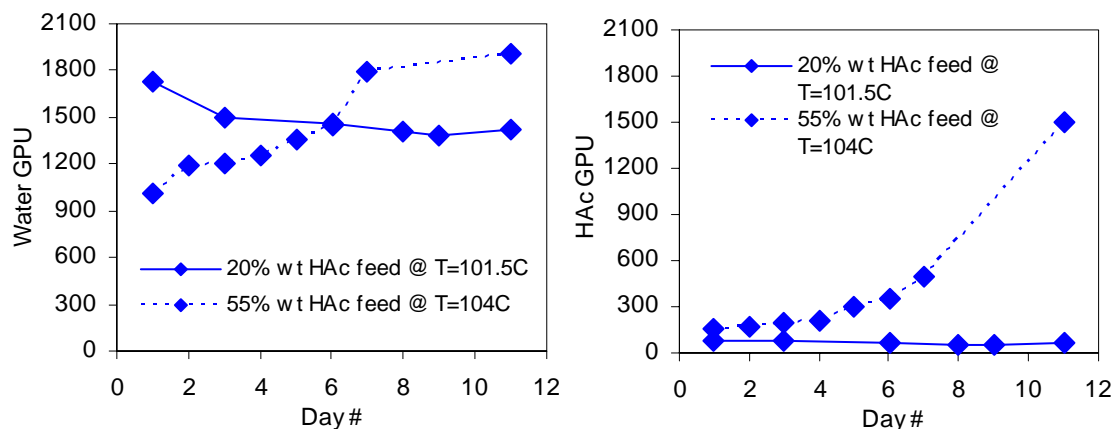


Figure 4.17: The variations of water and HAC permeances with time for 20% wt and 55% wt HAC concentration feeds

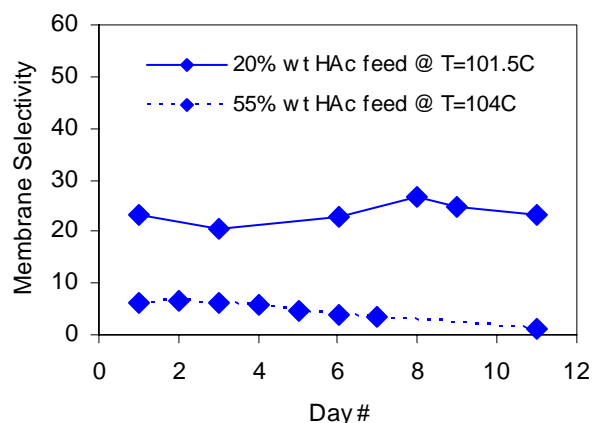


Figure 4.18: The variation of membrane selectivity with time for 20% wt and 55% wt HAC concentration feeds

A small depression of the water permeance is observed in the initial days for 20% wt HAC/H₂O feeds as the polymer has not reached steady state due to the HAC conditioning effects. The selectivity is considered constant as the scattered data are still in a small and acceptable range. No significant differences exist as compared to the experimental results in Chapter 4.5.5, in which water is used to wash the pervaporation modules periodically and store them at the waiting status.

The HAc permeance increases much more drastically than the water permeance with time for 55% wt HAc concentration feeds. The selectivity almost drops down to one on day #11. This clearly indicates that the HAc-induced plasticization associated with the high HAc concentration feed swells the polymer with time. More and more free volume can be created as long as the polymer chains respond to swelling stresses from HAc. The increased free volume favors the passage of the “slow” molecules such as HAc much more than water and causes a huge increment in the HAc permeance. As a consequence, the membrane selectivity is reduced dramatically even though the water permeance results show that the membrane continues to function to some degree. Figure 4.19 shows water and HAc transport through the membrane under the HAc-induced swelling condition.

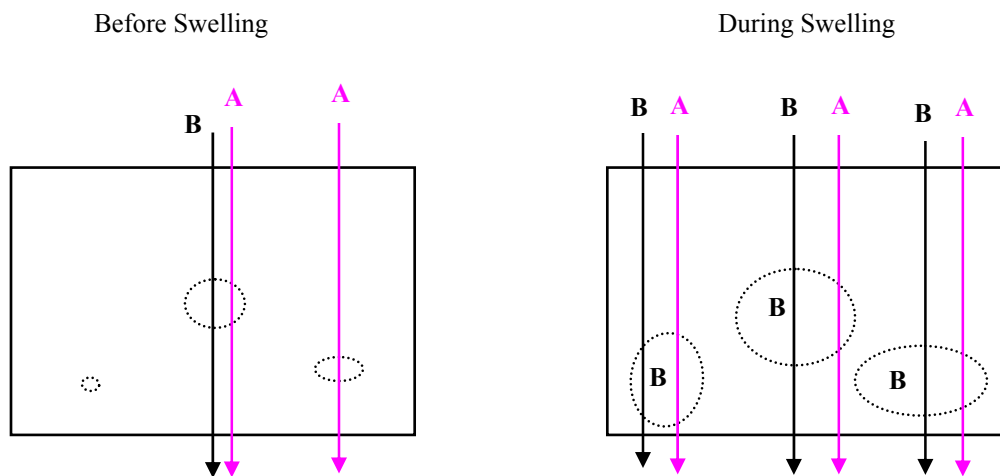


Figure 4.19: Cartoon pictures showing plasticization effects caused by the presence of HAc in a membrane system. The symbol of \bigcirc represents the free volume accessible to A/water or B/HAc in the glassy polymer. The purple arrows represent transport pathway of water, while the black arrows represent transport pathway of HAc. Additional arrows shown in “during swelling” case illustrate the increased flux of water and HAc during the B/HAc-induced plasticization (the polymer matrix is swelled). Clearly, more HAc molecules go through the polymer, thereby reducing the membrane selectivity.

In industry, a cross-flow separator is commonly used due to its high efficiency [21-22], as shown in Figure 4.20. The fiber used to separate 20% wt HAc/H₂O feeds must face the higher HAc concentration solution as well at the final stage of the separator.

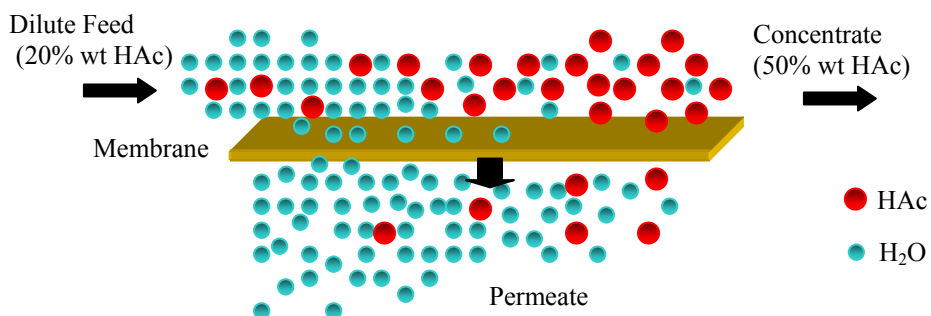


Figure 4.20: Cartoon picture showing the separating process in a cross-flow separator

The high HAc concentration feed has been shown to cause considerable deterioration in the fiber performance with time; therefore, it is necessary to investigate whether this effect is lethal for a 20% wt HAc/H₂O mixture-conditioned fiber. When the testing of FB4.7_3 module was finished with 20% wt HAc feeds in the first 11 days, a substitute solution with 55% wt HAc concentration was used to conduct a pervaporation test on the 12th day. Thereafter, pure DI water and a model 20% wt HAc solution were used for pervaporation tests on day #13 and #14, respectively. The schematic testing procedures are shown in Figure 4.21. Figure 4.22 illustrates the pervaporation results of FB4.7_3 module during these four days.

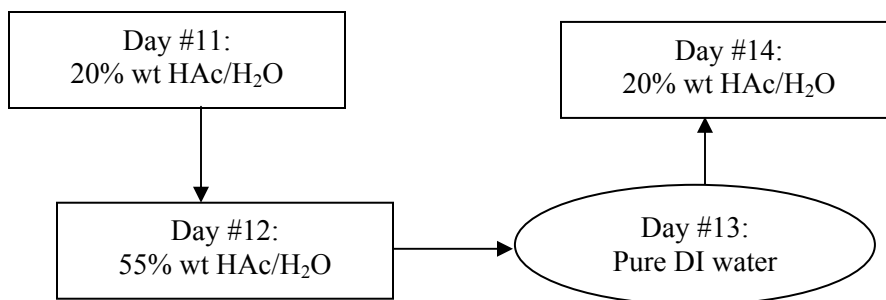


Figure 4.21: Schematic testing procedures for FB4.7_3 module

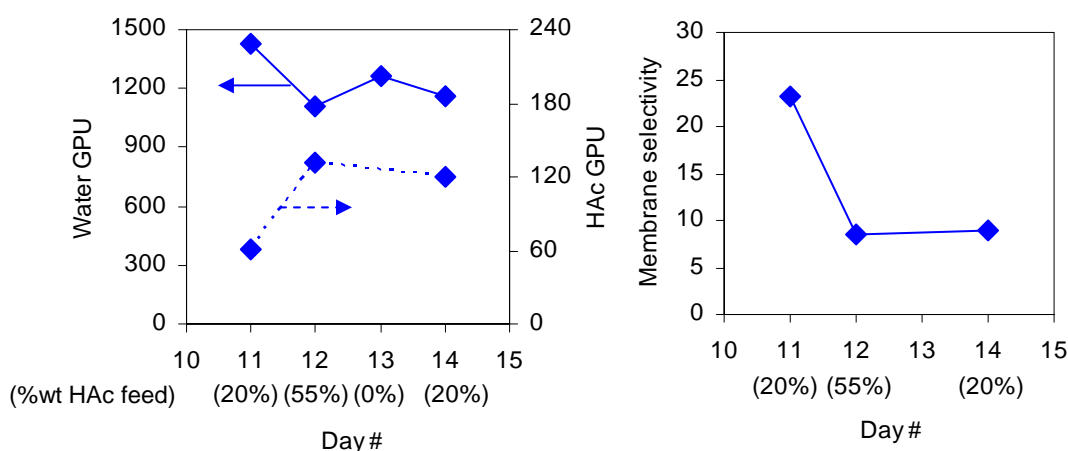


Figure 4.22: Permeance and selectivity for FB4.7_3 module on day #11, 12, 13, and 14

As expected, the membrane selectivity decreases dramatically with a reduction of the water permeance and an increment of the HAc permeance when changing to a 55% wt HAc concentration feed. The swelling from the high acetic acid concentration feed increases the free volume and changes the free volume distribution. The HAc-induced plasticization helps itself through the membrane much more than water, resulting in the low membrane selectivity. However, both pure DI water and a 20% wt HAc solution feed on the 13th and 14th day can not return the membrane back to the original status. This indicates that the membrane morphology has been irreversibly changed. The increased free volume due to the 55% wt HAc concentration feed on day #12 can not shrink back,

resulting in the low membrane selectivity even with a 20% wt HAc concentration feed on day #14. The relatively constant water permeability on day #12 and 14 further indicates that the additional free volume due to 55% wt HAc-induced swelling is captured by acetic acid instead of water. Although the polymer chains can be recovered to their original status easily when stored in a water bath and washed by water frequently, FB4.7_3 module behaves totally different due to the long term exposure procedures, i.e. from 20% wt HAc feeds for 11 days, through a 55% wt HAc feed and pure DI water feed, to a 20% wt HAc feed eventually. The operating history, especially the HAc-induced conditioning procedure, influences the membrane separation performance of FB4.7_3 module.

Transport phenomena in a glassy asymmetric hollow fiber are very complicated in an aggressive environment. First, a glassy polymer is in thermodynamic non-equilibrium state and has “excess” un-relaxed free volume among the polymer chains. Second, the swelling penetrant can change the polymer morphology and alter its discrimination of shape and size for penetrants. In addition to the membrane material and its morphology, the operating history can be another important factor that determines the membrane separation. Therefore, identification of these crucial factors is helpful to improve the membrane separation performance.

4.6 Summary

Adaptation of a regular gas separation Matrimid[®] hollow fiber (O.D. ~ 250 μm) into pervaporation has been proved feasible. With shell feed, the pressure buildup in the bore side along the axial direction of a hollow fiber plays an important role in the fiber

performance. Typically the membrane selectivity is underestimated as the bore pressure buildup affects highly permeable gases such as water more seriously. A large bore size fiber has been experimentally proved to be a good solution to minimize the bore pressure buildup. In fact, the membrane selectivity ($\alpha_{\text{mem}} \sim 20\text{-}30$) and water flux ($\sim 4.5 \text{ kg/m}^2\text{hr}$) are increased by about 150% with a diameter (O.D. $\sim 500 \text{ }\mu\text{m}$) twice as large as the regular fiber in a model 20% wt HAc concentration feed. Further, a decrease in the HAc flux was observed with the increased bore size due to the reduction in the HAc-induced plasticization. The large bore size fibers can decrease the HAc concentration in the bore side and thus reduce its swelling effects on the fibers. This “win-win” situation makes large bore size defect-free Matrimid[®] hollow fibers very attractive for pervaporation of HAc and water mixtures in industry.

Strong HAc-induced plasticization occurs with high HAc concentration feeds. This is detrimental to the fiber performance because the membrane selectivity is decreased drastically. Acetic acid functions not only as a “slow” penetrant, but also as a swelling agent in this research. In other words, HAc is more competent to capture the increased “transient gaps” arising from the HAc-induced plasticization. The HAc-induced swelling effects favor itself through the membrane much more than water, resulting in the low membrane selectivity. The application of thermal annealing will be described in Chapter 6 to suppress the HAc-induced plasticization [18-19, 23].

4.7 References

- [1] Kirk, R.E. and Othmer, D.F. *Encyclopedia of chemical technology*. John Wiley & Sons, Inc. 4th Ed. New York. 2000, 18, 1006-1012.
- [2] Personal Communication with Dr. Steve Pietsch from BP, 2004-2005.

- [3] Petlyuk, F.B. *Distillation theory and its application to optimal design of separation units*. Cambridge, UK: New York: Cambridge University Press, 2004.
- [4] Stichlmair, J. and Fair, J.R. *Distillation: principles and practices*. John Wiley & Sons, Inc. New York 1998.
- [5] Huang, R.Y.M. *Pervaporation membrane separation processes*. Elsevier Science Publishing Company, Inc. New York. 1991, 1-46.
- [6] Lee, E.K. and Koros, W.J. *Membrane, Synthetic, Application*. Encyclopedia of Physical Science and Technology, 2001.
- [7] Kesting, R.E. and Fritzsche, A.K. *Polymeric gas separation membranes*. John Wiley and Sons, Inc. New York 1993.
- [8] Kaschemkat, J., Hilgendorff, W., Boddeker, K.W., and Kneifel, K. German Patent Application DE 3713973 A1.
- [9] Membrane Technology and Research, Inc., 1360 Willow Road, Menlo Park, CA 94025, U.S.A.: Product Information 1988.
- [10] SEMPAS Membranetechnik GmbH, Rosenbergstr. 103, 7000 Stuttgart 1, West Germany: Product Information 1989.
- [11] Rautenbach, R. and Albrecht, R. *The separation potential of pervaporation: II. Process design and economics*. J. Membr. Sci. 1985, 25, 25-54.
- [12] Wijmans, J.G. *Process performance = membrane properties + operating conditions*. J. Membr. Sci. 2003, 220, 1-3.
- [13] Guo, W.F., Chung, T.S., and Matsuura, T. *Pervaporation study on the dehydration of aqueous butanol solutions: A comparison of flux vs. permeance, separation factor vs. selectivity*. J. Membr. Sci. in press.
- [14] Vu, D.Q. *Formation and characterization of asymmetric carbon molecular sieve and mixed matrix membranes for natural gas purification*. Ph.D. Dissertation, The University of Texas at Austin, 2001.
- [15] Manos, P. *Solvent exchange drying of membranes for gas separation*. United States Patent 4,120,098.
- [16] Park, H.C., Moon, Y.S., Rhee, H.W., Won, J., Kang, Y.S., and Kim, U.Y. *Effect of solvent exchange on the morphology of asymmetric membranes, in membrane formation of modification*, Pinnau, I. and Freeman, B., Ed. 2000, ACS: Washington, D.C. 110-124.

- [17] Chern, R.T., Koros, W.J., Sanders, E.S., and Yui, R. *Second component effects in sorption and permeation of gases in glassy polymers*. J. Membr. Sci. 1983, 15, 157-169.
- [18] Wind, J.D., Sirard, S.M., Paul, D.R., Green, P.F., Johnston, K.P. and Koros, W.J. *Relaxation dynamics of CO₂ diffusion, sorption, and polymer swelling for plasticized polyimide membranes*. Macromolecules. 2003, 36(17), 6442-6448.
- [19] Wind, J.D., Sirard, S.M., Paul, D.R., Green, P.F., Johnston, K.P. and Koros, W.J. *Carbon dioxide-induced plasticization of polyimide membranes: pseudo equilibrium relationships of diffusion, sorption, and swelling*. Macromolecules. 2003, 36(17), 6433-6441.
- [20] Al-Juaied, M.A. *Carbon dioxide removal from nature gas by membranes in the presence of heavy hydrocarbons and by aqueous diglycolamine[®]/Morpholine*. Ph.D. Dissertation, The University of Texas at Austin, 2004.
- [21] Baker, R.W. *Membrane technology and applications*. The McGraw-Hill Companies, Inc. 2000.
- [22] Porter, M.C., *Handbook of industrial membrane technology*. Noyes Publications, Park Ridge, NJ 1990.
- [23] Bos, A., Punt I.G.M., Wessling, M., and Strathmann, H. *Plasticization-resistant glassy polyimide membranes for CO₂/CO₄ separations*. Sep. Purif. Technol. 1998, 14, 27-29.

Chapter 5: Mathematical Model to Demonstrate Bore Pressure Change Effects on Fiber Performance

5.1 Introduction

The pressure change in the bore side of a hollow fiber is typically trivial for gas separation with shell feed. Due to high flux associated with pervaporation of HAc/H₂O mixtures, however, the bore pressure change turns out to be significant and can not be neglected any more [1-2]. Thus, it is necessary to develop a mathematical model to take the bore pressure change into consideration. The overall production rate can be reduced since an increase of the pressure in the bore side decreases the driving force across the membrane wall. Several analytical and numerical solutions have appeared in the literature to describe the pressure drop in hollow fiber membranes [2-9]. Pan [3-4] attempted to model multicomponent permeation systems with high flux in asymmetric hollow fiber membranes including the permeate pressure variation. Chern et al. [5] reported that the pressure buildup in the fiber lumen was substantial for smaller fibers when the permeator was operated at high permeation rates for the shell feed mode. Thorman et al. [10] studied the pressure drop and separation in a binary system through a bundle of silicone rubber capillary tubing. The Poiseuille equation, coupled with the permeation equation, was used to describe the flow behavior of pure gases through the tubes. Lim et al. [11] modified the Hagen-Poiseuille equation to account for fiber permeability and gas compressibility.

At the initial stage of this work, the aim was to investigate the feasibility of adapting 250 μm diameter Matrimid[®] hollow fiber membranes (water-selective) to pervaporation of a model 20% wt HAc/H₂O mixture. Considering the pressure change in

the bore side of the fibers, a simple model to describe the bore pressure change was established with the Hagen-Poiseuille equation. This model indicated that a significant pressure change associated with high flux existed in the bore side for 250 μm outer diameter fibers. A large bore size fiber should be a good solution to minimize the effects of the bore pressure change in pervaporation. As expected, the experimental results with a large bore size fiber exhibited a significant increase in the water flux and membrane selectivity. However, a big discrepancy in the HAc flux existed between the experimental and model results. That is, the reduction of the HAc flux was observed in a large bore size fiber instead of increment due to the bore pressure change. This clearly suggested that the lower swelling effect generated by the lower HAc pressure change inside the larger bore was mainly responsible for the decreased HAc flux. It appeared that HAc permeability was a strong HAc-concentration dependent variable due to the HAc-induced plasticization on the fibers, while the water permeability was weakly dependent on HAc concentration for a model 20% wt HAc/H₂O feed.

5.2 Model Development

The finite element method was used to simulate the pressure change in the bore side of a hollow fiber. A hollow fiber was divided into a number of differential elements and a mass balance was built in each differential element. The shell feed mode was applied to separate HAc/H₂O mixtures at about 101°C. Figure 5.1 illustrates the schematic diagram of this method for a “one-ended single-fiber” module. This concept can be easily extended to a double-ended one.

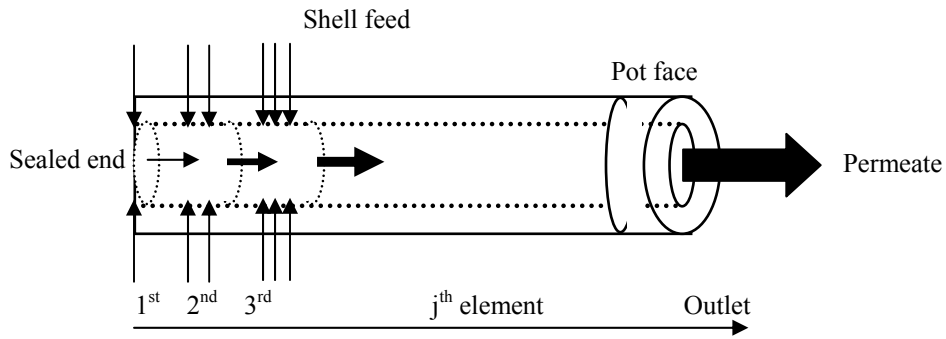


Figure 5.1: Schematic diagram of the finite element method for a one-ended module

The key assumptions involved in the mathematical model are as follows:

- (1) The behavior of the permeate gases is ideal and laminar;
- (2) The hollow fiber-based pervaporation module is isothermal ($\sim 101^\circ\text{C}$);
- (3) Shell feed is used;
- (4) The pressure in the shell side (feed side) is constant (1 atm);
- (5) Operation is at the steady state;
- (6) The total number of 10 is used to divide the available length (~ 20 cm) of a hollow fiber into differential elements.

The Hagen-Poiseuille equation is used to model the bore pressure change of a hollow fiber [3-4, 12].

$$\frac{d(p^2)}{dz} = \frac{256RT\mu}{\pi d^4} \left(\frac{dn_{\text{mol}}}{dt} \right) \quad (5.1)$$

where p is the pressure in the bore side, z is the fiber length, R is the universal gas constant, T is temperature, d is the inner diameter, μ is gas viscosity, n_{mol} is the total mole permeates that are obtained on the downstream/bore side, and t is time.

For the j^{th} element of a hollow fiber shown in Figure 5.2, equation 5.1 can be integrated to yield:

$$p_{j-1}^2 - p_j^2 = \frac{256RT\mu_j}{\pi d^4} \frac{F_j}{\Delta z} \quad (5.2)$$

where p_{j-1} and p_j are the pressures in and out the j^{th} element along the axial direction of a hollow fiber, Δz is the fiber length in the j^{th} element, F_j is the mole flowrate along the axial direction and assumed to be constant in the j^{th} element, and μ_j is the average gas viscosity in the j^{th} element that is estimated based upon the following equation,

$$\mu_j = \mu_{\text{H}_2\text{O}} y_{j,\text{H}_2\text{O}} + \mu_{\text{HAc}} (1 - y_{j,\text{H}_2\text{O}}) \quad (5.3)$$

where $\mu_{\text{H}_2\text{O}}$ and μ_{HAc} represent H_2O and HAc viscosities, and $y_{j,\text{H}_2\text{O}}$ represents the H_2O concentration in the j^{th} element.

The j^{th} Element

$$\left(\frac{\mathcal{P}}{\ell} \right)_{\text{H}_2\text{O}} \cdot \Delta p_{j,\text{H}_2\text{O}} \cdot (\pi D \cdot \Delta z) + \left(\frac{\mathcal{P}}{\ell} \right)_{\text{HAc}} \cdot \Delta p_{j,\text{HAc}} \cdot (\pi D \cdot \Delta z)$$

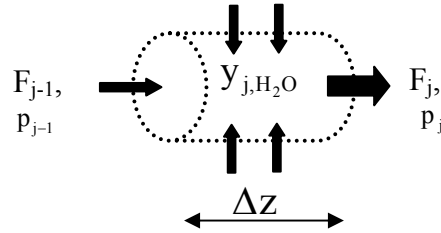


Figure 5.2: Schematic diagram of the j^{th} element in a hollow fiber

Thus, the H_2O concentration in the j^{th} element, $y_{j,\text{H}_2\text{O}}$, can be obtained as follows:

$$y_{j,H_2O} = \frac{F_{j-1} \cdot y_{j-1,H_2O} + \left(\frac{\mathcal{P}}{\ell}\right)_{H_2O} \cdot \Delta p_{j,H_2O} \cdot (\pi D \cdot \Delta z)}{F_{j-1} + \left[\left(\frac{\mathcal{P}}{\ell}\right)_{H_2O} \cdot \Delta p_{j,H_2O} \cdot (\pi D \cdot \Delta z) + \left(\frac{\mathcal{P}}{\ell}\right)_{HAc} \cdot \Delta p_{j,HAc} \cdot (\pi D \cdot \Delta z)\right]} \quad (5.4)$$

where $\left(\frac{\mathcal{P}}{\ell}\right)_{H_2O}$ and $\left(\frac{\mathcal{P}}{\ell}\right)_{HAc}$ are the average permeances of water and acetic acid for a given HAc feed concentration. The symbol of $\Delta p_{j,H_2O}$ is the partial pressure difference across the membrane for component H_2O in the j^{th} element, and $\Delta p_{j,HAc}$ is the partial pressure difference across the membrane for component HAc in the j^{th} element. D is the outer diameter. $\Delta p_{j,H_2O}$ and $\Delta p_{j,HAc}$ are defined as:

$$\begin{cases} \Delta p_{j,H_2O} = x_{H_2O} \gamma_{H_2O} p_{H_2O}^* - y_{j,H_2O} p_j \\ \Delta p_{j,HAc} = (1 - x_{H_2O}) \gamma_{HAc} p_{HAc}^* - (1 - y_{j,H_2O}) p_j \end{cases} \quad (5.5)$$

where x_{H_2O} and $(1 - x_{H_2O})$ are the respective mole fractions of H_2O and HAc in the feeding liquid, γ_{H_2O} and γ_{HAc} are the activity coefficients for H_2O and HAc, $p_{H_2O}^*$ and p_{HAc}^* are the saturated vapor pressures at the operating temperature for H_2O and HAc, y_{j,H_2O} and $(1 - y_{j,H_2O})$ are the respective mole fractions of H_2O and HAc in the bore side in the j^{th} element, and p_j is the total pressure in the bore side in the j^{th} element.

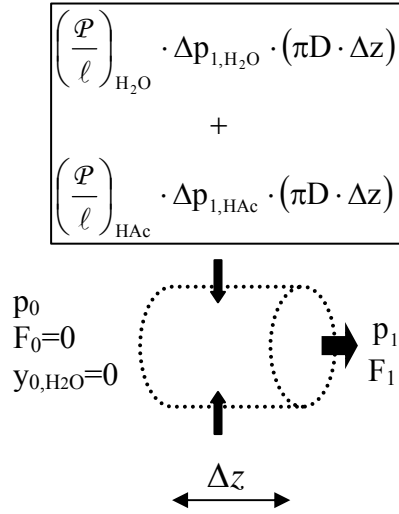
Therefore, the mass balance in the j^{th} element can be expressed as:

$$F_j = F_{j-1} + \left[\left(\frac{\mathcal{P}}{\ell}\right)_{H_2O} \cdot \Delta p_{j,H_2O} \cdot (\pi D \cdot \Delta z) + \left(\frac{\mathcal{P}}{\ell}\right)_{HAc} \cdot \Delta p_{j,HAc} \cdot (\pi D \cdot \Delta z)\right] \quad (5.6)$$

where F_{j-1} and F_j are the flowrates in and out the j^{th} element.

The first and last differential elements of a hollow fiber, i.e. the sealed end and pot face, are shown in Figure 5.3 due to their unique properties.

1st Element / Sealed End of Fiber



Last Element / Pot Face

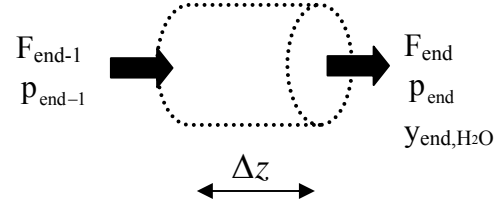


Figure 5.3: Schematic diagram of sealed end and pot face of a fiber

No in-flowrate exists for the sealed end element and no permeation occurs in the pot face of a fiber. Equations 5.7 (a-c) and 5.8 (a-c) show the bore pressure change, total mass balance, and H₂O concentration inside the bore for the sealed end and pot face element, respectively.

$$\left\{ \begin{array}{l} p_0^2 - p_1^2 = \frac{256RT\mu_1}{\pi d^4} \frac{F_1}{\Delta z} \quad (5.7_a) \\ F_1 = F_0 + \left[\left(\frac{\mathcal{P}}{\ell} \right)_{H_2O} \cdot \Delta p_{1,H_2O} \cdot (\pi D \cdot \Delta z) + \left(\frac{\mathcal{P}}{\ell} \right)_{HAc} \cdot \Delta p_{1,HAc} \cdot (\pi D \cdot \Delta z) \right] \quad (5.7_b) \\ y_{1,H_2O} = \frac{F_0 \cdot y_{0,H_2O} + \left(\frac{\mathcal{P}}{\ell} \right)_{H_2O} \cdot \Delta p_{1,H_2O} \cdot (\pi D \cdot \Delta z)}{F_1} \quad (5.7_c) \end{array} \right.$$

$$\left\{ \begin{array}{l} p_{\text{end-1}}^2 - p_{\text{end}}^2 = \frac{256RT\mu_{\text{end}}}{\pi d^4} \frac{F_{\text{end}}}{\Delta z} \\ F_{\text{end}} = F_{\text{end-1}} \\ y_{\text{end,H}_2\text{O}} = y_{\text{end-1,H}_2\text{O}} \end{array} \right. \quad \begin{array}{l} (5.8_a) \\ (5.8_b) \\ (5.8_c) \end{array}$$

where F_0 and F_1 are the flowrates in and out the 1st element, $\Delta p_{1,\text{H}_2\text{O}}$ is the partial pressure difference across the membrane for H_2O in the 1st element, and $\Delta p_{1,\text{HAc}}$ is the partial pressure difference across the membrane for HAc in the 1st element. The symbols of p_0 and p_1 are the total pressures in and out the 1st element in the bore side along the axial direction of a hollow fiber, $F_{\text{end-1}}$ and F_{end} are the flowrates in and out the last element, $p_{\text{end-1}}$ and p_{end} are the total pressures in and out the last element in the bore side along the axial direction of a hollow fiber, $y_{0,\text{H}_2\text{O}}$, $y_{1,\text{H}_2\text{O}}$, $y_{\text{end-1,H}_2\text{O}}$, and $y_{\text{end,H}_2\text{O}}$ represent the H_2O concentrations in the 1st, 2nd, penultimate, and last element, and μ_1 and μ_{end} are viscosities in the 1st and last element, respectively.

The bore pressure at the sealed end of a fiber p_0 , the average H_2O permeance

$\left(\frac{\mathcal{P}}{\ell}\right)_{\text{H}_2\text{O}}$, and the average HAc permeance $\left(\frac{\mathcal{P}}{\ell}\right)_{\text{HAc}}$ are three initial guesses. The total

flowrate and water concentration at the sealed end are equal to zero, i.e. $F_0=0$ and $y_{0,\text{H}_2\text{O}}=0$. The pot face is modeled as a straight pipe without permeation through the fiber wall. The equations 5.2-5.8 are iterated until the following three boundary conditions are satisfied.

1) The modeled outlet total pressure, p_{end} , matches the measured outlet pressure,

$p_{\text{end,measure}}$;

2) The modeled outlet flowrate, F_{end} , matches the measured outlet flowrate,

$F_{\text{end,measure}}$;

3) The modeled outlet mole fraction of component H_2O , $y_{\text{end,H}_2\text{O}}$, matches the measured outlet mole fraction, $y_{\text{end,H}_2\text{O,measure}}$.

Macro[®] function in Microsoft Excel[®] 2002 was used to solve these coupled non-linear equations by iterations to obtain the values of p_0 , $\left(\frac{\mathcal{P}}{\ell}\right)_{\text{H}_2\text{O}}$, and $\left(\frac{\mathcal{P}}{\ell}\right)_{\text{HAc}}$.

Some important points have to be clarified before the modeling work is discussed in the following sections.

1) Experimental results of water and HAc fluxes are calculated based upon equation 5.9.

$$\begin{cases} \text{Flux}_{\text{H}_2\text{O,Expt.}} (\text{kg} / \text{m}^2 \text{hr}) = \frac{F_{\text{end,measure}}}{\pi DL} \\ \text{Flux}_{\text{HAc,Expt.}} (\text{kg} / \text{m}^2 \text{hr}) = \frac{F_{\text{end,measure}} (1 - y_{\text{end,H}_2\text{O,measure}})}{\pi DL} \end{cases} \quad (5.9)$$

2) The water and HAc permeabilities without bore pressure change correction can be simply calculated by equation 5.10.

$$\begin{cases} (\mathcal{P})_{\text{H}_2\text{O,No bore pressure change correction}} (\text{Barrers}) = \frac{\text{Flux}_{\text{H}_2\text{O,Expt.}}}{x_{\text{H}_2\text{O}} \gamma_{\text{H}_2\text{O}} p_{\text{H}_2\text{O}}^* - 0} \cdot \ell_{\text{skin}} \\ (\mathcal{P})_{\text{HAc,No bore pressure change correction}} (\text{Barrers}) = \frac{\text{Flux}_{\text{HAc,Expt.}}}{x_{\text{HAc}} \gamma_{\text{HAc}} p_{\text{HAc}}^* - 0} \cdot \ell_{\text{skin}} \end{cases} \quad (5.10)$$

3) The water and HAc permeabilities of each fiber with bore pressure change correction ($\mathcal{P}_{\text{H}_2\text{O,pressure change correction}}$ and $\mathcal{P}_{\text{HAc,pressure change correction}}$) are obtained from iterations of the equations 5.2-5.8. The experimental results of $p_{\text{end,measure}}$, $F_{\text{end,measure}}$, and $y_{\text{end,H}_2\text{O,measure}}$ for each fiber are used as boundary conditions. The bore pressure at the

sealed end, p_0 , and the pressure distribution inside the bore are solved automatically once the iterations are completed.

4) The model expectation of water and HAc fluxes is derived following step 3). That is, the corrected water and HAc permeabilities are used to calculate the water and HAc fluxes as below.

$$\begin{cases} \text{Flux}_{\text{H}_2\text{O},\text{Model}} (\text{kg} / \text{m}^2 \text{hr}) = \frac{P_{\text{H}_2\text{O},\text{pressure change correction}}}{\ell_{\text{skin}}} \cdot (x_{\text{H}_2\text{O}} \gamma_{\text{H}_2\text{O}} p_{\text{H}_2\text{O}}^*) \\ \text{Flux}_{\text{HAc},\text{Model}} (\text{kg} / \text{m}^2 \text{hr}) = \frac{P_{\text{HAc},\text{pressure change correction}}}{\ell_{\text{skin}}} \cdot (x_{\text{HAc}} \gamma_{\text{HAc}} p_{\text{HAc}}^*) \end{cases} \quad (5.11)$$

All parameters have been defined in terms of the equations 5.1-5.8.

5.3 Results and Discussion

The model was used to investigate the bore pressure change effects on hollow fibers for pure gas permeation tests, pure DI water feed tests, and 20% wt HAc concentration feed tests. HAc and water transport behaviors in the polymer can be better understood from the model results.

5.3.1 Model Results with Pure Gas Permeation Tests

Although the model is developed for separating mixtures, it can be easily extended to correct the bore pressure change in pure component permeation tests. The component mole fraction is absolutely assigned as one. The experimental parameters of FB1.4 fiber for pure gas permeation tests including N_2 , O_2 , and He, are listed in Table 5.1. These values were applied as inputs in the model to correct the bore pressure change.

Table 5.1: Parameters used as model inputs for FB1.4 fiber in pure gas permeation tests

Parameters	Values
P_{end} (psi)	14.7
F_{end} (cc(STP)/sec)	N ₂ : 0.0083, O ₂ : 0.058, He: 0.75
Y_{end}	1
Outer diameter (μm)	231
Inner diameter (μm)	135
Available separation length (cm)	18.2
Length of pot face (cm)	5
Temperature (°C)	34
Pressure in the feed side (psi)	100.5

Table 5.2 shows corrected (bore pressure change involved) and uncorrected (no bore pressure change involved) results of FB1.4 fiber with pure gas permeation tests.

Table 5.2: Comparison between uncorrected and corrected bore pressure changes for FB1.4 fiber

	Uncorrected	Corrected	% Increment
N ₂ (GPU)	0.55	0.552	0.36
O ₂ (GPU)	3.8	3.9	2.6
He (GPU)	50	56	12.1
$\alpha_{\text{O}_2/\text{N}_2}$	6.9	7.1	2.8
$\alpha_{\text{He}/\text{N}_2}$	90	101	12.2

As it can be seen, all the permeances increase when the bore pressure change is taken into account in the model. Clearly the bore pressure change affects highly permeable gases significantly since the real (corrected) He permeance increases about 12.1% compared to 0.36% of the N₂ permeance from the model results. The higher flux associated with highly permeable gases causes more significant pressure buildup inside the bore of a hollow fiber. This can decrease the pressure driving force across the membrane and the corresponding flux more dramatically. Therefore, the true membrane selectivity is undoubtedly underestimated if one fails to correct the bore pressure change for high/low permeable gas pairs such as He/N₂. Figure 5.4 shows the modeled pressure distribution along the axial direction of a hollow fiber for N₂, O₂, and He permeations.

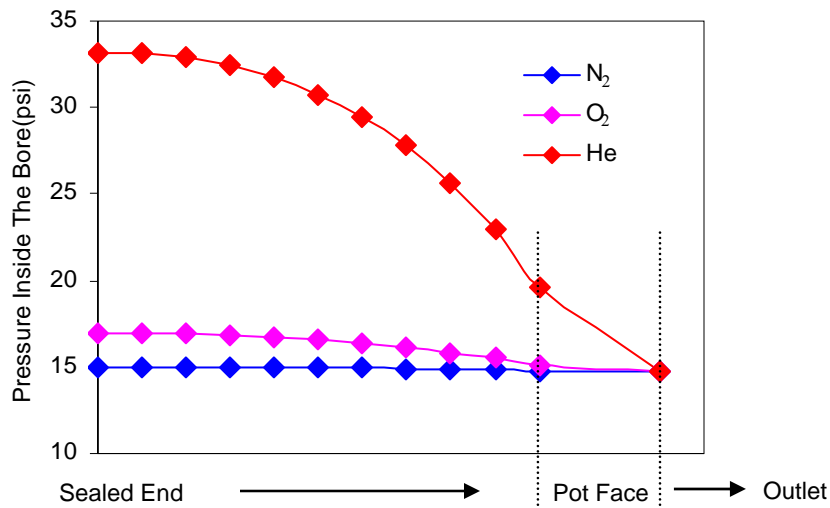


Figure 5.4: Modeled pressure distribution of N₂, O₂, and He inside the bore of FB1.4 fiber

The negative effects caused by the bore pressure change should be distinguished from the substrate resistance as both can reduce permeance and selectivity. The bore pressure change is relevant to the macro-configuration of a hollow fiber, while the

substrate resistance is related to the micro-structure of any membrane material. Therefore, the inherent material property can be obtained once the bore pressure change is corrected using this model.

In terms of equation 5.1,

$$\frac{d(p^2)}{dz} = \frac{256RT\mu}{\pi d^4} \left(\frac{dn_{\text{mol}}}{dt} \right) \quad (5.1)$$

it is apparent that an increase of “d” (inner diameter of a hollow fiber) can effectively decrease $\frac{d(p^2)}{dz}$ (the bore pressure change), while maintaining the same flowrate of $\left(\frac{dn_{\text{mol}}}{dt} \right)$. In other words, spinning a large bore size fiber is a good solution to minimize the bore pressure change, especially for highly permeable gases.

5.3.2 Model Results for Pervaporation Tests with Pure DI Water Feeds

Pure DI water feeds were used in pervaporation to investigate the effects of the bore pressure change on different size fibers. Water does not show any noticeable effects on the polymer, as discussed in Chapter 4. Thus, the model results that take the bore pressure change into consideration should represent the inherent fiber properties.

Table 5.3 shows the inner diameter and skin thickness of hollow fibers that are used in the model. The skin thickness is estimated based upon pure gas permeation tests, which have been described in Chapter 3.

Table 5.3: Inner diameter and skin thickness of hollow fibers used in the model
 *: Calculated based upon pure gas permeation tests (N₂ and O₂) using Equation 3.3

Fiber Identification	Inner Diameter/Bore Size (μm)	Thickness of Skin Layer (μm)*
DW21.3_1	130	0.37
FB1.4_1	165	0.59
FB4.5	229	0.88
FB2.6_1	290	0.77
FB4.7_2	311	0.69
FB4.7_1	331	0.69
FB4.12_1	452	0.60

The water permeability can be obtained for each fiber as the bore pressure change is corrected. It should be pointed out that the water permeability instead of water permeance is used here, in order to avoid the possible influences of skin thickness. Theoretically the same water permeability should be achieved regardless of the fiber size since negligible interaction exists between water and the polymer. Figure 5.5 shows the model results of the water permeability with and without bore pressure change correction for different size fibers.

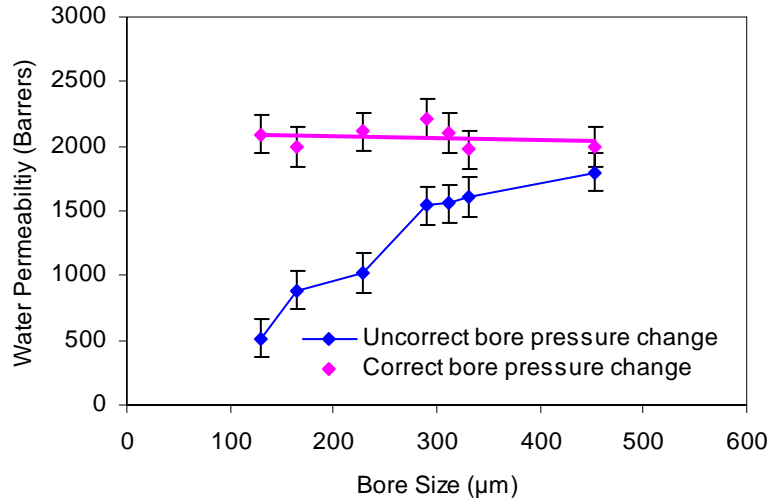


Figure 5.5: Variation of water permeability vs. bore size with and without bore pressure change correction

As it can be seen, the water permeability is almost constant with the bore pressure change correction for different size fibers in contrast to uncorrected results. This further confirms that water has negligible effects on the polymer. The bore pressure change must be corrected due to high water flux through the membrane; otherwise, the underestimated water permeability will be regarded as the inherent polymer properties. The modeled water pressure distribution inside the different bore size fiber along the axial direction is shown in Figure 5.6. The pressure buildup inside a small bore fiber is much larger than that of a large bore size fiber. This can reduce the pressure driving force across the membrane and decrease the water flux more dramatically.

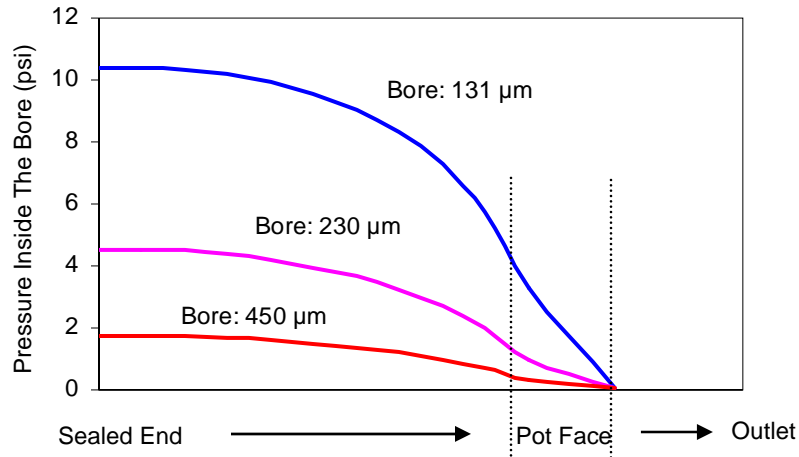


Figure 5.6: Modeled pressure distribution inside the bore for different bore size fibers

Figure 5.7 shows the variation of water flux with the bore size for both model and experimental results. The difference of water flux between the model and experimental results decreases with an increment of the bore size. Less than 10% discrepancy can be observed as the bore size increases to 350 μm . In this research, a hollow fiber with the bore size larger than 450 μm is difficult to spin due to the limited resource. However, the available results clearly indicate that a large bore size fiber is a good solution to minimize the bore pressure change. In addition, it is reasonable to neglect the bore pressure change if the bore size is larger than 350 μm or the outer diameter is larger than 500 μm in this work.

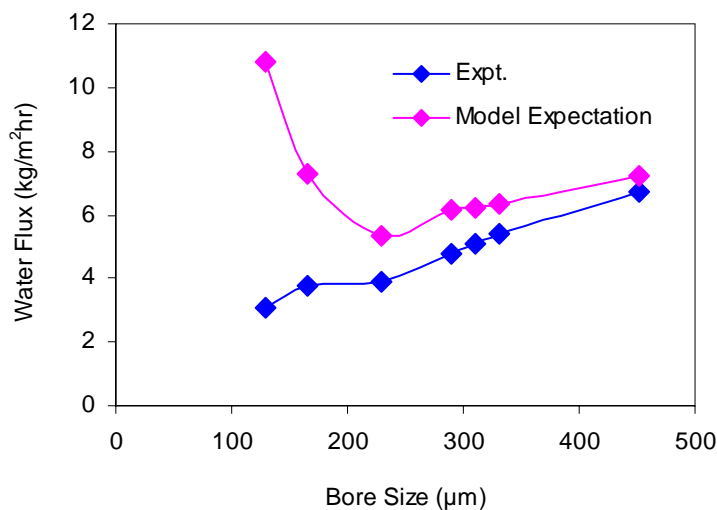


Figure 5.7: Comparison of water flux between model and experimental results for different bore size fibers with pure DI water feeds

5.3.3 Model Results for Pervaporation Tests with 20% HAc/H₂O Feeds

20% wt HAc/H₂O feeds were used in pervaporation for different size hollow fibers. Due to the HAc-induced swelling effects shown in Chapter 4, the bore pressure change has to be corrected based on the average water and HAc permeability for each fiber. The water and HAc permeability are assumed constant for the given bore size fiber in the model. Figure 5.8 shows the variation of water flux with different bore size fibers for model and experimental results. It was observed that the experimental results were very close to the model expectation as the bore size was bigger than 350 μm. This is in good agreement with the previous discussion. The bore pressure change associated with high water flux through the fiber wall can be significantly decreased in a large bore size fiber.

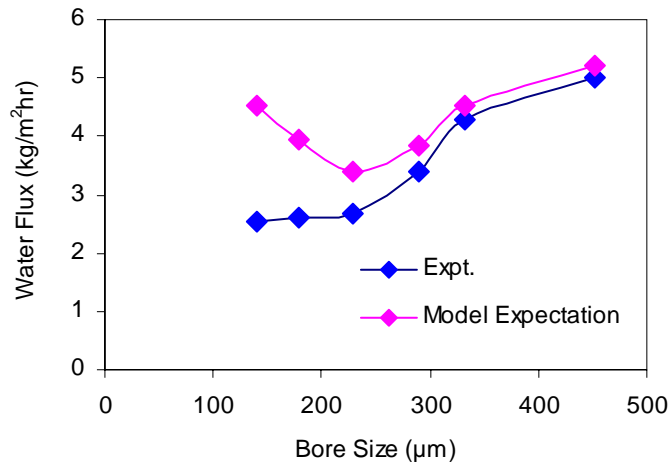


Figure 5.8: Comparison of water flux between model and experimental results for different bore size fibers with 20% wt HAc/H₂O feeds

The model and experimental results of the HAc flux are shown in Figure 5.9 for different size fibers. The bore pressure change influences highly permeable penetrant significantly; however, the fluxes of all the penetrants should be affected. The HAc flux might not increase as much as the water flux in a large bore size fiber because of its “slow” penetrant properties theoretically.

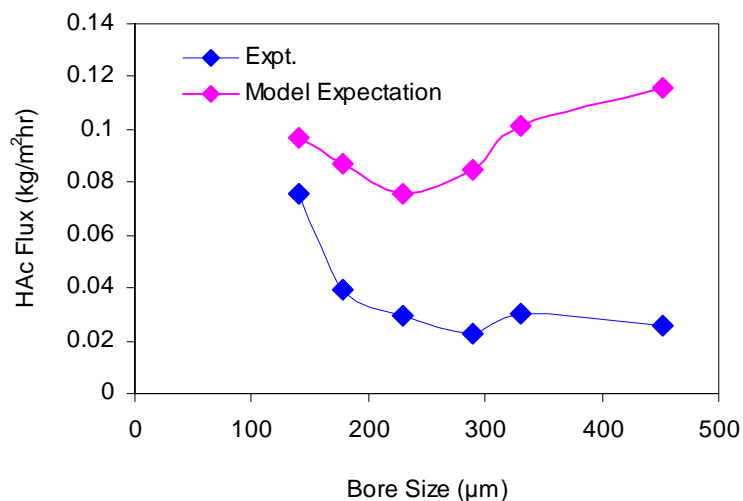


Figure 5.9: Comparison of HAc flux between model and experimental results for different bore size fibers with 20% wt HAc/H₂O feeds

It is clear that a big difference exists between the model and experimental results. The discrepancy tends to be larger with the increment of the bore size. As opposed to the model expectation, in which HAc would not decrease in a large bore size fiber due to the low bore pressure change, the *depression* of the HAc flux was observed *experimentally*. This indicates that HAc has strong swelling effects on the polymer. The decreased swelling effects in the bore side of a large bore size fiber are responsible for the reduced HAc flux through the polymer. In fact, two opposite factors, the bore pressure change and HAc-induced swelling, affect the HAc transport behavior. It is of interest to investigate which one is more dominant. With the same HAc concentration feeds (20% wt HAc), the corrected HAc permeability and the modeled *average HAc partial pressure inside the bore* are calculated for different bore size fibers with the bore pressure change considered, as shown in Figure 5.10.

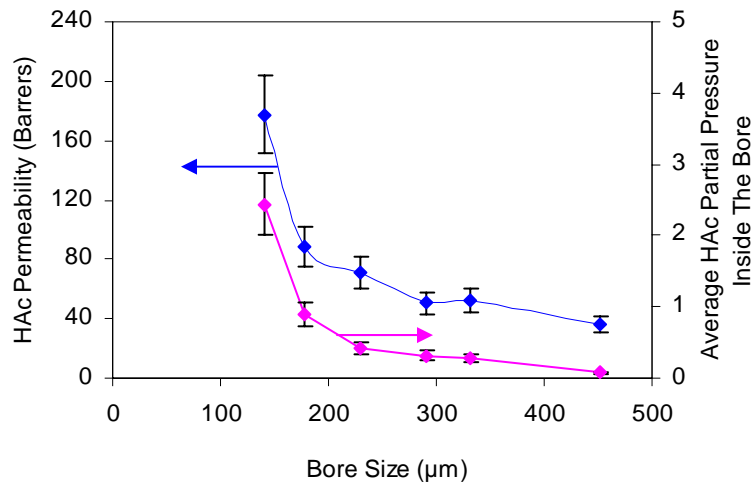


Figure 5.10: HAc permeability and HAc partial pressure inside the bore for different bore size fibers with bore pressure change correction

The HAc permeability drops down in a large bore size fiber even with the bore pressure change correction. Moreover, the decreased average HAc partial pressure inside

the large bore was observed in the model as well. Both suggest that the HAc-induced swelling in the bore side, instead of the bore pressure change, is a determinant factor for the non-constant HAc permeability. The HAc permeability is a HAc concentration-dependent variable and relies upon the swelling condition inside the bore. A large bore size fiber can decrease the pressure change in the bore side and thus reduce the HAc-induced swelling effects. Therefore, it is not surprising that the decreased HAc permeability can be observed with an increment of the bore size.

Although the bore pressure change plays an important role in the water flux, it is not clear whether the HAc-induced swelling in the bore side has any effects on the water transport through the polymer. Thus, the water permeability is calculated for different bore size fibers with the bore pressure change correction, as shown in Figure 5.11.

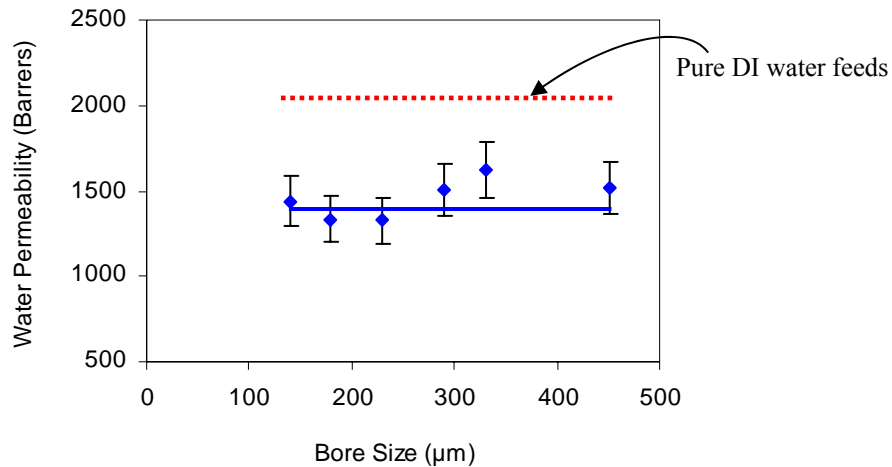


Figure 5.11: Water permeabilities with bore pressure change correction for different bore size fibers

The water permeability is not absolutely constant and the maximum deviation is about 12%. This suggests that the HAc-induced swelling effects in the bore side might

influence the water transport for the 20% wt HAc/H₂O mixture feed but not significantly. It is noticed that the water permeability decreases with 20% wt HAc/H₂O mixture feeds in contrast to pure DI water feeds. HAc is more capable of competing for the additional transport sites even under the swelling condition, resulting in the reduction of the water permeability in a mixture feed. This further confirms that the HAc-induced swelling effect on the hollow fiber mostly facilitates the HAc transport through the polymer instead of water.

5.4 Summary

A mathematical model was developed to demonstrate the effects of the pressure change in the bore side of a hollow fiber. The bore pressure change can affect fluxes of all the penetrants, but highly permeable penetrants are influenced much more seriously. The true membrane selectivity will be underestimated for high/low permeable gas pairs without the bore pressure change correction if the highly permeable gas is the end-product. A large bore size fiber has been proved to be very effective to minimize the bore pressure change from this model.

The water flux increases up to 150% in a large bore size fiber for pervaporation with 20% wt HAc/H₂O mixture feeds in contrast to a small bore size fiber. Further, the water permeability with the bore pressure change correction varies much less than the HAc permeability in the model. This indicates that water is relatively “neutral” to the polymer and the decreased average driving force from the bore pressure change is a key to determine its productivity. The HAc-induced swelling effects in the bore side are relatively negligible for the water permeability; however, they can *influence the HAc*

permeability significantly. The HAc-induced swelling effects are much more dominant on the HAc transport through the membrane than the effects of the bore pressure change on the average HAc driving force across the membrane. The decreased HAc permeability can be observed with an increment of the bore size due to the decreased HAc-induced swelling in a large bore size fiber in the model. This significant discovery was not anticipated in our original research plan and was an important outcome of this coupled experimental and theoretical study.

The separation factor is improved in a large bore size fiber due to the increased water flux and decreased HAc flux. This “win-win” situation can be further explained by the decreased HAc permeability and relatively constant water permeability in a large bore size fiber from the modeling work.

5.5 References

- [1] Nader M. A. and Abbas, A. *Modeling an industrial reverse osmosis unit*. Desalination. 1999, 126, 33-39.
- [2] Lim, S. P., Tan, X., and Li, K. *Gas/vapor separation using membranes: Effect of pressure drop in lumen of hollow fibers*. Chem. Eng. Sci. 2000, 55, 2641-2652.
- [3] Pan C. Y. and Habgood H. W. *Gas separation by permeation: Part I. Calculation methods and parametric analysis*. Canadian J. Chem. Eng. 1978, 56, 197-209.
- [4] Pan C. Y. and Habgood H. W. *Gas separation by permeation: Part II. Effect of permeate pressure drop and choice of permeate pressure*. Canadian J. Chem. Eng. 1978, 56, 210-217.
- [5] Chern, R. T., Koros, W. J., and Fedkiw, P. S. *Simulation of a hollow fiber gas separator: The effects of process and design variables*. Ind. Eng. Chem., Process, Design and Development. 1985, 24, 1015-1022.
- [6] Goran, T. and Milan, V. *Pressure drops and hydraulic resistances in a three-phase hollow fiber membrane contactor with frame elements*. Chem. Eng. Proc. 2001, 40, 3-11.

- [7] Mellis, R., Gill, W. N., and Belfort, G. *Fluid dynamics in a tubular membrane: theory and experiment*. Chem. Eng. Commun. 1993, 122, 103-125.
- [8] He, G., Zhou, Y., Xu, R., and Zhu, B. *Study on pressure drop in hollow-fiber membrane for gas separation*. Mo Kexue Yu Jishu. 1993, 13(2), 22-28.
- [9] Wang, R., Liu, S. L., Lin, T. T., and Chung, T. S. *Characterization of hollow fiber membranes in a permeator using binary gas mixtures*. Chem. Eng. Sci. 2002, 57(6), 967-976.
- [10] Thorman, J. M., Rhim, H., and Hwang, S. *Gas separation by diffusion through silicone rubber capillaries*. Chem. Eng. Sci. 1975, 30(7), 751-754.
- [11] Lim, S. P. and Li, K. *Internally staged permeator for gas/vapor separation: effect of pressure drop in annuli of annular hollow fibers*. Chem. Eng. Sci. 2001, 56, 3907-3913.
- [12] Thundiyil, M.J. and Koros, W.J. *Mathematical modeling of gas separation permeators – for radial crossflow, countercurrent, and cocurrent hollow fiber membrane modules*. J. Membr. Sci. 1997, 125, 275-291.

Chapter 6: Pervaporation of HAc/H₂O Mixtures Using Thermally Annealed Hollow Fibers

6.1 Introduction

Advanced pervaporation separations are trending towards the application of membranes due to their low energy and capital costs. However, the trade-off between polymer permeability (productivity) and selectivity (efficiency), especially with aggressive organic solvents that can cause severe plasticization, limits the adoption of this membrane technology. The previous chapter illustrates this issue with regard to HAc interactions with Matrimid[®]. Although research is on-going for developing new polymers to improve the membrane performance, an alternative route to enhancing the selectivity of the currently available membranes can be achieved by a thermal annealing method.

The Matrimid[®] hollow fibers used in this work are spun by the “dry-jet, wet-quench” spinning method, as shown in Figure 3.2. Due to rapid phase separation in the air gap, the formed outer selective skin layer of a hollow fiber is in a thermodynamic non-equilibrium state and has “excess” un-relaxed free volume. Once this fiber experiences aggressive solvents like acetic acid, the polymer chains can be swelled and dilated, resulting in the membrane selectivity being lower than the intrinsic value.

A membrane can be treated at an elevated temperature to improve its performance, which is usually called “thermal annealing”, “heat cure” or “heat treatment”. Kawakami et al. [1] cured 6FDA-m-DDS dense film membranes at 150, 200, and 250°C, and found that the packing density and the fluorescence intensity of this polyimide increased sharply with the increasing curing temperature. An increase in intermolecular and/or intra-molecular interactions by a charge transfer complex was

proposed. Krol et al. [2] investigated the gas separation of propane/propylene using the polyimide Matrimid[®] 5218 with different heat treatment environments. They observed that the densification of the fiber morphology occurred due to heat treatment and mild heat treatment appeared to be effective in suppressing the propylene-induced plasticization. Barsema et al. [3] examined the intermediate structures between annealing and carbonization when exposing the polyimide membranes at different heating temperatures between 300 and 525°C. Gas permeation measurements with He, N₂, O₂, CO₂, and C₃H₆ indicated that the structure became more dense at temperatures below the T_g of the polymer, while the formation of charge transfer complexes took place above the T_g. When compared with the untreated membranes, all heat treated membranes showed good resistance to plasticization by C₃H₆. Bos et al. [4] stabilized the Matrimid membranes by heat treatment at 350°C to suppress the CO₂-induced plasticization. Chemical crosslinking was believed to have occurred since the heat treated film did not dissolve in the original casting solvent any more. Wind et al. [5-7] found that both thermal annealing and covalent cross-linking of the polyimide films could reduce swelling to prevent large increases in the CO₂ diffusion coefficient at high feed pressures. The CO₂ permeability and polymer free volume strongly depended on the annealing temperature. Hibshman et al. [8] investigated the annealing effects on the polyimide-organosilicate hybrid membranes. The transport properties of these hybrid membranes were evaluated using pure gases such as He, N₂, O₂, CO₂, and CH₄. However, thermal annealing has not been investigated in depth in liquid separation to suppress the swelling effects from aggressive organic solvents in contrast to gas separation.

In this work, Matrimid[®] hollow fibers were treated at high temperatures but still below T_g ($305^{\circ}\text{C} \sim 315^{\circ}\text{C}$) to improve the membrane performance. The chemical structure of Matrimid[®] is shown in Figure 6.1. It contains alternating electron donor and electron acceptor, which correspond to the phenylene group and aromatic imide group, respectively [9-11]. If enough mobility can be obtained through heat treatment, the aromatic imide group and phenylene group in different polymer chains will approach each other closely enough to allow π -electron interaction, which leads to the formation of charge transfer complexes. This behavior increases the packing density of the polymer chains and decreases the free volume in the outer selective skin layer. Thus, mobility of the polymer chains is dramatically restricted so that the rigid configuration formed among the adjacent polymer chains provides high size and shape discrimination between penetrants and also suppresses the penetrants-induced plasticization [12].

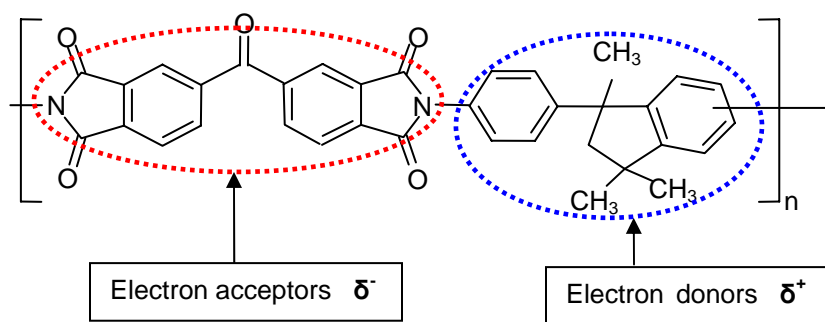


Figure 6.1: Chemical structure of Matrimid[®] showing electron acceptive and donative groups [9-11]

6.2 Spectroscopy Technology

Generally speaking, spectroscopy uses the interaction of energy with a sample to perform an analysis. The data that is obtained from spectroscopy is called a spectrum. A spectrum can be a plot of the detected energy intensity versus the wavelength (or mass or

momentum or frequency, etc.) of the energy. This plot contains a lot of information such as atomic and molecular energy levels, molecular geometries, chemical bonds, interactions of molecules, and related processes. Fourier Transform Infrared Spectroscopy (FTIR), Nuclear Magnetic Resonance (NMR), and Micro-Fluorescence are used to analyze membrane samples in this work due to their rapid and efficient features.

6.2.1 FTIR

FTIR is an analytical technique used to measure the absorption of various infrared light wavelengths by the material of interest. The absorbed energy can be converted by an organic molecule into energy of molecular rotation or vibration based upon the absorbed frequencies of infrared radiation. Thus, these infrared absorption bands identify specific molecular components and structures. Absorption bands that locate in the range of 4000 – 1500 cm^{-1} are typically from functional groups (e.g. -OH, C=O, N-H, CH₃, etc.). The region between 1500 - 400 cm^{-1} is referred to as intra-molecular phenomena that are highly specific for each material [13-14]. Bruker Tensor 27 with TGA-IR is used in this work to measure FTIR spectra.

6.2.2 ¹H NMR

Nuclei with an odd number of protons, neutrons, or both, have "nuclear spin" [14-15] and they are randomly oriented in the absence of a magnetic field. When a nucleus with a non-zero spin is placed in a magnetic field, the nuclear spin can align in either the same direction or in the opposite direction as the field. These two nuclear spin alignments have different energies and application of a magnetic field lifts the degeneracy of the

nuclear spins. In other words, absorption of the radiation causes the nuclear spin to realign or flip in the higher-energy direction. After reemitting radio frequency (RF) radiation, the nuclei will return back to the lower energy state. Nuclear magnetic resonance (NMR) spectroscopy is the absorption of radiofrequency radiation by a nucleus in a strong magnetic field. The spins of nuclei are sufficiently different so that NMR experiments can be sensitive for only one particular isotope of one particular element. This makes NMR spectroscopy extremely useful for determining the structure of molecules. The NMR behavior of ^1H nuclei is examined in this project since it normally provides more structure information than ^{13}C NMR for our polymer. The ^1H NMR model used in this work is Varian 300 MHz spectrometer.

6.2.3 Fluorescence Spectroscopy

Fluorescence is the phenomenon in which light absorption of a given wavelength by a fluorescent group is followed by the emission of light at the longer wavelengths. Theoretically fluorescence contains three steps including excitation, excited-state, and fluorescence emission, as shown in Figure 6.2.

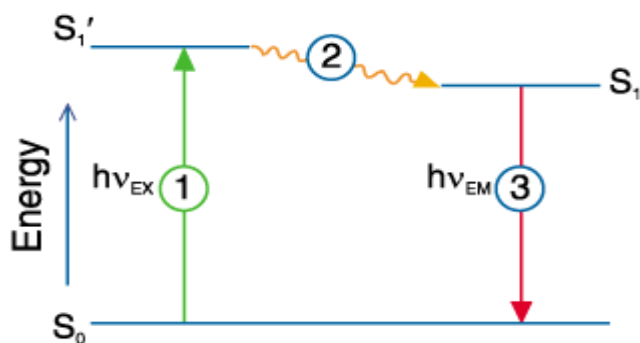


Figure 6.2: Jablonski diagram illustrating the processes involved in the creation of an excited electronic singlet state by optical absorption and subsequent emission of fluorescence [16].

In the first step, a photon of energy, $h\nu_{\text{EX}}$, that is supplied by an external source such as an incandescent lamp or a laser, is absorbed by the fluorophore, creating an excited electronic singlet state (S'_1). In the second step, this excited state exists for a finite time (typically 1–10 nanoseconds) and the fluorophore is subject to a multitude of possible interactions with its molecular environment. Thus, the energy of S'_1 can be partially dissipated, yielding a relaxed singlet excited state (S_1) from which fluorescence emission originates. However, not all the molecules initially excited by absorption (step 1) will return to the ground state (S_0) by fluorescence emission. Other processes such as collisional quench, fluorescence resonance energy transfer, and intersystem cross may also depopulate S_1 . In the last step, a photon of energy, $h\nu_{\text{EM}}$, is emitted, returning the fluorophore to its ground state S_0 . Due to energy dissipation during the excited-state (step 2), the energy of this photon is lower, and therefore of longer wavelength, than the excitation photon $h\nu_{\text{EX}}$. The distribution of wavelength-dependent intensity that causes fluorescence is referred to as the fluorescence excitation spectrum, and the distribution of wavelength-dependent intensity of emitted energy is known as the fluorescence emission spectrum. Clearly the emission intensity is proportional to the amplitude of the fluorescence excitation spectrum at the excitation wavelength [17-20].

Fluorescence has proven to be a powerful technique for studying molecular interactions in analytical chemistry, biochemistry, cell biology, physiology, nephrology, cardiology, photochemistry, and environmental science. However, very few literatures have been reported in membrane structure and function with fluorescence probes [1, 9, 21]. Micro-fluorescence (SEE #1000, 50X Objective) is used in this project to investigate

morphology changes of polymer chains and formation of charge transfer complexes for virgin and annealed fibers.

6.3 One Application of Fluorescence Technology in Benzophenone-Type polyimides

Q. Jin etc. [9] investigated the fluorescence spectrum of a benzophenone-type aromatic polyimide, i.e. PI(BTDA/DPM), as shown in Figure 6.3.

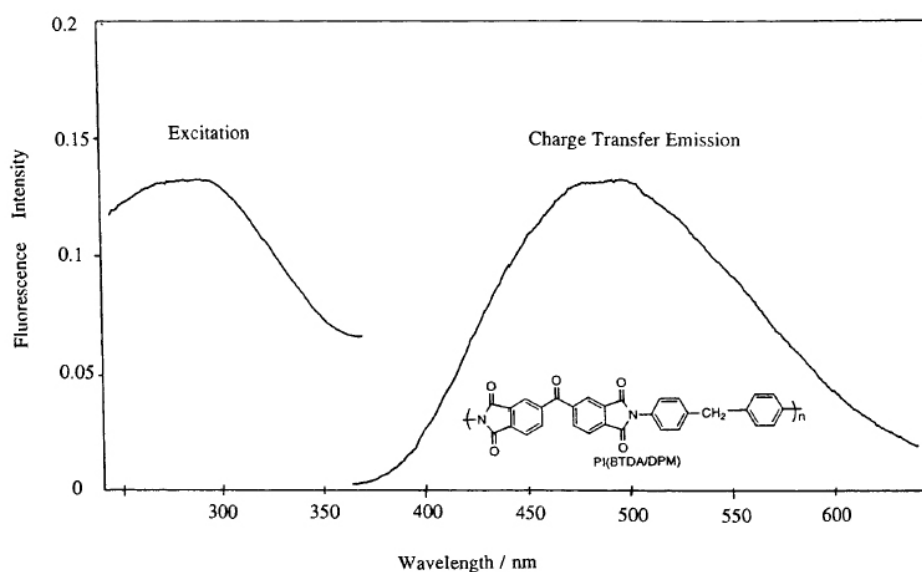


Figure 6.3: Fluorescence spectrum of a benzophenone-type aromatic polyimide PI (BTDA/DPM) film

The wavelength of 300 nm was used to excite the PI film and the fluorescence was observed at 500 nm. Compared to the model compound of BTDA, in which the phosphorescence peaks appeared at 440 and 480 nm, the authors claimed that the 500 nm fluorescence peak was attributed to the formation of charge transfer complexes. The authors also proposed that both intra- and inter-molecular charge transfer complexes existed in this benzophenone-type polyimide with aromatic diamine based upon UV

absorption spectra. Figure 6.4 shows the electron acceptor and donor, and charge transfer complexes for PI(BTDA/DPM) polymer used in this paper.

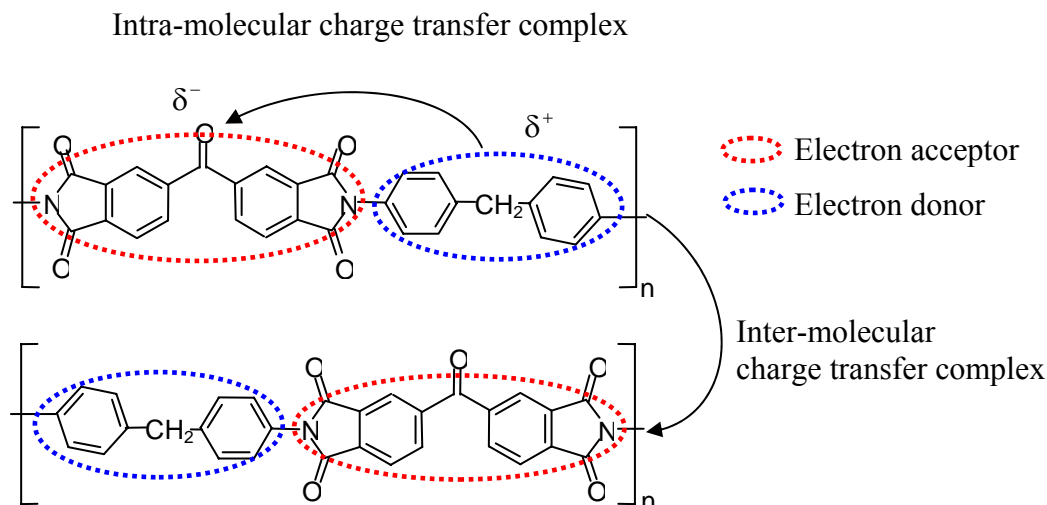


Figure 6.4: Intra- and inter-molecular charge transfer complexes for PI(BTDA/DPM) polymer [9]

6.4 Thermal Annealing Procedures

An oven is used to conduct heat treatment of the fibers. First, the oven is heated at the required temperature for 3 hours and drawn in vacuum until the environment reaches steady state. The hollow fibers are then placed into the oven immediately. After the desired time period for heat treatment, the fibers are taken out of the oven and placed on a Kimwipe® at room temperature for 1 hour. Next the pervaporation module can be assembled using these thermally annealed fibers for pervaporation tests. The detailed operating procedures for pervaporation experiments are described in Chapter 4.

Due to some limitations in our experimental setup, the highest annealing temperature can not exceed 220°C.

6.5 Separation Results with and without Thermal Annealing for 20% wt HAc Concentration Feeds

A model 20% wt HAc/H₂O mixture was used as a feed solution for pervaporation tests at the temperature of 101.5°C. The effects of annealing variables on the fiber performance were investigated below.

6.5.1 Heating Temperature

As stated in Chapter 3, the nascent fibers must be placed into a vacuum oven at 110°C for one hour to remove the residual solvents. The thermal treatment temperature for the fibers should be at least higher than 110°C, thus 150°C, 180°C, and 220°C were selected to perform heat treatment in vacuum with the FB5.6 state fibers for one hour. Once these fibers were ready, the pervaporation modules of FB5.6_21, FB5.6_31 and FB5.6_41 were prepared based upon different heating temperatures. In the mean time, FB5.6_11 module was made of a virgin fiber without any heat treatment as a reference. Pervaporation tests were conducted at 101.5°C using 20% HAc concentration feeds. Figure 6.5 and 6.6 show the permeance and selectivity of these four modules, respectively.

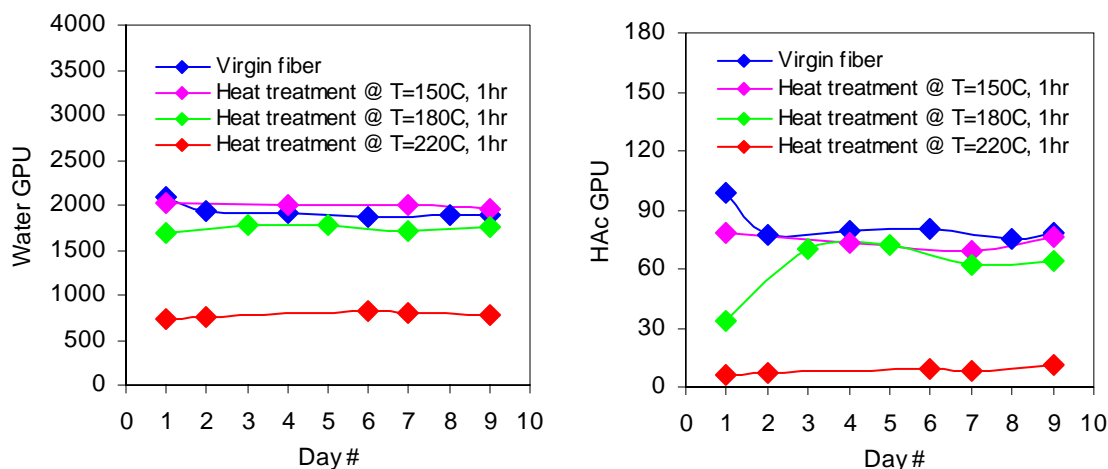


Figure 6.5: Effects of heating temperature on water and acetic acid permeances

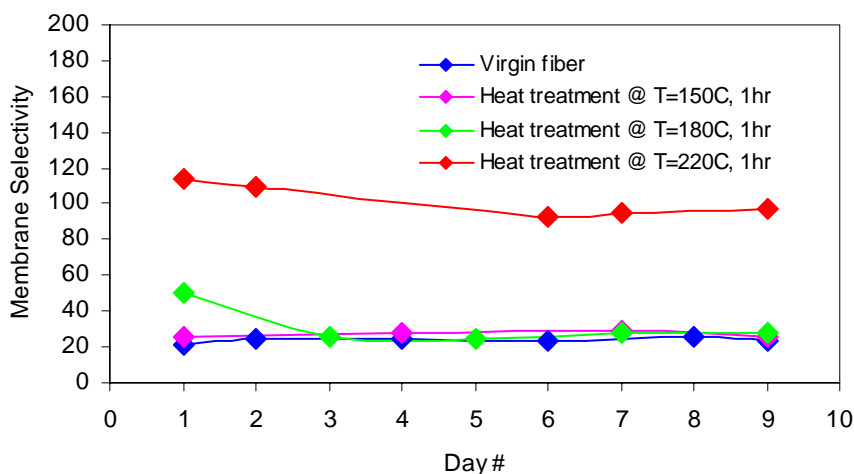


Figure 6.6: Effects of heating temperature on the membrane selectivity α_{mem}

The fiber with heat treatment at 220°C exhibits a significant enhancement in the membrane selectivity. Clearly this heating temperature enables the polymer chains to obtain enough mobility to allow charge transfer complexes being formed. The decreased free volume and altered free volume distribution hinder the HAc transport much more dramatically than water. Therefore, the membrane selectivity is improved while the permeances of both penetrants are reduced. In addition, the improved rigidity of the polymer chains due to heat treatment can suppress the swelling effects from acetic acid.

Thus, this fiber can maintain very good membrane selectivity ($\alpha \sim 95$) for up to 9 days. The fibers that are heated at 150°C and 180°C behave similar to the virgin fiber. The membrane selectivities are quite close in these three modules. This indicates that heat treatment at 150°C and 180°C can not provide enough energy to enhance noticeable shape and size discrimination ability of the polymer. Therefore, heating temperature must be optimized high enough but below T_g to keep the polymer in the glassy state. Table 6.1 shows the comparison between a virgin hollow fiber and an annealed hollow fiber.

Table 6.1: Comparison of separation results between a virgin hollow fiber and an annealed hollow fiber

Feed: 20% wt HAc/H ₂ O mixture	Hollow fiber without heat treatment (Selective skin: 0.61 μm)	Hollow fiber with heat treatment@ T=220°C 1hour (Selective skin: 0.61 μm)
Water Flux (kg/m ² hr)	4.98	1.65
HAc Flux (kg/m ² hr)	0.036	0.0033
Selectivity $\alpha_{\text{H}_2\text{O}/\text{HAc}}$	25	95

6.5.2 Spectroscopy Results for Annealed Hollow Fibers

Since a significant increase of the membrane selectivity has been observed with annealed fibers, it is necessary to investigate whether chemical reaction occurs with thermal annealing. It was observed that these annealed fibers can be dissolved in solvents such as NMP and CH₂Cl₂ easily. The FTIR spectrum of Matrimid obtained at room temperature is given in Figure 6.7 and corresponds well with the Matrimid spectra

obtained by other investigators [22-23]. The spectra of the untreated and treated Matrimid fibers are almost identical. This suggests that heat treatment in this work is not intense enough to cause any chemical crosslinking, while still sufficient to improve the membrane selectivity.

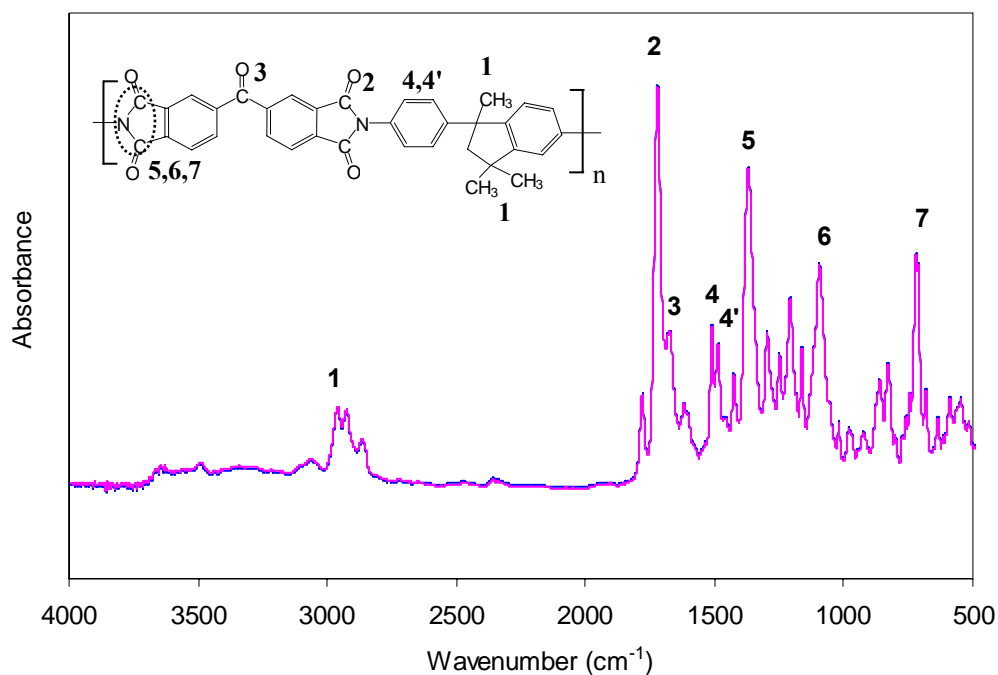


Figure 6.7: Chemical structure of Matrimid[®] and FTIR absorption spectra for virgin and annealed fibers at room temperature

The ¹H NMR measurement was conducted on the Matrimid[®] fibers with and without heat treatment. Clearly all the spectra are almost identical regardless of thermal annealing, as shown in Figure 6.8. This NMR study further validates that no chemical reaction occurs with thermal annealing.

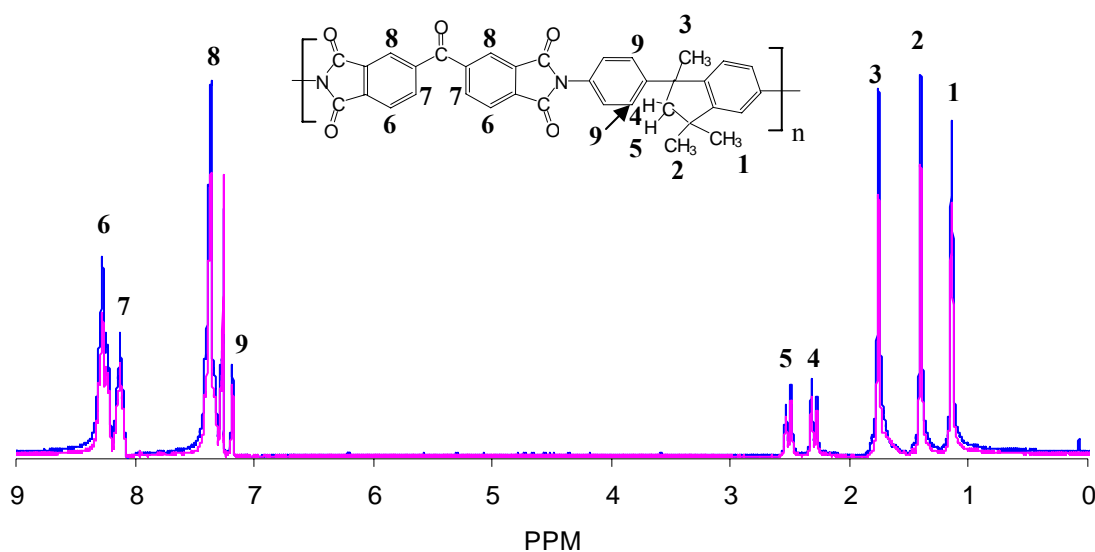


Figure 6.8: Chemical structure of Matrimid® and ^1H NMR absorption spectra for virgin and annealed fibers at room temperature

As stated in Chapter 6.2.3, fluorescence behavior is sensitive to the micro-environmental change with the molecular interaction [21]. Therefore, fluorescence techniques are reliable and convenient tools to study the formation of charge transfer complexes and densification of polymer chains [9]. All the fibers for fluorescence measurements should be prepared with the same methodology and evaluated using identical instrumental parameters so that the comparison is meaningful. The variation is only the curing temperature for each fiber. Figure 6.9 shows the variations of micro-fluorescence emission spectra for the fibers cured at different temperatures.

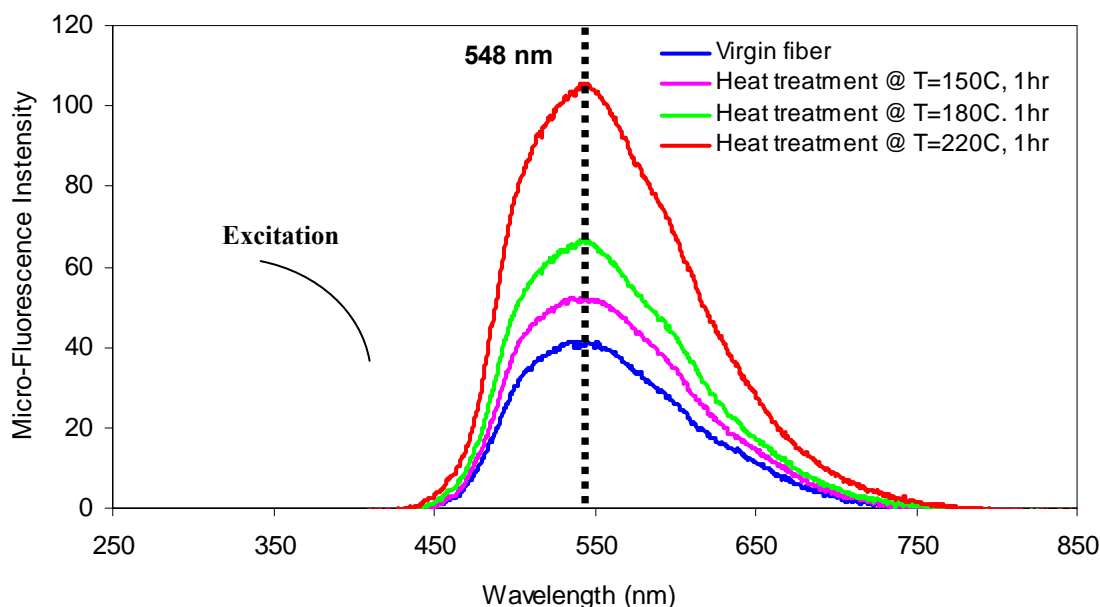


Figure 6.9: Variations of micro-fluorescence emission spectra for the fibers cured at different temperatures

When excited at the wavelength of 365 nm, the fluorescence emission spectra bands were observed at about 548 nm for all the fibers. The emission intensity increased with an increase in the heating temperature. This supports the fact that charge transfer complexes undoubtedly exist in the Matrimid[®] fiber. In contrast to the polymer of PI(BTDA/DPM) in Q. Jin's paper (Figure 6.3), three alkyl groups of Matrimid[®] can promote charge transfer complexes more stable and stay at the lower energy level. It is not surprising that the wavelength of Matrimid[®] fluorescence emission spectrum is longer than that of PI(BTDA/DPM).

Experimentally it is not easy to distinguish intra-molecular charge transfer complexes and inter-molecular charge transfer complexes in the Matrimid[®] fiber, since both of them are concurrently formed. However, the increased fluorescence intensity is an apparent indication that inter-molecular interactions between parallel planar structures

become dominant and the inter-molecular packing density is increased with thermal annealing [1]. In other words, thermal annealing helps the polymer chains to relax and rearrange between adjacent coplanar molecules, which decreases the chain interstitial space accordingly and produces strong inter-molecular charge transfer complexes. Thus the fluorescence emission is significantly increased with an increase of thermal annealing temperature. The closely localized configuration of aromatic polyimide benzene rings and formation of charge transfer complexes in the Matrimid[®] fiber suppress the mobility of polymer chains and provide high size and shape discrimination between penetrants.

6.5.3 Heating Time

In addition to the heating temperature, the duration of heat treatment is another important variable that is worth investigating. In industry, long time heat treatment is not practical; conversely the formation of charge transfer complexes might fail if the annealing time is too short. One, five, and twelve hours were selected to cure the FB5.6 state fibers at 220°C in vacuum. FB5.6_22, FB5.6_32 and FB5.6_42 modules were prepared using different heating times. FB5.6_11 module made of a virgin fiber was used as a reference. The micro-fluorescence emission spectra are shown in Figure 6.10.

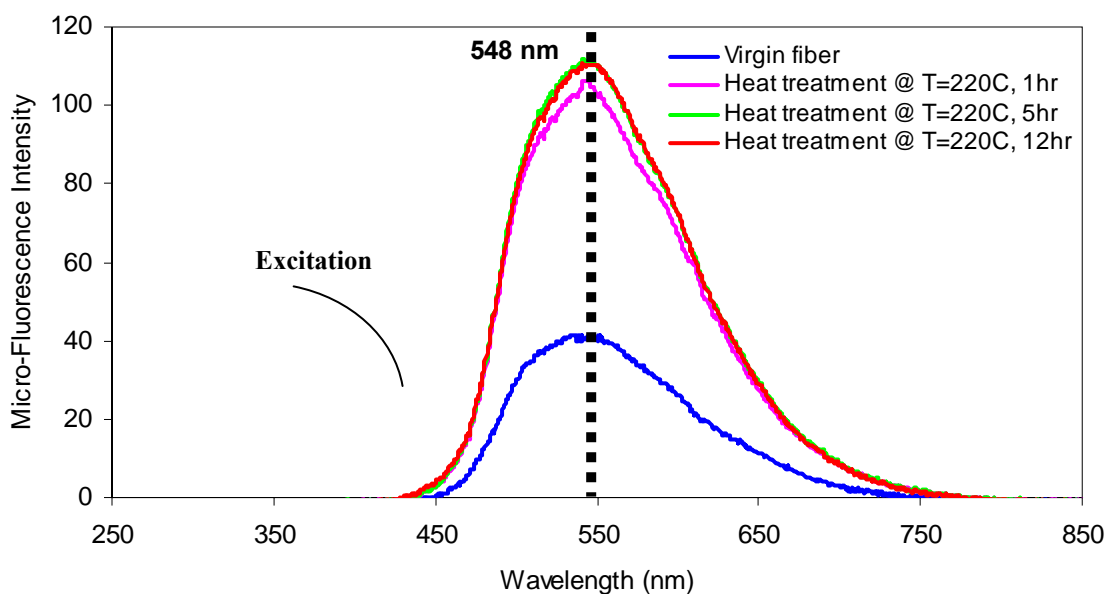


Figure 6.10: Variations of micro-fluorescence emission spectra for the fibers cured at different times

As excited at the wavelength of 365 nm, the fluorescence emission peaks were observed at about 548 nm for all the fibers. The emission intensity increased dramatically with annealed fibers. However, only small enhancement of emission intensity was observed for the longer annealing times. This indicates that one hour thermal annealing is enough to form stable charge transfer complexes in the outer skin layer of a hollow fiber, which results in the higher selectivity towards larger molecular transportation. The improvement of membrane selectivity will be very limited even with long time annealing. The permeation results of virgin and annealed fibers for different annealing times are illustrated in Figure 6.11.

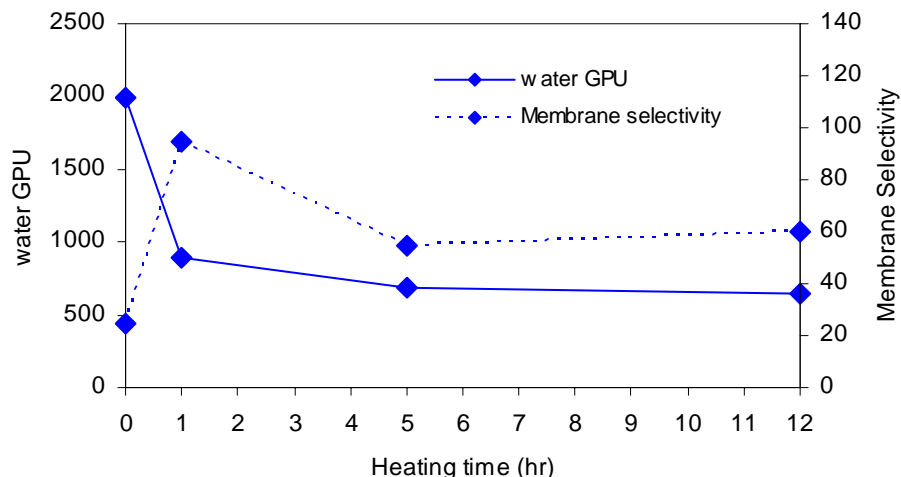


Figure 6.11: Effects of annealing times on water permeance and membrane selectivity

Both water permeance and membrane selectivity decrease when annealing time increases to 5 and 12 hours in contrast to the fiber with 1 hour heat treatment. The morphology changes of polymer chains in the outer skin layer of hollow fibers should be similar for these three annealing times based upon micro-fluorescence spectra. However, the substrate layer and macrovoids underneath the outer skin of a hollow fiber might collapse due to long time curing. This causes the densification of the substrate and influences transport properties of the “fast” gas molecules significantly. Two opposite factors matter for water and HAc transport through the membrane. Sufficient curing time is helpful to form charge transfer complexes and decrease the free volume in the selective layer. This can increase the membrane selectivity and decrease the water flux. However, the additional substrate resistance arising from over-curing can affect water much more than acetic acid, resulting in the decreased permeance and selectivity. This argument can be proven by pure gas permeation tests. The fibers with the same heat treatment procedure were tested using N₂, O₂, and He at 35°C, as shown in Table 6.2.

Table 6.2: Pure gas permeation results for hollow fibers with different annealing times

Fibers Identification (O.D. ~ 520 μm)	N ₂ (GPU)	O ₂ (GPU)	He (GPU)	Selectivity $\alpha_{\text{O}_2/\text{N}_2}$	Selectivity $\alpha_{\text{He}/\text{N}_2}$
FB5.6_60 (No heat treatment)	0.49	3.37	44	6.9	90
FB5.6_61 (Heat treatment @ 220°C, 1 hr)	0.26	1.67	23	6.4	88
FB5.6_62 (Heat treatment @ 220°C, 5 hrs)	0.22	1.15	14	5.5	62
FB5.6_63 (Heat treatment @ 220°C, 12 hrs)	0.23	1.14	13	5.0	59

The annealed fibers demonstrate the lower permeance because of the free volume loss and formation of charge transfer complexes in the outer selective layer. The passage of the “fast” gases, such as O₂ and He, through the 5 or 12 hours-annealed fiber is affected much more than that of the 1 hour-annealed fiber. The additional substrate resistance arising from the longer thermal treatment time is believed to hinder fast gases more significantly and lower the selectivity of $\alpha_{\text{O}_2/\text{N}_2}$ and $\alpha_{\text{He}/\text{N}_2}$.

The membrane selectivities of HAc/H₂O mixtures are still improved to some degree with over-heated fibers in contrast to the selectivity of 30 for a virgin fiber. Nevertheless, the heat treatment time has to be optimized to minimize the substrate resistance and maximize the intensity of charge transfer complexes in the selective layer. One-hour curing time appears sufficient since it pushes the membrane selectivity up to 95 for a model 20% wt HAc/H₂O solution feed.

6.5.4 Heating Environment

Vacuum equipment is usually involved in the annealing step in most open literatures [5-8]. If expensive vacuum can be avoided in heat treatment of hollow fibers, while maintaining similar fiber performance, annealing will be very attractive for industrial application. In this section, the FB5.6 state hollow fibers were thermally cured in air and vacuum at 220°C for 1 hour separately. Thereafter, FB5.6_111 and FB5.6_211 modules were prepared for pervaporation tests with 20% wt HAc/H₂O mixture feeds. Figure 6.12 shows the separation results.

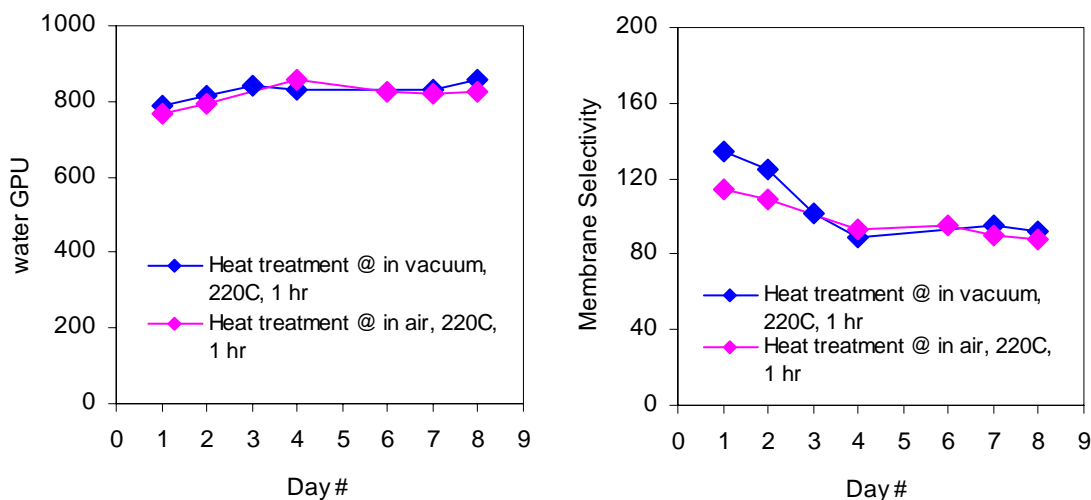


Figure 6.12: Effects of heating environments on water permeance and membrane selectivity

As it can be seen, the water permeance and membrane selectivity are very close for both air and vacuum annealed fibers. This indicates O₂ (in air) does not affect the rearrangement of polymer chains and modification of interstitial chain space. Some differences exist for the membrane selectivity between air annealed and vacuum annealed fibers in the initial two days, but still in an acceptable error range. It should be noted that even a small change of the free volume distribution can cause different separation results.

The air and vacuum annealed fibers can be easily dissolved in solvents such as NMP and CH_2Cl_2 . The same FTIR spectra as Figure 6.7 were obtained for virgin, air annealed, and vacuum annealed fibers. This indicates that no chemical reaction occurs with air or vacuum heating. Heat treatment in this work is not intense enough to cause any chemical crosslinking, but is still sufficient to improve the fiber performance. In addition, heat treatment can be completed in air instead of the costly vacuum condition.

6.5.5 Long Term Separation Performance with Annealed Fibers

Although heat treatment is very effective to increase the membrane selectivity of HAc/ H_2O mixtures, long-term performance experiments have to be carried out to determine how permanent these effects will be. In terms of the above discussion, the optimal variables for heat treatment are shown in Table 6.3.

Table 6.3: Optimal heating variables

Temperature	220°C
Time	1 hour
Curing Environment	In air

Figure 6.13 illustrates the permeance and separation factor for a hollow fiber (FB5.6_511) with heat treatment at 220°C in air for 1 hour. A model 20% wt HAc/ H_2O mixture was used not only as a feed solution for pervaporation but also a soaking bath to store the fiber, which closely added real industrial operations. It is apparent that the fiber is very robust and maintains good separation performance for at least one month without any pure DI water involved. The swelled polymer chains from the acetic acid

conditioning effects cause the decreased membrane selectivity at the initial stage, since a small change of the free volume distribution can affect the fiber performance significantly. To the best of our knowledge, no long-term experimental results have been published previously for separating acetic acid and water mixtures. Most data were collected in a very short time period (6 ~ 10 hours) [24-25].

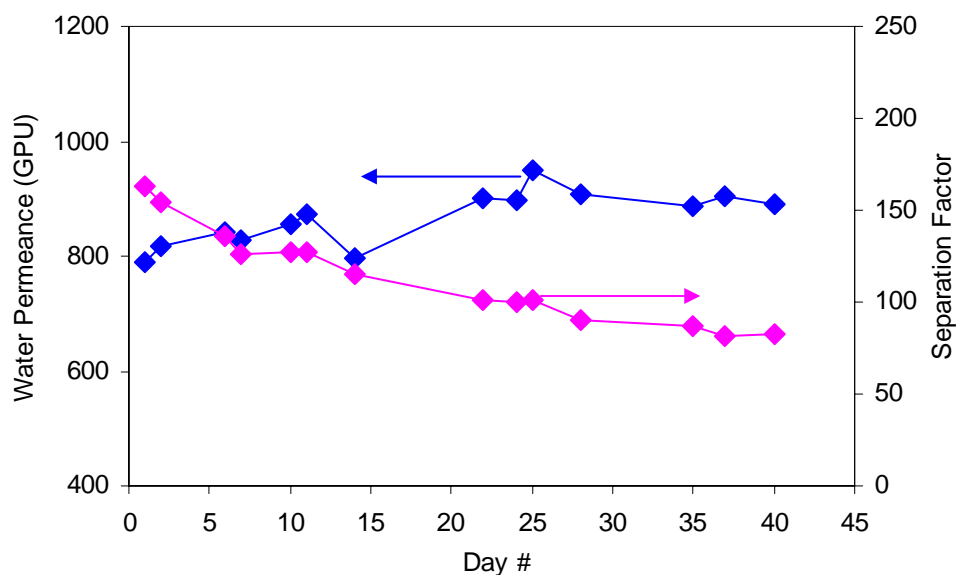


Figure 6.13: Permeance and separation factor of module FB5.6_511 for long term separation experiments

6.6 Separation Results with and without Thermal Annealing for 50% wt HAc Concentration Feeds

The fibers that are thermally cured based on the optimal heating variables in Table 6.3 demonstrate a significant enhancement of the separation factor with a model 20% wt acetic acid-water mixture. The highest acetic acid concentration in an aqueous solution that has been reported is about 10% wt [24-25] using polyimide membranes. Therefore, it is interesting to investigate whether heat treatment works with higher HAc

concentration feeds as well. A model 50% wt HAc/H₂O solution was used as a feed for pervaporation tests at the temperature of 103.5°C and also as a soaking bath.

6.6.1 Heating Time

The FB5.6 state fibers were heat-treated at 220°C in air for 1 hour and 12 hours, respectively. Thereafter, FB5.6_211 and FB5.6_212 modules were prepared to conduct pervaporation tests with a model 50% wt HAc/H₂O mixture feed. As a reference, FB5.6_210 module made of a virgin fiber was used to perform the same test. Figure 6.14 shows the permeation and selectivity results for these three modules.

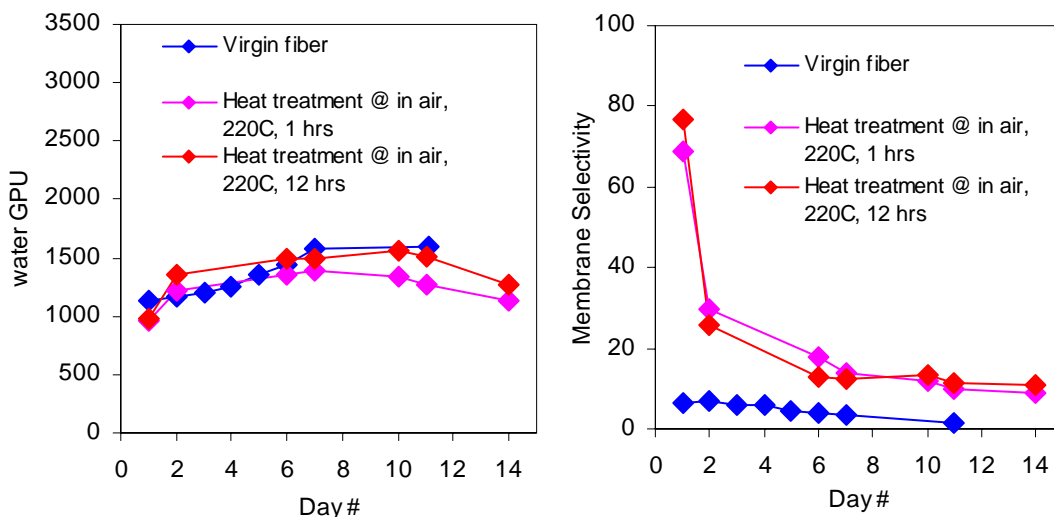


Figure 6.14: Effects of heating time on water permeance and membrane selectivity with a model 50% wt HAc/H₂O mixture feed

Throughout the 14 day test, the membrane selectivity of the annealed fibers is about 10. Two competing factors can affect the fiber performance in this case. First, the loss of free volume and formation of charge transfer complexes in the outer skin layer due to heat treatment. Second, swelling effects arising from high acetic acid

concentration feeds. It is clearly shown that heat treatment improves the rigidity of the polymer chains that can suppress the HAc-induced plasticization. However, this suppression is not sufficient to avoid the decrease of the membrane selectivity in high HAc concentration feeds over extended periods of time. That is, a strong interaction between high HAc concentration feeds and the polymer can activate polymer chain segments and may change the free volume and its distribution significantly. The HAc-induced swelling in a virgin fiber is more drastic because almost no selectivity is shown on day #11.

It has also been observed that no large difference exists for the fibers with heat treatments of 1 hour or 12 hours. This indicates the HAc-induced plasticization dominates with the high HAc concentration feed and charge transfer complexes from thermal annealing are not intense enough to suppress the HAc-induced plasticization. Even with annealed hollow fibers, the skin layer can be dramatically swelled when exposed to 50% wt HAc concentration solutions. In an extreme case, bulk diffusion will control the transport of both penetrants, if the free volume is increased drastically by the HAc-induced swelling stress. The membrane selectivity undoubtedly drops down to one.

6.6.2 Heating Environment

The effects of heating environment on the fiber performance, air or vacuum, have been investigated by pervaporation tests with a model 20% wt HAc concentration feed at 101.5°C in Chapter 6.5.4. Similar behaviors were observed for both fibers. However, it is still interesting to examine whether heating environment can affect the annealed fibers

with the higher HAc concentration feeds. Figure 6.15 shows separation results at 103.5°C with 50% wt HAc/H₂O mixture feeds for air annealed and vacuum annealed fibers.

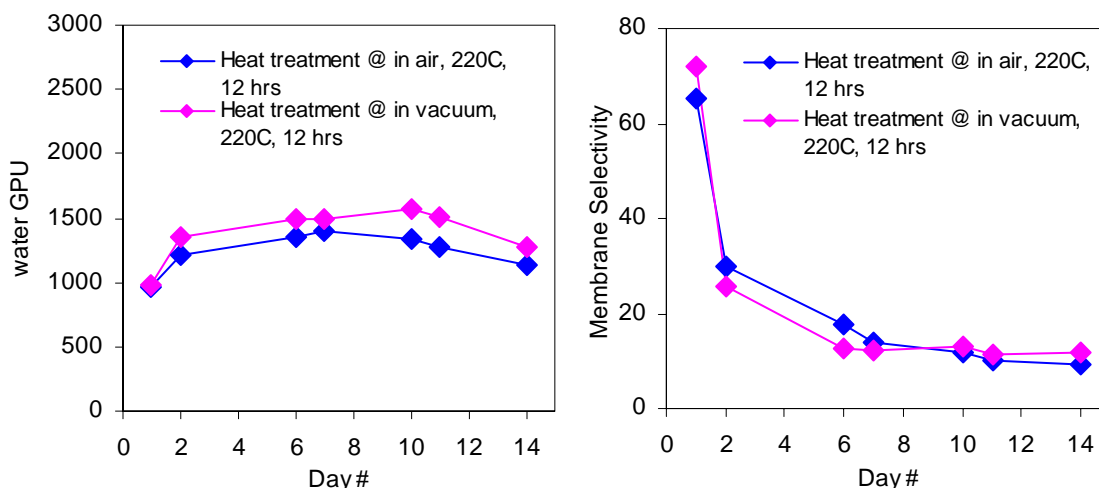


Figure 6.15: Effects of heating environments on water permeance and membrane selectivity with a model 50% wt HAc/H₂O mixture feed

No significant differences exist between air and vacuum-based annealing environments. This further confirms that heating environment does not have profound effects on the fiber performance and the air-based annealing technology will be very attractive for industrial applications. Charge transfer complexes formed from thermal curing suppress the mobility of the polymer chains; however, heat treatment is not sufficiently intensive to inhibit the high HAc concentration-induced swelling. Therefore, the membrane selectivity decreases with time.

6.7 Modeling Work to Estimate Overall Selectivity of Annealed Fibers in a Cross-Flow Separator

It has been clearly illustrated that heat treatment can significantly improve the fiber selectivity. The membrane selectivity increases to 95 with a 20% wt HAc

concentration feed and to 10 with a 50% wt HAc concentration feed. Although a dead-end flow separator is used in this research because of its convenient set-up, the concept can be easily extended to other operation types. A cross-flow separator is usually utilized in industry due to its high efficiency [26-27]. The schematic diagrams of dead-end flow and cross-flow separators are shown in Figure 6.16.

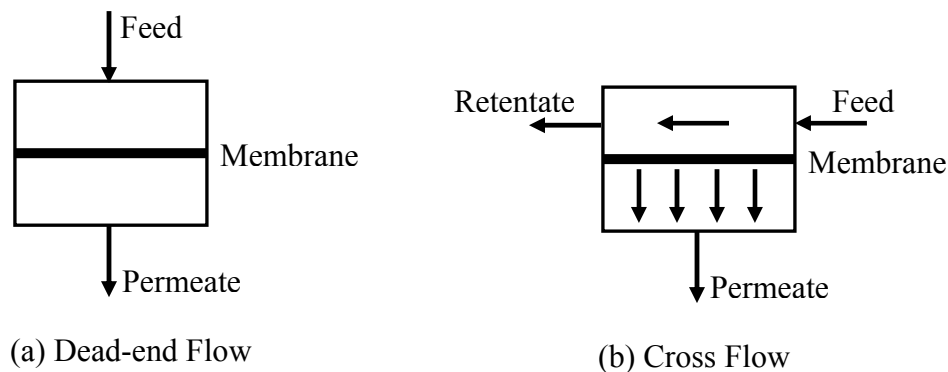


Figure 6.16: Schematic diagrams of dead-end flow and cross-flow separators

A mathematical model was developed to evaluate the annealed fiber performance in a cross-flow separator below.

6.7.1 Permeabilities of Water and Acetic Acid

Large bore size fibers (O.D. $\sim 520 \mu\text{m}$) from the FB5.6 state were annealed at 220°C in air for 1 hour. Thereafter, pervaporation modules were fabricated to conduct pervaporation tests with 20%, 30%, 40%, and 50% HAc concentration feeds for five days. The *average* permeance and membrane selectivity varying with different HAc concentration feeds are shown in Figure 6.17.

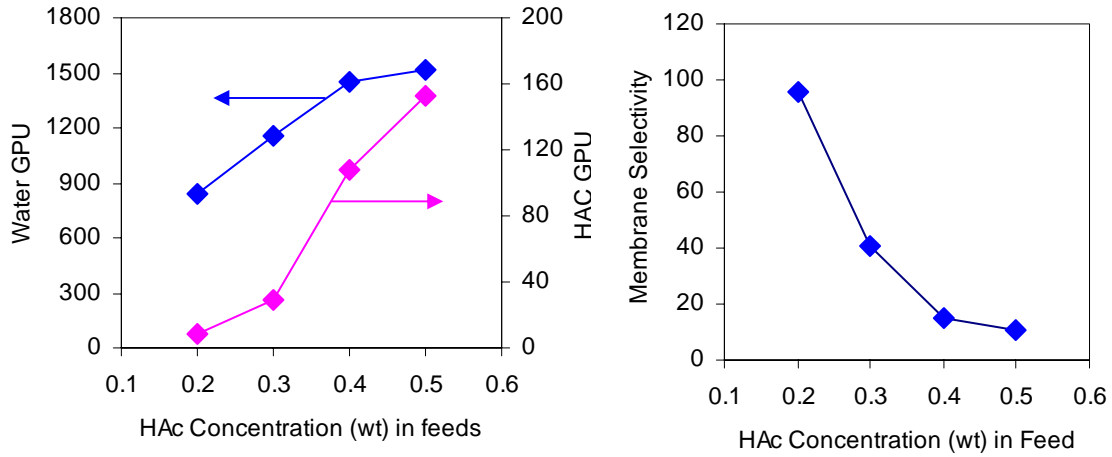


Figure 6.17: Water and HAC permeances and membrane selectivity vs. HAC concentration (% wt) in feeds

As shown above, the relative increment of the HAC permeability is much larger than that of the H₂O permeability and the membrane selectivity drops down quickly with high HAC concentration feeds. This indicates that the HAC-induced swelling starts to dominate with the increase of the HAC concentration in feeds. Both the water and acetic acid permeances are concentration dependent.

Piecewise linear functions are used to correlate the variation of penetrant permeance with the HAC concentration in feeds. The regression functions are described in equation 6.1, 6.2, and 6.3.

$$\begin{cases} \left(\frac{\mathcal{P}}{\ell}\right)_{\text{HAc}} = 202x_{\text{HAc}} - 31.6 & 20\% \text{wt} \leq x_{\text{HAc}} \leq 30\% \text{wt} \\ \left(\frac{\mathcal{P}}{\ell}\right)_{\text{HAc}} = 790x_{\text{HAc}} - 208 & 30\% \text{wt} \leq x_{\text{HAc}} \leq 40\% \text{wt} \\ \left(\frac{\mathcal{P}}{\ell}\right)_{\text{HAc}} = 500x_{\text{HAc}} - 92 & 40\% \text{wt} \leq x_{\text{HAc}} \leq 50\% \text{wt} \end{cases} \quad (6.1)$$

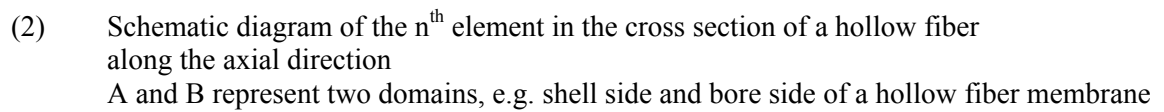
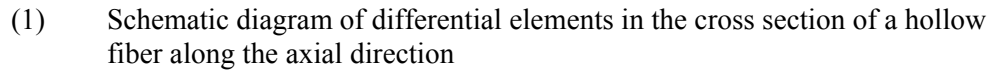
$$\begin{cases} \left(\frac{\mathcal{P}}{\ell}\right)_{\text{H}_2\text{O}} = 3460x_{\text{HAc}} + 150 & 20\%\text{wt} \leq x_{\text{HAc}} \leq 30\%\text{wt} \\ \left(\frac{\mathcal{P}}{\ell}\right)_{\text{H}_2\text{O}} = 4330x_{\text{HAc}} - 111 & 30\%\text{wt} \leq x_{\text{HAc}} \leq 40\%\text{wt} \\ \left(\frac{\mathcal{P}}{\ell}\right)_{\text{H}_2\text{O}} = 470x_{\text{HAc}} - 1433 & 40\%\text{wt} \leq x_{\text{HAc}} \leq 50\%\text{wt} \end{cases} \quad (6.2)$$

$$\begin{cases} \alpha_{\text{H}_2\text{O}/\text{HAc}} = -547.16x_{\text{HAc}} + 205.11 & 20\%\text{wt} \leq x_{\text{HAc}} \leq 30\%\text{wt} \\ \alpha_{\text{H}_2\text{O}/\text{HAc}} = -259.56x_{\text{HAc}} + 118.83 & 30\%\text{wt} \leq x_{\text{HAc}} \leq 40\%\text{wt} \\ \alpha_{\text{H}_2\text{O}/\text{HAc}} = -44.523x_{\text{HAc}} + 32.818 & 40\%\text{wt} \leq x_{\text{HAc}} \leq 50\%\text{wt} \end{cases} \quad (6.3)$$

where x_{HAc} represents the HAc concentration in feeds, $\alpha_{\text{H}_2\text{O}/\text{HAc}}$ represents the membrane selectivity, and $\left(\frac{\mathcal{P}}{\ell}\right)_{\text{HAc}}$ and $\left(\frac{\mathcal{P}}{\ell}\right)_{\text{H}_2\text{O}}$ represents the HAc and H₂O permeance, respectively.

6.7.2 Model Development

A mathematical model was developed based upon mass balance in a cross-flow separator, which is shown in Figure 6.18. Two parallel domains outside and inside a fiber were evenly divided into a number of differential elements and mass balance was built in each element.



162

- (4) Shell feed is used in this model, which can be easily extended to bore feed;
- (5) The total pressure on the shell side (feed side) is constant and 1 atm;
- (6) Operation is at the steady state;
- (7) The length of a fiber is assumed to be 1 meter, which is practical in industry;
- (8) The outer diameter of the fiber is about 500 μm . The fluxes with annealed fibers are decreased dramatically, as described in Chapter 6.5.1. Thus, it is reasonable to assume the bore pressure change is negligible with 1 m long annealed fiber module based upon the modeling work in Chapter 5;
- (9) Multiple fibers are bundled to make a pervaporation module. The number of fibers used in the model is absolutely defined as 10^5 . Thus, the total available separation area is 157 m^2 , while the occupied volume is only 196 cm^3 .

For the n^{th} element in domain A, mass balance equations are given below:

$$F_n = F_{n-1} - \left(\frac{\mathcal{P}}{\ell} \right)_{\text{HAc}} \cdot (x_{\text{HAc}(n-1)} p_T) \cdot (\pi D^2 \cdot N \cdot \frac{L}{n}) - \left(\frac{\mathcal{P}}{\ell} \right)_{\text{H}_2\text{O}} \cdot ((1 - x_{\text{HAc}(n-1)}) \cdot p_T) \cdot (\pi D^2 \cdot N \cdot \frac{L}{n}) \quad (6.4)$$

$$x_{\text{HAc}(n)} = \frac{F_{n-1} \cdot x_{\text{HAc}(n-1)} - \left(\frac{\mathcal{P}}{\ell} \right)_{\text{HAc}} \cdot (x_{\text{HAc}(n-1)} \cdot p_T) \cdot (\pi D^2 \cdot N \cdot \frac{L}{n})}{F_n} \quad (6.5)$$

where F_{n-1} and F_n are flowrates in and out the n^{th} element in the shell side. The symbol of $x_{\text{HAc}(n)}$ is the mole fraction in the n^{th} element in the shell side, and thus the mole fraction of water is $(1 - x_{\text{HAc}(n)})$ in the n^{th} element in the shell side. The symbol of p_T represents the total pressure in the shell side and is 1 atm in this case, D is the outer diameter of a hollow fiber, and L is the available length of a hollow fiber. The symbols of n and N

represent the total number of the differential elements in the hollow fiber and the total number of the fibers used in separation, respectively.

For the n^{th} element in domain B, mass balance equations are given below:

$$f_n = f_{n-1} + \left(\frac{\mathcal{P}}{\ell} \right)_{\text{HAc}} \cdot (x_{\text{HAc}(n-1)} p_T) \cdot (\pi D^2 \cdot N \cdot \frac{L}{n}) + \left(\frac{\mathcal{P}}{\ell} \right)_{\text{H}_2\text{O}} \cdot ((1 - x_{\text{HAc}(n-1)}) \cdot p_T) \cdot (\pi D^2 \cdot N \cdot \frac{L}{n}) \quad (6.6)$$

$$y_{\text{HAc}(n)} = \frac{f_{n-1} \cdot y_{\text{HAc}(n-1)} + \left(\frac{\mathcal{P}}{\ell} \right)_{\text{HAc}} \cdot (x_{\text{HAc}(n-1)} \cdot p_T) \cdot (\pi D^2 \cdot N \cdot \frac{L}{n})}{f_n} \quad (6.7)$$

where f_{n-1} and f_n are flowrates in and out the n^{th} element in the bore side. The symbol of $y_{\text{HAc}(n)}$ is the mole fraction in the n^{th} element in the bore side, and thus the mole fraction of water is $(1 - y_{\text{HAc}(n)})$ in the n^{th} element in the bore side.

The total mass balance can be easily expressed:

$$\begin{cases} F_o = F_R + f_p \\ F_o \cdot x_{\text{HAc}(o)} = F_R \cdot x_{\text{HAc}(R)} + f_p \cdot y_{\text{HAc}(P)} \end{cases} \quad (6.8)$$

where F_o is the total flowrate entering into a separator, F_R and f_p are the total flowrates leaving a separator from the shell side and bore side, respectively. The symbol of $x_{\text{HAc}(o)}$ represents the initial HAc concentration entering in a separator, $x_{\text{HAc}(R)}$ and $y_{\text{HAc}(P)}$ represent the HAc concentrations leaving the shell side and bore side, respectively.

As stated in Chapter 1, the acetic acid concentrations entering into and leaving the separator are specified as 20% wt and 50% wt, respectively. Therefore, the initial and boundary conditions can be written as follows:

$$\left\{ \begin{array}{l} x_{\text{HAc(o)}} = 20\% \text{ wt;} \\ y_{\text{HAc(o)}} = 0; \\ f_o = 0; \\ x_{\text{HAc(R)}} = 50\% \text{ wt;} \\ n = 100; \\ N = 10^5; \\ p_T = 1\text{atm;} \\ D = 500\mu\text{m;} \\ L = 100\text{cm;} \end{array} \right. \quad (6.9)$$

Once the initial flowrate of a model 20% wt HAc/H₂O mixture is given, the HAc concentration on the permeate side, retentate flowrate, and permeate flowrate, i.e. $y_{\text{HAc(p)}}$, F_R , and F_p can be calculated using the equations 6.1-6.8. The HAc concentration distribution in the shell and bore side along the axial direction can be obtained as well. The overall or average membrane selectivity can be generated by the following equation,

$$\bar{\alpha} = \frac{\int_0^L \alpha(L) \cdot dL}{L} \quad (6.10)$$

6.7.3 Simulation Results

Goal Seek[®] function in Microsoft Excel[®] 2002 was used to solve the equations 6.1-6.8 based upon the initial and boundary conditions in equation 6.9. The total flowrate entering in the separator should be 591 kg/hr to satisfy the separation requirement for the given separation area. The HAc concentration distributions in the shell and bore side along the axial direction of fibers are shown in Figure 6.19. Figure 6.20 shows the normalized water and HAc flowrates in the shell and bore sides along the axial direction

of hollow fibers, i.e. $\frac{F_n \cdot (1 - x_{HAc(n)})}{F_o \cdot (1 - x_{HAc(o)})} \times 100\%$, $\frac{F_n \cdot x_{HAc(n)}}{F_o \cdot x_{HAc(o)}} \times 100\%$,

$\frac{f_n \cdot (1 - y_{HAc(n)})}{F_o \cdot (1 - x_{HAc(o)})} \times 100\%$, and $\frac{f_n \cdot y_{HAc(n)}}{F_o \cdot x_{HAc(o)}} \times 100\%$ vs. distance down the fiber length.

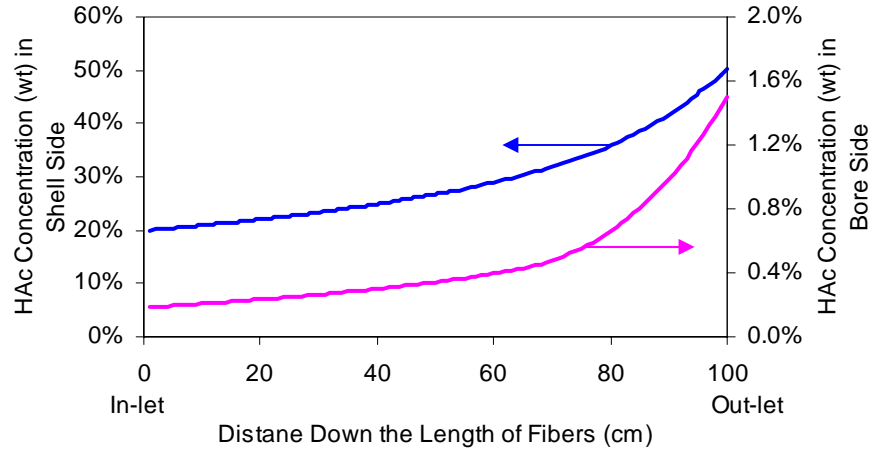


Figure 6.19: HAC concentration distribution in the shell and bore sides for a hollow fiber-based cross-flow separator

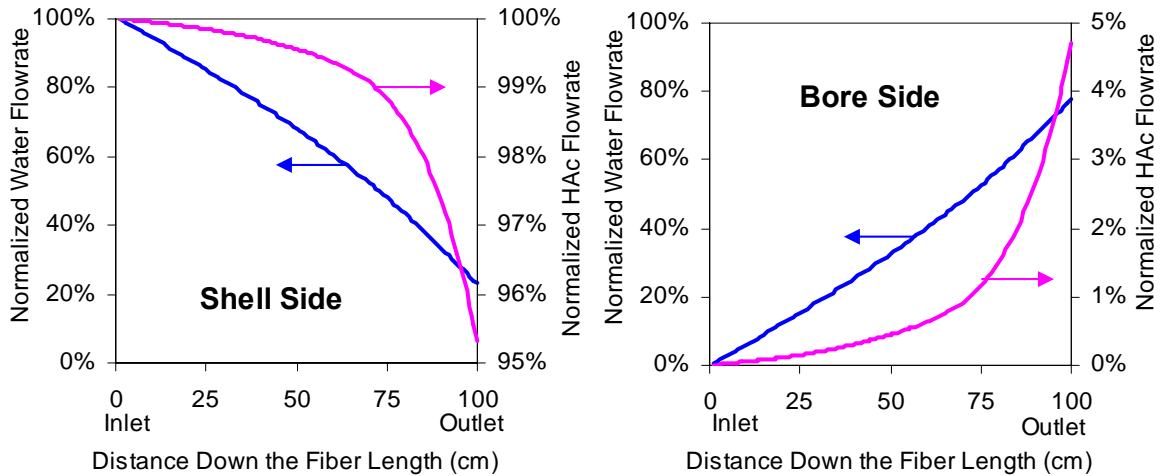


Figure 6.20: Normalized HAC and H₂O flowrate distribution on the shell and bore sides for a hollow fiber-based cross-flow separator

It is clear that a hollow fiber-based cross-flow separator is very efficient to separate HAC/H₂O mixtures even with some loss at the final stage due to significant

swelling effects from the high HAc concentration feed on the fibers. Most water (80% mass) is removed through the membrane. The overall membrane selectivity retains around 44, as calculated from equation 6.10.

In this research, the initial HAc concentration in feeds is restricted to be 20% wt based on industrial requirements. The feed flowrate should be optimized to get the best fiber performance when the separation area is fixed. For example, the feed flowrate of 591 kg/hr is obtained if the HAc concentration in the retentate is maintained as 50% wt. The lower flowrate can drive the HAc concentration in the shell side larger than 50% wt quickly, resulting in more significant swelling problems at the final stage of the separator. However, the higher flowrate can not completely take advantage of the membrane separation and lead to relatively low percentage for the removed water. Figure 6.21 (A)

shows the HAc loss $(\frac{f_p \cdot y_{HAc(p)}}{F_o \cdot x_{HAc(o)}} \times 100\%, \text{ efficiency})$ and mass percentage for the

removed water $(\frac{f_p \cdot (1 - y_{HAc(p)})}{F_o \cdot (1 - x_{HAc(o)})} \times 100\%, \text{ productivity})$ vs. the normalized feed flowrate.

The variation of the overall membrane selectivity with the normalized feed flowrate is shown in Figure 6.21 (B).

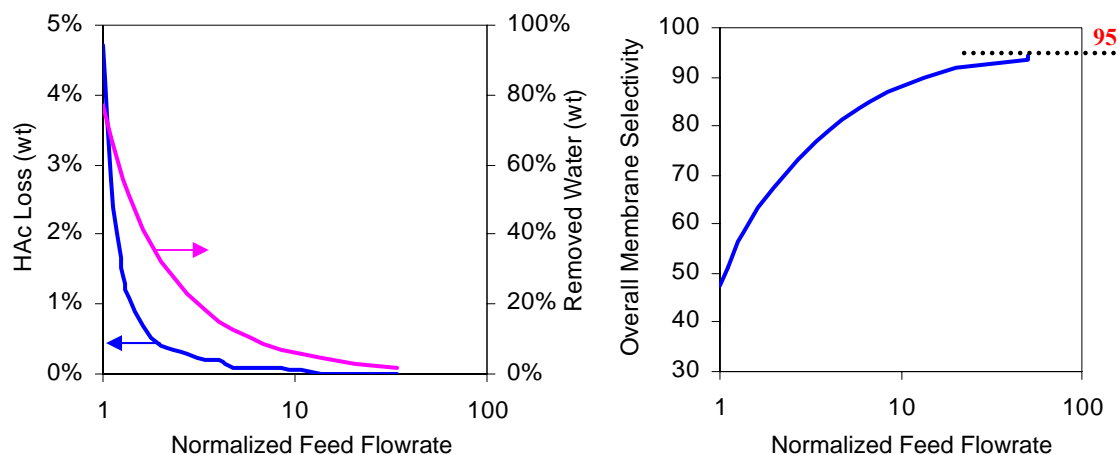


Figure 6.21: (A) HAC loss and removed water (% wt) vs. normalized feed flowrate
(B) Overall membrane selectivity vs. normalized feed flowrate

The mass percentage of HAC loss can be decreased as the feed flowrate increases; however, the mass percentage of removed water will be reduced as well. When the feed flowrate is sufficiently high, very small mass percentage of water is removed from the system and overall membrane selectivity goes up to the asymptote of 95.

6.8 Summary

Thermal annealing applied to Matrimid[®] hollow fibers significantly improves the membrane selectivity of acetic acid and water mixtures. Free volume loss and formation of charge transfer complexes arising from heat treatment increase the size and shape discrimination of water and acetic acid molecules. The hindrance to the segmental mobility among the polymer chains in annealed membranes suppresses the HAC-induced swelling. Only the physical structure of the polymer changes but no chemical reaction occurs with thermal annealing.

The heating variables were investigated and optimized for the fiber structure used in this work. The temperature of 220°C, heating time of 1 hour, and air-based heating environment are optimal for a model 20% wt HAc feed. The membrane selectivity of 95 was achieved with acceptable water flux of 1.6 kg/m²hr. Thermal annealing does not work effectively with high HAc concentration feeds. The membrane selectivity and water flux are about 10 and 2.0 kg/m²hr for a 50% wt HAc concentration feed, respectively. However, these results are still attractive, since almost no selectivity exists for virgin fibers with the same feed for the extended time period. This indicates that heat treatment is capable of suppressing the HAc-induced plasticization, but not sufficiently intensive in more aggressive environments such as a 50% wt HAc concentration feed.

In order to evaluate the performance of annealed fibers in industrial applications, a model to simulate a cross-flow separator was developed. If operating parameters can be optimized properly, the overall membrane selectivity of annealed fibers is still satisfactory even with an aggressive environment.

The thermal annealing technology has been successfully developed in pervaporation of HAc/H₂O mixtures. This method turns out to be very attractive for scale-up and commercial applications because the heating process is simple and no expensive vacuum equipment is involved. In addition, use of an inert N₂ blanket during annealing may also be attractive and would not add much cost. Thermal annealing can be applied to other pervaporation hollow fiber membranes, provided that the chemical structure of a membrane material is feasible to form charge transfer complexes. Fluorescence spectroscopy has been proved very helpful for first calibration of charge transfer complexes and packing density of the polymer chains. The next chapter will

compare the sorption-induced swelling between virgin and annealed fibers to better understand the interaction between penetrants and the polymer.

6.9 References

- [1] Kawakami, H., Mikawa, M., and Nagaoka, S. *Gas transport properties in thermally cured aromatic polyimide membranes*. J. Membr. Sci. 1996, 118, 223-230.
- [2] Krol, J.J., Boerrigter, M., and Koops, G.H. *Polyimide hollow fiber gas separation membranes: preparation and the suppression of plasticization in propane/propylene environments*. J. Membr. Sci. 2001, 184, 275-286.
- [3] Barsema J.N., Klijnstra, S.D., Balster, J.H., Van der Vegt, N.F.A., Koops, G.H., and Wessling, M. *Intermediate polymer to carbon gas separation membranes based on Matrimid PI*. J. Membr. Sci. 2004, 238, 93-102.
- [4] Bos, A., Punt I.G.M., Wessling, M., and Strathmann, H. *Plasticization-resistant glassy polyimide membranes for CO₂/CO₄ separations*. Sep. Purif. Tech. 1998, 14, 27-29.
- [5] Wind, J.D., Paul, D.R., and Koros, W.J. *Natural gas permeation in polyimide membranes*. J. Membr. Sci. 2004, 228, 227-236.
- [6] Wind, J.D., Sirard, S.M., Paul, D.R., Green, P.F., Johnston, K.P., and Koros, W.J. *Carbon dioxide-induced plasticization of polyimide membranes: Pseudo-equilibrium relationships of diffusion, sorption, and swelling*. Macromolecules. 2003, 36, 6433-6441.
- [7] Wind, J.D., Staudt-Bickel, C., Paul, D.R., and Koros, W.J. *Solid-state covalent cross-linking of polyimide membranes for carbon dioxide plasticization reduction*. Macromolecules. 2003, 36, 1882-1888.
- [8] Hibshman, C., Cornelius, C.J., and Marand, E. *The gas separation effects of annealing polyimide-organosilicate hybrid membranes*. J. Membr. Sci. 2003, 211, 25-40.
- [9] Jin, Q., Yamashita, T., and Horie, K. *Polyimides with alicyclic diamines. II. hydrogen abstraction and photocrosslinking reactions of benzophenone-type polyimides*. J. Polym. Sci.: Part A: Polym. Chem. 1994, 32, 503-511.
- [10] Hasegawa, M., Kochi, M., Mita, I., and Yokota, R. *Molecular aggregation and fluorescence spectra of aromatic polyimides*. Eur. Polym. J. 1989, 25, 349-354.

- [11] Wachsman, E. D. and Frank, C. W. *Effect of cure history on the morphology of polyimide: Fluorescence spectroscopy as a method for determining the degree of cure*. Polymer. 1988, 29, 1191-1197.
- [12] Personal Communication with Prof. Mostafa A. El-Sayed and Dr. Wei Qian from Laser Dynamic Lab, Georgia Tech, 2005.
- [13] Silverstein, R., Bassler, G., and Morrill, T. *Spectrometric identification of organic compounds*. 5th Ed. John Wiley & Sons, Inc. 1991.
- [14] Skoog, D.A., Holler, F.J., and Nieman, T.A. *Principles of instrumental analysis*. 5th Ed. Saunders Golden Sunburst Series, Saunders College Publishing, 1998.
- [15] Duer, M.J. *Introduction to solid-state NMR spectroscopy*. Oxford, UK; Malden, MA: Blackwell, 2004.
- [16] <http://probes.invitrogen.com/handbook/figures/0664.html>.
- [17] Gullbault, G.G. *Fluorescence: theory, instrumentation, and practice*. Marcel Dekker, Inc., New York, 1967.
- [18] Pringsheim, P. *Fluorescence and phosphorescence*. Interscience publishers, Inc., New York, 1949.
- [19] Skoog, D.A., West, D.M., and Holler, F.J. *Fundamentals of analytical chemistry*. 7th Ed. Saunders College Publishing, 1996.
- [20] Castellan G.W. *Physical chemistry*. 3rd Ed. The Benjamin/Cummings Publishing Company, Inc. 1983.
- [21] Cho, D., and Drzal, L. *Effect of thermal cure on the fluorescence of MatrimidTM 5292 bismaleimide resin*. J. Mater. Sci. Lett. 2003, 22, 459-461.
- [22] Guerra, G., Choe, S., William, D.J., Karasz, F.E., and MacKnight, W.J. *Fourier transform infrared spectroscopy of some miscible polybenzimidazole/polyimide blends*. Macromolecules. 1988, 21, 231-234.
- [23] Bos, A. *High pressure CO₂/CH₄ separation with glassy polymer membranes - Aspects of CO₂-induced plasticization*. Ph.D. Dissertation, The University of Twente at Netherlands, 1996.
- [24] Huang, J.G., Cranford, R.J., Matsuura, T., and Roy, C. *Sorption and transport behavior of water vapor in dense and asymmetric polyimide membranes*. J. Membr. Sci. 2004, 241, 187-196.

- [25] Huang, J.G., Cranford, R.J., Matsuura, T., and Roy, C. *Water vapor permeation properties of aromatic polyimides*. J. Membr. Sci. 2003, 215, 129-140.
- [26] Baker, R.W. *Membrane technology and applications*. McGraw-Hill. 2000.
- [27] Porter, M.C., *Handbook of industrial membrane technology*. Noyes Publications, Park Ridge, NJ 1990.

Chapter 7: Sorption-Induced Swelling Tests

7.1 Introduction

The solution diffusion mechanism has been well developed to describe transport properties of low molecular weight compounds in non-porous glassy polymer membranes [1-2]. Rigid and glassy Matrimid[®] membranes are capable of separating gases based upon subtle differences in penetrant size and shape [3-4]. They are most permeable to the smallest components in a mixture and least permeable to the largest components when diffusivity dominates in the permeability. However, different behavior can be observed if solubility is primarily responsible for permeability behavior of penetrants instead of diffusion coefficients [5-9]. In addition, the transport mechanism tends to be more complicated as strong plasticization occurs due to the interaction between penetrants and polymers [10-14]. The penetrant-induced swelling can influence both solubility and diffusivity of all the penetrants. It is necessary to investigate the contribution of solubility on separation performance under the HAc-induced plasticization conditions that have been observed in Chapter 4 and 6.

The dual mode theory is commonly used to describe the sorption behavior of a glassy polymer because it is in a thermally non-equilibrium status [15-16]. The non-equilibrium “excess” free volume or microvoids formed from inter-segmental packing defects provide one type of sorption sites, typically called the “Langmuir sites”. The other type of sorption sites is associated with normally densified regions of the polymer, which obey the Henry’s law and involve dilation of the matrix to accommodate sorbed penetrants. The penetrant molecules sorbed in the Langmuir sites are typically much less

mobile than those in the Henry's law sorption sites [17]. Moreover, the solubilities of solvents in glassy polymers are generally history dependent since they are non-equilibrium materials [18-21].

The goal during this chapter is to investigate the interaction between penetrants and the fibers with and without heat treatment. A method is developed to simulate sorption-induced swelling behavior for hollow fibers. The swelling comparison between virgin and annealed fibers is provided, which proves that thermally annealed membranes can suppress the swelling from acetic acid significantly.

7.2 Sorption-Induced Swelling Experiments

Dynamic and equilibrium sorption-induced swelling tests of acetic acid and water mixtures were performed on Matrimid[®] hollow fiber membranes. Due to a non-homogenous configuration of a hollow fiber, i.e. an ultra-thin densified skin layer supported by an open porous substructure, the gravimetric method [22] can not be applied in the sorption test of a hollow fiber membrane. First, it is very difficult to remove liquid droplets from the fiber surface without damaging the skin layer. Second, it is not possible to completely expel the penetrants present on the bore side of a hollow fiber. Therefore, a new method has to be developed to examine the penetrant sorption in a hollow fiber. The measurement of the fiber length extension is used to characterize the sorption-induced swelling condition on hollow fiber membranes as a measure of the most important sorption within the densified matrix that gives rise to plasticization effects. At the constant temperature of 26°C, hollow fiber modules are soaked in different HAc concentration solutions. The length of each module is measured at the selected time

intervals. The module used in the swelling tests is slightly different from the pervaporation module. In this case, a hollow fiber is sealed by epoxy in both ends to avoid solvents flowing into the bore side. Figure 7.1 shows the schematic of a module immersed in a model HAc/H₂O solution.

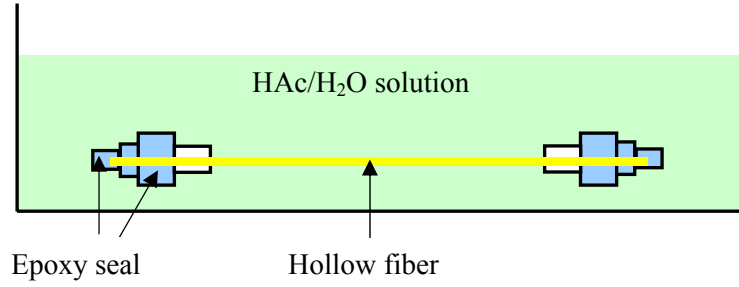


Figure 7.1: Experimental set-up for a hollow fiber-based swelling test

The length extension can be expressed as follows:

$$S_t = \left(\frac{L_t - L_o}{L_o} \right) \times 100\% \quad (7.1)$$

where S_t represents the length extension due to the penetrant-induced swelling at time t , L_t is the measured length of a fiber at time t , and L_o is the initial length of a dry hollow fiber.

Each test is repeated two times for completeness and reproducibility with an inherent error of about $\pm 0.5\%$. The volume of solution should be large enough to prevent concentration changes in HAc/H₂O solutions due to sorbate uptake in hollow fiber modules. While length dilation does not necessarily reflect the full 3-dimensional swelling of the fibers, it is the only measurement that we can confidently make at this point.

7.3 Swelling Effects on Hollow Fibers with and without Heat Treatment

Instead of gravimetric measurements, the length extension was measured at 26°C to simulate the mass uptake of solvents in a hollow fiber due to its non-homogenous configuration. No length extension was observable when a fiber module was soaked in pure DI water. This is indicative of negligible water sorption within measurement accuracy of $\pm 0.5\%$ in the polymer. The kinetic and equilibrium length extension data of virgin and annealed fibers in acetic acid and water mixtures are shown in Figure 7.2 and 7.3, respectively. The annealed fibers were treated in air at 220°C for 1 hour. The length of a dry fiber is about 20 cm.

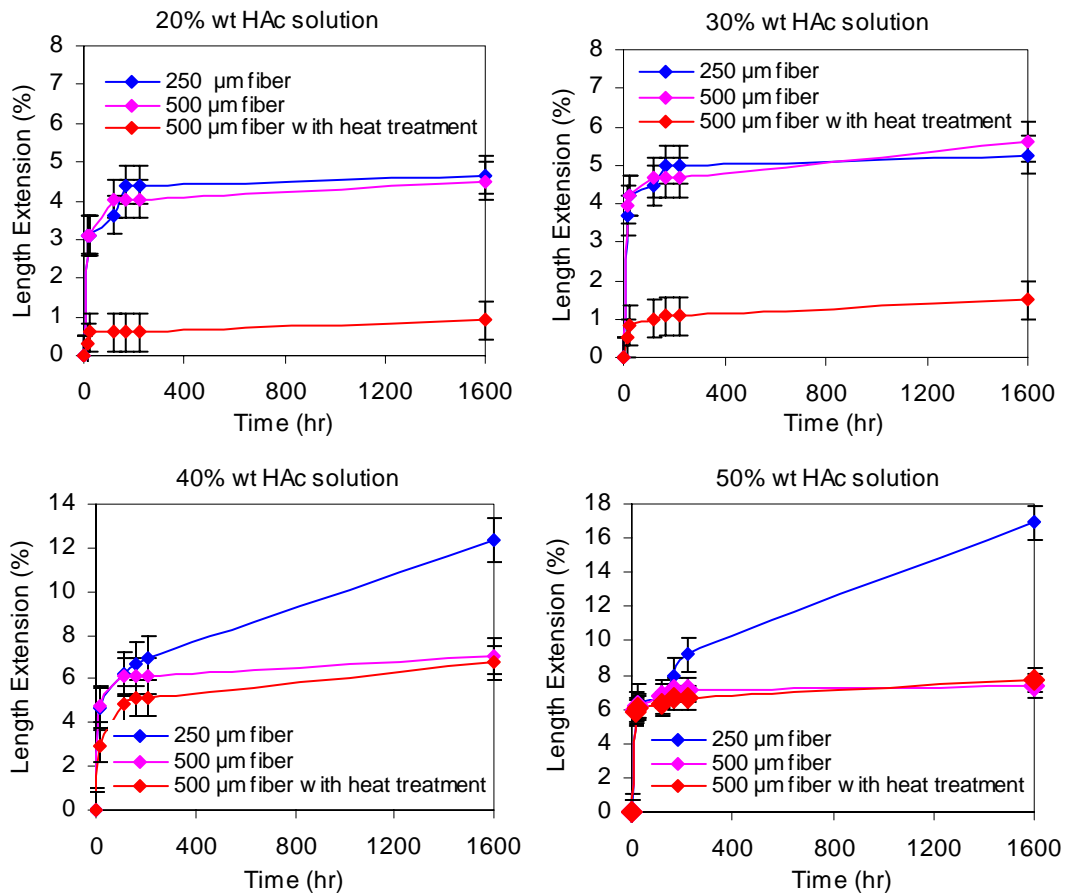


Figure 7.2: Length extension measurement of hollow fibers with and without heat treatment in different HAc concentration solutions

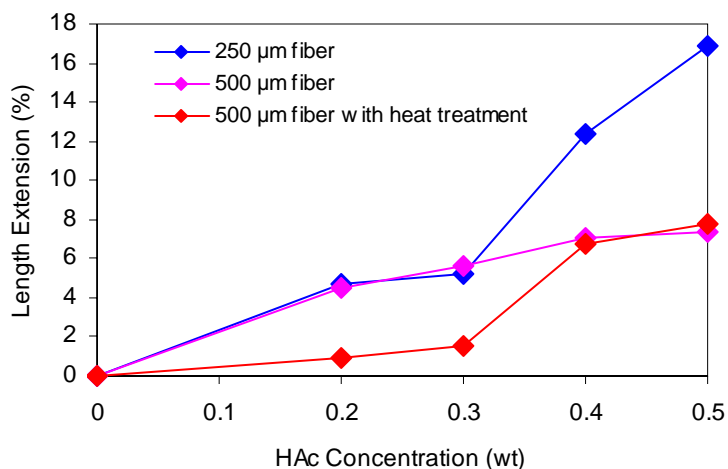


Figure 7.3: Equilibrium data of length extension for virgin and annealed fibers

Several interesting aspects of the data should be addressed. When compared to the sorption-induced swelling data of virgin fibers, the length extension of the thermally annealed fiber is very low in 20% and 30% wt HAc concentration solutions. This is in excellent agreement with the separation results in Chapter 6 and supports the fact that heat treatment can stabilize the membrane by reducing the free volume and promoting the formation of charge transfer complexes [23-24]. Thus, the separation performance can be significantly improved for annealed fibers as the swelling degree from acetic acid in the polymer decreases to 0.5% for a 20% wt HAc/H₂O mixture. However, this heat curing method is not robust enough to prevent the swelling effects from the higher HAc concentration solution. Clearly HAc-induced plasticization tends to be much more severe in the 40% and 50% wt HAc concentration solutions, resulting in similar length extension amounts between the virgin fiber and annealed fiber. It has also been observed that the length extension amount of the 250 μm diameter virgin fiber demonstrates an upswing in the 40% and 50% wt HAc concentration solutions. This might suggest that more rapidly

quenched small diameter hollow fibers are much more easily swelled in more aggressive environments.

The HAc solubility in the polymer plays an important role in the membrane selectivity in contrast to the almost negligible water sorption. The swelled polymer chains due to the high HAc concentration feed favor more HAc sorption into the polymer (solubility). This swelling, in turn, enables large increase in diffusivity and permeability. In other words, the HAc permeability and solubility can increase significantly in high HAc concentration solutions. Nevertheless, the membrane selectivity decreases since the water permeability exhibits a rather limited increment under the HAc-induced swelling condition. This is believed to occur, since the swelling effect benefits the larger penetrant more than the smaller one.

7.4 Summary

Chapters 4 and 6 focus on gathering data to evaluate the fiber performance in separating acetic acid and water mixtures. Although excellent membrane selectivity was achieved using thermally annealed hollow fiber membranes, inherent responsible mechanisms such as the interaction between penetrants and the polymer, are still not clear. In this chapter, an acceptable method has been developed to examine the sorption-induced swelling in the membranes to help probe this issue. The length extension is measured to study the HAc-induced swelling in the hollow fibers.

No measurable water-induced swelling exists in virgin and annealed membranes. The HAc induced swelling (and hence sorption) in annealed fibers is dramatically decreased with the low HAc concentration solutions such as 20% and 30% wt. This

supports the suggestion that the formation of charge transfer complexes and reduction in the free volume due to heat treatment can suppress the sorption of penetrants significantly. In addition to the improved shape and size discrimination for water and acetic acid molecules, the decreased HAc sorption from thermal annealing is also responsible for the large reduction of the HAc permeance. As a result, the membrane selectivity is increased significantly with a 20% wt HAc concentration feed.

However, a significant increase in the length extension of both the virgin and annealed membranes was observed in 40% and 50% HAc concentration solutions. This indicates that the HAc-induced swelling is a dominant factor in explaining permeation and selectivity results in high HAc concentration solutions. The polymer chains are dilated and more free volume is produced, which can increase the HAc solubility and diffusivity more significantly than water. Therefore, the membrane selectivity drastically falls down even with thermally annealed fibers.

The sorption-induced swelling data for virgin and annealed membranes are in qualitative agreement with the pervaporation results. This can help us to gain the basic understanding about the interaction between penetrants and the polymer.

7.5 References

- [1] Paul, D.R. and Y.P. Yampol'skii, *Polymeric gas separation membranes*. Boca Raton: CRC Press 1994.
- [2] Mulder, M., *Basic principles of membrane technology*. Kluwer Academic Publishers: Dordrecht. 1996.
- [3] Freeman B.D. and Pinnau I. *Polymer membranes for gas and vapor separation* ACS SYMPOSIUM SERIES 733 1999.

- [4] Stern, S.A. *Polymers for gas separations: the next decade*. J. Membr. Sci. 1994, 94, 1-65.
- [5] Lue, S.J. and Peng, S.H. *Polyurethane (PU) membrane preparation with and without hydroxypropyl- β -cyclodextrin and their pervaporation characteristics*. J. Membr. Sci. 2003, 222, 203-217.
- [6] Vieth, W.R., Dao, L.H., and Pedersen, H. *Nonequilibrium microstructural and transport characteristics of glassy poly(ethylene terephthalate)*. J. Membr. Sci. 1991, 60(1), 41-62.
- [7] Patel, N.P., Hunt, M.A., Lin-Gibson, S., Bencherif, S., and Spontak, R.J. *Tunable CO₂ transport through mixed polyether membranes*. J. Membr. Sci. 2005, 251(1-2), 51-57.
- [8] Koros, W.J. *Simplified analysis of gas/polymer selective solubility behavior*. J. Polym. Sci., Polym. Phys. Ed. 1985, 23(8), 1611-1628.
- [9] Kazama, S., Teramoto, T., and Haraya, K. *Carbon dioxide and nitrogen transport properties of bis(phenyl)fluorene-based cardo polymer membranes*. J. Membr. Sci. 2002, 207(1), 91-104.
- [10] Wind, J.D., Staudt-Bickel, C., Paul, D.R., and Koros, W.J. *The effects of crosslinking chemistry on CO₂ plasticization of polyimide gas separation membranes*. Ind. Eng. Chem. Res. 2002, 41(24), 6139-6148.
- [11] Lue, S.J., Wang, F. J., and Hsiaw, S. *Pervaporation of benzene/cyclohexane mixtures using ion-exchange membrane containing copper ions*. J. Membr. Sci. 2004, 240(1-2), 149-158.
- [12] Prabhakar, R., Merkel, T.C., Freeman, B.D., Imizu, T., Higuchi, A., Sarti, G.C., and Doghleri, F. *Effect of fluorocarbon-hydrocarbon interactions on solubility and permeability properties of polymers*. Polym. Mater. Sci. Eng. 2001, 85, 253-254.
- [13] Story, B.J., Koros, W.J. *Sorption and transport of carbon dioxide and methane in chemically modified poly(phenylene oxide)*. J. Membr. Sci. 1992, 67(2-3), 191-210.
- [14] Shimazu, A., Miyazaki, T., Maeda, M., and Ikeda, K. *Relationships between the chemical structures and the solubility, diffusivity, and permselectivity of propylene and propane in 6FDA-based polyimides*. J. Polym. Sci., Part B: Polym. Phys. 2000, 38(19), 2525-2536.
- [15] Frb, A.J. and Paul, D.R. *Gas sorption and transport in polysulfone*. J. Membr. Sci., 1981. 8, 11-22.

- [16] Paul, D.R. *Gas Sorption and Transport in Glassy Polymers*. Ber. Bunsenges Phys. Chem. 1979, 83, 294-302.
- [17] Kesting, R.E. and Fritzsche, A.K. *Polymeric gas separation membranes*. John Wiley & Sons, Inc. 1993.
- [18] Struik, L.C.E. *Physical aging in amorphous polymers and other materials*. Elsevier: Amsterdam. 1978.
- [19] Lee, E.K. and Koros, W.J. *Membrane, synthetic, applications*. Encyclopedia of Physical Science and Technology. 2001, 279-344.
- [20] Fleming, G.K. and Koros, W.J. *Dilation of polymers by sorption of carbon dioxide at elevated pressures: silicone rubber and unconditioned polycarbonate*. Macromolecules. 1986, 19, 2285-2291.
- [21] Jordan, S.M., Koros, W.J. and Fleming, G.K. *The effects on carbon dioxide exposure on pure and mixed gas permeation behavior of polymers: comparison of glassy polycarbonate and silicone rubber*. J. Membr. Sci. 1987, 30, 191-212.
- [22] Damle, S. *Membrane Based Separations of Organic Solutes from Supercritical Carbon Dioxide*. Ph.D. Dissertation, The University of Texas at Austin, 2004.
- [23] Kawakami, H., Mikawa, M., and Nagaoka, S. *Gas transport properties in thermally cured aromatic polyimide membranes*. J. Membr. Sci. 1996, 118, 223-230.
- [24] Krol, J.J., Boerrigter, M., and Koops, G.H. *Polyimide hollow fiber gas separation membranes: preparation and the suppression of plasticization in propane/propylene environments*. J. Membr. Sci. 2001, 184, 275-286.

Chapter 8: Conclusions and Recommendations for Future Work

8.1 Summary of Conclusions

The primary objective of this dissertation was to demonstrate the fundamental feasibility of adapting gas separation hollow fibers into pervaporation membranes for organic-containing feeds. The model system of acetic acid and water mixtures was used for a proof-of-concept study. The membrane performance under reasonably realistic processing conditions (20% wt HAc/H₂O feeds, 101°C and one atmosphere) was examined to determine the effectiveness of this approach. It has been shown that a hollow fiber-based membrane is a promising alternative to the costly distillation technology. In particular, different requirements between gas and liquid separation were defined. The research work presented in this dissertation not only illustrates that a glassy polymer is a good candidate for liquid separation (HAc/H₂O mixtures), but also provides helpful techniques, such as a large bore size defect-free hollow fiber spinning and thermal annealing, to improve the membrane performance with aggressive feeds. The knowledge gained in this project can be used to guide future researchers' work in many areas such as hollow fiber spinning from novel polymers, aggressive organic-organic solvent pervaporation, and post treatment of commercial polymers. The flow diagram in Figure 8.1 highlights our achievements.

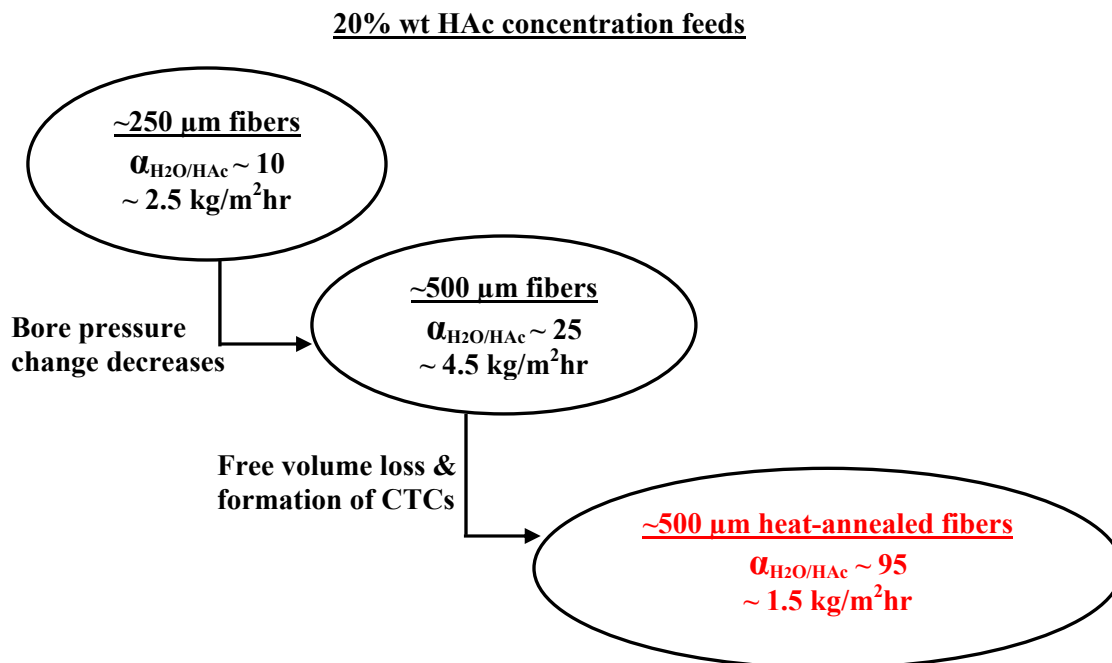


Figure 8.1: Flow diagram showing our achievements

8.1.1 Spinning a Large Bore Size Defect-Free Fiber

A scientific basis was successfully developed to spin a large bore size defect-free Matrimid® hollow fiber using an available first generation spinneret and spinning equipment. Each step, including dope preparation, spinning, solvent exchange, drying, and pure gas permeation, has been discussed with theoretical and practical considerations. Based upon the knowledge of spinning a small bore size fiber (O.D. ~ 250 μm) in our group, the spinning steps were modified and optimized to obtain a large bore size defect-free fiber (O.D. ~ 500 μm).

- The formulation of the dope composition was refined and optimized. The concentration spectrum of each chemical was narrowed down. The evaporation of more volatile solvents in the air gap can lead to quick vitrification of a fiber's outer periphery [1]. The optimal concentration of

more volatile solvents in the dope should be high enough to obtain a thin defect-free separation layer, while not causing any difficulties in the spinning process.

- The take-up rate is an important spinning variable to control the outer diameter of fibers: the slower the take-up rate, the larger the fiber diameter. The minimum rate is about 12 m/min. A take-up rate lower than this threshold causes a serious “crinkling” problem, in which the fiber does not have a straight cylindrical form. When the nascent fibers with a relatively high velocity in the air gap hit an aqueous quench bath, high surface tension and bath viscosity apparently hamper the ability of fibers to go through the bath unless the pulling velocity of a take-up drum is high enough to overcome water viscous resistance.
- The optimal dope extrusion rate is about 180ml/hr for our existing spinneret. A higher rate is very hard to handle in the spinning process and might cause incomplete phase separation in the quench bath, while a lower rate decreases the productivity of fiber fabrication.
- The bore fluid extrusion rate is responsible for the bore size of a hollow fiber. Although a large bore is required in pervaporation, the substrate wall tends to be thinner with the higher bore fluid extrusion rate. This leads to the reduction of mechanical support from the substrate.

8.1.2 Pervaporation of HAc/H₂O Mixtures Using Hollow Fibers

A lab scale pervaporation module was assembled and a hollow fiber-based pervaporation set-up was established. Both a regular size fiber (O.D. $\sim 250\ \mu\text{m}$) and large size fiber (O.D. $\sim 500\ \mu\text{m}$) were used to separate 20% wt model HAc/H₂O mixtures. The membrane selectivity (~ 25) and water flux ($\sim 4.5\ \text{kg/m}^2\text{hr}$) were improved by about 150% with a diameter (O.D. $\sim 500\ \mu\text{m}$) twice as large as the regular fiber. This is in good agreement with the model expectation. The membrane performance can be severely deteriorated due to the high bore pressure change associated with the large water flux in pervaporation in a small diameter hollow fiber.

Generally, highly permeable gas molecules are affected much more seriously than slow ones by the bore pressure change. Therefore, the true membrane selectivity for a high/low permeable gas pair can be underestimated in a small bore size fiber. A large bore size fiber is a good solution to minimize the negative effects of the bore pressure change. As expected, the water flux increased significantly with a large bore size fiber. However, the *depression* of the HAc flux was observed with a large bore size fiber. This important observation *was not anticipated at the outset of this work*. Apparently the HAc permeability is a concentration-dependent variable. The polymer is less swollen because of the low HAc pressure change (low HAc concentration) in the bore side of large fibers, which hinders the passage of acetic acid molecules. Clearly we are in a win-win situation with the large bore size fibers, because both selectivity and productivity are improved dramatically using the large bore size fiber for a 20% wt HAc concentration feed.

Pure DI water feeds were also investigated in pervaporation and the fiber demonstrated a constant permeability with time. It is believed that the swelling interaction between water and the polymer is negligible.

8.1.3 Model to Simulate Pressure Change in Bore Side of Hollow Fibers

A mathematical model was developed to simulate the pressure change in the bore side of a hollow fiber in a high flux pervaporation process. The simulation results showed that the pressure change in a large bore (O.D. $\sim 500\ \mu\text{m}$) was much smaller than in a small one (O.D. $\sim 250\ \mu\text{m}$). The expected maximum water permeance from the modeling work is very close to the experimental results with a large bore size fiber. This indicates that a $500\ \mu\text{m}$ outside diameter fiber can effectively minimize the negative effects of the bore pressure change. A diameter larger than $500\ \mu\text{m}$ fiber might offer slightly better membrane selectivity, but it would sacrifice the available separation area.

The comparison between the model and experimental results suggests that the water permeability is weakly HAc-concentration dependent, while the HAc permeability is strongly HAc-concentration dependent for a model 20% wt HAc/H₂O feed. In terms of the modeled selectivity and permeance that take the bore pressure change into account, the membrane selectivity and flux can be predicted with different size fibers. Although system parameters are different, this model can also be extended for separating other binary mixtures.

8.1.4 Investigation of Thermally Annealed Fibers in Separating HAc/H₂O Mixtures

A large bore size hollow fiber was tested by the pure gas permeation method using N₂, O₂, and He. The membrane selectivities of $\alpha_{\text{O}_2/\text{N}_2}$ and $\alpha_{\text{He}/\text{N}_2}$ are very close to the intrinsic results (dense films), thereby indicating defect-free fibers. The average membrane selectivity of about 25 could be achieved for these fibers in separating 20% wt HAc/H₂O mixtures. Unlike low-sorbing gas molecules such as N₂ and O₂, the fibers were found being swelled significantly in separating HAc/H₂O solutions, because acetic acid molecules can plasticize the polymer and facilitate the passage of the “slow” gas molecules, i.e. acetic acid in this research, while not affecting the “fast” molecules as significantly. It is believed that this situation reflects the creation of a proportionally larger fraction of large size transient gaps in the plasticized matrix than in the unplasticized one.

Thermal annealing (below T_g) has been studied in gas separation [2-5], but very limited research has been published in pervaporation. A glassy polymer is a non-equilibrium material and has excess un-relaxed free volume. The diffusion coefficient of a penetrant in a glassy polymer membrane mainly depends on two factors,

- The size and shape of a penetrant
- Structure of a polymer including segmental mobility of the polymer chains, the free volume and its distribution

Thermal annealing can reduce the free volume, effectively increasing the discrimination of the size and shape of penetrants. Meanwhile, the formation of charge transfer complexes due to heat treatment can improve the rigidity of the polymer chains and thus

suppress the plasticization caused from acetic acid molecules. A membrane selectivity of about 95 can be obtained with a 20% wt HAc concentration feed at about 101.5°C.

The annealing parameters such as heating temperature, heating time, and heating environment were investigated to see how strong their effects are on the fiber performance.

- Heating temperature

It has been observed that the optimal heating temperature is about 220°C. Heating temperatures higher than 220°C could not be tested in this work due to the limitation of experimental facilities. With heating temperatures lower than 220°C, fibers could not be annealed intensively enough, resulting in lower membrane selectivities.

- Heating time

The best heating time is 1 hour for the currently optimized fiber morphology. Evidence for the transition layer collapse was observed for the over-heated fibers (longer than 5 hours) in pure gas permeation and pervaporation tests. This overheating generates excess substrate resistance. Thus, the resulting membrane selectivity is somewhat decreased because the substrate resistance hinders water/fast gas molecules much more severely than HAc/slow ones. A more “open” transition layer fiber may enable further annealing time to tune selective skin layer properties via the procedure.

- Heating environment

Thermal annealing was performed under air and vacuum conditions. The fiber did not show any difference between these two heating environments. This is potentially helpful in industry because creation of expensive vacuum can be avoided. A more conservative but still economical approach might use inert N₂ blankets during annealing.

- Long term performance

A fiber was treated under the optimal heating conditions. Thereafter, a 20% wt acetic acid-water mixture was used not only as a feed solution for pervaporation but also as a soaking bath to store the fiber. The fiber was very robust and maintained stable separation performance for at least one month. Earlier authors [6] only demonstrated their pervaporation results for short time periods (6 ~ 7 hours) for separating HAc/H₂O mixtures.

FTIR and ¹H NMR tests were completed with virgin and annealed fibers, and no noticeable difference was observed. This indicates that no chemical reaction such as chemical crosslinking occurs with thermal annealing. A significant increase in micro-fluorescence emission intensity was observed with the increased heating temperature. This provides concrete proof that charge transfer complexes are formed and intensified by the higher thermal temperature. With thermal annealing, the reduction of free volume and formation of inter-molecular charge transfer complexes improve the discrimination of shape and size for penetrants and suppress the HAc-induced swelling; thus, the membrane selectivity can be significantly increased.

Higher HAc concentration feeds such as 50% wt were also studied in pervaporation using annealed fibers. The high HAc concentration-induced plasticization resulted in low membrane selectivity (~ 10). However, this value is still much better than that of virgin fibers (~ 1.5).

A model was also developed to simulate an annealed fiber-based cross-flow separator that was very close to realistic operations. The overall membrane selectivity for a 20% wt HAc feed with a 50% wt HAc final product retained an average value of about 44, although some losses exist due to the strong swelling from the 50% wt HAc concentration solution at the final stage of the separator. Nevertheless, these results are still satisfactory for industrial viability.

8.1.5 Sorption-Induced Swelling Tests

Sorption-induced swelling tests were used to probe the interaction between penetrants and the polymer. The length extension measurement was applied in hollow fibers to characterize the HAc-induced swelling. The sorption of pure DI water on fibers was first investigated and no measurable changes were observed. This further proves that the interaction between water and the polymer is weak. Therefore, the sorption-induced swelling for acetic acid and water mixtures could be reasonably assumed to be acetic acid, although this assumption might not be accurate especially under the swelling conditions. Further tests should investigate this more carefully.

A significant reduction of acetic acid-induced swelling was observed from virgin to annealed fibers in the 20% wt HAc concentration solution because the length extension is decreased from 4.0% to 0.5%. Due to potentially non-isotropic swelling, this factor of

8X lower swelling cannot be safely extrapolated to a 8X lower sorption uptake. Nevertheless, the trends should be likely similar. This indicates that the “excess” free volume of virgin fibers decreases dramatically due to heat treatment. In addition, the formation of charge transfer complexes in annealed fibers strongly restricts segmental mobility of the polymer chains and thus limits the sorption of solvents.

The sorption-induced swelling studies for a hollow fiber were also conducted in the higher HAc concentration solutions such as 50% wt. The difference in sorption between virgin and annealed fibers was very small. The HAc-induced plasticization is dominant in the polymer as heat treatment is apparently not intense enough to suppress the HAc-induced swelling. As a result, the length extension amount reaches almost 8% for virgin and annealed fibers.

Transport phenomena of acetic acid and water molecules through hydrophobic Matrimid[®] membranes are very complicated since many factors have to be considered. The diffusion coefficient of water is a dominant factor for its high flux, while both diffusivity and solubility of acetic acid are responsible for its permeation. In addition, the HAc diffusion and solution coefficients are strong concentration-dependent variables.

8.2 Recommendations for Future Work

The work described in this dissertation is of theoretical and practical natures, and it has also raised some interesting questions. In order to fully understand the phenomena that have been described and allow scale up for future industry applications, additional fundamental work remains to be done. This section contains recommendations for the next step of this project.

8.2.1 Performance Evaluation for Contaminated Feeds

It is important to evaluate how well the fiber performs with industrial streams. Based upon the information from our industry sponsor, methyl acetate (MeAc), methanol (MeOH), and p-xylene are three major contaminants in separating acetic acid and water mixtures. Future work should examine the effects of these chemicals on the fiber performance.

a) *Identify the influences of MeAc, MeOH, and p-xylene on the fiber performance*

Each component should be studied individually to avoid complicated interaction situations. Since water does not have noticeable interaction with the polymer, a binary system of each chemical and water should be a good starting point in separating mixtures. Further, sorption tests should be conducted to investigate the effects of each solvent on the polymer matrix.

b) *Evaluate the separation performance with a full “cocktail” mixture*

Once individual effects of contaminants are well studied, full “cocktail” mixtures should be investigated because they may have nonlinear effects on the fibers.

c) *A valid analytical technique should be developed for a full “cocktail” mixture*

A valid analytical method has to be established to examine a solution containing more than three chemicals, since the refractometer is generally used to test only a binary system. Head-space GC might be a good tool to measure multi-component solutions [7].

8.2.2 Plasticization by HAc and Potential Contaminates

The experimental results in this work clearly show that high HAc concentration solutions can dramatically plasticize the polymer and thus deteriorate the membrane selectivity. Moreover, potential contaminants such as MeAc, MeOH, and p-xylene might also induce large swelling stresses on the polymer chains and impair the membrane performance. Thermal annealing as described in this dissertation can solve the swelling problems to some degree; however, additional work is required to deal with more aggressive environments. Several attempts have been made to stabilize membranes in the open literatures as noted below.

- Cross-linking

In terms of polyimides structure, the imide link can be used as a site to cross-link with diamino compounds [8]. Benzophenone groups can also be cross-linked by exposure of UV radiation [9]. The utilization of a proper covalent cross-linking agent to cross-link 6FDA-based polyimides is another promising technique to stabilize membranes against CO₂ plasticization up to 40 atm feed pressure [2-3].

- Blending

Blends have been used to improve membrane stability [10]. One form of blending is to combine a high performance polymer with a highly stable polymer. Another form involves adding oligomers or monomers to a polymer to form interpenetrating networks. The cross-linked blends of an acetylene-terminated monomer (ATM) with a commercially available

poly(etherimide) can improve thermal and chemical stability and increase gas selectivity as compared to the uncrosslinked blends [11].

- ***A new high performance polymer***

Torlon[®] [poly(amide imide) (PAI)] has some physical properties that are similar to polyimides, but is generally tougher under stresses and less permeable to organics due to the amide group. Further, PAIs can accept higher loadings of inorganic materials with more homogeneous dispersion compared to polyimides [12]. *Therefore, Torlon[®] might be a potential candidate for the next generation membrane material and future work should focus on spinning a Torlon[®]-based hollow fiber membrane.* The chemical structure of Torlon[®] is shown in Figure 8.2.

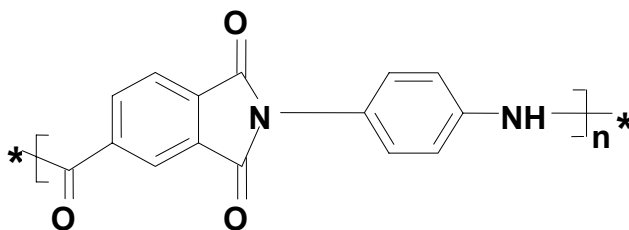


Figure 8.2: Chemical structure of Torlon[®]

8.3 References

- [1] Wallace, D.W. *Crosslinked hollow fiber membranes for natural gas purification and their manufacture from novel polymers*. Ph.D. Dissertation, The University of Texas at Austin, 2004.
- [2] Wind, J.D., Sirard, S.M., Paul, D.R., Green, P.F., Johnston, K.P., and Koros, W.J. *Carbon dioxide-induced plasticization of polyimide membranes: Pseudo-equilibrium relationships of diffusion, sorption, and swelling*. *Macromolecules*. 2003, 36, 6433-6441.

- [3] Wind, J.D., Staudt-Bickel, C, Paul, D.R., and Koros, W.J. *Solid-state covalent cross-linking of polyimide membranes for carbon dioxide plasticization reduction*. Macromolecules. 2003, 36, 1882-1888.
- [4] Bos, A., Punt I.G.M., Wessling, M., and Strathmann, H. *Plasticization-resistant glassy polyimide membranes for CO₂/CO₄ separations*. Sep. Purif. Technol. 1998, 14, 27-39.
- [5] Kawakami, H., Mikawa, M., and Nagaoka, S. *Gas transport properties in thermally cured aromatic polyimide membranes*. J. Membr. Sci. 1996, 118, 223-230.
- [6] Huang, J.G., Cranford, R., Matsuura, T., and Roy, C. *Development of polyimide membranes for the separation of water vapor from organic compounds*. J. Appl. Poly. Sci. 2002, 85, 139-152.
- [7] Chai, X.S., Hou, Q.X., Zhu, J.Y., Chen, S.L., Wang, S.F., and Lucia, L. *Carboxyl groups in wood fibers. I. Determination of carboxyl groups by headspace gas chromatography*. Ind. Eng. Chem. Res. 2003, 42, 5440-5444.
- [8] Liu, Y., Wang R., and Chung, T.S. *Chemical cross-linking modification of polyimide membranes for gas separation*. J. Membr. Sci. 2001, 189, 231-239.
- [9] Kita, H., Inada, T., Tanaka, K., and Okamoto, K. *Effect of photocrosslinking on permeability and permselectivity of gases through benzophenone-containing polyimide*. J. Membr. Sci. 1994. 139-147.
- [10] Bos, A., Punt, I.G.M., Strathmann, H., and Wessling, M. *Suppression of gas separation membrane plasticization by homogeneous polymer blending*. AIChE J. 2001, 47, 1088-1093.
- [11] Rezac, M. E. and Schoberl, B. *Transport and thermal properties of poly(ether imide)/acetylene-terminated monomer blends*. J. Membr. Sci. 1999, 156, 211-222.
- [12] Hoppin, C. R. *Characterization of Torlon[®] Films*. 2004 (Internal report in Dr. William Koros' group).

Appendix A: Manufacture of Lab-Scale Hollow Fiber Modules for Gas Permeation [1]

An asymmetric hollow fiber has to be potted into a housing for gas permeation tests. The fibers have to be sealed in such a manner as to allow gas to contact one side of the fiber, while a low pressure or vacuum is maintained on the other side, so that mass transfer can occur across the membrane. This requires an airtight seal that is referred to as a tubesheet. The tubesheet is usually formed with epoxy or similar materials. The housing with potted hollow fibers is called a module [2-3].

A.1 Parts

Swagelok[®] tubing and fittings are used for module housing components, as shown in Figure A.1. Scotch-weld epoxy adhesive is used to mount fibers into the house. The table below lists the main parts needed to make a hollow fiber module.

Table A.1: Parts for assembling double-ended lab scale hollow fiber modules

Name	Manufacturer	Notes
Ferrules	Swagelok [®]	Brass or Stainless Steel
Nut	Swagelok [®]	Brass
Female Adapter	Swagelok [®]	Brass
Male Adapter	Swagelok [®]	Brass
Tee	Swagelok [®]	Stainless Steel
Metal Tubing	Swagelok [®]	Stainless Steel
Cap	Swagelok [®]	Stainless Steel
Plug	Swagelok [®]	Stainless Steel
Tygon Tubing	Fisher Scientific	
Scotch-weld Epoxy	Grainger	

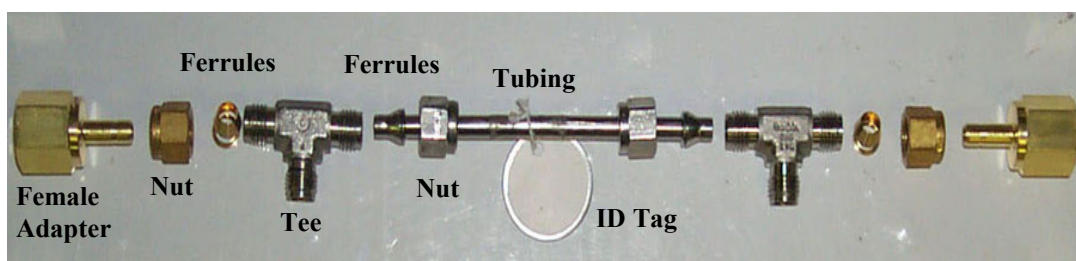


Figure A.1: Parts for assembling double-ended lab scale hollow fiber modules

A.2 Procedures

A “blank” module is first prepared (Figure A.2). Fibers are then pulled through the housing using a thin string. Standard Teflon[®] tape is used to pack into one of the female adapters around the fibers, which can prevent epoxy from dripping into the housing.



Figure A.2: Parts for a blank module

A 1-cm piece of $\frac{3}{16}$ " Tygon[®] tubing has to be hooked with a brass male $\frac{1}{4}$ " NPT adapter, which is shown in Figure A.3. After the epoxy is poured into the brass female adapter, the male adapter has to be screwed into the female adapter until the epoxy fills the Tygon tubing piece. The Tygon tubing can be snapped off the module, once the epoxy gets cured (~10 minutes). The pot face should be clean to ensure the open fiber bore. The other pot face should be formed in the same manner.



Figure A.3: Brass male adapter with Tygon tubing piece

A.3 References

- [1] Wallace, D.W. *Crosslinked hollow fiber membranes for natural gas purification and their manufacture from novel polymers*. Ph.D. Dissertation, The University of Texas at Austin, 2004.
- [2] Carruthers, S.B. *Integral skin formation in hollow fiber membranes for gas separations*. Ph.D. Dissertation, The University of Texas at Austin, 1997.
- [3] Djoekita, G., Vu, D.Q., and Koros, W.J. *Pervaporative Introduction of Organic Vapors into High-Pressure Gas Feeds*. J. Appl. Polym. Sci. 2001, 80(2), 311-315.

Appendix B: Pure Gas Permeation Tests for Hollow Fiber Modules

This appendix contains the procedures used for pure gas permeation tests. All tests are run in a temperature-controlled permeation box.

B.1 Setup

Bore vs. Shell Feed

Testing can be done by feeding the gas on either the bore or shell side of a module. The pressure change in the bore side has to be corrected with shell feed, since the pressure change inside the bore influences fast gases more significantly than slow gases. This issue has been described in chapter 5.

The “Christmas Tree”

Set up Swagelok[®] fittings (Union Crosses and Tees) to attach the feed inlet of the modules to the feed gas port in the permeation system, and be certain that a pressure transducer is hooked up to the feed as well. The whole unit with Swagelok[®] fittings and modules is called a “Christmas Tree”.

Testing Order

Start with highly permeable gas first (He), then less permeable gas (O₂), and finally the slowest gas (N₂) for pure gas permeation tests. This testing order avoids overestimating membrane selectivity. *The testing order is very important*, especially for polymers with very low gas permeability such as Torlon[®].

B.2 Purge Modules

- 1) Zero the pressure transducer.
- 2) Open the retentate outlet on all the modules.
- 3) Open the gas cylinder and pressurize the entire system. Gas should be flowing through the entire system and exiting through the retentate of each module. Let the gas flow for at least 5 seconds.
- 4) Close the main cylinder valve. The pressure should drop slowly in the system.
- 5) Open the cylinder valve when the regulator pressure reads ~20 psi.
- 6) Repeat steps 4 and 5 three more times.
- 7) The entire system has been purged, or 'rinsed', a total of four times with "clean gas."
- 8) Close the retentate of each module.
- 9) Adjust the feed pressure as desired, close the door of the permeation system.
- 10) Wait 15 min. The permeation flowrates and inner box temperature should equilibrate.

B.3 Testing

- 1) (*0-15 minutes*) During the 15 min. equilibration, the following steps should be done:
 - a. Record the active length of each module
 - b. Record the # of fibers in each module
 - c. Record the box temperature
 - d. Wet the bubble flowmeter.

2) (> 15 minutes) Measure each module's permeate flowrate w/ a bubble flowmeter.

e. Let the bubble travel for at least 15 seconds, and preferably an easily measured distance.

i. GOOD--10.00 mL in 17.67 seconds

ii. GOOD--200 mL in 31.27 sec

iii. BAD--10.00 mL in 11.21 seconds (too short, too much error).

f. Smallest measurable flowrate is ~ 0.5 mL / minute.

g. Electronic Flowmeters do NOT seem to be as accurate or precise at low flowrates (< 100 ml/min). A Bubble Flowmeter should be used.

h. Record the feed pressure for each flowrate measurement.

3) (> 45 minutes) Test the modules *again* 45 min after equilibration (1 hr after pressurization).

i. If there's greater than a **5%** difference between the '45 minute measurement' and the '15 min measurement', wait another 45 minutes and measure a 3rd time.

j. Keep testing until there is less than a **5%** change over 45 minutes. Only 2 measurements are generally necessary if the system was purged well.

4) Calculate permeances and selectivities for the membranes. Retest as desired.

5) Close all cylinder valves, turn off the pressure transducer, clean up.

B.4 Analysis

1) Permeance

- a. The equation shown here results in units of GPU. Constants in the equation convert common measurement units to those required for GPU.

$$\text{b. } \left(\frac{\mathcal{P}}{\ell} \right)_A [\text{GPU}] = 10^6 \cdot \frac{(\text{Permeate flow}) \cdot 273.15}{T \cdot A \cdot \Delta p \cdot 5.17}$$

- i. Permeate flow is in ml/sec.
- ii. T is the testing temperature in Kelvin.
- iii. A is the area available for permeation in cm^2 .
- iv. Δp is the pressure drop between upstream and downstream sides of the membrane in psi.

2) Ideal selectivity

$$\text{c. } \alpha_{A/B} = \frac{\left(\frac{\mathcal{P}}{\ell} \right)_A}{\left(\frac{\mathcal{P}}{\ell} \right)_B}$$

3) Uncertainty

- d. Uncertainty for permeance is estimated from the precision of the bubble flow meter, pressure transducer, and stopwatch to be about $\pm 5\%$.

Appendix C: Fabrication of Hollow Fiber-Based Pervaporation Modules

A concept to manufacture hollow fiber-based pervaporation modules is similar to gas permeation modules in Appendix A [1]. An asymmetric hollow fiber must be mounted into a vessel, so as that liquid or vapor can contact one side of the fibers and run through the fiber wall to the other side with low pressure. Figure C.1 shows the pervaporation module used in this work for separating acetic acid-water mixtures.



Figure C.1: Pervaporation module used for separating acetic acid-water mixtures

C.1 Parts

Swagelok[®] fittings are used for assembling a pervaporation module. The table below lists the main parts needed to make a pervaporation module.

Table C.1: Parts for assembling a hollow fiber-based pervaporation module

Name	Manufacturer	Notes
Female Adapter	Swagelok [®]	Brass
Male Adapter	Swagelok [®]	Brass
Ultra-Torr Reducing Union, 1/2" - 1/4"	Swagelok [®]	Stainless Steel
Ferrules	Swagelok [®]	Brass
Nuts	Swagelok [®]	Brass
Cylindrical Reaction Vessel	Lab Glass	Glass
Tygon Tubing	Fisher Scientific	
Scotch-weld Epoxy	Grainger	

C.2 Procedures

Unlike gas permeation modules, in which 20-50 fibers are used to make a module, only *one fiber* is used to make a pervaporation module.

A cylindrical reaction vessel has to be processed to add two pieces of short glass tubing along the diameter direction, as shown in Figure C.1. An ultra-torr reducing union can be hooked with the glass tubing. After a female adapter is connected with the ultra-torr fitting, a fiber is then pulled through the vessel. Standard Teflon[®] tape is used to pack into the female adapter around the fiber, which can prevent epoxy from dripping into the vessel. A 1-cm piece of $\frac{3}{16}$ " Tygon[®] tubing is used to hook with a brass male $\frac{1}{4}$ " NPT adapter. Once the epoxy is poured into the brass female adapter, the male adapter has to be screwed into the female adapter until the epoxy fills the Tygon tubing piece. The Tygon tubing can be snapped off from the module, after the epoxy gets cured (~10 minutes). The pot face should be clean to ensure the open fiber bore. The other pot face should be formed in the same manner.

C.3 Notes

The Scotch-weld epoxy has been used for all the gas permeation modules due to its cheap and convenient properties. Generally it takes at most 30 minutes to get this epoxy cured. However, some other epoxies should be considered if a module has to withstand tough environments such as high temperature, high pressure, and aggressive feeds. Stycast[®] 2651 from Emerson & Cuming, Loctite[®] Depend[®] 330[™] adhesive from McMaster-Carr are more durable seals in contrast to the Scotch-weld epoxy. Table C.2 shows the technical parameters for these two epoxies.

Table C.2: Technical parameters for Stycast[®] 2651 and Loctite[®] Depend[®] 330[™] epoxies

Epoxy	Stycast [®] 2651	Loctite [®] Depend [®] 330 [™]
Tensile strength (psi)	~ 7000	~ 3300
Upper Temperature Tolerance (°C)	~130	~ 120
Cure Time (hr)	~ 24	1~2 minutes becomes hard, then needs 24 hr to reach full strength
Resistant	water	water, hydrocarbon oils, and common organic solvents
Bonds	stainless steel, marble, and concrete	Aluminum, stainless steel, marble, glass, concrete, and wood

C.4 References

- [1] Wallace, D.W. *Crosslinked hollow fiber membranes for natural gas purification and their manufacture from novel polymers*. Ph.D. Dissertation, The University of Texas at Austin, 2004.

Appendix D: Pervaporation Tests for Hollow Fiber Modules

This appendix contains the procedures followed for pervaporation tests. Figure D.1 shows the pervaporation setup.

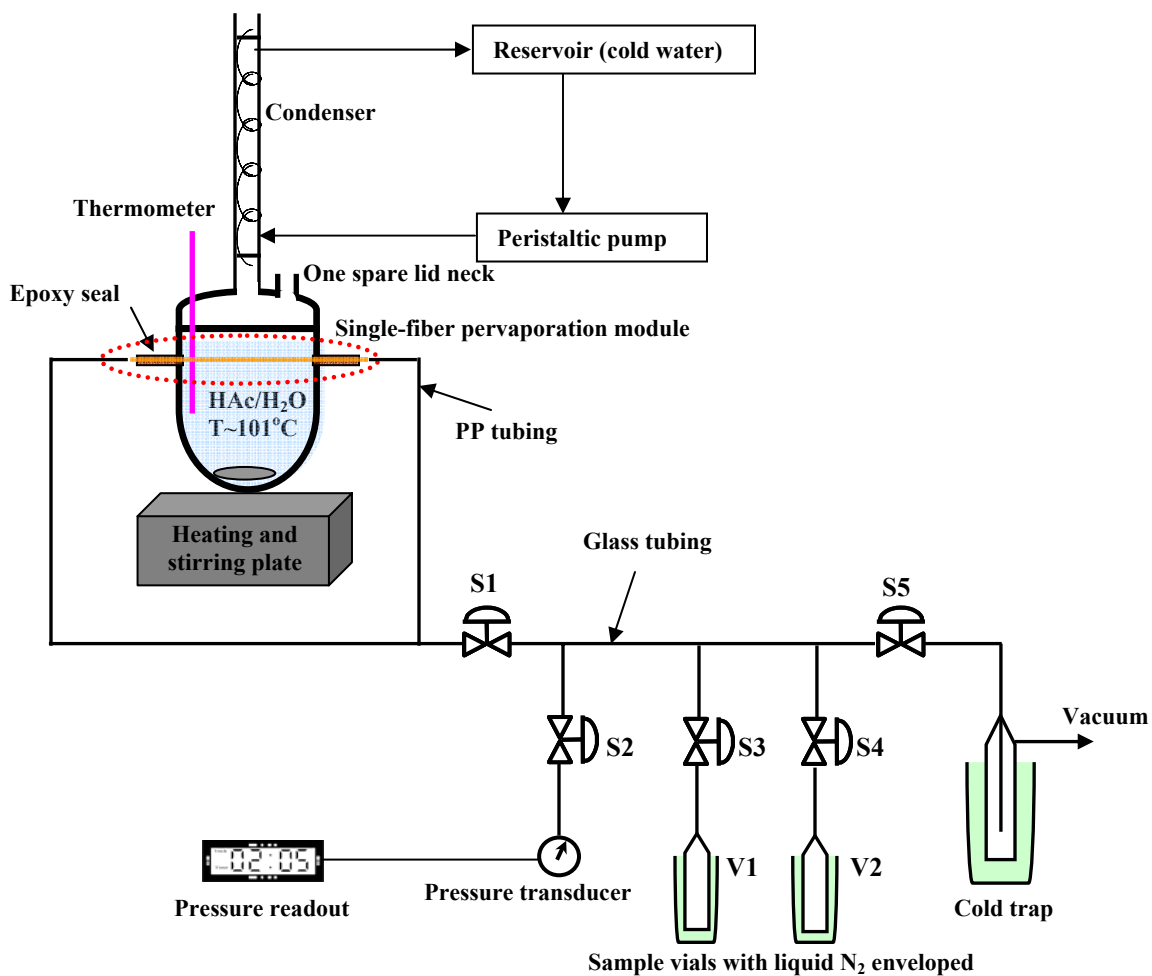


Figure D.1: A hollow fiber-based pervaporation system

D.1 Bore vs. Shell Feed

Unlike pure gas permeation tests, shell feed is applied for pervaporation experiments. It is difficult to circulate a feed solution inside the bore with an inner diameter of 150 - 350 μm in this work. With shell feed, excellent circulation is available so that both concentration-polarization and external mass transfer resistance can be effectively minimized. However, the pressure change inside the bore associated with high flux should be corrected to obtain the inherent polymer permeability and selectivity, which has been described in Chapter 5.

D.2 Operation Procedures

- 1) Connect a pervaporation module with a pervaporation system. Carefully pour a liquid feed into the vessel and put a stir bar into the liquid. Meanwhile, take 2 ml feed liquid for the refractometer test ($RI_{\text{feed_b4}}$).
- 2) Place a reaction vessel lid and Teflon O-ring on the top of the vessel and clamp them together.
- 3) Insert a thermometer and a condenser into the lid necks. Place a hot plate underneath the module.
- 4) Fill a reservoir with cold water and turn on a peristaltic pump.
- 5) Turn on the hot plate and start to heat and circulate the feed liquid.
- 6) Weigh collecting vials V1 and V2 together (w_1).
- 7) Hook connecting vials V1 and V2 with the pervaporation system.
- 8) Open valves S1, S2, S3, S4, S5.
- 9) Immerse the cold trap in a dewar flask filled with liquid nitrogen.

- 10) Start the vacuum pump.
- 11) Pull vacuum for 2-3 hours to purge the downstream until the vacuum gets stable (steady state).
- 12) Periodically check the vacuum and temperature through the pressure readout and thermometer, respectively.
- 13) Prepare a stopwatch and two dewar flasks filled with liquid nitrogen.
- 14) When the vacuum is below 0.5 torr and stable, and temperature reaches the required value, record pressure and temperature.
- 15) Quickly close valve S5 and immerse two collecting vials in those two liquid nitrogen dewars. Start timing.
- 16) Check the vacuum again. It should increase first and then decrease below 2 torr and get stable.
- 17) The collecting time differs from 2 hour to 5 hours depending on the amount of permeates needed and membrane materials.
- 18) Check the vacuum and temperature. Take out hot water from the reservoir and fill in cold water periodically to get the condenser function well. Fill in liquid nitrogen in those two dewars periodically as well.
- 19) Close valve S1 when time is up. Stop timing.
- 20) Record the temperature. Turn off the hot plate.
- 21) Check the vacuum. The pressure should decrease until get stable. Record the pressure.
- 22) Close valves S3 and S4.
- 23) Take off two liquid nitrogen dewars from collecting vials.

- 24) Let collecting vials warm to room temperature.
- 25) Stop both the vacuum pump and peristaltic pump. Take off the liquid nitrogen dewar from the cold trap.
- 26) Take collecting vials off the system. Use parafilms to cover their top immediately.
- 27) Weigh two vials together (permeates inside the vials) (w2).
- 28) Collect 2 ml feed liquid from the vessel.
- 29) Conduct refractometer tests for the permeate and liquid feed (RI_{permeate} and $RI_{\text{feed_af}}$).
- 30) Open valves S1, S3, S4, S5. Take off the cold trap from the system, clean it and assemble it back to the system.
- 31) Leave the pervaporation vessel on the hot plate or take it off from the system, depending on the experimental plan.

D.3 Analysis

1) Permeance

- a. The equation shown here results in units of GPU. Constants in the equation convert common measurement units to those required for GPU.

$$\text{b. } \left(\frac{\mathcal{P}}{\ell} \right)_{\text{H}_2\text{O}} [\text{GPU}] = 10^6 \cdot \frac{(\text{Permeate flow}) \cdot (1 - y_{\text{HAc}})}{A \cdot \Delta p \cdot 2.9}$$

- i. Permeate flow is in g/hr.

- ii. y_{HAc} is the *mass* concentration of HAc in the permeate, which is calculated based upon the refractive index of $\text{RI}_{\text{permeate}}$.
- iii. A is the area available for permeation in cm^2 .
- iv. Δp is the pressure drop between upstream and downstream sides of the hollow fiber membrane in cmHg .

2) Separation factor

$$\text{c. } \beta_{\text{H}_2\text{O}/\text{HAc}} = \frac{(1 - y_{\text{HAc}})/y_{\text{HAc}}}{(1 - x_{\text{HAc}})/x_{\text{HAc}}}$$

- v. x_{HAc} is the mass concentration of HAc in the feed liquid, which is calculated based upon the average refractive index of $(\text{RI}_{\text{feed-b4}} + \text{RI}_{\text{feed-af}})/2$. y_{HAc} is the mass concentration of HAc in the permeate, which is calculated in terms of the refractive index of $\text{RI}_{\text{permeate}}$.
- vi. $\text{RI}_{\text{feed-b4}}$ and $\text{RI}_{\text{feed-af}}$ should not exhibit too much difference if the condenser functions well. In addition, the relatively large feed liquid is used in this work in contrast to a single-fiber module.

3) Ideal selectivity

$$\text{d. } \alpha_{\text{H}_2\text{O}/\text{HAc}} = \frac{\left(\frac{\mathcal{P}}{\ell}\right)_{\text{H}_2\text{O}}}{\left(\frac{\mathcal{P}}{\ell}\right)_{\text{HAc}}}$$

3) Uncertainty

- e. Uncertainty for fluxes is estimated from the precision of the balance and stopwatch to be about $\pm 2\%$.
- f. The permeance and membrane selectivity have to be corrected based upon the model work in chapter 5, depending on the bore size of a hollow fiber.

D.4 Emergency Stop

Keep an eye on the vacuum. If the vacuum loses too fast, close S1 and S5. Turn off the hot plate. Check the membrane and epoxy. In most cases, it is due to the broken fiber and epoxy leakage.

D.5 Notes

- 1) The pervaporation system is made of glass. Handle carefully and do not try to pull or twist any glass connection parts.
- 2) Replace cold water in the reservoir every hour to ensure the condenser function well. Keep the cold trap in liquid nitrogen when the test is running.
- 3) Change pump oil every three months.

Appendix E: Exploration of Reverse Osmosis Technology

E.1 Introduction

Reverse osmosis (RO) is a solvent selective membrane separation process in which the applied upstream pressure must exceed the osmotic pressure difference across the membrane. Water is the typical solvent in most existing RO applications and desalting seawater and brackish water by RO has been commercialized for several decades [1]. Generally in RO, feed water flows along the membrane surface under the required pressure and the permeated water is collected on the other side of the membrane. In the mean time, the concentrated water, containing dissolved and undissolved materials that can not go through the membrane, is discharged to the environment from where it originates. Figure E.1 shows a typical RO membrane desalination system with an energy recovery turbine.

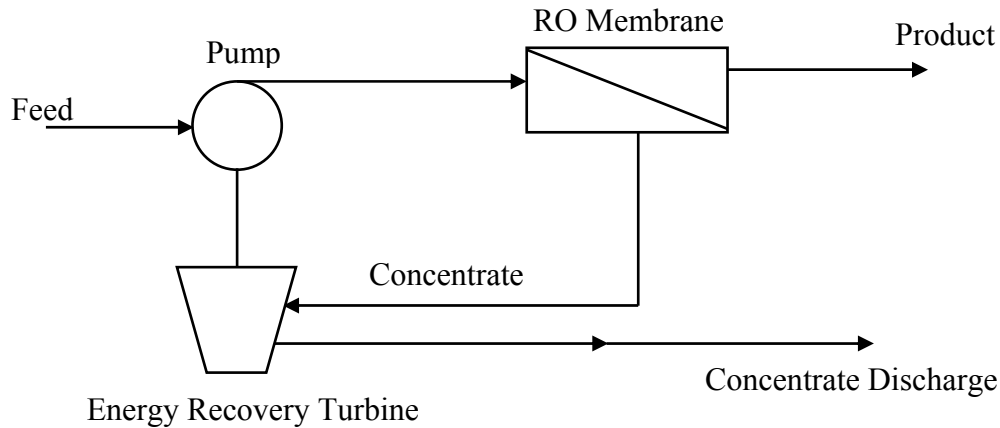


Figure E.1: Typical RO membrane desalination system with energy recovery [2]

In contrast to other conventional water treatment processes, reverse osmosis has proven to be the most efficient and energy-saving method for removing salts, chemical contaminants, and heavy metals such as lead from drinking water. Thus, it should be very interesting to investigate the possibility of applying annealed fibers in a RO system for separating HAc/H₂O mixtures. Figure E.2 shows the flowchart of a hollow fiber-based RO separator.

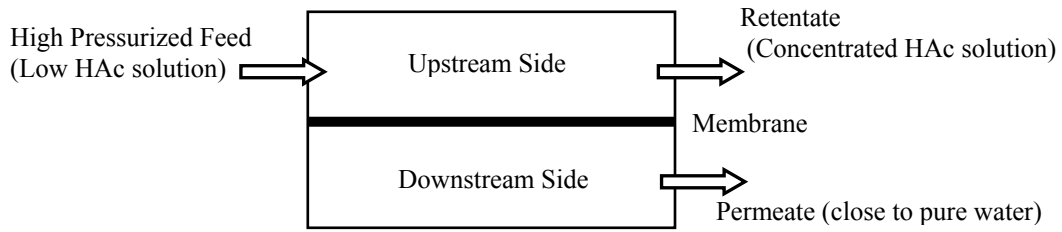


Figure E.2: Flowchart of a hollow fiber-based RO separator

E.2 RO Model

As stated in Chapter 2, the solution-diffusion model (SD) is used to describe the transport of penetrants through a non-porous skin layer of a hollow fiber. Due to the specific mechanism in a RO system, the modified SD model in separating HAc/H₂O mixtures is defined as below [3-4]:

$$\alpha_{\text{H}_2\text{O}/\text{HAc}}' = \underbrace{\left[\frac{D_{\text{H}_2\text{O}}}{D_{\text{HAc}}} \right]}_{\text{Diffusion}} \underbrace{\left[\frac{K_{\text{H}_2\text{O}}}{K_{\text{HAc}}} \right]}_{\text{Solubility}} \underbrace{\left[\frac{(\Delta p - \Delta \pi) V_1 / RT}{\Delta \omega_{\text{HAc}}} \right]}_{\text{RO Driving_Force}} \quad (\text{E.1})$$

where $\alpha_{\text{H}_2\text{O}/\text{HAc}}$ is the RO membrane selectivity, $D_{\text{H}_2\text{O}}$ and D_{HAc} are the diffusion coefficients of water and HAc through the membrane, respectively. The parameters of $K_{\text{H}_2\text{O}}$ and K_{HAc} are the water and HAc partition coefficients that equal the ratio of the component mass concentration in the membrane to that in the external solution. The parameter of $\Delta\omega_{\text{HAc}}$ is the difference in *mass* fractions of HAc in the external solutions in contact with the upstream and downstream faces of the membrane. The quantity $(\Delta p - \Delta\pi)$ represents the effective driving force for water permeation taken to be the difference between the transmembrane pressure and the transmembrane osmotic pressure. The parameter of V_1 is the partial molar volume of water (cm^3/mol), R is the gas universal constant ($82.07 \text{ cm}^3 \text{ atm} / \text{mol} \cdot \text{K}$), and T is temperature (K).

The effectiveness of RO driving force on the membrane performance, DFE, is defined as the last term of equation 8.1. This term characterizes the contribution from the RO system and is independent of membrane materials.

$$\text{DFE} = \frac{(\Delta p - \Delta\pi)V_1 / RT}{\underbrace{\Delta\omega_{\text{HAc}}}_{\text{RO Driving_Force}}} \quad (\text{E.2})$$

The transmembrane osmotic pressure, $\Delta\pi$, can be expressed as below [4-5]:

$$\Delta\pi = -\frac{RT}{V_1} \ln\left(\frac{x_{\text{H}_2\text{O},\text{up}}}{x_{\text{H}_2\text{O},\text{down}}}\right) \quad (\text{E.3})$$

where $x_{\text{H}_2\text{O},\text{up}}$ and $x_{\text{H}_2\text{O},\text{down}}$ represent the *mole* fractions of water on the upstream and downstream sides, respectively.

Liquids are usually moved by pumps, generally rotating equipment. The energy cost, E (Btu/lb), for an adiabatic pump can be expressed as below [6]:

$$E = 0.003 \cdot V \cdot \Delta p \quad (E.4)$$

where V is the specific volume of liquids (cm^3/g), and Δp is the applied pressure (psi).

Clearly the osmotic pressure is a key to design a RO cross-flow separator. Figure E.3 shows the variation of the osmotic pressure with the HAc concentration on the upstream side and downstream side. For example, with a 50% wt HAc/ H_2O mixture on the upstream side and a 20% wt HAc/ H_2O mixture on the downstream, the osmotic pressure is about 300 atm.

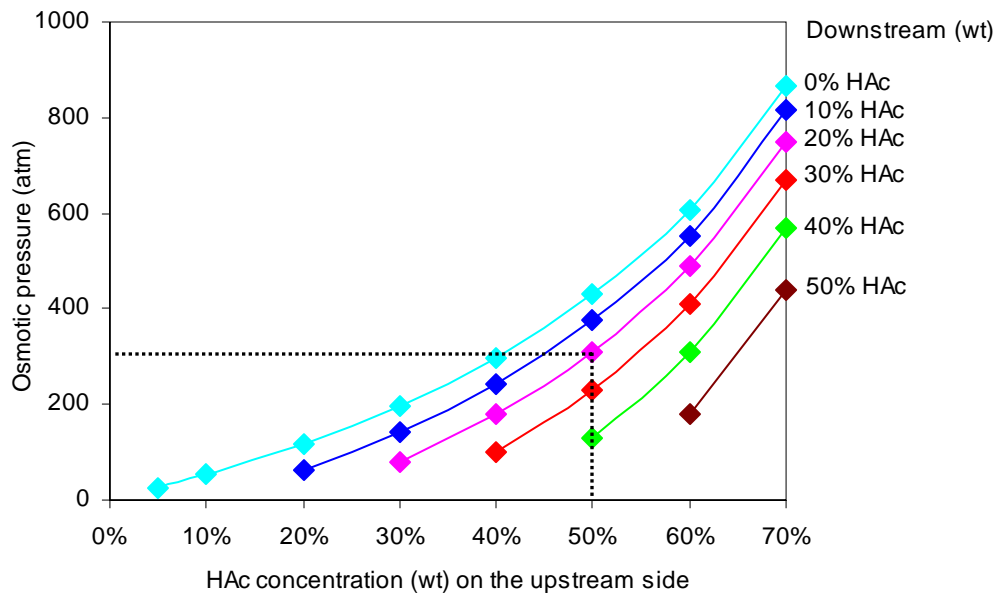


Figure E.3: Osmotic pressure vs. HAc concentration on the upstream and downstream sides of the membrane

The following assumptions have to be made to evaluate the annealed hollow fiber performance in a RO system theoretically.

$$1) \alpha_{\text{H}_2\text{O}/\text{HAc}} = \left[\underbrace{\frac{D_{\text{H}_2\text{O}}}{D_{\text{HAc}}}}_{\text{Diffusion}} \right] \left[\underbrace{\frac{K_{\text{H}_2\text{O}}}{K_{\text{HAc}}}}_{\text{Solubility}} \right] = \phi(x_{\text{HAc}}). \text{ This selectivity illustrates the mobility}$$

and solubility-controlled behavior associated with the membrane material itself. Since the membrane selectivity is strongly concentration dependent in this project, the piecewise linear functions shown in equation 6.3 will be used to in the RO calculation;

- 2) The operation temperature is 101.5°C;
- 3) $V_1 \approx 18.72 \text{ cm}^3 / \text{mol}$ for HAc/H₂O mixtures at 101.5°C;
- 4) The transport of water and HAc through the membrane are independent, so a “frame of reference” correction is NOT needed;
- 5) Shell feed is used;
- 6) The applied pressure in the shell side is constant;
- 7) Bore pressure change is negligible because of large bore size annealed fibers;
- 8) A model 20% wt HAc/H₂O concentration solution is fed into a cross-flow separator;
- 9) The module length is 100 cm;
- 10) The change of liquid volumes is independent of the applied pressure. The critical temperatures (T_C) and critical pressures (P_C) of water and HAc are shown in Table E.1.

Table E.1: T_C and P_C for water and HAc [7-8]

Compounds	T_C ($^{\circ}\text{C}$)	P_C (atm)
Water	374.2	218.3
HAc	57.1	320

A hypothetical RO cross-flow separator is shown in Figure E.4. A model 20% wt HAc solution is concentrated to 30% wt HAc on the retentate side using hollow fiber membranes, while almost pure DI water is collected on the permeate side.

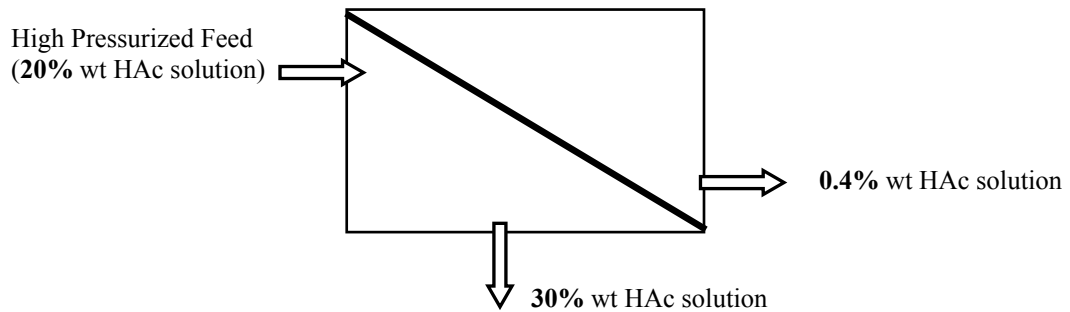


Figure E.4: Hypothetical RO cross-flow separator

Figure E.5 illustrates the variations of osmotic pressure and the HAc concentration on the upstream side with the distance down the length of hollow fibers.

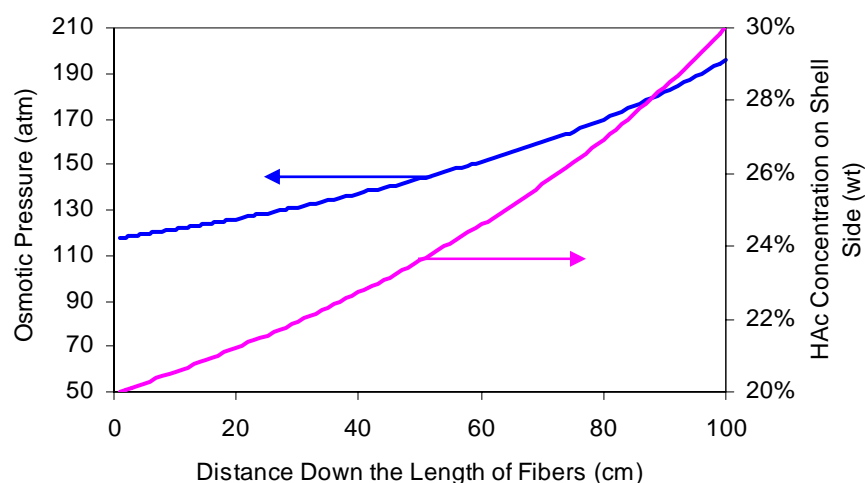


Figure E.5: Variations of osmotic pressure and HAc concentration on the upstream side vs. distance down the length of hollow fibers

The osmotic pressure increases due to the concentrated HAc solution on the upstream side along the distance down the length of fibers. The overall membrane selectivity and energy cost with the applied pressure are shown in Figure E.6.

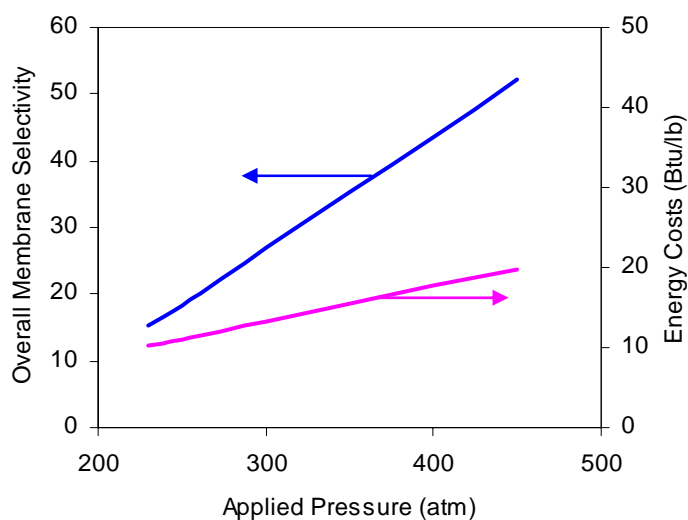


Figure E.6: Overall membrane selectivity and energy cost vs. applied pressure

Only 18 Btu/lb is needed to acquire the overall membrane selectivity of 44 that is the best selectivity in pervaporation in this research. In fact, the energy cost can be further depressed by an energy recovery turbine [9]. That is, a part of the concentrated retentate under pressure can be re-circulated so as that less feed solution has to be pressurized to achieve the required flow rate over the membrane.

Typically the energy consumption of about 121 Btu/lb is necessary in an optimized thermal separation in a state-of-the-art seawater system [10]. The effective “thermal equivalent” energy for RO membranes is much lower than thermal energy even including 33% efficiency for the electricity generation of pumps [10].

The energy-saving RO technology is very attractive in separating HAc/H₂O mixtures because energy becomes increasingly critical in the future. However, it also raises new challenges such as whether membranes can hold high RO pressure. Nevertheless, RO technology is still worthy of future researchers’ investigation for separating water-organic solvent systems using advanced membrane materials.

E.3 References

- [1] Lee, E.K. and Koros, W.J. *Membrane, Synthetic, Applications*. Encyclopedia of Physical Science and Technology. 2001, 313-318.
- [2] National Research Council. *Review of the desalination and water purification technology roadmap*. The National Academies Press, Washington, D.C. 2004.
- [3] Koros, W.J., Fleming, G.K., Jordan, S.M., Kim, T.H., and Hoehn, H.H. *Polymeric membrane materials for solution-diffusion based permeation separations*. Prog. Polym. Sci. 1988, 13, 381-385.
- [4] Parekh, B.S. *Reverse osmosis technology: Application for high-purity-water production*. Marcel Dekker, Inc. 1988, 1-43.

- [5] Castellan, G.W. *Physical chemistry*. The Benjamin/Cummings Publishing Company, Inc. 3rd Ed. 1983, 288-291.
- [6] Smith, J.M., Van Ness, H.C., and Abbott, M.M. *Introduction to chemical engineering thermodynamics*. McGraw-Hill Higher Education. 2001, 272-274.
- [7] Steam tables: Properties of saturated and superheated steam. ABB Combustion Engineering. 1967.
- [8] <http://www.flexwareinc.com/gasprop.htm>.
- [9] Hoornaert, P. *Reverse osmosis*. Pergamon International Information Cooperation, 1984, 82-87.
- [10] Koros, W.J. *Evolving beyond the thermal age of separation processes: Membranes can lead the way*. AIChE J. 2004, 50 (10), 2326-2334.

Bibliography

- A. El-Sayed, M. and Qian, W. Personal Communication with Prof. and Dr. Wei Qian from Laser Dynamic Lab, Georgia Tech, 2005.
- Al-Juaied, M.A. *Carbon dioxide removal from nature gas by membranes in the presence of heavy hydrocarbons and by aqueous diglycolamine[®]/Morpholine*. Ph.D. Dissertation, The University of Texas at Austin, 2004.
- Aref-Azar, A. and Hay, J. N. *Physical Aging in Glassy Polymers, an I. R.. Spectroscopic Investigation of Poly(ethylene terephthalate)*. Polymer. 1982, 23, 1129-1132.
- Bai, J., Fouda, A.E., Matsuura, T., and Hazlett, J.D. *Study on the preparation and performance of polydimethylsiloxane-coated polyetherimide membranes in pervaporation*. J. Appl. Polym. Sci. 1993, 48, 999-1008.
- Ballweg A.H., Brtischke H.E.A., Schneider W.H. and Tiisel G.F. *Pervaporation Membranes*. Proceedings of the Fifth International Alcohol Fuels Symposium. John McIndoe, Dunedin, New Zealand. 1982.
- Baker, R.W. *Membrane technology and applications*. The McGraw-Hill Companies, Inc. 2000.
- Barrer, R.M. *Diffusion and permeation in heterogeneous media, in Diffusion in polymers*. J. Crank and G.S. Park, Editors. 1968, Academic Press: New York. 165-217.
- Barsema J.N., Klijnstra, S.D., Balster, J.H., Van der Vegt, N.F.A., Koops, G.H., and Wessling, M. *Intermediate polymer to carbon gas separation membranes based on Matrimid PI*. J. Membr. Sci. 2004, 238, 93-102.
- Binning R.C., R.J. Lee, Jennings J.F. and Martin E.C. *Separation of Liquid Mixtures by Permeation*. Ind. Eng. Chem. 1961, 53, 45-50.
- Bird R. B., Stewart W. E. and Lightfoot E. N. *Transport Phenomena* John Wiley & Sons, Inc., New York, 1960.
- Blume I., Wijmans J.G. and Baker R.W. *The separation of dissolved organics from water by pervaporation*. J. Membr. Sci. 1990, 49(3), 253-286.
- Boom, R.M., Boomgaard, T.v.d., Berg, J.W.A.v.d., and Smolders, C.A. *Linerarized cloudpoint curve correlation for ternary systems consisting of one polymer, one solvent and one non-solvent*. Polymer. 1993, 34, 2348-2356.
- Bos, A. *High pressure CO₂/CH₄ separation with glassy polymer membranes - Aspects of CO₂-induced plasticization*. Ph.D. Dissertation, The University of Twente at Netherlands, 1996.

- Bos, A., Punt, I.G.M., Strathmann, H., and Wessling, M. *Suppression of gas separation membrane plasticization by homogeneous polymer blending*. AIChE J. 2001, 47, 1088-1093.
- Bos, A., Punt, I.G.M., Wessling, M., and Strathmann, H. *Plasticization-resistant glassy polyimide membranes for CO₂/CH₄ separations*. Sep. Purif. Technol. 1998, 14, 27-39.
- Bueche, F. *Physical properties of polymers*. New York: Interscience, Inc. 1962.
- Carruthers, S.B. *Integral skin formation in hollow fiber membranes for gas separations*. Ph.D. Dissertation, The University of Texas at Austin, 1997.
- Carruthers, S.B., Ramos, G.L., and Koros, W.J. *Morphology of integral-skin layers in hollow-fiber gas-separation membranes*. J. Appl. Poly. Sci. 2003, 90, 399-411.
- Castellan, G.W. *Physical chemistry*. The Benjamin/Cummings Publishing Company, Inc. 3rd Ed. 1983, 288-291.
- Chai, X.S., Hou, Q.X., Zhu, J.Y., Chen, S.L., Wang, S.F., and Lucia, L. *Carboxyl groups in wood fibers. 1. Determination of carboxyl groups by headspace gas chromatography*. Ind. Eng. Chem. Res. 2003, 42, 5440-5444.
- Chan, A.H., Koros, W.J. and Paul, D.R. *Analysis of hydrocarbon gas sorption and transport in ethyl cellulose using the dual sorption/partial immobilization models*. J. Membr. Sci. 1978, 3, 117-130.
- Chern, R. T., Koros, W. J., and Fedkiw, P. S. *Simulation of a hollow fiber gas separator: The effects of process and design variables*. Ind. Eng. Chem. Process, Design and Development. 1985, 24, 1015-1022.
- Chern, R.T., Koros, W.J., Sanders, E.S., and Yui, R. *Second component effects in sorption and permeation of gases in glassy polymers*. J. Membr. Sci. 1983, 15, 157-169.
- Cho, D., and Drzal, L. *Effect of thermal cure on the fluorescence of MatrimidTM 5292 bismaleimide resin*. J. Mater. Sci. Lett. 2003, 22, 459-461.
- Chung, T.S., E.R. Kafchinski, and R. Vora, *Development of a Defect-Free 6FDA-Durene Asymmetric Hollow Fibers and its Composite Hollow Fibers*. J. Membr. Sci. 1994, 88, 21-36.
- Clausi, D. T. *Formation and characterization of asymmetric polyimide hollow fiber membranes for gas separations*. Ph.D. Dissertation, The University of Texas at Austin, 1998.
- Clausi, D.T., McKelvey, S.A and W.J. Koros, *Characterization of substructure resistance in asymmetric gas separation membranes*. J. Membr. Sci. 1999, 160, 51-64.

Clausi, D.T., Koros, W.J. *Formation of defect-free polyimide hollow fiber membranes for gas separations*. J. Membr. Sci. 2000, 167, 79-89.

Damle, S. *Membrane Based Separations of Organic Solutes from Supercritical Carbon Dioxide*. Ph.D. Dissertation, The University of Texas at Austin, 2004.

Davis T.E. and Overman D. C. *Process for Drying Water-Wet Membranes* United States Patent 4,430,807, Dow Chemical 1984.

Deng, S., Sourirajan, S., Matsuura, T. *Study of polydimethylsiloxane/aromatic polyamide laminated membranes for separation of acetic acid/water mixtures by pervaporation process*. Sep. Sci. Technol. 1994, 29, 1209-1216.

Djoekita, G., Vu, D.Q., and Koros, W.J. *Pervaporative Introduction of Organic Vapors into High-Pressure Gas Feeds*. J. Appl. Polym. Sci. 2001, 80(2), 311-315.

Dorkendo, K.D. and Pfromm, P.H. *Experimental evidence and theoretical analysis of physical aging in thin and thick amorphous glassy polymer films*. J. of Polym. Sci. Part B: Polym. Phy. 1999, 37, 2239-2251.

Duer, M.J. *Introduction to solid-state NMR spectroscopy*. Oxford, UK; Malden, MA: Blackwell, 2004.

Ekiner, O.M., Hayes, R.A., and Manos, P. *Reactive post treatment for gas separation membranes*. United States Patent 5,091,216, E.I. du Pont de Nemours 1992.

Ekiner, O.M. and Hayes, R.A. *Phenylindane-containing polyimide gas separation membranes*. United States Patent 5,015,270, E.I. du Pont de Nemours, 1991.

Ekiner, O.M. and Vassilatos, G. *Polyaramide hollow fiber for hydrogen/methane separation-spinning and properties*. J. Membr. Sci. 1990, 53, 259-273.

Fleming, G.K. and Koros, W.J. *Dilation of polymers by sorption of carbon dioxide at elevated pressures: silicone rubber and unconditioned polycarbonate*. Macromolecules. 1986, 19, 2285-2291.

Frb, A.J. and Paul, D.R. *Gas sorption and transport in polysulfone*. J. Membr. Sci. 1981, 8, 11-22.

Freeman B.D. and Pinnau I. *Polymer membranes for gas and vapor separation* ACS SYMPOSIUM SERIES 733 1999.

Goran, T. and Milan, V. *Pressure drops and hydraulic resistances in a three-phase hollow fiber membrane contactor with frame elements*. Chem. Eng. Proc. 2001, 40, 3-11.

Gray-Weale, A.A. and Henchman, R.H. *Transition-state theory model for the diffusion coefficients of small penetrants in glassy polymers*. Macromolecules. 1997, 30(23), 7296-7306.

Greenfield, M.L. and Theodorou, D.N. *Molecular modeling of methane diffusion in glassy atactic polypropylene via multidimensional transition state theory*. Macromolecules. 1998, 31(20), 7068-7090.

Gudernatsch, W., Kimmerle, K., Stroh, N., and Chmiel, H. *Recovery and concentration of high vapor pressure bioproducts by means of controlled membrane separation*. J. Membr. Sci. 1998, 36, 331-342.

Guerra, G., Choe, S., William, D.J., Karasz, F.E., and MacKnight, W.J. *Fourier transform infrared spectroscopy of some miscible polybenzimidazole/polyimide blends*. Macromolecules. 1988, 21, 231-234.

Gullbault, G.G. *Fluorescence: theory, instrumentation, and practice*. Marcel Dekker, Inc., New York, 1967.

Guo, W.F., Chung, T.S., and Matsuura, T. *Pervaporation study on the dehydration of aqueous butanol solutions: A comparison of flux vs. permeance, separation factor vs. selectivity*. J. Membr. Sci. in press.

Hasegawa, M., Kochi, M., Mita, I., and Yokota, R. *Molecular aggregation and fluorescence spectra of aromatic polyimides*. Eur. Polym. J. 1989, 25, 349-354.

Hayes R. A. *Polyimide Gas Separation membranes* United States Patent 4,705,540, E.I. Du Pont de Nemours, 1987.

He, G., Zhou, Y., Xu, R., and Zhu, B. *Study on pressure drop in hollow-fiber membrane for gas separation*. Mo Kexue Yu Jishu. 1993, 13(2), 22-28.

Henis, J.M.S. and Tripodi, M.K. *Composite hollow fiber membranes for gas separation: the resistance model approach*. J. Membr. Sci. 1981, 8, 233-246.

Henis, J.M.S. and Tripodi, M.K. *Multicomponent membranes for gas separations*. United States Patent 4,230,463, Monsanto Co. 1980.

Henis, J.M.S. and Tripodi, M.K. *Multicomponent membranes for gas separations*. United States Patent 4,230,463, Monsanto Co. 1980.

Hibshman, C., Cornelius, C.J., and Marand, E. *The gas separation effects of annealing polyimide-organosilicate hybrid membranes*. J. Membr. Sci. 2003, 211, 25-40.

Hines, A.L. and Maddox, R.N. *Mass transfer fundamentals and applications*. Prentice Hall Inc. 1985.

Ho, W.S.W. and Sirkar, K.K. *Membrane handbook*. Van Nostrand Reinhold, New York 1992.

Hofmann, T., Hapke, R.L., Sengupta, A., and Roberts, D.L. *Acetic acid and butyric acid recovery from aqueous solutions by pervaporation*. Presented at the Conference of the North American Membrane Society, San Diego, CA, 1991.

Hoornaert, P. *Reverse osmosis*. Pergamon International Information Cooperation. 1984, 82-87.

<http://probes.invitrogen.com/handbook/figures/0664.html>.

<http://www.flexwareinc.com/gasprop.htm>.

Huang, J.G., Cranford, R.J., Matsuura, T., and Roy, C. *Sorption and transport behavior of water vapor in dense and asymmetric polyimide membranes*. J. Membr. Sci. 2004, 241, 187-196.

Huang, J.G., Cranford, R.J., Matsuura, T., and Roy, C. *Water vapor permeation properties of aromatic polyimides*. J. Membr. Sci. 2003, 215, 129-140.

Huang, J.G., Cranford, R., Matsuura, T., and Roy, C. *Development of polyimide membranes for the separation of water vapor from organic compounds*. J. Appl. Poly. Sci. 2002, 85, 139-152.

Huang, R.Y.M. *Pervaporation membrane separation processes*. Elsevier Science Publishing Company, Inc. New York. 1991, 1-46.

Huang, S.C., Ball, I.J., and Kaner, R.B. *Polyaniline membranes for pervaporation of carboxylic acids and water*. Macromolecules. 1998, 31, 5456-5464.

Hoppin, C. R. *Characterization of Torlon[®] Films*. 2004 (Internal report in Dr. William Koros' group).

Ismail, A.F. and Yean, L.P. *Review on the development of defect-free and ultrathin-skinned asymmetric membranes for gas separation through manipulation of phase inversion and rheological factors*. J. Appl. Poly. Sci. 2003, 88, 442-451.

Jin, Q., Yamashita, T., and Horie, K. *Polyimides with alicyclic diamines. II. hydrogen abstraction and photocrosslinking reactions of benzophenone-type polyimides*. J. Polym. Sci.: Part A: Polym. Chem. 1994, 32, 503-511.

Jordan, S.M., Koros, W.J. and Fleming, G.K. *The effects on carbon dioxide exposure on pure and mixed gas permeation behavior of polymers: comparison of glassy polycarbonate and silicone rubber*. J. Membr. Sci. 1987, 30, 191-212.

Kaschemkat, J., Hilgendorff, W., Boddeker, K.W., and Kneifel, K. German Patent Application DE 3713973 A1.

Kawakami, H., Mikawa, M., and Nagaoka, S. *Gas transport properties in thermally cured aromatic polyimide membranes*. J. Membr. Sci. 1996, 118, 223-230.

Kazama, S., Teramoto, T., and Haraya, K. *Carbon dioxide and nitrogen transport properties of bis(phenyl)fluorene-based cardo polymer membranes*. J. Membr. Sci. 2002, 207(1), 91-104.

Kesting, R.E. and Fritzsche, A.K. *Polymeric gas separation membranes*. John Wiley and Sons, Inc., New York 1993.

Kirk, R.E. and Othmer, D.F. *Encyclopedia of chemical technology*. John Wiley & Sons, Inc. 4th Ed. New York. 2000, 18, 1006-1012.

Kita, H., Inada, T., Tanaka, K., and Okamoto, K. *Effect of photocrosslinking on permeability and permselectivity of gases through benzophenone-containing polyimide*. J. Membr. Sci. 1994. 139-147.

Kim, T. H., Koros, W. J., Husk, G. R., and O'Brien, K. C. *Relationship between gas separation properties and chemical structure in a series of aromatic polyimides*. J. Membr. Sci. 1988, 37, 45-62.

Kirk, R.E. and Othmer, D.F. *Encyclopedia of chemical technology*. John Wiley & Sons, Inc. 4th Ed. New York. 2000, 18, 1006-1012.

Koros, W.J. *Simplified analysis of gas/polymer selective solubility behavior*. J. Polym. Sci., Polym. Phys. Ed. 1985, 23(8), 1611-1628.

Koros, W.J. *Evolving beyond the thermal age of separation processes: Membranes can lead the way*. AIChE J. 2004, 50 (10), 2326-233

Koros, W.J. and Fleming, G.K. *Membrane-based gas separation*. J. Membr. Sci. 1993, 83, 1-80.

Koros, W.J., Fleming, G.K., Jordan, S.M., Kim, T.H., and Hoehn, H.H. *Polymeric membrane materials for solution-diffusion based permeation separations*. Prog. Polym. Sci. 1988, 13, 381-385.

Koros, W.J. and Hellums, M.W. *Transport properties, in encyclopedia of polymer science and engineering*, 2nd ed., John Wiley and Sons: New York, 1989; Supplement. Vol., 724-803.

Koros, W.J. and Paul, D.R., *CO₂ sorption in poly(ethylene terephthalate) above and below the glass transition*. J. Poly. Sci.: Phys. Ed. 1978, 16, 1947-1964.

- Koros, W.J. and Paul, D.R. et al. *Carbon dioxide sorption and transport in polycarbonate*. J. Polym. Sci., Polym. Phys. 1976 Ed. 14, 687-702.
- Koros, W.J., Pinnau, I. *In polymeric gas separation membranes*; Pual, D.R. and Yampol'skii, Y.P., Eds.; CRC Press: Boca Raton, LA, 1994; Chapter 5.
- Kovacs, A. J. *La Contraction Isotherme du Volume des Polyme' res Amorphes*. J. Polym. Sci. 1958, 30, 131-147.
- Krol, J.J., Boerrigter, M., and Koops, G.H. *Polyimide hollow fiber gas separation membranes: preparation and the suppression of plasticization in propane/propylene environments*. J. Membr. Sci. 2001, 184, 275-286.
- Lee, E.K. and Koros, W.J. *Membrane, Synthetic, Applications*. Encyclopedia of Physical Science and Technology. 3rd Ed. Academic Press. 2001, 279-344.
- Lide, D.R. *Handbook of chemistry and physics*. CRC Press. 1995-1996, 76th, 6-57.
- Lide, D.R. *Handbook of chemistry and physics*. CRC press. 1995-1996, 76th, 3.3-3.330.
- Lim, S. P., Tan, X., and Li, K. *Gas/vapor separation using membranes: Effect of pressure drop in lumen of hollow fibers*. Chem. Eng. Sci. 2000, 55, 2641-2652.
- Lim, S. P. and Li, K. *Internally staged permeator for gas/vapor separation: effect of pressure drop in annuli of annular hollow fibers*. Chem. Eng. Sci. 2001, 56, 3907-3913.
- Liu, Y., Wang R., and Chung, T.S. *Chemical cross-linking modification of polyimide membranes for gas separation*. J. Membr. Sci. 2001, 189, 231-239.
- Loeb, S. and Sourirajan, S. *Sea water demineralization by means of an osmotic membrane*. Adv. Chem. Ser. 1962, 38, 117-132.
- Lue, S.J. and Peng, S.H. *Polyurethane (PU) membrane preparation with and without hydroxypropyl-b-cyclodextrin and their pervaporation characteristics*. J. Membr. Sci. 2003, 222, 203-217.
- Lue, S.J., Wang, F. J., and Hsiaw, S. *Pervaporation of benzene/cyclohexane mixtures using ion-exchange membrane containing copper ions*. J. Membr. Sci. 2004, 240(1-2), 149-158.
- Machado, P.S.T., Habert, A.C. and Borges, C.P. *Membrane formation mechanism based on precipitation kinetics and membrane morphology: flat and hollow fiber polysulfone membranes*. J. Membr. Sci. 1999, 155, 171-183.
- Mahajan, R., *Formation, characterization and modeling of mixed matrix membrane materials*. Ph.D. Dissertation, The University of Texas at Austin at Austin, 2000.

- Makino, H., Kusuki, Y., Harada, T., and Shimazaki, H. United States Patent 4,373,400, 1983.
- Makino, H., Kusuki, Y., Harada, T., and Shimazaki, H. United States Patent 4,440,643, 1984.
- Makino, H., Kusuki, Y., Harada, T., Shimazaki, H., and Isida, T. United States Patent 4,528,004, 1985
- Makino, H., Kusuki, Y., Yoshida, H., and Nadamura, A. United States Patent 4,378,324, 1983.
- Manos, P. *Solvent exchange drying of membranes for gas separation*. United States Patent 4,120,098.
- McCaig, M.S. and Paul, D.R. *Effect of film thickness on the changes in gas permeability of a glassy polyarylate due to physical aging Part I. Experimental observations*. Polymer. 2000, 41, 629-637.
- McCaig, M.S., Paul, D.R., and Barlow, J.W. *Effect of film thickness on the changes in gas permeability of a glassy polyarylate due to physical aging Part II. Mathematical model*. Polymer. 2000, 41, 639-648.
- McHugh, A.J. and Tsay, C.S. *Dynamics of the phase inversion process*. J. Appl. Poly. Sci. 1992, 46, 2011-2021.
- McKelvey, S.A. *Formation and characterization of hollow fiber membranes for gas separation*. Ph.D. Dissertation, The University of Texas at Austin, 1997.
- Mckeley, S.A., Clausi, D.T., and Koros, W.J. *A guide to establishing hollow fiber macroscopic properties for membrane applications*. J. Membr. Sci. 1997, 124, 223-232.
- Mellis, R., Gill, W. N., and Belfort, G. *Fluid dynamics in a tubular membrane: theory and experiment*. Chem. Eng. Commun. 1993, 122, 103-125.
- Membrane Technology and Research, Inc., 1360 Willow Road, Menlo Park, CA 94025, U.S.A.: Product Information 1988.
- Mulder, M., *Basic principles of membrane technology*. Kluwer Academic Publishers: Dordrecht 1996.
- Nader M. A. and Abbas, A. *Modeling an industrial reverse osmosis unit*. Desalination. 1999, 126, 33-39.
- National Research Council. *Review of the desalination and water purification technology roadmap*. The National Academies Press, Washington, D.C. 2004.

- Ohya, H., Kudryavtsev, V.V., and Semenova, S.I. *Polyimide membranes: applications, fabrications, and properties*. Gordon and Breach Inc. 1996.
- Pan C. Y. and Habgood H. W. *Gas separation by permeation: Part I. Calculation methods and parametric analysis*. Canadian J. Chem. Eng. 1978, 56, 197-209.
- Pan C. Y. and Habgood H. W. *Gas separation by permeation: Part II. Effect of permeate pressure drop and choice of permeate pressure*. Canadian J. Chem. Eng. 1978, 56, 210-217.
- Parekh, B.S. *Reverse osmosis technology: Application for high-purity-water production*. Marcel Dekker, Inc. 1988, 1-43.
- Park, H.C., Moon, Y.S., Rhee, H.W., Won, J., Kang, Y.S., and Kim, U.Y. *Effect of solvent exchange on the morphology of asymmetric membranes, in membrane formation of modification*, Pinnau, I. and Freeman, B., Ed. 2000, ACS: Washington, D.C. 110-124.
- Patel, N.P., Hunt, M.A., Lin-Gibson, S., Bencherif, S., and Spontak, R.J. *Tunable CO₂ transport through mixed polyether membranes*. J. Membr. Sci. 2005, 251(1-2), 51-57.
- Paul, D.R. *Gas Sorption and Transport in Glassy Polymers*. Ber. Bunsenges Phys. Chem. 1979, 83, 294-302.
- Paul, D.R. and Koros, W.J. *Effect of partially immobilizing sorption on permeability and the diffusion lag time*. J. Poly. Sci., Poly. Phys. 1976, 14, 675-685.
- Paul, D.R. and Yampol'skii, Y.P. *Polymeric gas separation membranes*. CRC Press. Boca Raton, FL 1994.
- Paulsen, F.G., Shojaie, S.S., and Krantz, W.B. *Effect of evaporation step on macrovoid formation in wet-cast polymeric membranes*. J. Membr. Sci. 1994, 91, 265-282.
- Pesek, S.C. *Aqueous quenched asymmetric polysulfone flat sheet and hollow fiber membranes prepared by dry/wet phase separation*. Ph.D. Dissertation, The University of Texas at Austin, 1993.
- Pesek, S. C. and Koros, W.J. *Aqueous quenched asymmetric polysulfone membranes prepared by dry/wet phase separation*. J. Membr. Sci. 1993, 81, 71-81.
- Petlyuk, F.B. *Distillation theory and its application to optimal design of separation units*. Cambridge, UK: New York: Cambridge University Press, 2004.
- Pietsch, S., personal Communication with Dr. Steve Pietsch from BP, 2004-2005.
- Pinnau, I. and Freeman, B.D. *Membrane formation and modification*. ACS Symposium

Series 744, 1999.

Pinnau, I. and Koros, W.J. A Qualitative skin formation mechanism for membranes made by dry/wet phase inversion. *J. Poly. Sci., Poly. Phys. Ed.* 1993, 31, 419-427.

Porter, M.C., *Handbook of industrial membrane technology*. Noyes Publications, Park Ridge, NJ 1990.

Prabhakar, R., Merkel, T.C., Freeman, B.D., Imizu, T., Higuchi, A., Sarti, G.C., and Doghleri, F. *Effect of fluorocarbon-hydrocarbon interactions on solubility and permeability properties of polymers*. *Polym. Mater. Sci. Eng.* 2001, 85, 253-254.

Pringsheim, P. *Fluorescence and phosphorescence*. Interscience publishers, Inc., New York, 1949.

Rautenbach, R. and Albrecht, R. *The separation potential of pervaporation: II. Process design and economics*. *J. Membr. Sci.* 1985, 25, 25-54.

Reuvers, A.J., Van den Berg, J.W.A., and Smolders, C.A. *Formation of membranes by means of immersion precipitation. Part I. A model to describe mass transfer during immersion precipitation*. *J. Membr. Sci.* 1987, 45-65.

Rezac, M.E., Pfromm, P.H., Costello, L.M., and Koros, W.J. *Aging of thin polyimide-ceramic and polycarbonate-ceramic composite membranes*. *Ind. Eng. Chem. Res.* 1993, 32, 1921-1926.

Rezac, M. E. and Schoberl, B. *Transport and thermal properties of poly(ether imide)/acetylene-terminated monomer blends*. *J. Membr. Sci.* 1999, 156, 211-222.

Rhodes, E. *Spinnerets for hollow fiber membranes: design & modeling*. 2004 (Internal report in Dr. William Koros' group).

Sano, T., Ejiri, S., Yamada, K., Kawakami, Y., and Yanagishita, H. *Separation of acetic acid-water mixtures by pervaporation through silicalite membrane*. *J. Membr. Sci.* 1997, 123, 225-233.

SEMPAS Membranetechnik GmbH, Rosenbergstr. 103, 7000 Stuttgart 1, West Germany: Product Information 1989.

Shimazu, A., Miyazaki, T., Maeda, M., and Ikeda, K. *Relationships between the chemical structures and the solubility, diffusivity, and permselectivity of propylene and propane in 6FDA-based polyimides*. *J. Polym. Sci., Part B: Polym. Phys.* 2000, 38(19), 2525-2536.

Silverstein, R., Bassler, G., and Morrill, T. *Spectrometric identification of organic compounds*. 5th Ed. John Wiley & Sons, Inc. 1991.

- Skoog, D.A., Holler, F.J., and Nieman, T.A. *Principles of instrumental analysis*. 5th Ed. Saunders Golden Sunburst Series, Saunders College Publishing, 1998.
- Skoog, D.A., West, D.M., and Holler, F.J. *Fundamentals of analytical chemistry*. 7th Ed. Saunders College Publishing, 1996.
- Smith, J.M., Van Ness, H.C., and Abbott, M.M. *Introduction to chemical engineering thermodynamics*. McGraw-Hill Higher Education. 2001, 272-274.
- Smolders, C.A., Reuvers, A.J., Boom, R.M., and Wienk, I.M. *Microstructure in phase-inversion membranes. Part 1. Formation of macrovoids*. J. Membr. Sci. 1992, 73, 259-275.
- Spillman, R.W. *Economics of gas separation membranes*. Chem. Eng. Proc. January 1989, 41-62.
- Steam tables: Properties of saturated and superheated steam. ABB Combustion Engineering. 1967.
- Stern, S.A. *Polymers for gas separations: the next decade*. J. Membr. Sci. 1994. 94, 1-65.
- Stichlmair, J. and Fair, J.R. *Distillation: principles and practices*. John Wiley & Sons, Inc. New York 1998.
- Story, B.J., Koros, W.J. *Sorption and transport of carbon dioxide and methane in chemically modified poly(phenylene oxide)*. J. Membr. Sci. 1992, 67(2-3), 191-210.
- Struik, L. C. E. *Physical Aging in Amorphous Polymers and Other Materials*. Elsevier Science Publishing Company, Inc. New York, 1978.
- Tao, W., J.R. Collier, and B.J. Collier, *Evaluation of Interfacial Adhesion in Sheath/Core Composite Fibers*. J. Appl. Poly. Sci. 1993. 47, 1115-1122.
- Thorman, J. M., Rhim, H., and Hwang, S. *Gas separation by diffusion through silicone rubber capillaries*. Chem. Eng. Sci. 1975, 30(7), 751-754.
- Thundiyil M. J. and Koros W. J. *Mathematical modeling of gas separation permeators – for radial crossflow, countercurrent, and cocurrent hollow fiber membrane modules*. J. Membr. Sci. 1997, 125, 275-291.
- Tin, P.S., Chung, T.S., Liu, Y., Wang, R., Liu, S.L., and Pramode, K.P. *Effects of cross-linking modification on gas separation performance of matrimid membranes*. J. Membr. Sci. 2003, 225, 77-90.
- Tsay, C.S. and McHugh, A.J. *A rationale for structure and formation during phase*

inversion. J. Poly. Sci. Part B. 1992, 30, 309-313.

Vieth, W.R., Dao, L.H., and Pedersen, H. *Nonequilibrium microstructural and transport characteristics of glassy poly(ethylene terephthalate)*. J. Membr. Sci. 1991, 60(1), 41-62.

Vu, D.Q., *Formation and characterization of asymmetric carbon molecular sieve and mixed matrix membranes for natural gas purification*. Ph.D. Dissertation, The University of Texas at Austin, 2001.

Wachsman, E. D. and Frank, C. W. *Effect of cure history on the morphology of polyimide: Fluorescence spectroscopy as a method for determining the degree of cure*. Polymer. 1988, 29, 1191-1197.

Wallace, D.W. *Crosslinked hollow fiber membranes for natural gas purification and their manufacture from novel polymers*. Ph.D. Dissertation, The University of Texas at Austin, 2004.

Wang, D., Li, K, and Teo, T.K. *Highly permeable polyethersulfone hollow fiber gas separation membranes prepared using water as non-solvent additive*. J. Membr. Sci. 2000, 176, 147-158.

Wang, R., Liu, S. L., Lin, T. T., and Chung, T. S. *Characterization of hollow fiber membranes in a permeator using binary gas mixtures*. Chem. Eng. Sci. 2002, 57(6), 967-976.

Wijmans, J.G. *Process performance = membrane properties + operating conditions*. J. Membr. Sci. 2003, 220, 1-3.

Wind, J.D., Claudia, S.B., Paul, D.R., and Koros, W.J. *Solid-state covalent cross-linking of polyimide membranes for carbon dioxide plasticization reduction*. Macromolecules. 2003, 36, 1882-1888.

Wind, J.D., Paul, D.R., and Koros, W.J. *Natural gas permeation in polyimide membranes*. J. Membr. Sci. 2004, 228, 227-236.

Wind, J.D., Sirard, S.M., Paul, D.R., Green, P.F., Johnston, K.P., and Koros, W.J. *Relaxation dynamics of CO₂ diffusion, sorption, and polymer swelling for plasticized polyimide membranes*. Macromolecules. 2003, 36, 6442-6448.

Wind, J.D., Sirard, S.M., Paul, D.R., Green, P.F., Johnston, K.P. and Koros, W.J. *Carbon dioxide-induced plasticization of polyimide membranes: pseudo equilibrium relationships of diffusion, sorption, and swelling*. Macromolecules. 2003, 36(17), 6433-6441.

Wind, J.D., Staudt-Bickel, C., Paul, D.R., and Koros, W.J. *The effects of crosslinking chemistry on CO₂ plasticization of polyimide gas separation membranes*. Ind. Eng. Chem. Res. 2002, 41(24), 6139-6148.

Van de Witte, P., Dijkstra, P.J., Van den Berg, J.W.A., and Feijen, *Phase separation processes in polymer solutions in relation to membrane formation*. J. Membr. Sci. 1996, 117, 1-31.

Yoshikawa, M., Kuno, S.T., and Kitao, T. *Specialty polymeric membranes 3. Pervaporation separation of acetic acid/water mixtures through polymeric membranes having a pyridine moiety as a side group*. J. Appl. Polym. Sci. 1994, 51, 1021-1027.

Yoshikawa, M., Kuno, S.L., Wano, T., and Kitano, T. *Specialty polymeric membranes. 4. Pervaporation separation of acetic acid/water mixtures through modified polybutadiene membranes*. Poly. Bull. 1993, 31, 607-611.

Zimmerman, C.Z. Singh, A. and Koros, W.J., *Tailoring mixed matrix composite membranes for gas separations*. J. Membr. Sci. 1997, 137, 145-154.